ODESSA ASTRONOMICAL PUBLICATIONS

Volume 21
(2008)

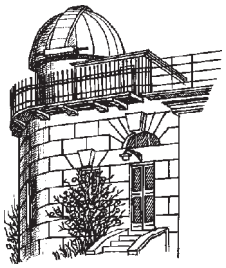

Odessa
«AstroPrint»

FOREWORD

This issue of the "Odessa Astronomical Publications" (V.21, 2008) contains a collection of material presented at the International Conference "Chemical and dynamic evolution of stars and galaxies" that was held in the framework of working group "Stellar atmospheres". This Conference was dedicated to the 70th anniversary of the professor Nikolay Sergeyevich Komarov (1938–2003), it was held in Odessa (Ukraine), Chernomorka, on August 25-29, 2008.

59 participants from Ukraine, Russia, Kazakhstan and Estonia attended Conference. The Memorial part of the conference and the first talk were devoted to the Komarov's life, his scientific, pedagogical and popularization activity. The scientific part of the Conference was presented in 45 contributions.

T. V. Mishenina

CONTENTS

Foreword
T.V.Mishenina 2
Contents 3
NIKOLAY SERGEYEVICH KOMAROV AND THE DEVELOPMENT OF THE SPECTROSCOPIC RESEARCHES IN ODESSA ASTRONOMICAL OBSERVATORY
T.V.Mishenina, A.V.Dragunova 5
PECULIARITIES OF THE NUCLEOSINTHESIS OF HEAVY ELEMENTS IN A DISK OF SPIRAL GALAXY
I.A.Acharova, Yu.N.Mishurov, J.R.Dlepine 9
HIGH PRECISE EFFECTIVE TEMPERATURES OF 182 MAIN SEQUENCE STARS
S.I.Belik, V.V.Kovtyukh, M.P.Yasinskaya 13
IS PZ MON A RED DWARF OR A RED GIANT?
N.I.Bondar', S.G.Sergeev 17
ROTATIONAL VARIATION OF THE MAGNETIC FIELD OF β CrB IN DIFFERENT SPECTRAL LINES
V.Butkovskaya, D.Baklanova, I.Han, K.M.Kim, D.Lyashko, D.Mkrtichian, S.Plachinda, G.Valyavin, V.Tsymbal 19
MAGNETIZATION OF STARS VS. THE EFFECTIVE TEMPERATURE
V.D.Bychkov, L.V.Bychkova, J.Madej 22
MAGNETIC FIELDS OF STARS
V.D.Bychkov, L.V.Bychkova, J.Madej 24
ADAPTIVE MODE OF THE MSS BTA
G.A.Chountonov, I.D.Najdenov 26
PECULIARITIES OF MIXING METALS IN INTERGALACTIC AND INTERSTELLAR MEDIA
S.Yu.Dedikov, Yu.A.Shchekinov, E.O.Vasiliev 29
MIXING METALS UNDER STRIPPING GALACTIC GASEOUS HALOES: RADIATIVE LOSSES
S.Yu.Dedikov, Yu.A.Shchekinov, E.O.Vasiliev 33
HD 158450: A MAGNETIC CHEMICALLY PECULIAR STAR IN A YOUNG STELLAR GROUP
N.A.Drake, E.G.Jilinski, V.G.Ortega, R. de la Reza, B.Bazzanella 35
ABUNDANCES OF COPPER AND ZINC IN STARS OF THE GALACTIC THIN AND THICK DISKS
T.I.Gorbaneva, T.V.Mishenina, N.Yu.Basak, C.Soubiran, V.V.Kovtyukh 37
ESTIMATION OF THE MASS AND THE SPECIFIC MOMENT OF ROTATION OF A BLACK HOLE IN THE CENTER OF SPHERICAL CLUSTER M15
A.A.Kisselev, Yu.N.Gnedin, N.A.Shakht, E.A.Grosheva, M.Yu.Piotrovich, T.M.Natsvlishvili 39
Non-LTE LINE FORMATION FOR S I
S.A.Korotin 42
EVOLUTIONARY CHANGES OF THE KINEMATICS OF THE GALACTIC THIN DISK STARS IN THE SOLAR NEIGHBOURHOOD
V.V.Koval, T.V.Borkova, V.A.Marsakov 45
SPECTRAL LUMINOSITY INDICATORS FOR FGK SUPERGIANTS AND CLASSICAL CEPHEIDS
V.V.Kovtyukh, F.A.Chekhonadskikh 48
HANSKY ALEKSEY PAVLOVITCH
Lemeshchenko N.D., Shevchyuk T.V. 53
CHEMICAL COMPOSITION AND EVOLUTIONARY STATUS OF SPECTRAL BINARY STAR 12 PER
V.V.Leushin, M.K.Kuznetsov 57
POPULATION OF THE Be STARS IN THE YOUNG OPEN CLUSTERS
S.L. Malchenko 60
OMEGA CENTAURI: GLOBULAR CLUSTER, STELLAR STREAM — DWARF GALAXY
V.A.Marsakov, T.V.Borkova 64
FORMATION OF SMALL-SCALE STRUCTURES IN THE INTERSTELLAR MEDIUM
E.E.Matvienko, E.O.Vasiliev, Yu.A.Shchekinov 70
DESTRUCTION OF THE INTERSTELLAR CLOUDS BY THE SHOCK WAVES
E.E.Matvienko, Yu.A.Shchekinov 74

THE LOCAL DWARF GALAXIES:BUILDING BLOCKS OF MASSIVE ONES?
I.THE FORNAX DWARF GALAXY
T.V. Nykytyuk 76
ON THE CORRELATION OF IR AND OPTICAL VARIABILITY IN NGC 4151
V.L.Oknyanskij, V.M.Lyuty, O.G.Taranova, E.A.Koptelova, V.I.Shenavrin 79
СТАНОВЛЕНИЕ И РАЗВИТИЕ НАЗЕМНОЙ СПЕКТРОСКОПИИ
Панчук В.Е. 81
О ПОЛЬЗЕ НЕКЛАССИЧЕСКИХ ПРЕДСТАВЛЕНИЙ АСТРОНОМИЧЕСКИХ СПЕКТРОВ
Панчук В.Е., Сачков М.Е., Якопов М.В. 85
THE ROLE OF PURE GALAXY CLUSTERS FOR STUDYING SUPERCLUSTER STRUCTURE
E.A.Panko 88
MODEL ATMOSPHERES OF PECULAR CARBON GIANTS
Ya.V.Pavlenko, L.A.Yakovina 92
GENERAL MAGNETIC FIELD OF THE SUN AS A STAR AS INDICATOR OF MASSIVE STREAMS FLOWING ON THE SUN
S.Plachinda, D.Baklanova, I.Han, K.-M.Kim, P.Reegen, G.Valyavin, W.Weiss 94
ACTIVIVE PHENOMENA OBSERVED IN ATMOSPHERIC LINES OF THE HERBIG AE STAR HD163296
M.A.Pogodin, M.M.Guimaraes, S.H.P.Alencar, W.J.B.Corradi, S.L.A.Vieira 97
THE MODELLING OF THE MASS—METALLICITY RELATION FOR THE LOCAL GROUP DWARF GALAXIES
M.V.Ryabova, Yu.A.Shchekinov 100
THE SEQUENTIAL STAR FORMATION IN GLOBULAR CLUSTERS
M.V.Ryabova, Yu.A.Shchekinov 102
THE LARGE SKY LENS
R.B.Shatsova, G.B.Anisimova 106
RADIO LOOPS IN ZONE OF AVOIDING OF OPEN CLUSTERS
R.B.Shatsova, M.L.Gozha 109
LITHIUM SPOTS IN THE NORTHERN roAP STAR HD 12098
A.V.Shavrina, Yu.V.Glagolevskij, N.A.Drake, N.S.Polosukhina, Ya.V.Pavlenko, D.O.Kudryavtsev 111
SPOTS STRUCTURE AND STRATIFICATION OF SOME CHEMICAL ELEMENTS IN THE ATMOSPHERE OF He-WEAK STAR HD 21699
A.V.Shavrina, Yu.V.Glagolevskij, J.Silvester, G.A. Chuntonov, Ya.V.Pavlenko, V.R. Khalack 115
SPECTROSCOPIC MONITORING OF NOVA VULPECULAE 2007 (V458 Vul)
T.N.Tarasova 120
QUASISYNTHETIC PHOTOMETRY
Tsymbal V. 124
STELLAR INVESTIGATION IN THE OPEN CLUSTER OF POLARIS
I.A.Usenko, A.S.Miroshnichenko, V.G.Klochkova, V.E.Panchuk 127
NEW ASPECT OF SMALL-AMPLITUDE CEPHEID SU CAS
I.A.Usenko, V.G.Klochkova, N.S.Tavolzhanskaya 131
FIRST SUPERNOVAE IN DWARF PROTOGALAXIES
E.O.Vasiliev, E.I.Vorobyov, Yu.A.Shchekinov 135
CRITICAL METALLICITY FOR POPULATION II STARS
E.O.Vasiliev, Yu.A.Shchekinov 139
Non-LTE LINE FORMATION FOR Zr I/II IN COOL STARS
A.B.Vinogradova, L.I.Mashonkina 141
ANALYSIS OF THE SPECTRAL ENERGY DISTRIBUTION OF THE COOLEST RCrB TYPE CARBON STAR DY Per
L.A.Yakovina, A.V.Shavrina, Ya.V.Pavlenko, A.F.Pugach 146
ρ PUPPIS: THE POSSIBILITY OF NON-RADIAL PULSATIONS
A.V.Yushchenko, T.N.Dorokhova, V.F.Gopka, C.Kim 150
ATMOSPHERIC PARAMETERS AND CHEMICAL COMPOSITION OF PECULIAR STARS HR465, HD91375, and HD25354
V.Yushchenko, V.Gopka, A.Yushchenko, A.Shavrina, S.Hubrig, F.Musaev 153
THE INFLUENCE OF ATMOSPHERIC ABSORPTION ON VISIBILITY OF GALAXIES
M.Biernacka, M.Chudy, P.Flin, M.Michniak, E.Panko 158

NIKOLAY SERGEYEVICH KOMAROV AND THE DEVELOPMENT OF THE SPECTROSCOPIC RESEARCHES IN ODESSA ASTRONOMICAL OBSERVATORY

T.V.Mishenina, A.V.Dragunova

Astronomical Observatory of Odessa National University,
Marazlievskaya, 1v, 65014 Odessa, Ukraine, *astro@paco.odessa.ua*

Figure 1: N.S.Komarov (1938-2003)

Komarov Nikolay Sergeyevich was born on June, 16th, 1938 in Sestroretsk Leningrad region in the family of navy officer. Two years after the family moved to Odessa where in 1955 Nikolay graduated from the school and entered the University, the mathematical branch of the Faculty of Physics and Mathematics. After the launch of the first artificial satellite of the Earth he has been moved to astronomical specialisation of the physics branch of the Faculty. In 1955-1960 he made a number of marks of the artificial satellite passing and became a champion in the number of marks. Nevertheless he has a great interest in spectroscopy. His master thesis was devoted to the spectra of meteors. This was made despite that fact that the main activity of the Observatory was in an area of the visual observation of variable stars and a photometrical research of the meteors and comets using the photo-plates. Having graduated University in 1960, Nikolay Sergeyevich began his work at the Odessa Astronomical Observatory (OAO). During a year he was engaged in the visual observations of variable stars on a 19-inch clock-workless telescope installed at the open platform in Mayaki observational station without any pavilion.

In 1961 N.S.Komarov was a post-graduate student. Prominent Odessa astronomer Sergey Vladimirovich Rublyov considerably influenced the further choice of the scientific interests of Nikolay Sergeyevich. Rublyov sent him to the Crimean Astrophysical Observatory (CrAO) where N.S.Komarov was engaged in the spectral observations on a 50-inch reflector with the purpose to obtain and collect the observational material for his PhD thesis. In CrAO another prominent astronomer Ivan Miheyevich Kopylov proposed to Komarov to start dealing with phenomenon of "metal" stars. The thesis "Kinematic and morphological characteristics of the "metal" stars" was successfully defended by Komarov in 1968, and he obtained the scientific degree of the Candidate of Physical and Mathematical sciences (PhD equivalent). Shortly after, he was appointed at the position of the head of department of astrophysics (the largest in Observatory at that time). Then, in 1970, N.S.Komarov headed the research sector, and later the department of astrospectroscopy (later this department of the physics of stars and galaxies became again the largest department in Observatory).

Nikolay Sergeyevich was the leader by his nature, he had good mathematical education, and he always has an intuition where the interesting and perspective line of investigation can be found. In 1967 V.A.Pozigun and N.S.Komarov constructed an infra-red (IR) – electrospectrophotometer (ESPM) and they started in the Soviet Union pioneer observations of the stars in the near IR region. With an advent of ESPM, the new epoch of spectroscopic investigations in OAO started. ESPM was attached to 17" telescope. As a detector the photomultiplier tube RCA7102 was used (it was brought by prof. V.P.Tsessevich from USA). The cooling was made by frozen carbon dioxide; the spectra were registered on a data tape. In September 1966 the observations of Vega and χ Cyg were obtained. At that time the military-industrial establishment of the USSR was very interested in spectral observation in the near IR region. To get the military

contracts on the determination of the energy distributions in the IR spectra of some stars it was necessary to establish the new observational stations in the sites with a good astronomical climate. The first observational station has been founded in Vannovsky (near Ashgabat, Turkmenistan). The 17" telescope with IR spectrometer was installed at that station, and it was in operation from 1970 to 1975. In 1970 two new spectrometers of the Seya-Namioka type were constructed with the aim of a signal registration in a visible spectral region, and one spectrometer with the discrete scanning for IR region. First the thermostabilization was made using the frozen carbon dioxide, and then by thermoelectric cooler created on the basis of the Komarov's technical project. The new equipment was used for observations at the peak Terskol in the North Caucasus (telescope AZT-7 and 80-cm telescope built in OAO). Then the spectrometer of the Seya-Namioka type was attached to the telescopes in the Abastumani Observatory (Georgia) in 1973–1974, and at Mondy (Sayan Mountains, at the Solar Observatory of Siberian branch Academy of Sciences of USSR). The telescopes were constructed by the Odessa Observatory engineers and astronomers L.S.Paulin, N.N.Fashchevskij, V.N.Ivanov, and equipped with the spectrometers and photometers that were constructed also in OAO. The telescopes were installed at the stations of MAO AS USSR (Pulkovo) at the pass Bezymyannyy (Caucasus), Armenia, and at Murghab (Pamir Mountains). In 1970, Nikolay Sergeyevich developed the project "Extinction Service" to investigate the atmospheric extinction by photometric methods. He involved Odessa astronomer N.I.Dorohov to this program in 1972. In 1976 N.I.Dorohov together with engineer V.Egorov elaborated the new EPM for photometric system WBVR. This photometer was used for observations at Mayaki station and Terskol station. In 1986 Odessa astronomer A.F.Pereverzentsev under the supervisory of N.S.Komarov made an electrophotometer for the photometric system UBVRI. Later it was installed on the pass Bezymyannyy (Armenia). In 1991 N.S.Komarov initiated creation of the two-channel EPM for 80-cm Odessa telescope on the Mnt. Dushak – Erekdag (Turkmenistan), and similar photometer for the 1m Odessa telescope installed in the Vyhorlat Observatory (Slovakia). Photometers were made by N.I.Dorokhov. All the works on automation of the observational process was initiated and supervised directly by N.S.Komarov. Nikolay Sergeyevich personally took part in the observations at all the Odessa Observatory stations. In addition he participated in the observations of solar eclipses and zodiacal light at the following places: Chukotka, Kamchatka, Sakhalin, mountains of Hindu Kush. In 1968 N.S.Komarov together with V.A.Pozigun decided to start the Observatory's computerization. The first computer "Promin'" was bought using the money from the military contracts gained by the Komarov's department. The spectroscopic investigations by N.S.Komarov were not limited only by simply obtaining the energy distributions in spectra. The study of the stellar fundamental parameters, spectroscopic analysis of the stellar atmospheres, the determination of the chemical composition and synthetic spectra calculations were carried out by his group, and then these works were continued in the department of spectroscopy ("Komarov's department" as it is now called in Observatory).

Creation by N.S.Komarov together with N.A.Sahibullin, A.Sapar and Y.Straume the workshop "Stellar atmospheres" favoured to the coordination of all the works carried out in USSR on the observation and interpretation of the high resolution spectra, and the modelling of the stellar atmospheres. In 1976, the first big meeting of this group was held in the Tartu Observatory (Tyravere, Estonia). In fact, the group continues its work up to now. In 2002 Komarov decided to enlarge the format of the existing workshop "Stellar atmospheres" to the International Conference "Chemical and dynamic evolution of the stars and galaxies".

In 1989, in the Special Astrophysical Observatory of the Russian Academy of Sciences N.S.Komarov defended his ScD thesis "Structure of the atmospheres of the cool giant stars", and then he gained the professor title. He published about 160 scientific papers and 3 monographs. He also prepared 56 scientific reports about the Observatory's works on contracts. Atmospheres of stars, especially cool stars, were interesting to N.S.Komarov. The presence of a large number of atomic and molecular absorption lines is the characteristic feature of spectra of these objects. And this is puzzling, intriguing, and at the same time attracting essence of this problem. In his monograph "Cool giant stars" N.S.Komarov generalised the main results obtained by him personally and under his supervisory. It should be noted that this book he devoted to the memory of his teacher S.V.Rublyov. In this work he summarized the results on absolute energy distributions in stellar spectra; spectral classification of giant stars; the analysis of the radiation blocking factor in stellar spectra by the atomic and molecular absorption lines; fundamental characteristics of stars (the scale of effective temperatures, absolute star sizes, bolometric magnitudes, surface gravities); structure of atmospheres of the cool stars (thermochemical equilibrium, synthetic spectrum calculations with an account of the molecular absorption; abundances of chemical elements). It should be also noted that N.S.Komarov supported such works at the Odessa Observatory as NLTE analysis of the stellar spectra; an investigation of the metallicity gradient in galactic disk using the calibrations "[Fe/H] – CN" for open clusters, the determination of the isotopic abundances; formation of the dust in the upper layers of atmospheres of giants etc.

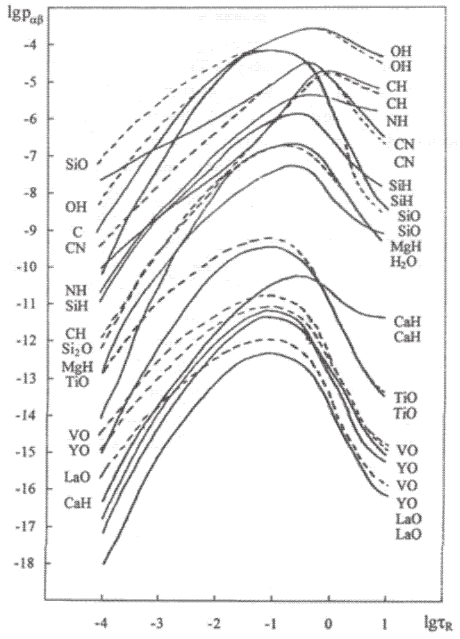

Figure 2: log $p_{\alpha\beta}$/log τ_R

Now let us turn to some concrete results obtained by N.S.Komarov. Taking into account the effective depths of the absorption line formation for a differential methods based on a curve of growth N.S.Komarov succeeded in determination the relative abundances of elements with a good accuracy of the order of 0.1dex (in 70-s!). Having based on the study of 12 open clusters he also showed that the matter in galactic spiral arms is distributed non-uniformly, and this non-uniformity is reflected in its chemical composition. As a result, it was possible to estimate the value of the radial metallicity gradient in a galactic disk: d[Fe/H]/dR = – (0.07 ± 0.03).

The most favourite plot of Nikolay Sergeyevich (that he always demonstrated, see Fig. 1) shows the partial pressure of the molecules in atmospheres of the cool stars as a result of thermochemical equilibrium (these calculations were made in the beginning of 80-s). In fact, this result is actual up to now. Idea about the temeperature inversion in the upper layers of the cool stars for many years was actively supported by N.S.Komarov was confirmed recently by the existence of chromospheres in K – M – giants.

More than ten PhD theses were prepared under his supervisory, and also due to his initiative. He was a member of a specialized councils on (both ScD and PhD) theses defence on astrophysics and radioastronomy, a member of professional astronomical societies, including International and European societies, a member of editorial boards of many scientific and popular scientific Journals and magazines. Nikolay Sergeyevich delivered a course of astrospectroscopy to the students of Odessa University, as well he delivered lectures to the participants of International Gamow's Summer Astronomical School, to auditorium of the former society "Znanie" and in "Planetarium". Nikolay Sergeyevich was also one of the organizers of workshops on spectrophotometric and photometric standards. He was the active participant of many international scientific conferences on the problems of spectroscopy, stellar atmospheres, cool stars, chemical evolutions of the Galaxy. Now the spectroscopic researches in OAO are continued, but the accent of these investigations is somewhat displaced – from energy distributions to the analysis of the high resolution spectra using the sophisticated astrophysical methods. Cool and hot stars, supergiants, giants and dwarfs, variable stars of the various types, pulsing and eclipsing binary stars, the stars belonging to the open and globular clusters are the subject of spectroscopic investigations. The calculations of synthetic spectra are now carried out using the NLTE approximation, the study of the chemical and dynamic evolution of the Galaxy and other galaxies is performed. Obtained results are published in the high-level international astronomical journals. There are many articles published by the followers of N.S.Komarov.

Besides of astronomy, N.S.Komarov had a great interest in yachting, he participated in the large yachting contests of the Black and Azov Sea. He has the daughter Natalia and the grandson – Nikolay Komarov Jr. He was the well-known astronomer, and the astronomical world respects him.

With this Conference, devoted to his memory, we with gratitude pay a tribute to him for his energy, work and merits.

References

Komarov N.S., Dragunova A.V., Karamysh V.F., Orlova L.F., Pozigun V.A.: 1979, *Photometric and spectral catalogue of the bright stars*, Naukova Dumka, Kiev, 536p.

Komarov N.S., Pozigun V.A., Belik S.A, Dragunova A.V., Gopka V.F., Zakozhurnikova N.N., Kantsen L.E., Karamysh V.F., Mishenina T.V., Orlova L.F., Pereverzentsev A.F., Russo T.A., Cherkass A.G.: 1983, *Spectrophotometrie of stars in the region of λ 550 900 nm.*, Naukova Dumka, Kiev, 312 p.

Komarov N.S.: 1999, *Cool giant stars*, Astroprint, Odessa, 216 p.

Komarov N.S.: 1967, Kinematic and Morphological Properties of Stars with Enhanced Metal Lines, *AZh*, **44**, 110.

Komarov N.S., Pozigun, V.A.: 1968, Stellar Energy Distribution at Infrared Wavelengths, *AZh*, **45**, 133.

Komarov N.S., Medvedev Yu.A., Mishenina T.V.: 1973, Spectrophotometry of M-type giant stars,

AZh, **50**, 1193.

Komarov N.S., Panchuk V.E.: 1974, Spectral classification of late-type stars, *AZh*, **51**, 593.

Komarov N.S., Dragunova A.V.: 1975, On selective absorption in stars of spectral class M. I. The influence of the blanketing effect on stellar magnitudes; the integrated blocking coefficient, *AZh*, **52**, 1251.

Komarov N.S., Tsymbal V.V.: 1980, Thermochemical equilibrium in the atmospheres of cool stars – Atoms and ions, *AZh*, **57**, 1010.

Komarov N.S., Shcherbak A.N.: 1980, The abundance of chemical elements in the solar neighborhood, *PAZh*, **6**, 637.

Komarov N.S., Mishenina T.V., Motrich V.D.: 1985, Determination of the NA content in the atmospheres of K giants, *AZh*, **62**, 740.

Korotin S.A., Komarov N.S.: 1989, The influence of non-LTE effects on the sodium abundance in the atmospheres of K giants, *AZh*, **66**, 866.

Gopka V.F., Komarov N.S., Mishenina T.V., Yuschenko A.V.: 1990, Analysis of the abundance of heavy elements in the atmospheres of K-giants – Barium and lanthanoids, *AZh*, **67**, 1204.

Korotina L.V., Komarov N.S.: 1992, Fundamental characteristics of cool giant stars, *AZh*, **69**, 1168.

Komarov N.S., Basak N.Yu.: 1993, The chemical composition of two Praesepe giant stars, *AZh*, **70**, 111.

Kovtyukh V.V., Komarov N.S., Depenchuk E.A.: 1994, Abundance of Helium and Other Chemical Elements in the Atmospheres of Classical Cepheides, *PAZh*, **20**, 215.

Dorokhov N.I., Dorokhova T.N., Komarov N.S., Mukhamednazarov S.: 1997, News from Mt. Dushak-Erekdag station of Odessa astronomical observatory, *OAP*, **10**, 123.

Komarov N.S., Dragunova A.V., Belik S.I.: 1998, Averaged energy distributions in the stellar spectra, *KFNT*, **14**, 274.

Komarov N.S., Zgonyajko N.S., Vasil'eva S.V.: 2001, Abundances of chemical elements in the atmospheres of k supergiants in the Small Magellanic Cloud, *KFNT*, **17**, 471.

Komarov N.S. : 2002, Evolution from the nuclides to the chemical elements, *OAP*, **15**, 23.

Belik S.I., Dragunova A.V., Komarov N.S.: 2004, Determination of fundamental characteristics for stars of the F, G, and K spectral types. The surface gravities and metallicity parameters, *KFNT*, **20**, 430.

PECULIARITIES OF THE NUCLEOSINTHESIS OF HEAVY ELEMENTS IN A DISK OF SPIRAL GALAXY

I.A. Acharova[1], Yu.N. Mishurov[1], J.R.D Lepine[2]

[1] Department of Space Research, Southern Federal University
Zorge Street, 5, Rostov-on-Don, 344090 Russia, *achar@phys.rsu.ru, mishurov@phys.rsu.ru*
[2]Instituto de Astronomia, Geofisica e Ciencias Atmosfericas,Universidade de Sao Paolo,
Cidade Universitaria, Sao Paolo, SP, Brazil*jacques@astro.iag.usp.br*

ABSTRACT. The goal of paper to see that different models for spiral pattern of galactic disks lead to distinguishable radial distribution of heavy elements. Moreover it will be explained why the distributions, demonstrated different chemical elements show different pattern. This fact has extremely importance for understanding of the processes, which occur in a galactic disk and allows to narrow down the possible class of their models.

Key words: Galaxy:abundances; Galaxy:structure

1. Introduction

The work is devoted research of influence of galactic spiral arms on formation of radial distribution of heavy elements abundance. It is widely believed that the radial distribution of heavy elements in the galactic disk retains important information about its structure and evolution.

Earlier, it was assumed that the radial distribution of metallicity in the Galaxy could be described by a simple linear function.In the last decade pupleshed observations, which demonstrate different peculiarities on this distribution [1-12]. Moreover, in these article was demonstrated that the radial abundance distributions for different chemical elements show different pattern.

We have to bear in mind that sources of heavy elements are different objects,which space distribution also different. As believed, the main source of oxygen, supernovae Type II (SN II). These stars are known to be concentrated in the spiral arms [13]. Moreover, the progenitors of stars of this type have very short lifetimes, implying that SN II have not moved significantly from their birth places. On the other hand, the progenitors of the sources of most of the iron ($\sim 70\,\%$) – type Ia supernovae (SN Ia) – may be several billions years old [14]. Even if they were born inside an arm, they have had enough time to move far from their birth place. Thus conserns other elements, distinction in yilds proportion from supernovaes reach up to several times.

The enrichment of the any volume of interstellar gas take place only when its located near its sources, so spatial distribution of heavy elements in young objects must repeat spatial distribution of its sources.

First of all, we mention the bimodal radial abundance pattern,i. e. rather steep gradient in the inner part of the galactic disc for galactocentric distances $r < 7.5$ kpc and a plateau up to 11 kpc for oxygen.

Of course, researches of thin structure of radial distribution of heavy elements are still far from the end, and we are only in the beginning of the way. Probably, future observations will be more informative. However as show our calculations, peculiarities in the radial distribution of heavy elements may be formed under the influence of galactic spiral arms. Thus different models of spiral structure lead to distinguishable pictures of the radial abundance distributions.

2. Basic ideas and equations

For research of chemical evolution of a galaxy traditionally use the equations formulated by Tinsley [15] and specified by Lacey & Fall [16]. We also use their approach, but with two essential additions: 1) the influence of spiral arms will be considered and 2) the effect of diffusion of elements will be taken into account.

The corresponding equations:

$$\frac{\partial \mu_s}{\partial t} = (1-R)\psi, \tag{1}$$

$$\frac{\partial \mu_g}{\partial t} = -(1-R)\psi + f, \tag{2}$$

$$\mu_g \frac{\partial Z}{\partial t} = P_Z\psi + f(Z_f - Z) + \frac{1}{r}\frac{\partial}{\partial r}(r\mu_g D\frac{\partial Z}{\partial r}), \tag{3}$$

where Z is the oxygen content, μ_s and μ_g are the surface densities for the stellar and gaseous disks correspondingly, ψ is the star formation rate (SFR; we use

the instantaneous recycling approximation), f is the in fall rate of matter onto the galactic disk, Z_f is its abundance (we adopt $Z_f = 0.17Z_\odot$), R is the stellar mass fraction returned into interstellar medium (ISM), P_Z is the part of the stellar mass ejected into ISM as a newly synthesized element (oxygen in our case), r is the galactocentric distance, t is time. The last term in equation (3) describes the heavy element diffusion due to turbulent motions in ISM. Let us now discuss the influence of spiral arms on radial oxygen distribution. SN II, according to observations, accurately concentrate in spiral arms. SN Ia do not show such close communication with spiral arms, they can be present out of arms and even out of a disk [13]. Therefore, first of all, influence of spiral arms will affect oxygen distribution. Here sees two possible channels.

The first is caused by that rate nucleosinthesis of oxygen is connected with rate of birth SN II. Rate of birth SN II depends on star formation rate, which is defined, according to Roberts [17], intensity of the galactic shock wave arising in interstellar gas at its flowing in a spiral arms. Such idea of influence of spiral arms on nucleosinthesis has been done by Oort 1974 [18].

Here it is necessary to tell, that there are different opinions concerning that, whether or not galactic shock waves influence on star formation rate. There are researches with arguments both for and against this assumption. As a whole, for today it is definitely may to speak, that the most massive stars (SN II, stars of classes O,B) really concentrate to spiral arms. At the same time the equations of chemical evolution include SFR ψ of stars all masses, including low masses. Thus, this problem still waits for the unambiguous decision.

Therefore we will pass to discussion of other effect which is connected by that enrichment of some volume of interstellar gas by oxygen will occur only when the volume appears close its sources, SN II, i. e. in spiral arms. Therefore rate of enrichment on the given radius is defined, it is obvious, frequency of occurrence of the considered volume of gas in arms.

The matter is that a spiral pattern as the density wave, rotates as a solid body, i. e. its angular velocity $\Omega(r)$ is constant. The galactic disk rotates differentially, its angular velocity Ω_P is function of radius. It is visible, that frequency of occurrence of an element of gas in arms is defined by a difference of rotation velocity of a disk matter and wave pattern velocity $\Omega(r) - \Omega_P$. Therefore quantity P_Z which is interpreted as the part of the stellar mass ejected into interstellar medium on the given radius in the form of new synthesised oxygen not be a constant as in previous researches, but proportional to the above difference. So we can write

$$P_Z \sim |\Omega(r) - \Omega_P|, \qquad (4)$$

Area where both these velocities coincide

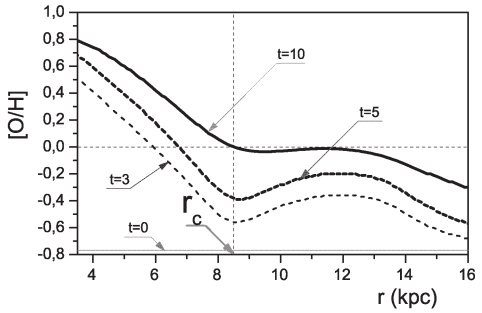

Figure 1: Evolution of the radial oxygen distribution in the model of a stationary long-lived spiral pattern with corotation resonance at solar position $r_C = r_\odot$. The Sun is at $r_\odot = 8.5$ kpc. Time is in Gyrs.

$\Omega(r_C) = \Omega_P$, is called the corotation. Frequency of entering into spiral arms the volume of ISM is close to zero near corotation, so here there is a feature: oxygen injection into interstellar medium will be suppressed. Competing process is turbulent diffusion of elements. With influence corotation and diffusion we connect the mechanism of occurrence of features in radial distribution of oxygen in a galactic disk.

3. Results and discussion

In what follows, we will examine the oxygen radial abundance patterns, predicted by various models for the spiral pattern, because it is the most sensitive indicator of the influence of spiral arms on galactic enrichment by heavy elements.

Results of research show, that different models of density waves pattern differ from each other in the oxygen radial distribution and evolution.

In models with long-lived (or quasi-stationary) spiral structure, the location of corotation resonance is crucial for the final pattern oxygen abundance. Only for a case with corotation radius being situated in the intermediate region of the galactic disc (it is close to solar position) the structure of such distribution like bimodal.Example of calculation in the frame of this model are presented on Fig. 1.

As to models with corotation resonance on the very end of a galactic disk or close to its centre, they do not show any features on radial distribution of an abundance in the area accessible to observations, it monotonic. In the first case, the gradient close to those which is traditionally resulted in observant works. If the corotation radius is located near the centre of Galaxy the oxygen gradient is too steep, that is not supported by any observations.These results are presented on Fig. 2 and Fig. 3.

Very interesting result are obtained in the model in

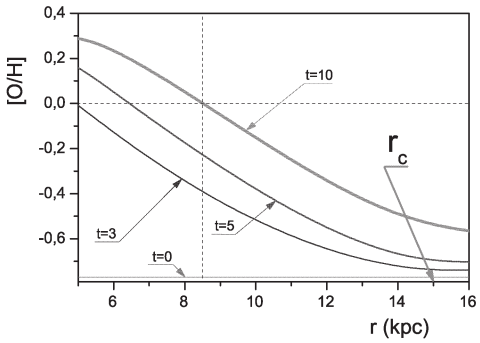

Figure 2: The same as in Fig.1 but for a model with corotation resonance at $r_C = 15$ kpc

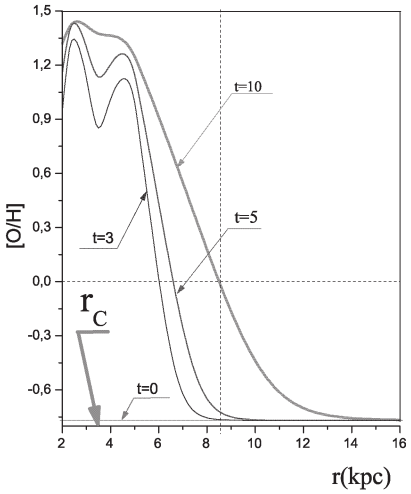

Figure 3: The same as in Fig.1 but for a model with corotation resonance at $r_C = 3.5$ kpc

which corotation radius drifts along r in time: abundance distribution depends on a direction and the region of the corotation resonance drift.

As to model in which corotation radius wanders over a large galactic radius (from outskirts to the inner part), abundance distribution linear (Fig. 4).

In the cases when the corotation resonance drifts from 9 to 7 kpc during the galactic disk life and in the opposite direction from 7 to 9 kpc we have similar pictures with a bimodal-like structure (Fig. 5).

The concept in which the spiral structure is a succession of transient (or short-lived) spiral waves, irrespective of time of existence of each private pattern, the resulting gradient appears too steep (Fig. 6).

Thus, our work strongly suggests that models of the chemical evolution of the Galactic disc must take into account the effect of the spiral pattern.

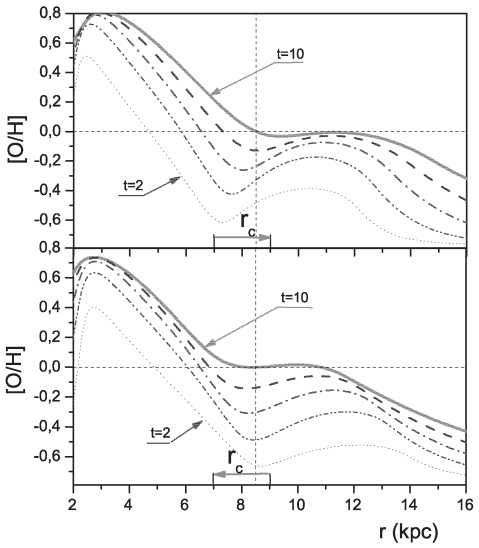

Figure 4: The same as in Fig. 1 but the pattern rotation velocity Ω_P changes so as the corotation resonance drifts between 15 kpc and 4 kpc

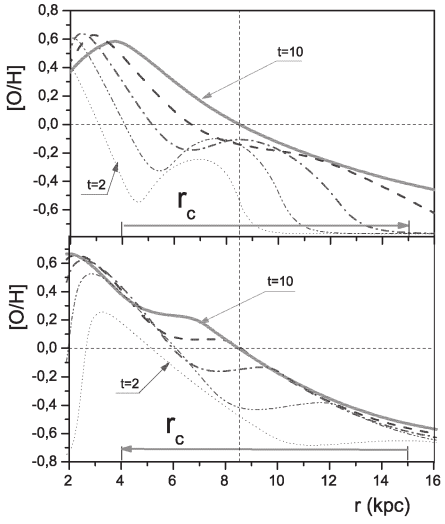

Figure 5: The same as in Fig. 1 but for the corotation resonance driftsbetween 7 kpc and 9 kpc

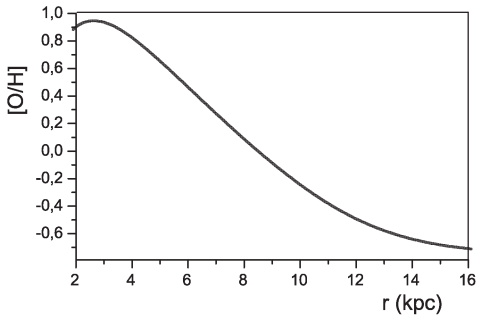

Figure 6: The final (at $t = 10$ Gyr) radial oxygen distribution for a succession of transient spiral density waves)

References

1. Vilchez J., Esteban C.: 1996, *Monthly Notices Roy. Astron. Soc.*, **280**, 720.
2. Daflon S., Cunha K.: 2004, *Astrophys. J.*, **617**, 1115.
3. Twarog B., Ashman K., Anthony-Twarog B.: 1997, *Astron. J.*, **114**, 2556.
4. Smartt S., Rolleston W.: 1997, *Astrophys. J. Lett.*, **481**, 47.
5. Caputo F., Marconi M., Musella I., Pont F.: 2001, *Astron. Astrophys.*, **372**, 544.
6. Andrievsky S., Kovtyukh V., Luck R., et.al.: 2002, *Astron. Astrophys.*, **381**, 32.
7. Andrievsky S., Bersier D., Kovtyukh V., et.al: 2002, *Astron. and Astrophys.*, **384**, 140.
8. Andrievsky S., Kovtyukh V., Luck R., et.al: 2002, *Astron. and Astrophys.*, **392**, 491.
9. Luck R., Gieren W., Andrievsky S., et.al:, 2003, *Astron. and Astrophys.*, **401**, 939.
10. Andrievsky S., Luck R., Martin P., Lepine J.: 2004, *Astron. and Astrophys.*, **413**, 159.
11. Maciel W., Quireza C.: 1999, *Astron. Astrophys.*, **345**, 629.
12. Maciel W., Costa R., Uchida M.: 2003 *Astron. and Astrophys.*, **397**, 667.
13. Bartunov O., Tsvetkov D., Filimonova I.: 1994, Astron. Soc. Pacific., **106**, 1276.
14. Matteucci F.: 2003, *Carnegi Astrophys. Ser., Eds A Mc William and M. Rauch. Cambridge Univ. Press* **I**, 52.
15. Tinsley B.: 1980 *Fundamentals of Cosmic Physics*, **5**, 287.
16. Lacey C., Fall S.: 1985, *Astrophys. J.* **290**, 154.
17. Roberts W.: 1969, *Astrophys. J.*, **158**, 123.
18. Oort J.H.: 1974, *IAU Symp. No. 58.*, 375.

HIGH PRECISE EFFECTIVE TEMPERATURES OF 182 MAIN SEQUENCE STARS

S.I. Belik, V.V. Kovtyukh, M.P. Yasinskaya

Odessa Astronomical Observatory, Odessa National University
T.G.Shevchenko Park, Odessa 65014 Ukraine,*val@deneb1.odessa.ua*

ABSTRACT. High precise temperatures ($\sigma = 10 - 15$ K) have been determined from line depth ratios for a set of 182 F-K field dwarfs of about solar metallicity (–0.5 < [Fe/H] < +0.4), based on high resolution (R=42 000), high S/N echelle spectra.

Key words: Stars: fundamental parameters; stars: effective temperatures; stars: dwarfs.

1. Introduction

The key to our analysis of the stellar spectra is the line-depth ratio technique, pioneered by Gray (1994) and successively improved by our group. This technique allows the determination of $T_{\rm eff}$ with an exceptional precision. It relies on the ratio of the central depths of two lines that have very different functional dependences on $T_{\rm eff}$. The method is independent of the interstellar reddening and only marginally dependent on individual characteristics of stars, such as rotation, microturbulence and metallicity.

Briefly, a set of 105 line ratio – $T_{\rm eff}$ relations was obtained in Kovtyukh et al. (2003), with the mean random error of a single calibration being 60–70 K (40–45 K in most cases and 90–95 K in the least accurate cases). The use of ∼70–100 calibrations per spectrum reduces the uncertainty to 5–7 K. These 105 relations use 92 lines, 45 with low (χ <2.77 eV) and 47 with high (χ >4.08 eV) excitation potentials, and have been calibrated with the 45 reference stars in common with Alonso et al. (1996), Blackwell & Lynas-Gray (1998) and di Benedetto (1998). The zero-point of the temperature scale was directly adjusted to the Sun ($T_{\rm eff}$=5777 K is adopted for the Sun), based on 11 solar reflection spectra taken with ELODIE, leading to an uncertainty in the zero-point of about 1 K. The application range for the calibrations is -0.5 <[Fe/H]< +0.4.

In the present study we add 182 new spectra to the sample, increasing the total number of dwarfs with precisely determined $T_{\rm eff}$ to 550.

2. Observations

The spectra used in this paper were extracted from the most recent version of the library of stellar spectra collected with the ELODIE echelle spectrograph at the Observatoire de Haute-Provence by Soubiran et al. (1998) and Prugniel & Soubiran (2001). The description of the instrument mounted on the 1.93 m telescope can be found in Baranne et al (1996).

The spectral range of the spectra is 4400–6800 ÅÅ and the resolution is R=42 000. The signal to noise ratio (S/N) of the spectra range from 40 to 680, with the large majority having $S/N > 100$. Spectrum extraction, wavelength calibration and radial velocity measurement were performed at the telescope with the on-line data reduction software while straightening of the orders, removing of cosmic ray hits, bad pixels and telluric lines were performed as described in Katz et al (1998). Further processing of the spectra (continuum placement, measuring equivalent widths, etc.) was carried out by us using the DECH20 software (Galazutdinov, 1992). Equivalent widths and depths R_λ of lines were measured manually by means of a Gaussian fitting. The Gaussian height was taken as a measure of the line depth. This method produces line depth values that agree with the parabola technique used by Gray (1994).

3. Results

In Table 1 for each star we report the mean $T_{\rm eff}$, the mean square deviation for each determination (σ), number of the calibrations used (N), and the standard error of the mean (σ(mean)). For comparison, we also provide $T_{\rm eff}$ as determined in Masana, Jordi and Ribas (2006). For the majority of stars we get an error which is smaller than 10 K.

Masana, Jordi and Ribas (2006) present a method to determine effective temperatures, angular semi-diameters and bolometric corrections for population I and II FGK type stars based on V and 2MASS IR pho-

Table 1: The computed $T_{\rm eff}$ for MS-stars.

HD	$T_{\rm eff}$ K	σ	N	σ (mean)	$T_{\rm eff}$ (Masana)	HD	$T_{\rm eff}$ K	σ	N	σ (mean)	$T_{\rm eff}$ (Masana)
000330	6042	49	68	5.9	5764	044966	6237	103	58	13.5	–
000739	6491	62	40	9.8	–	045654	6385	271	43	41.3	–
001461	5728	35	121	3.1	–	046871	6087	53	62	6.7	5992
001497	5859	72	112	6.8	5776	048410	5899	69	79	7.7	5946
001581	5954	62	65	7.7	–	048591	5784	201	52	27.9	–
001832	5799	107	107	10.4	5747	048684	5955	88	95	9.1	5907
002330	5991	78	91	8.2	6178	049932	6507	38	20	8.6	–
003229	6478	44	47	6.4	–	049933	6674	131	18	30.8	–
003268	6263	82	53	11.2	6221	050039	6332	73	45	10.8	6377
003801	6115	48	85	5.2	6259	059360	5908	129	52	17.8	5799
004813	6211	46	72	5.5	–	059468	5570	65	105	6.3	–
005600	6209	163	43	24.8	6454	059967	5781	63	100	6.3	–
007228	6150	165	34	28.3	6127	059984	6166	154	47	22.5	–
007476	6549	78	35	13.2	–	061421	6662	53	24	10.7	–
007570	6054	42	94	4.3	–	063077	6057	107	67	13.0	5814
008997	4655	282	48	40.7	–	064235	6325	185	36	30.8	–
009966	5844	81	107	7.9	5845	064606	5340	129	102	12.8	–
010126	5554	73	109	7.0	5539	065430	5227	64	111	6.1	5157
010132	5382	59	115	5.5	–	067230	6698	123	10	38.8	–
010556	6003	58	93	6.0	6073	067827	6081	66	92	6.9	5942
010647	6163	49	62	6.3	–	068168	5707	47	119	4.4	–
013555	6551	47	28	9.0	6509	068284	5901	127	64	15.9	5843
014214	6035	44	110	4.2	–	068380	6491	75	31	13.5	6739
014802	5960	74	99	7.4	–	069056	5594	60	111	5.7	5598
015632	5761	41	122	3.7	5728	070937	6291	322	15	83.0	6495
016673	6292	31	35	5.2	6224	070958	6639		1		6458
016895	6364	64	57	8.5	–	071595	6569	93	33	16.2	6679
019902	5595	51	119	4.7	5531	072659	5907	63	65	7.8	5998
020367	6022	46	112	4.3	6019	072945	6310	60	65	7.4	–
020807	5855	96	97	9.8	–	075880	5683	59	92	6.2	–
022556	6183	96	62	12.2	5954	075935	5434	40	111	3.8	–
023596	5931	74	100	7.4	–	076932	6089	139	55	18.7	–
025069	5119	96	97	9.7	–	078660	5684	66	92	6.9	5710
025444	5828	52	104	5.1	–	079126	5987	66	58	8.6	5885
025457	6374	96	16	24.0	6403	083870	5688	275	40	43.5	–
025825	5982	44	108	4.2	5974	085533	5659	68	109	6.5	5547
026756	5638	75	112	7.1	5642	089744	6253	70	73	8.2	6149
026767	5815	38	114	3.6	–	097503	4538	47	73	5.5	4496
026784	6190	80	31	14.3	6221	100563	6407	70	57	9.3	6489
027406	6013	86	48	12.5	–	101013	5262	74	100	7.4	–
027857	5750	58	91	6.1	5965	103432	5622	47	111	4.4	5608
028344	5947	28	110	2.7	5939	104956	6102	68	52	9.4	6112
028821	5650	89	90	9.4	5800	105113	5986	61	101	6.1	–
028992	5875	35	99	3.6	6021	105755	6173		1		5854
029419	6034	35	112	3.3	5987	107213	6194	76	49	10.9	6254
029587	5754	80	91	8.4	5722	108019	5973	110	80	12.3	5938
030376	5529	68	114	6.4	5519	108863	5181	94	110	9.0	–
030708	5740	55	123	4.9	5936	109098	5841	79	111	7.5	5828
032070	5611	89	89	9.5	5565	109247	5765	147	39	23.6	–
032963	5741	34	112	3.2	–	110223	6119	143	25	28.6	6163
033256	6572	42	19	9.5	–	111513	5796	54	111	5.1	–
033636	5935	74	53	10.1	5930	112914	4898	77	98	7.8	–
034445	5815	51	104	5.0	5867	114642	6453	73	22	15.5	–
034745	6109	77	57	10.2	6136	114762	6255	20	2	14.3	5919
037495	6650	47	4	23.3	–	115617	5509	74	108	7.1	–
038309	5776	253	53	34.8	–	115954	5818	68	106	6.6	5870
038393	6388	26	29	4.8	–	116091	5876	83	82	9.2	–
042548	6708	49	10	15.6	6661	117635	5239	65	87	7.0	–
043042	6514	75	25	15.1	–	118096	4305	105	76	12.1	–
043318	6340	46	55	6.2	–	120136	6337	78	27	15.0	–
043856	6227	50	43	7.6	6092	120510	6467	71	37	11.6	6372

Table 1 (Continued)

HD	$T_{\rm eff}$ K	σ	N	σ (mean)	$T_{\rm eff}$ (Masana)	HD/BD	$T_{\rm eff}$ K	σ	N	σ (mean)	$T_{\rm eff}$ (Masana)
120567	5184	89	111	8.4	–	174457	5831	99	116	9.2	5875
122518	5893	85	96	8.7	5919	175806	6047	100	84	10.9	6150
122727	5702	80	111	7.6	5699	180945	6474	85	21	18.5	6374
124115	6472	116	5	51.9	6458	181096	6126	158	32	27.9	–
124425	6441	58	3	33.3	6435	182274	6427	163	19	37.4	6330
125706	5849	86	92	9.0	5793	186226	6305	125	54	16.9	–
128429	6569	108	9	36.0	6388	189259	6726	76	11	22.9	6768
129171	5860	63	107	6.1	5893	190360	5564	47	116	4.4	–
134044	6164	48	77	5.5	6545	190437	6121	100	59	13.1	–
140209	5742	75	112	7.1	–	191533	6251	45	60	5.8	–
140901	5553	55	107	5.4	–	197967	6322	70	71	8.4	6176
140913	5902	58	93	6.0	5951	198023	6551	131	19	30.1	6567
142860	6334	88	30	16.0	–	198343	4555	204	24	41.6	–
147887	5833	141	80	15.8	5946	201191	4334	44	62	5.6	–
148049	6105	105	64	13.1	6058	203608	6235	96	32	17.1	–
150177	6171	89	2	63.1	6107	209458	6098	39	97	4.0	6051
157881	4146	165	6	67.6	–	211976	6376	81	61	10.3	6493
160693	6075	2	2	1.3	5788	211998	5599	205	49	29.2	–
161797	5602	56	112	5.2	–	215648	6291	68	46	10.1	–
163714	6021	84	66	10.4	–	216435	5921	39	107	3.8	–
165670	6355	52	40	8.2	–	217107	5585	54	119	5.0	–
165908	6098	21	2	14.7	–	218059	6352	79	43	12.0	6342
166073	6380	117	36	19.4	6399	219420	6267	44	65	5.4	–
166183	6283	116	43	17.7	6317	220221	4892	46	89	4.8	–
167407	5957	89	91	9.3	5988	222368	6270	59	76	6.7	–
168151	6652	69	15	17.7	–	283704	5499	49	121	4.4	–
170291	6311	86	49	12.3	6299	+11 9332	5230	40	100	4.0	–
170579	6280	171	43	26.0	6346	+26 2461	6014	149	38	24.3	–
171888	6167	70	81	7.8	6207	+52 2815	4325	134	33	23.3	–
171951	6124	66	72	7.8	–	SUN	5777	31	100	3.1	–
172675	6295	82	38	13.4	–						

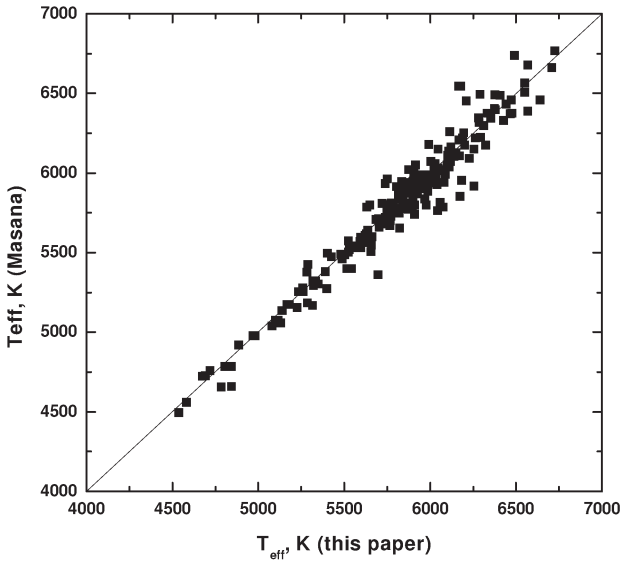

Figure 1: Comparison of our $T_{\rm eff}$ with estimates from Masana, Jordi and Ribas (2006).

tometry. Accurate calibration is accomplished by using a sample of solar analogues, whose average temperature is assumed to be equal to the solar effective temperature of 5777 K. By taking into account all possible sources of error they estimate associated uncertainties to better than 1 angular semi-diameter for unreddened stars. They determined $T_{\rm eff}$, angular semi-diameters, radii and bolometric corrections in the V and K bands for the 10 999 FGK stars.

Table 1 contains our final $T_{\rm eff}$ determinations for 182 MS stars. As one can see from Table 1, for the majority of stars we get an error which is smaller than 10 K. The consistency of the results derived from the ratios of lines representing different elements is very reassuring. It shows that our 105 calibrations are essentially independent of micro-turbulence, LTE departures, abundances, rotation and other individual properties of stars.

The temperatures of Masana, Jordi and Ribas (2006) are in a good agreement with our estimates – see Fig. 1.

4. Conclusion

The high-precision temperatures were derived for a set of 182 dwarfs, which may serve as temperature standards in the 4000–6750 K range. These temperatures are precise to within 10–35 K for the major fraction of the sample.

Acknowledgements. This work is based on spectra collected with the 1.93-m telescope of the OHP (France). Dr. C. Soubiran is acknowledged for help with spectral material.

References

Alonso A., Arribas S., Martínez-Roger C.: 1996, *A&ASS*, **117**, 227.
Baranne A., Queloz, D., Mayor, M., et al.: 1996, *A&ASS*, **119**, 373.
Blackwell D.E. & Lynas–Gray A.E. 1998, *A&ASS*, **129**, 505.
di Benedetto G.P.: 1998, *A&A*, **339**, 858.
Galazutdinov G.A.: 1992, *Prepr. SAO RAS*, **92**, 28.
Gray D.: 1994, *PASP* **106**, 1248.
Katz D., Soubiran C., Cayrel R., Adda M., Cautain R.: 1998, *A&A*, **338**, 151.
Kovtyukh, V.V., Soubiran, C., Belik, S.I., Gorlova N.I.: 2003, *A&A*, **411**, 559.
Masana E., Jordi C., Ribas I.: 2006, *A&A*, **450**, 735.
Moultaka J., Ilovaisky S. A., Prugniel P., Soubiran C.: 2004, *PASP*, **116**, 693.
Prugniel P. & Soubiran C.: 2001, *A&A*, **369**, 1048.
Soubiran C., Katz D., Cayrel R.: 1998, *A&AS*, **133**, 221.

IS PZ MON A RED DWARF OR A RED GIANT?

N.I. Bondar', S.G. Sergeev
SRI "Crimean Astrophysical observatory"
Nauchny, 98409, Ukraine, *bondar@crao.crimea.ua*

ABSTRACT. Hipparcos data (ESA 1997) give for PZ Mon a parallax π = 0.71 ±1.17 mas that is not in agreement with earlier estimations of distance to the star of 15–30 ps and with its status of K- dwarf. There are presented spectra of PZ Mon in the region 3750–6150 Å with resolution of ∼7 Å, which were carried out in the Nasmith focus of 2.6 m reflector in the Crimean Astrophysical observatory. Intensities of molecular absorptions in this spectral range are determined relative a nearby continuum and their relations between absolute magnitudes are considered. The calculated M_v=6.74 and r=29 ps correspond to an earlier classification of PZ Mon as a red dwarf.

Key words: Stars: stellar spectra, red dwarfs; individual: PZ Mon.

Spectral and photometric features of PZ Mon indicate that the star belongs to flare red dwarfs. Different authors estimated of distance to the star as 16–30 ps (Munch L., Munch G. 1955, Gliese 1982; Stobie et al. 1989; Gershberg et al. 1999). The value of X-ray luminosity measured by *Einstein* is logL_x=28.1. According relation between X-ray luminosity and a distance obtained for red dwarfs by Metanomski et al. (1998) the star is not far than 30 ps. But *Hipparcos* measurements given a parallax of 0.71 ± 1.17 mas. According this value and taking into account that the brightness of the star V=9.03 Saar (1998) found that a distance is not less than 500 ps. He studied high resolution spectra in the range of 6170 ± 20 Å for a red dwarf and a red giant. Basing on the obtained result and photometric features of PZ Mon he suggests that the star is K1 - giant in a RS CVn system.

In March 2008 two CCC-spectra of PZ Mon were carried out in the Nasmith focus of 2.6 m reflector at the Crimean Astrophysical Observatory. The range of 3700-6100 Å are covered, a spectral resolution was ∼ 7 Å. A low spectral resolution did not allow to use such indicator of an absolute stellar magnitude as the ratio I_{4063}/I_{4077} (Martynov 1976). Pettersen and Hawley (1989) presented results of a spectral survey of red dwarfs where using low resolution spectra in the region of 3600 – 9000 Åthey found empirical relations between absolute magnitudes and intensity of diatomic and triatomic molecules.

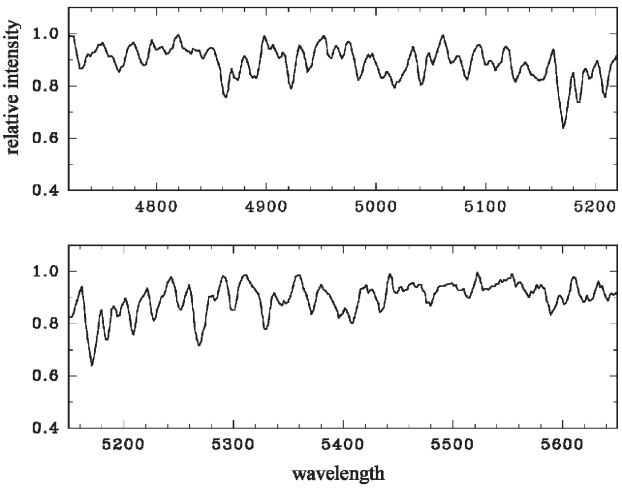

Figure 1: Spectrum of PZ Mon in the visual region

Basing on these relations for estimation of M_v, we chosen in the PZ Mon spectra bands of TiO (4760, 4950, 5450 Å) and band of CaOH (5550 Å). The bands intensities were determined relative a nearby peaks towards the blue. Measurements in TiO-bands given M_v=5–7.2, intensity of the CaOH (5550 Å) absorption corresponds to M_v=9.1, and the mean value of M_v is 6.74. Then a distance to PZ Mon is not more than 29 ps, that is in agreement with values M_v=6.97 and r=25.7 ps, obtained by Pettersen and Hawley (1989). So, photospheric properties, intensities of molecular absorptions in the visual range, indicate that PZ Mon is a red dwarf. But we suggest that for red dwarfs and red giants there is needed a comparative analysis of high resolution spectra in wide region to take obviously evidences in this question.

Acknowledgements. We are very thankful to Dr. P.P.Petrov for useful advices and discussion of methodical questions.

References

Gershberg R.E., Katsova M.M., Lovkaya M.N. et al.: 1999, *Astron. Astrophys.,* **201**, 119.
Gliese W.: 1982, *Astron. Astrophys. Suppl.,* **47**, 471.
ESA 1997: 1997, *The Hipparcos and Tycho Catalogs*, ESA SP-1200.

Martynov D.Ja.: 1979, *Kurs obschei astrofiziki.* M. Nauka. 640p.

Metanomski A.D., Pasquini L., Krautter J. et al.: 1998, , *Astron. Astrophys. Suppl.,* **131**, 197.

Munch L., Munch G.: 1955, *Tonantz. Tac. Bol.,* No. 13, 36.

Pettersen B.R., Hawley S.L.: 1999, *Astron. Astrophys.,* **201**, 187.

Saar S.H.: 1998, *IBVS,* No. 4580.

Stobie R.S., Ishida K., Peacock J.A.: 1989, *Month. Not. R. Astr. Soc.,* **238**, 709.

ROTATIONAL VARIATION OF THE MAGNETIC FIELD OF β CrB IN DIFFERENT SPECTRAL LINES

V. Butkovskaya[1], D. Baklanova[1], I. Han[2], K.M. Kim[2], D. Lyashko[3,4], D. Mkrtichian[5], S. Plachinda[1], G. Valyavin[2], V. Tsymbal[3,4]

[1] Crimean Astrophysical Observatory, Nauchny, Crimea, 98409, Ukraine
[2] Korea Astronomy and Space Science Institute, 36-1 Whaam-dong, Yuseong, Daejeon, Korea 305-348
[3] Tavrian National University, Yaltinskaya 4, Simferopol, Crimea, 95007, Ukraine
[4] Institut fur Astronomie, Turkenschanzstrasse 17, 1180 Vienna, Austria
[5] ARCSEC, Sejong University, Seoul 143-747, Korea

ABSTRACT. The results of spectropolarimetic study of one of the coolest Ap-stars β CrB are presented. It was shown that effective magnetic fields measured in different spectral lines and folded in phase with the rotational period of the star significantly differ from each other in amplitudes and mean values of the magnetic field curves.

Key words: Stars: magnetic fields; stars: peculiar; stars: individual: β CrB

1. Introduction

An unexplained effect on some chemically peculiar magnetic stars is that the values of effective magnetic field of the same star measured by different authors are significantly different from each other in shapes, amplitudes and mean values (see, for example, Leone and Catanzano 2001). This effect is illustrated in the Fig. 1, where the effective magnetic fields of one of the coolest Ap-stars β CrB obtained from data of different authors are folded in phase with the 18.478-day rotation period of the star. One can see that while magnetic fields measured by Wade et al. (2000) and our data vary sinusoidally with stellar spin period, magnetic field curve obtained from the measurements of Borra and Landstreet (1980) exhibits secondary bump in the phase of the field minima.

It should be noted, that different researchers use different bulks of spectral lines for stellar effective magnetic field measurement. For example, Borra and Landstreet (1980) measured magnetic field of β CrB in the line H_β, Wade et al. (2000) used bulk of lines in the spectral range of 4500-6000 Å and we used nine spectral lines in the range of 6136-6162 Å (see Fig. 1). Plachinda and Tarasova (1999) noted that systematic differences exist in the mean longitudinal magnetic field of β CrB measured in the two lines of Fe I and singe line of Ca I. One can suppose that the differences in magnetic field curves can be the result of non-uniform distribution of chemical elements (Wade and Smolkin 2004) and temperature inhomoheneties existing on the surface of β CrB (Plachinda and Tarasova 1999). I.e. magnetic field curves obtained in spectral lines of different chemical elements correspond to different parts of stellar surface and therefore, in assumption of dipole field configuration, corresponds to different magnetic field strength.

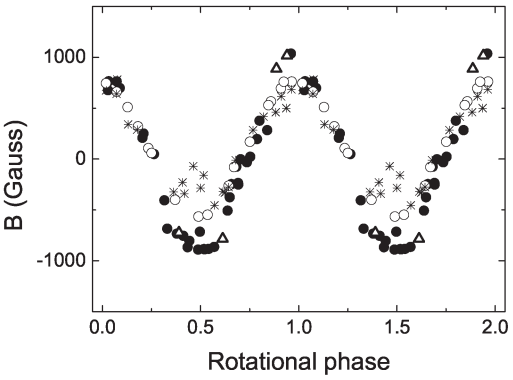

Figure 1: Effective magnetic field of β CrB obtained from data of Borra and Landstreet (1980) (crosses) and Wade et al. (2000) (open circles) and our data: CrAO (field circles) and BOAO (open triangles).

Studying effective magnetic field of β CrB in the individual spectral lines we paid attention to the fact that not only magnetic fields measured in spectral lines of different chemical elements but also magnetic fields measured in different spectral lines of the same chemical element exhibit systematic difference. The results of the initial study are presented in this paper.

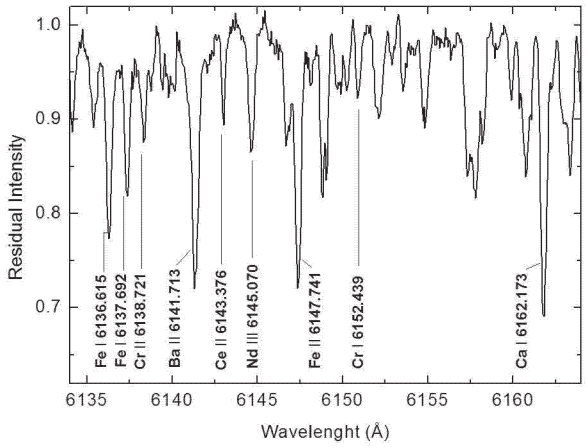

Figure 2: Spectral lines used for effective magnetic field of β CrB measurements.

2. Observations

An intensive spectropolarimetric study of the β CrB has been performed in the nine individual lines (Fig. 2) during 32 nights from 1993 to 2004 using coude spectrograph of the 2.6-m Shajn telescope at the Crimean Astrophysical Observatory and during 4 nights in 2007 and 2008 using eshelle spectrograph BOES at the Bohyunsan Optical Astronomy Observatory (BOAO, South Korea). Signal-to-noise ratios of a single spectrum were 150-350 with resolving power of spectra approximately 30000 (CrAO) and 45000 (BOAO). The study of the magnetic field of the star was carried out with the same equipment and 'Flip-Flop' procedure that have been discussed in detail by Butkovskaya & Plachinda (2007).

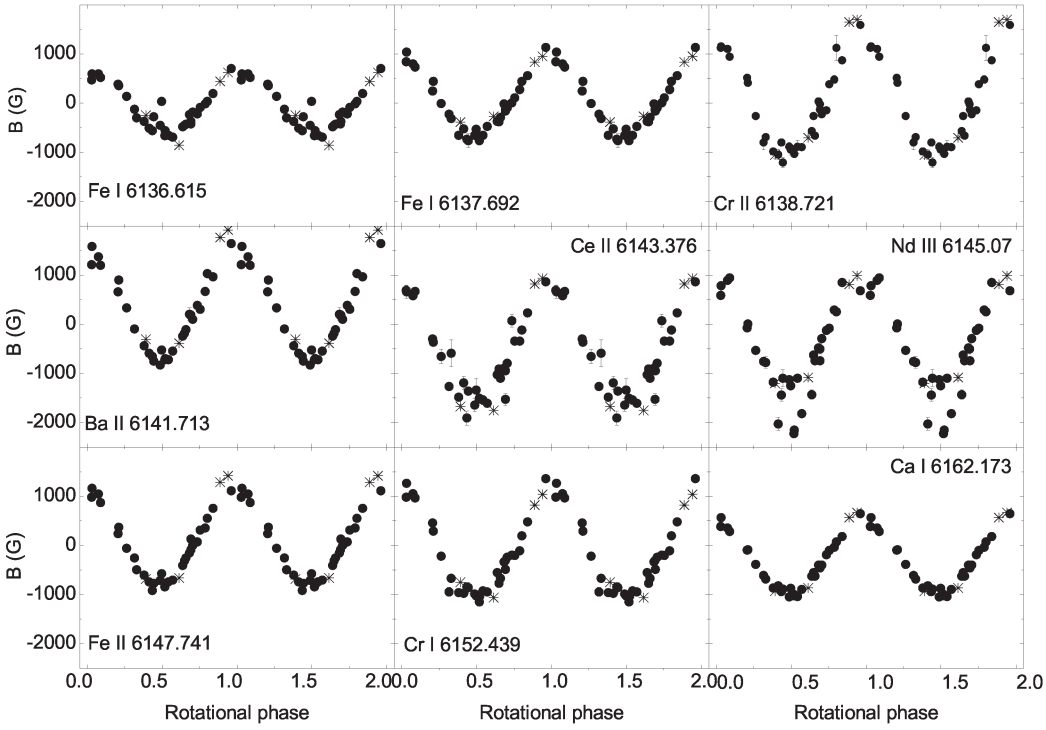

Figure 3: Effective magnetic field of β CrB measured in different spectral lines and folded in phase with the 18.478-day rotation period of the star.

3. Results

The rotational variations of the effective magnetic field of β CrB measured using individual spectral lines are presented in Fig. 3. One can see that all the magnetic field curves are well fitted by sinusoids, but these sinusoids significantly differ in amplitude and mean value from each other. The amplitudes and the mean values of the magnetic field curves are given in Table 1. In the first, second and third columns the chemical elements, wavelength and excitation potential are presented, in the two last columns the amplitudes B_e and the mean magnetic fields B_0 are given in Gauss.

Table 1: Parameters of the magnetic field curves.

Elem.	λ (Å)	Excit (eV)	Amplitude B_e (G)	Mean B_0 (G)
Fe I	6136.615	2.453	582 ± 36	23 ± 26
Fe I	6137.692	2.588	821 ± 24	137 ± 17
Cr II	6138.721	6.484	1250 ± 49	159 ± 36
Ba II	6141.713	0.704	1158 ± 38	459 ± 28
Ce II	6143.376	1.696	1221 ± 63	-448 ± 45
Nd III	6145.070		1273 ± 74	-261 ± 53
Fe II	6147.741	3.889	998 ± 28	177 ± 20
Cr I	6152.439	4.207	1100 ± 41	-11 ± 30
Ca I	6162.173	1.899	774 ± 18	-224 ± 13
All lines			855 ± 29	14 ± 21

Table 1 shows that amplitudes and mean values of individual magnetic field curves significantly differ from each other. The parameters of magnetic curves obtained using different lines of the same chemical element (Cr I 6152.439 and Cr II 6138.721; Fe I 6136.615, Fe I 6137.692 and Fe II 6147.741) show systematic differences. Moreover, the parameters of magnetic curves obtained using spectral lines of the same chemical element with the same ionization state and almost equal excitation potentials (Fe I 6136.615 and Fe I 6137.692) show systematic differences also. Strongly negative mean magnetic fields exhibit Ce II 6143.376, Nd III 6145.070, and Ca I 6162.173. We can expect that Ca as well as Fe are uniformly distributed on the stellar surface, therefore, the magnetic field obtained using the spectral lines of these elements would be equal within the measurement errors. Nevertheless, in the case of β CrB we see significant shift in the mean magnetic fields from 137 ± 17 Gs (Fe I 6137.692) to negative value -224 ± 13 (Ca I 6162.173).

Acknowledgements. V. Butkovskaya, D. Baklanova, D. Lyashko, S. Plachinda and V. Tsymbal acknowledge support from the Ukrainian Fundamental Research State Fund (25.2/074, M/364). D. Lyashko, S.Plachinda and V. Tsymbal acknowledges support in part from the Austrian Science Fund (P17890).

References

Borra E.F., Landstreet J.D.: 1980, *ApJSS,* **42**, 421.
Butkovskaya V., Plachinda S.: 2007, *A&A,* **469**, 1069.
Leone F., Catanzano G., Catalano S.: 2000, *A&A*, **355**, 315.
Leone F., Catanzano G.: 2001, *A&A*, **365**, 118.
Wade G.A., Donati J.-F., Landstreet J.D., Shorlin S.L.S.: 2000, *MNRAS*, **313**, 851.
Wade G.A., Smolkin: 2004, in: *Proc. Int. Conf., eds.: Glagolevskij Yu.V., Romanyuk I.I., Nizhny Arkhyz,* p.205.

MAGNETIZATION OF STARS VS. THE EFFECTIVE TEMPERATURE

V.D. Bychkov[1], L.V. Bychkova[1], J. Madej[2]

[1] Special Astrophysical Observatory of the Russian Academy of Sciences
Nizhnij Arkhyz, 369167 Russia, *vbych@sao.ru*
[2] Warsaw University Observatory
Al. Ujazdowskie 4, 00-478 Warsaw, Poland, *jm@astrouw.edu.pl*

ABSTRACT. Using all published magnetic measurements there were detected some dependences of frequency of occurrence of magnetic field value for all types of peculiarity (Bychkov et al., 2003a, 2008). On the basis of it we normalized these dependences for the most "non-magnetic" Am-stars and we draw the relative "magnetization" (MA) for peculiarity types for Ap-stars (Bychkov et al., 2003b). At the same time chemically peculiar stars neatly block to the two groups: "weak" - magnetic (Am and Hg-Mn stars) and "strong" - magnetic (SrCrEu, Sr, Si, He-w and He-r stars). "Strong" - magnetic group outnumbers "weak" - magnetic group on magnetic activity on average 5-10 times more, as shown in Fig. 3. This is mathematical expression of well-known observing fact. One of the most important and simpliciter measurable physical characteristic of stars atmospheres is effective temperature. This paper is devoted to the dependence of "magnetization" on T_{eff}.

Key words: Stars: magnetic fields of stars: fundamental parameters

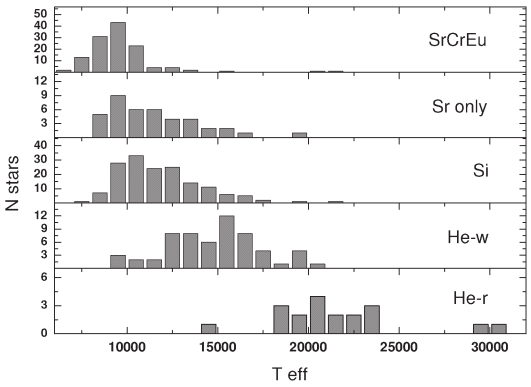

Figure 1: Quantity of stars for each type vs. T_{eff}

1. Starting data and dependences

Fig. 1 shows T_{eff} distribution of "magnetic" Ap-stars and Fig. 2 shows the same distribution of "non-magnetic" Ap-stars. These distributions base on the same extracts, which were used for construction of dependences (Bychkov et al., 2003a, 2008). Effective temperatures were taken from Hauk & North (1993), Glagolevskij (1994, 2002), Sokolov (1998) or were counted up on dependences from Paunzen et al. (2005). In Fig. 1 one can clearly see the dependence of stars distribution for different types of peculiarity. The T_{eff} dependence of relative MA is shown in Fig. 3.

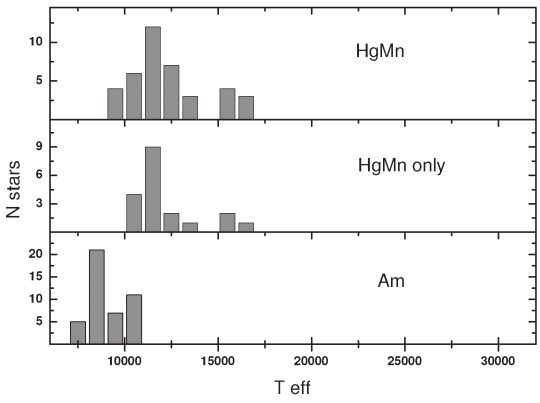

Figure 2: Quantity of stars for each type vs. T_{eff}

2. Discussion

As shown in Fig. 3 MA for "strong" - magnetic stars group distinctly decrease with increasing of T_{eff}. As all members of "strong" - magnetic Ap-stars locate on

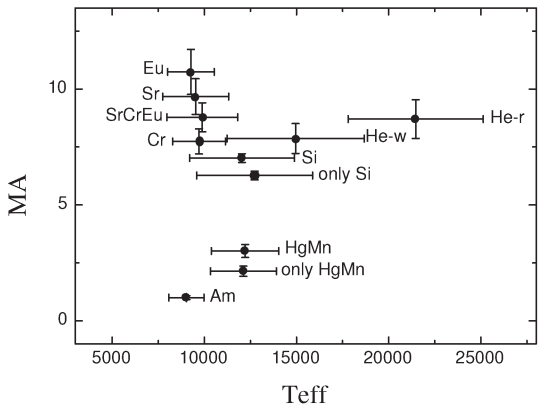

Figure 3: Magnetization MA vs. T_{eff}

the main sequence, one can see with T_{eff} increasing the increasing of stars mass and the decreasing of stars age. For example, He-r stars are almost two orders younger and 6 times more massive then SrCrEu stars on average. All of these contrary to hypothesis of "relic mechanism" of magnetic field origin (Moss 1989, 2001; Landstreet & Mathys 2000). If relic mechanism would work, the situation would be opposite: the younger and more massive the stars will have the strong magnetic fields. Haiashi phase, in which convective destroys relic magnetic field, is most strong in low-massive stars with strong magnetic fields. Arguably, "relic mechanism" gives only initial, inoculating magnetic field. There are two unsolved problems:

1. Why strong magnetic fields are observed solely in some types of chemically peculiar stars?
2. Does common mechanism for origin of magnetic fields exist for all these stars?

Acknowledgements. This work was supported by grant No. N203 4061 33 from the Polish Committee for Scientific Research.

References

Bychkov V.D., Bychkova L.V., Madej J.: 2003, *A&A*, **407**, 631.

Bychkov V.D., Bychkova L.V., Madej J.: 2005, *A&A*, **430**, 1143.

Bychkov V.D., Bychkova L.V., Madej J., 2008, *MNRAS, (in press).*

Lebedev V.S., Bychkov V.D., Bychkova L.V., Madej J.: 2006, *Proc. Inter. Conf. "Physics of magnetic stars"*, 169.

MAGNETIC FIELDS OF STARS

V.D. Bychkov[1], L.V. Bychkova[1], J. Madej[2]

[1] Special Astrophysical Observatory of the Russian Academy of Sciences
Nizhnij Arkhyz, 369167 Russia, *vbych@sao.ru*
[2] Warsaw University Observatory
Al. Ujazdowskie 4, 00-478 Warsaw, Poland, *jm@astrouw.edu.pl*

ABSTRACT. Now it is known about 1212 stars of the main sequence and giants (from them 610 stars — it is chemically peculiarity (CP) stars) for which direct measurements of magnetic fields were spent (Bychkov et al.,2008). Let's consider, what representations were generated about magnetic fields (MT) of stars on the basis of available observations data.

Key words: Stars: magnetic fields of stars: basic properties

1. The store observations data about measurements of magnetic fields of stars

For all 1212 stars have been received in the sum of 15240 estimations of a magnetic field. Observers investigated basically Ap stars as the most interesting objects. Magnetic field it was measured at the others basically with survey objective no more than 5 times.
Dependence of quantity of stars in from number of measurements for them made on Fig.1 is represented. Stars are divided on bins by quantity of measurements with step 5. The first bin contains stars with number of measurements from 1 up to 5, the second from 6 up to 10 and etc. In the first bin (no more than 5 measurements) 1061 star that makes 88% from total namber (on fig.1 the first bin is cut off from above). In figure also not put 5 stars the magnetic field for which was measured more than 200 times. All 5 stars are magnetic CP stars with very well studied magnetic behaviour.
Distribution is represented on fig.2 for the measured stars on visible star sizes. Apparently from this figure, bright stars approximately up to m_v $6m$, have been rather in regular intervals investigated.

On fig.3 show quantity of individual measurements of a magnetic field (MF) received in current of each year since the moment of the first measurements of MT on stars. It is necessary to pay attention that for construction of the histogram the published estimations were used only. And as not all the estimations received last years are published, it is necessary to expect increase in number of estimations for last years. Figure testifies that stable, escalating interest to research of stars magnetism is observed.

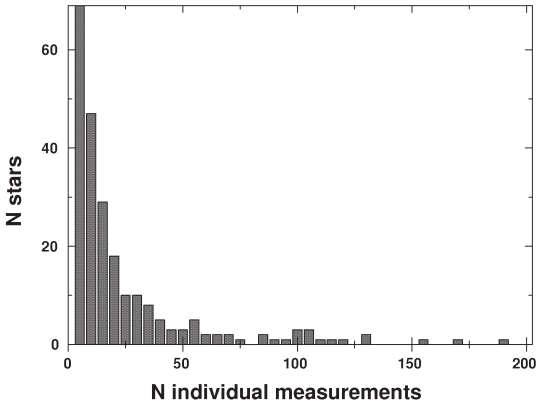

Figure 1: N stars vs. N individual measurements.

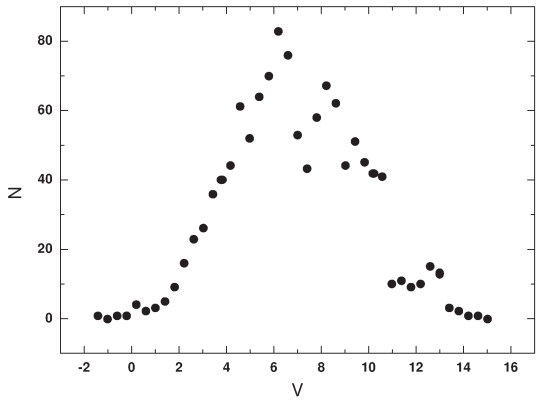

Figure 2: N stars vs.m_v of stars.

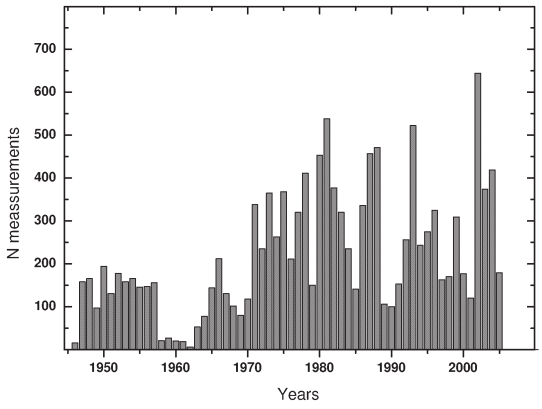

Figure 3: N measurements vs. years.

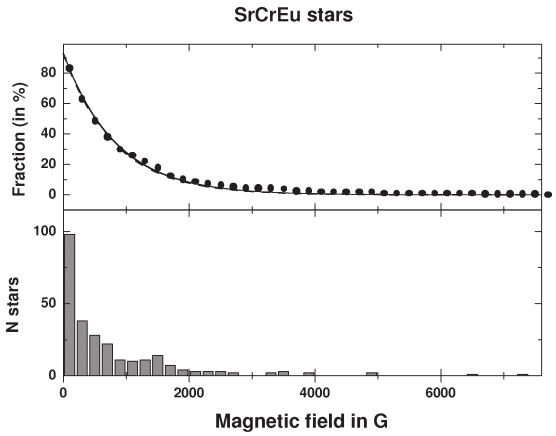

Figure 4: Integrated distribution function $N_{int}(B)$ in percent (upper panel), and the number distribution function $N(B)$ (lower panel) for SrCrEu stars vs. magnetic field in G.

2. Magnetic field of stars

Accessible data of observations have allowed to generate the next representations about magnetic fields of stars:

1. Strong magnetic global fields has some part CP of stars.
2. Exponent the law is observed in distribution of intensity of magnetic fields CP of stars (Bychkov et al., 2003, 2008). As an example such distributions we will show on fig.4 distribution for SrCrEu (strontium-chromium-europium) CP of stars.
3. Magnetic variability for 157 stars is studied (Bychkov et al., 2005).
4. Variability of magnetic field for 86% CP stars looks like a simple harmonic. Hence MF has simple dipolar structure for these stars. For 14% stars —changeability carries complex, more often two-componental character, and, possibly, MT has multipolar structure (Bychkov et al., 2005). It is possible influence dissimilar distributions of a chemical composition on a surface (Lebedev et al., 2006).
5. Changeability of MT with small amplitude (up to several tens G) is known for 6 stars of solar type and 3 early supergiants.
6. The stars of main sequence G, K, M spectral classes have local magnetic field spots structures.

Acknowledgements. This work was supported by grant No.N203 4061 33 from the Polish Committee for Scientific Research.

References

Bychkov V.D., Bychkova L.V., Madej J.: 2003, *A&A*, **407**, 631.

Bychkov V.D., Bychkova L.V., Madej J.: 2005, *A&A*, **430**, 1143.

Bychkov V.D., Bychkova L.V., Madej J.: 2008, *MNRAS, (in press).*

Lebedev V.S., Bychkov V.D., Bychkova L.V., Madej J.: 2006, *Proc. Inter. Conf. "Physics of magnetic stars"*, 169.

ADAPTIVE MODE OF THE MSS BTA

G.A. Chountonov, I.D. Najdenov

Special Astrophysical Observatory RAS
Nizhnij Arkhyz, *chunt@sao.ru*

ABSTRACT. The study of instability of the Main stellar spectrograph of the 6-m Telescope together with system of registration of a spectrum by means of the CCD shows that there is a drift of a spectrum along a dispersion, corresponding to the tenth of a pixel (the hundredth part of Å) in an hour. To eliminate this drift, i.e. to keep a spectrum from displacement, the plane-parallel glass plate was installed behind a slit of the spectrograph. The angle of inclination of this plate changes depending on a mismatch of positions of the current and comparison basic spectra. A lamp of hollow cathode is used. The scheme of this device is described. The results of tests are presented. The time of correction takes about one minute that allows to keep the position of the ThAr spectrum within ±0.0006 Å.

Key words: Stars: high precision spectral measurements

Introduction

The Main stellar spectrograph (MSS) equipped by the analyzer of polarization with double slicer, serves as one of the main tools for the measurements of stellar magnetic fields on the 6-m Telescope [Vasiliev et al., 1977, Chountonov, 2004]. Besides the measurements of magnetic fields, the MSS is used also for the chemical abundance studies and the precise registration of the profiles of the hydrogen lines used for the determination of atmospheric models. It is possible to distinguish two types of instabilities of any spectrograph causing the shift of a stellar spectrum during its registration:

– the shift of a spectrum connected with the movement of the center of gravity of a stellar image at the slit of spectrograph,

– the shift caused actually by spectrograph and the CCD system.

Instability of the MSS and CCD

This work is devoted to the second type of instability. After studying behaviour of the ThAr spectrum with time, we have developed and created a system of a current spectrum stabilisation by means of comparison of its position with that of the comparison spectrum. There is an analogue of the image stabilizer applied in digital cameras. Other variants of containment, for example, by moving a slit of spectrograph or the CCD are also possible. However, they seems to us more difficult in realization. The MSS was investigated by means of visual and photographic plate methods in 70-th during commissioning time (see, review [Panchuck et al., 2007]). The both, long- and short-term drifts of a spectrum were revealed. We have carried out the instability measurements using the equipment for measurements of magnetic fields of stars: the analyzer of circular polarization with double images slicer and the CCD (2Kx2K) developed in SAO. In Figure 1 we show a typical ThAr spectrum.

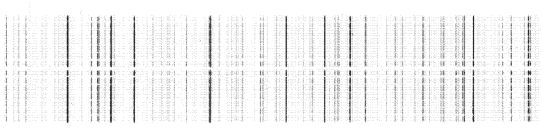

Figure 1: The ThAr spectrum registered with slicer.

In Figure 2 (a, b, c) we present the results of spectra shift measurements with time (number of exposition is on an abscissa axis and a difference of positions of current and comparison spectra is on axis of ordinates) on 1-st (a) and 14-th (b) slicers and their difference (c). A spectrum of the hollow cathode ThAr lamp was used. The light from this lamp was passed through the analyzer of polarization with double images slicer. One hundred expositions of spectra were registered with one minute exposition. The readout time of each frame was 20 sec. We can see a good correlation of spectra shifts of these two cuts which means the reliability of results. The software package in MIDAS environment, created in SAO [Najdenov et al., 2008] was used for reduction of spectra and definition of shifts. As it can be seen from the Figures, the short-term (minute) instability and drift are observed. To exclude influence of failures caused by cosmic particles, the opportunity of accumulation of several frames with the subsequent

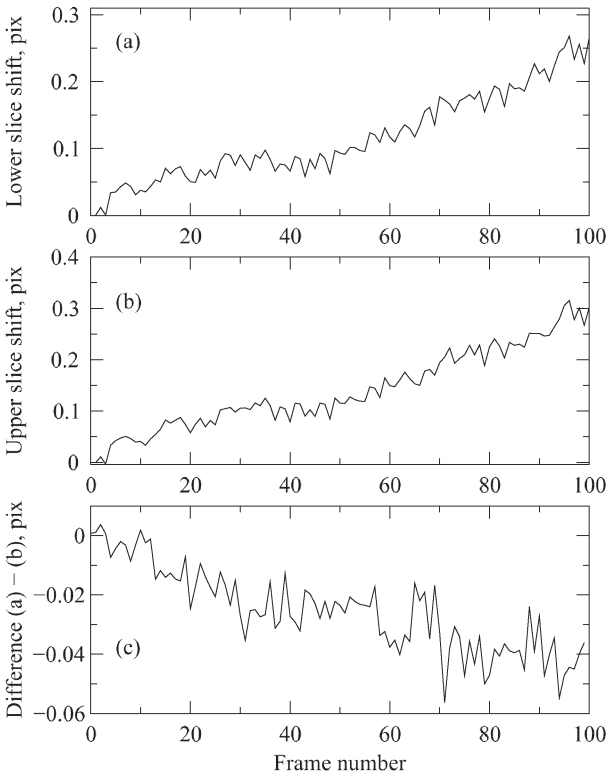

Figure 2: The position of ThAr spectrum for 1-st slice (a), 14-th slice (b) and their difference (c) with time.

clearing of cosmic particles traces was used. The MSS has won to itself glory unpromising that is located on load-bearing elements of the 6-m Telescope. Its elements are on large distances from each other and in different temperature conditions.

Main parameters of the MSS spectrum stabilizer

— a range of stabilization is about ±1 pix from the mean position of a plane-parallel plate, that is ±0.12 Å at 4500 Å

— a step of stabilization is 0.0011 pixels or 0.00014 Å

— time of correction is about one minute. For this time the spectrum drifts on 0.0006 Å.

Testing of the MSS spectrum stabilizer

The block diagram of the device for stabilization of a spectrum position for the MSS is represented on Figure 3. The computer 1 (PC1 under Windows) operates the CCD. After registration of a spectrum it copies a file with the image to the computer 2 (PC2 under LINUX). PC2 carries out an extraction of spectrum, calculates the difference of positions of current and comparison spectra, translates it into number of steps of the step motor and sends this value

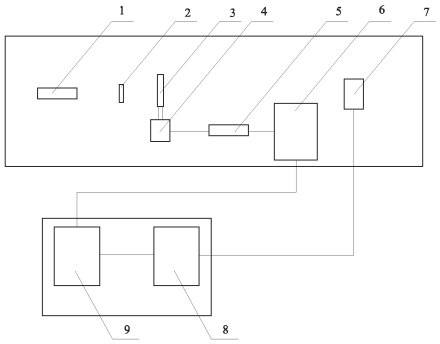

Figure 3: The block diagram of the device for stabilization of the spectrum position: 1 - ThAr lamp, 2 - slit of the MSS, 3 - plane-parallel plate, 4 - the step motor, 5 - the controller, 6 - PC3, 7 - CCD, 8 - PC1, 9 - PC2.

to computer 3 (PC3 under LINUX). PC3 turns a plane-parallel plate 3 on a necessary angle through the controller 5 and the step motor with a reducer 4. PC1 and PC2 are located in an management room, other elements on Nesmyth focus balcony. All procedure of correction can be repeated, if noncompensated value exceeds admissible value. The comparison spectrum is created preliminary in position of a plate of +1000 steps from the end contact. In this position the plate is almost perpendicular to the optical axis of the spectrograph. The relation "step/pixels" has to be about 0.0011. A plate thickness 6 mm are provided with displacement of a spectrum within the limits of not less than ±1 pix. The pixel size is 13 microns. One step corresponds to 0.00014 Å in the blue part of a spectrum.

Results of tests of the device for stabilization of a spectrum position

To check the work of the device, we have installed the additional inclined glass plate in a beam of light after the slicer. This plate causes artificial shift of a spectrum. In this condition of the device the comparison spectrum was created. On Figure 4 it corresponds to a point 1 on an abscissa axis. Then we have removed an additional plate. The position of a spectrum changed noticeably, approximately on 1.1 pixels (point 2). After that the program of shift compensation was started and the shift was compensated for three cycles.

It is possible to see from Figure 2c that a dispersion of a spectrum position about 0.005 pixels on one minute exposition. The drift during the exposition of 2 hours corresponds to 0.04 pixels. It is possible to explain that the spectrum turns with time also.

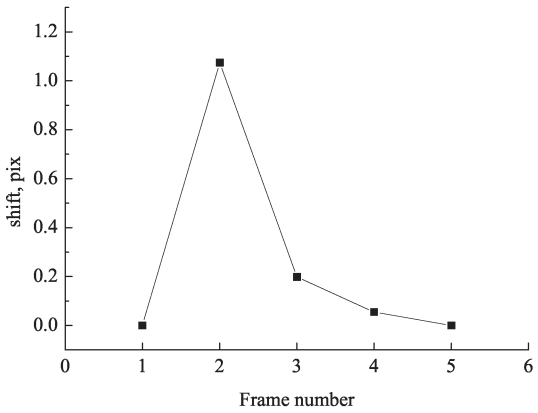

Figure 4: The compensation of an artificial shift of the spectrum.

Conclusions

The device for the MSS spectrum stabilization was created and is in trial operation on the 6-m Telescope. It allows, with an interval of one minute or often less, to carry out the correction of ThAr spectrum position with an accuracy of about 0.0006 Å. The device can be used for increasing the accuracy of radial velocity measurements of stars. It can be advanced by a principle stated in the work [Chountonov et al., 2000], by carrying out of a part of the electronic image containing a comparison spectrum, for calculation of the corrections, returning of a spectrum in a starting position and, thus, corrections of a spectrum of a star during accumulation without interruption an exposition. In the future, a fast photodetector with internal amplification EM CCD can be used for electronic correction of the image by simultaneous or consecutive registration of a star spectrum and a comparison spectrum.

Acknowledgements. The authors are thankful to V.Vlasjuk for discussion, G.A.Mal'kova, V.L.Plokhotnichenko and N.A.Vikul'ev - for help.

References

Vasiliev A.S. et al.: 1977, *Optical Mechanical Industry,* **2**, 31.

Chountonov G.A.: 2004, *Proceedings of International Conference on Magnetic Fields*, N.Arkhyz, 27–31 Aug 2003 /Eds. Yu.V. Glagolevskij, D.O. Kudryavtsev, I.I. Romanyuk, 2004, p. 286–291.

Panchuk V.E. et al.: 2007, *SAO report N 212.*

Najdenov I.D. et al.: 2008, *SAO report N 315.*

Chountonov G.A. et al.: 2000, *Proceedings of International Conference on Magnetic Fields of Chemically Peculiar and Related Stars*, N.Arkhyz, Russia, Eds. Yu.V. Glagolevskij, I.I. Romanyuk. p.249.

PECULIARITIES OF MIXING METALS IN INTERGALACTIC AND INTERSTELLAR MEDIA

S.Yu. Dedikov[1], Yu.A. Shchekinov[1,2], E.O. Vasiliev[3,4]

[1] Department of Physics, Southern Federal University, Rostov-on-Don 344090 Russia, *svsde@mail.ru, yus@phys.rsu.ru*
[2] Special Astrophysical Observatory, Nizhny Arkhyz 369167 Russia
[3] Institute of Physics, Southern Federal University, Rostov-on-Don 344090 Russia, *eugstar@mail.ru*
[4] Institute of Astronomy, Moscow 119017 Russia

ABSTRACT. We review the current status of the problem of metal mixing in the intergalactic and interstellar media. We give simple arguments for inefficiency of mixing metals because of a saturation of hydrodynamic (Rayleigh-Taylor and Kelvin-Helmholz) instabilities. We describe mixing in two typical processes: stripping of a galactic gaseous halo and cloud-cloud collision. We show that statistical features of metal distribution observed in the intergalactic medium is close to those obtained in our numerical simulations.

Key words: interstellar and intergalactic medium, metals, enrichment, mixing, hydrodynamic instabilities

1. Observations vs. simulations

After the reionization the metallicty of the intergalactic medium (IGM) reaches a value [Z]~ -3 and is kept at this level during a very long time, at least between redshifts $z = 2 - 5$ (Songaila 2001). This fact contradicts to the conventional theoretical models of the enrichment of the IGM with metals, which predict the increase of metallicity with age of the universe (Nath & Trentham 1997, Ferrara et al 2000). A possible solution can be connected with a strong and fast enrichment of the IGM by first stellar systems at $z \sim 10$ (Madau et al 2001). The spatial distribution of metals in this model appears to be more or less homogeneous. Moreover, the assumption of homogeneity is very often utilized in the estimates of metal budget in the IGM (Songaila 2001, Ferrara et al 2005). However, recent observations of metal absorptions in the intergalactic medium show extremely inhomogeneous distribution of metals on wide spatial scales (Simcoe et al 2006, Schaye et al 2007, Hao et al 2007). Inhomogeneous distribution of metals in the IGM was predicted theoretically by Dedikov & Shchekinov (2004) on the basis of numerical simulations of stripping of galactic gaseous haloes. In general this result can be obtained from a simple analisys of hydrodynamic (Rayleigh-Taylor and Kelvin-Helmholtz) instabilities, which are mainly responsible for metal mixing in the IGM (Dedikov & Shchekinov 2004).

The distribution of metals in the interstellar medium (ISM) is believed to be homogeneous due to multiple actions from stellar winds, supernovae explosions and other dynamic processes. However, recent observations suggest that the distribution of species such as deuterium (Jenkins et al. 1999) and oxygen (Meyer et al 1998) in the ISM are far from being homogeneous. De Avillez & MacLow (2002) have numerically simulated mixing of metals in a mono-phase ISM. They concluded that the timescale for complete mixing is quite long, ~ 350 Myr, and the mixing efficiency strongly changes with spatial scales. Moreover, in realistic coinditions of a multi-phase ISM mixing time obviously increases.

In this paper we briefly describe general properties of mixing process and how they manifest themself in the IGM and ISM.

2. Instabilities and mixing of metals

Mixing or erasing of chemical inhomogeneites in the IGM and ISM acts under irregular gaseous motions, which in turn are often supported by hydrodynamic instabilities, such as Rayleigh-Taylor (RT) and Kelvin-Helmholtz (KH) instabilites, developed when an enriched gas clump moves through diffuse medium. During the motion of a cloud through the intercloud medium the development of KH instability begins from a characteristic scale equal initially to the cloud radius (Klein et al 1994, Vietri et al 1997). Further on such large scale vortices cascade to produce inhomogeneities of smaller scales. As a result the cloud surface increases and the dynamic friction

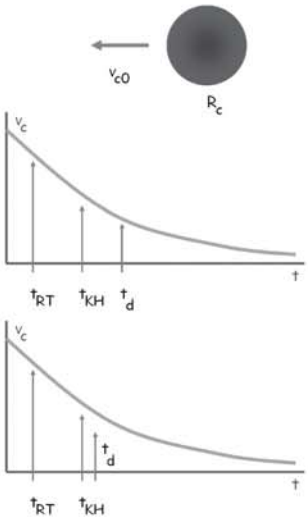

Figure 1: Schematic description of the saturation of instabilities: upper graph shows the interrelation between the characteristic times: the dynamic friction time t_d, the time scales of KH and RT instabilities $t_{\rm KH}$ and $t_{\rm RT}$ – in the initial state; lower graph shows this interrelation after a few KH time scales when the cloud surface increases due to progressive cascading of vortices (Dedikov & Shchekinov 2004, Shchekinov et al 2008).

time shortens. The cloud decelerates progressively, its velocity gradually decreases, $v_c \to 0$, and KH instability slows down proportionally. This process manifests as a saturation of the instability. Once the saturation is reached the mixing freezes out. As KH and dynamic friction time scales are usually close to each other, as schematically shown in Figure 1, the instability saturates quickly.

3. Mixing in the IGM

General features of metal mixing in the intergalactic medium under stripping of a galactic gaseous halo are presented in Figures 2 and 3, where the metallicity, density and temperature maps at times 1.27 and 2.54 Gyr are shown for an adiabatic (nonradiative) case. Note that although radiative losses by hydrogen and metals change the maps qualitatively, statistical properties of the metal distribution remain essentially unchanged (see Dedikov et al., this volume).

Figure 4 demonstrates the metallicity histogamm for stripping of a galactic gaseous halo. The resulted distributon of metals differs substantially from that produced by turbulent diffusion (the distribution corresponding to mixing by turbulent diffusion is depicted as dash line in Figure 4, the details can be found in Dedikov & Shchekinov 2004). This reflects the fact

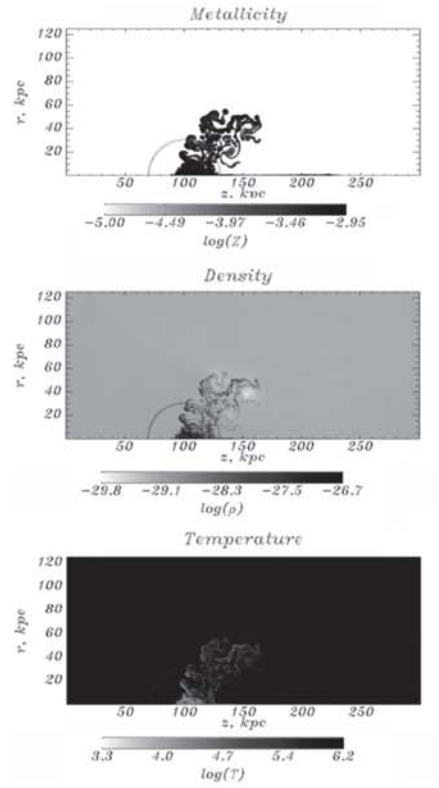

Figure 2: Metallicity, density and temperature distributions for stripping of a galactic gaseous halo at time $t = 1.27$ Gyr.

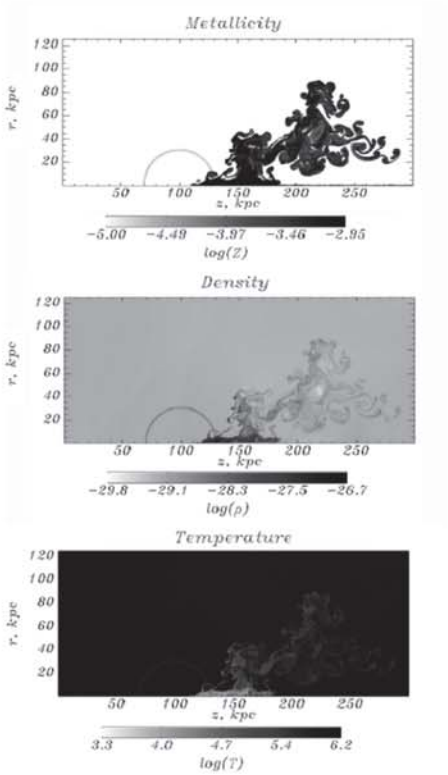

Figure 3: Same as in Figure 1 at time $t = 2.54$ Gyr.

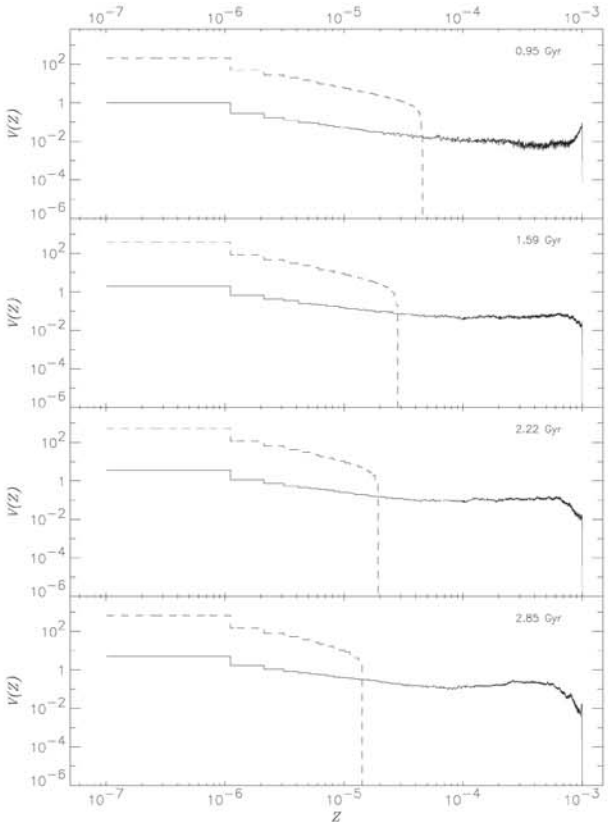

Figure 4: Metallicity histogamm for stripping of a galactic gaseous halo. The corresponding distribution produced by turbulent diffusion is depicted by dash line.

that metals mixed by cascading vortices remain confined into restricted pockets contrary to a diffusion model where they are redistributed homogeneously through the whole computational zone. Such pockets are surrounded by the background low-metallicity medium. This picture resembles an intermittent distribution (Dedikov & Shchekinov 2004).

Overall, asymptotically a highly inhomogeneous spacial metal distribution establishes with a numerous spots of low and high metallicity. From intuitive arguments one can expect an interrelation between the metallicity in such spots and their size. In order to determine this interrelation we applied a procedure similar to the cluster analysis: the metal distribution is presented as a relief map, which then is cutted at a given metallicity level Z_0, so that the regions with the metallicity $Z > Z_0$ isolate each other, and their surfaces can be explicitly calculated. If one assumes that the size of a given region is a square root of its surface, the "metallicity-size" relation in the form shown in Figures 5 and 6 can be found (Dedikov & Shchekinov 2004, Dedikov et al., 2009): Figures 5 presents the "metallicity-size" relation for stripping of a galactic gaseous halo at time 1.27 Gyr, while Figure

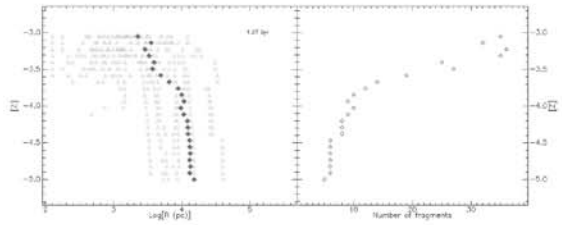

Figure 5: "Metallicity-size" (left panel) and number of fragments-metallicity (right) distributions for stripping of a galactic gaseous halo at time $t = 1.27$ Gyr. The metallicity and size for each isolated region is depicted by open symbols. Filled symbols present the mean size for a given metallicity.

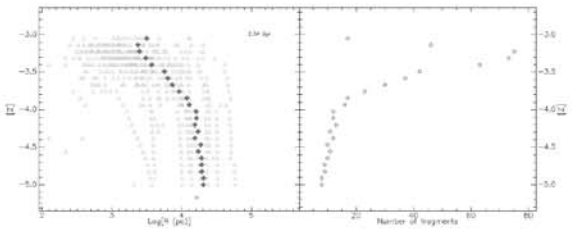

Figure 6: Same as in Figure 5 at time $t = 2.54$ Gyr.

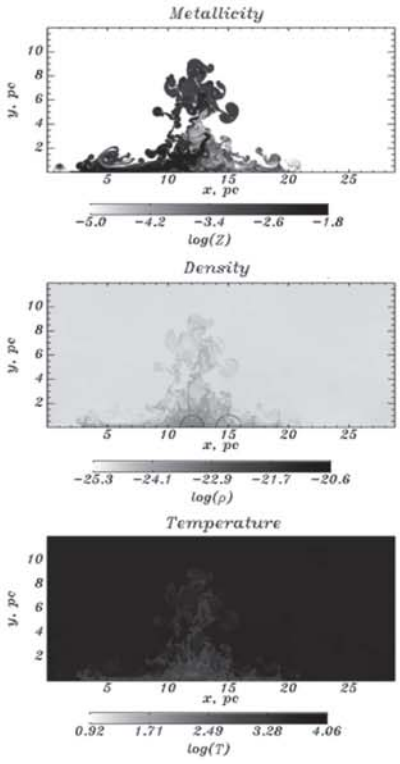

Figure 7: Metallicity, density and temperature distributions for cloud-cloud collision at time $t = 4.76$ Myr. The contours in the middle panel correspond to the initial positions of the clouds.

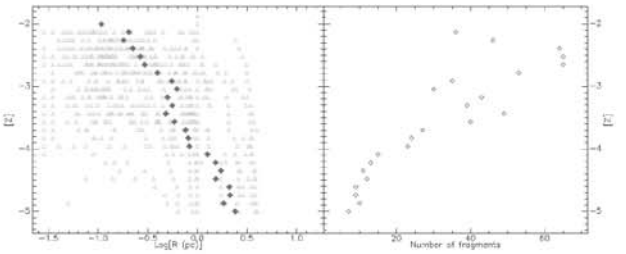

Figure 8: "Metallicity-size" (left panel) and number of fragments-metallicity (right) distributions for cloud-cloud collision at time $t = 4.76$ Myr.

6 – at 2.54 Gyr. Right panels in Figures 5 and 6 represent the number of fragments-metallicity relations. It is clearly seen from here that more metallic regions are smaller in size and more numerous. Thus, the detection of such regions in the IGM can be difficult and the metal bugdet in the IGM is underestimated.

4. Mixing in the ISM

Mixing of chemical species in the ISM obviously takes shorter characteristic time in comparison with that in the IGM, mainly because of highly developed turbulent motions supported by numerous shock waves from supernovae explosions and stellar winds. However, mixing still remains quite slow (de Avillez & Mac Low 2002), which is determined by the rate of shock waves passing through a given volume of the ISM. Another reason is connected with the enrichment from newly formed stellar clusters. Thus, one can expect that metal distribution in the ISM reveals strong spacial variations as it occurs in the IGM.

Another possible mixing process in the ISM is connected with cloud-cloud collisions. Here we present results for collisions of nearly equal clouds (5% difference in radius) with $n = 10$ cm^{-3}, $T = 100$ K, with metallicities $[Z] = 10^{-1}$ and 10^{-3}, and equal velocities $v = 5$ km s^{-1} (Vasiliev et al., in preparation). We apply the same statistical procedure to analyze the distribution of metals resulting in this process. Figure 7 presents the maps of metallicity, density and temperature for this model, while Figure 8 shows the corresponding "metallicity-size" and number of fragments-metallicity diagramms. One shoud note that the dependence of "metallicity-size" looks similar to that for stripping of gaseous halos (Figures 5 and 6).

5. Conclusion

In this paper we briefly reviewed properties of metal mixing in the intergalactic (IGM) and interstellar (ISM) media, which can be summarized as follows

- slowing down relative gas motions leads to saturation of hydrodynamic instabilites and results in a freezing of chemical inhomogeneities;
- mixing of metals remains therefore incomplete, and the distribution of metals is kept highly inhomogenious on small scales, so that the most metal-rich material is confined into small-sized pockets.

Recent observations confirm indeed fairly inhomogeneous distribution of metals in the IGM and ISM. We found that statistical characteristics of metal distribution oberved in the intergalactic medium looks similar to those obtained in the numerical simulations, and show the features usual for gaseous flows with saturation of hydrodynamic instabilities.

Acknowledgements. This work is supported by the RFBR grant 08-02-91321, the Federal Agency of Education grant RNP 2.1.1.3483. EOV is supported by the RFBR through the mobility programme grant 08-02-90706.

References

de Avillez M.A., Mac Low M.-M.: 2002, *ApJ*, **581**, 1047.

Dedikov S.Yu. and Shchekinov Yu.A.: 2004, *Asron. Rep.* **48**, 9.

Dedikov S.Yu., Shchekinov Yu.A., Vasiliev E.O.: *Astron. Bull.* in press.

Ferrara A., Pettini M., Shchekinov Yu.A.: 2000, *MNRAS*, **319**, 539.

Ferrara A., Scannapieco E., Bergeron J.: 2005, *ApJL*, **634**, 37.

Hao H., et al.: 2007, *ApJ*, Lett. **659**, 99.

Jenkins E.B., Tripp T.M., Woniak P.R., Sofia U.J. and Sonneborn G.: 1999, *ApJ*, **520**, 182.

Klein R.I., McKee C.F., Colella P.: 1994, *ApJ*, **420**, 213.

Madau P., Ferrara A., Rees M.: 2001, *ApJ*, **555**, 92.

Meyer D.M., Jura M. and Cardelli J.A.: 1998, *ApJ*, **493**, 222.

Nath B., Trentham N.: 1997, *MNRAS*, **291**, 505.

Schaye J., Carswell R.F., Kim T.-S.: 2007, *MNRAS*, **379**, 1169.

Shchekinov Yu.A., Shustov B.M., Vasiliev E.O., Dedikov S.Yu.: 2008, in: *Ultraviolet Universe.*

Simcoe R.A., Sargent W.L.W., Rauch M., Becker G.: 2006, *ApJ*, **637**, 648.

Songaila A.: 2001, *ApJ*, **561**, L153.

MIXING METALS UNDER STRIPPING GALACTIC GASEOUS HALOES: RADIATIVE LOSSES

S.Yu. Dedikov[1], Yu.A. Shchekinov[1,2], E.O. Vasiliev[3,4]

[1] Department of Physics, Southern Federal University
Rostov-on-Don 344090 Russia, *svsde@mail.ru, yus@phys.rsu.ru*
[2] Special Astrophysical Observatory, Russian Academy of Sciences
Nizhnij Arkhyz, Karachai-Cherkess Republic 369167 Russia
[3] Institute of Physics, Southern Federal University
Rostov-on-Don 344090 Russia, *eugstar@mail.ru*
[4] Institute of Astronomy, Russian Academy of Sciences
Moscow 119017 Russia

ABSTRACT. We present two-dimensional numerical model for mixing of metals in the intergalactic medium under stripping of a galactic gaseous halo both in adiabatic and radiative cases. A particular attention is paid to influence of radiative losses on mixing efficiency. We conclude that the statistical features of metal distribution are quite similar to those in adiabatic case.

Key words: intergalactic medium, metals, enrichment, mixing.

1. Introduction

It was recognized during last several years that the intergalactic medium (IGM) at redshift $z \leq 5.5$ is already polluted with metals, as seen from observations of CIV and SiIV absorptions in Lyα forest systems in quasar spectra. The metallicity Z of the IGM averaged over a wide interval of column densities ($10^{12} \leq N(\mathrm{CIV}) \leq 10^{15}$ cm^{-2}) is $Z = -3$, while in the interval $10^{13} \leq N(\mathrm{CIV}) \leq 10^{14}$ cm^{-2} metallicity is substantially lower, which shows that metals are distributed in the IGM inhomogeneously. The averaged metallicities in both column density intervals remain nearly independent on z up to $z \simeq 5.5$, and show decline at larger z (Songaila 2001). This fact, together with observations of Gunn-Peterson effect at redshift $z \sim 6$ (Songaila & Cowie 2002), possibly indicate that after an initial pollution of metals from the first objects their content and the degree of the inhomogeneity in the IGM remained invariant at later epochs.

Recent observations of absoption systems in the spectra of distant quasars (Schaye et al 2007) and environments of galaxies at $z = 2 - 3$ (Simcoe et al 2006) present new arguments for strong inhomogeneity of the intergalactic medium in wide range of spatial scales. Earlier the similar conclusion about inhomogeneous distribution of metals in the IGM was numerically obtained by Dedikov & Shchekinov (2004). In adiabatic conditions they have simulated the mixing mechanism connected with stripping of a metal enriched envelope around a galaxy by ram pressure of the outflowing intergalactic gas. Here we present the similar model with radiative losses.

2. Model

We consider the following simple model (more details can be found in Dedikov & Shchekinov 2004): a metal-enriched gas is ejected from a galaxy by an explosive mechanism and, therefore, forms a sufficiently thin shell. We simulate numerically in 2D description dynamics of such a metal enriched thin shell with the outer radius $R = 31$ kpc and thickness $\Delta R = 1$ kpc moving through the IGM with the velocity $u = 100$ km s^{-1}. We neglect the effects of gravitational field of a parent galaxy on the shell. For the sake of simplicity the shell is assumed to be in hydrostatic equilibrium at the initial moment. These simplifications are justified, because we consider a mixing of metals in the IGM inrespective to the properties of a parent galaxy. Gas densities in the shell, outside the shell and inside the shell are assumed equal to $n_{sh} = 4.4 \times 10^{-4}$ cm^{-3}, $n_{igm} = 4.4 \times 10^{-6}$ cm^{-3} and $n_h = 4.4 \times 10^{-6}$ cm^{-3}, respectively. The corresponding temperatures are $T_{sh} = 10^4$ K, $T_{igm} = 10^6$ K, $T_h = 10^6$ K and metallicities (i.e. the ratio of metal density to gas density) are $Z_{sh} = 10^{-3}$, $Z_{igm} = 0$, $Z_h = 0$.

We use the Zeus-2D hydrodynamics code (Stone & Norman 1992) in the cylindrical coordinates (r, z). The computational area of $\Delta r \times \Delta z = 125 \times 300$ kpc is

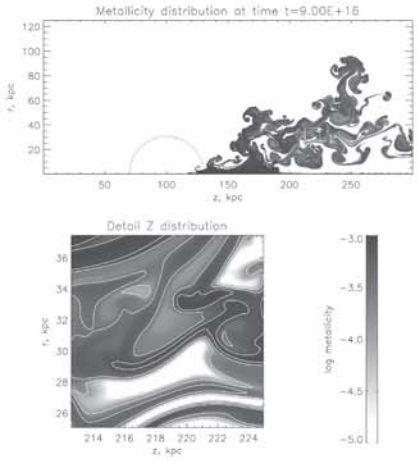

Figure 1: Metallicity distribution in the whole computational area and in the selected region. The initial position of the shell is marked by the dashed lines.

divided into 1000×2400 grid points. The intergalactic gas flows with velocity $u = 100$ km s^{-1} at z direction. Metallicity as a passive scalar variable is accounted for by adding the transfer equation to the Zeus-2D code. The cooling term include Lyα losses from hydrogen and cooling in the fine structure of single ionized carbon, atomic oxygen and metastable lines of CII and OI (Penston 1970, Hollenbach & McKee 1989). We solve the energy equation using the Newton-Raphson iterative procedure.

3. Results and conclusions

General features of metal mixing are demonstrated in Figure 1, where is presented a metallicity distribution at time $t = 2.85$ Gyr for the adiabatic case. It is clearly seen that enrichment is extremely inhomogeneous in the regions of non-zero metallicity. Average metallicity in this region $\langle Z \rangle = 4.6 \times 10^{-4}$, but a major contribution is due to high-metallicity spots $Z \geq 6.0 \times 10^{-4}$, which volume fraction is 12.5% in all. In the model with radiative losses the cooling is important in regions with greatest metal abundance, because they cool faster and therefore collapse faster. This is displayed in more extended metal distribution along z-axis while along radial direction. Another distinction consist with the time of mixing: for the case with radiative losses this value is greater.

Figure 2 presents histograms of the number of cells with metallicity at a given interval (since the number of intervals is large, the histogram practically corresponds to the metallicity distribution function) for both adiabatic and radiative cases. One can find a statistically insignificant difference between two cases.

The resulted distributon of metals essentially differs from that of a diffusion process. In particular, this

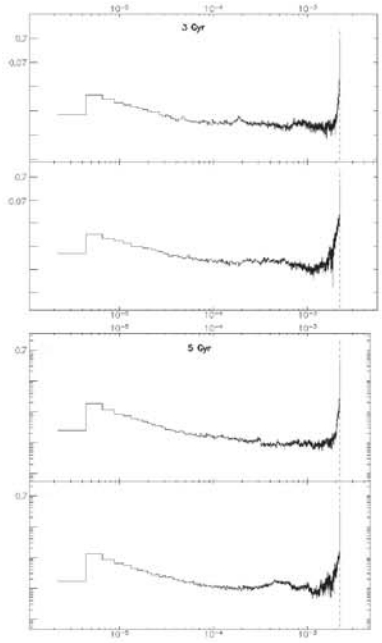

Figure 2: Metallicity distribution for adiabatic (upper) and radiative (lower) cases.

reflects the fact that metals in our numerical model are spread over a larger number of numerical cells with high metallicity than in a simple diffusion model. Moreover, the sufficient scatter in number of cells with near values of metallicities is observed in regions with high metallicities. It argues that on the small scales metals are distributed in well isolated spots and exchange between them is limited. Such properties of the mixing process correspond to the process with intermittency (Dedikov & Shchekinov 2004).

Acknowledgements. This work is supported by the RFBR grant 08-02-91321, the Federal Agency of Education grant RNP 2.1.1.3483. EOV is supported by the RFBR through the mobility programme grant 08-02-90706.

References

Dedikov S.Yu., Shchekinov Yu.A.: 2004, *Asron. Rep.*, **48**, 9.
Hollenbach D. & McKee C.F.: 1989, *ApJ*, **342**, 306.
Penston M.V.: 1970, *ApJ*, **162**, 771.
Schaye J., Carswell R.F., Kim T.-S.: 2007, *MNRAS*, **379**, 1169.
Simcoe R.A., Sargent W.L.W., Rauch M., Becker G.: 2006, *ApJ*, **637**, 648.
Songaila A.: 2001, *ApJ*, **561**, L153.
Songaila A., Cowie L.L.: 2002, *AJ*, **123**, 2183.
Stone J.M., Norman M.L.: 1992, *ApJSS*, **80**, 753.

HD 158450: A MAGNETIC CHEMICALLY PECULIAR STAR IN A YOUNG STELLAR GROUP

N.A. Drake[1], E.G. Jilinski[2,3], V.G. Ortega[2], R. de la Reza[2], B. Bazzanella[2]

[1] Sobolev Astronomical Institute, St. Petersburg State University, Universitetski pr., 28, St. Petersburg 198504, Russia, *drake@on.br*
[2] Observatório Nacional/MCT, Rua Gen. José Cristino, 77, Rio de Janeiro 20921-400, Brazil
[3] Pulkovo Observatory, Russian Academy of Sciences, St. Petersburg 196140, Russia

ABSTRACT. We report on the discovery of the Zeeman resolved spectral lines, corresponding to the very large magnetic field modulus $\langle H \rangle = 11.1$ kG, in the spectrum of the chemically peculiar star HD 158450 belonging to the recently discovered Mamajek 2 stellar group. We determined fundamental parameters and projected rotation velocity of the star. Dynamical 3D mean orbit calculations showed that Mamajek 2 stellar group has an age of 135 ± 5 Myr. Based on this age, we estimate that HD 158450 has completed about 12% of its main-sequence life. The importance of the detailed study of HD 158450, a member of a stellar group with a well determined age, for understanding the origin and evolution of stellar magnetic fields is discussed.

Key words: Stars: magnetic fields; stars: individual: HD 158450, HD 66318

1. Introduction

The new stellar group, named Mamajek 2, was discovered by Mamajek (2006) on the basis of common parallel motions and similar trigonometric parallaxes of the stars. It contains the bright B8 giant μ Oph and eight further B and A-type stars. In his work Mamajek (2006) proposes the coevality of this group located at a present distance of 170 pc from the Sun with an age of 120 ± 25 Myr. This author suggests that the Mamajek 2 group may have formed in the same star forming region as the Pleiades, NGC 2516 and α Persei cluster and the AB Dor stellar group.

The dynamical age of this group calculated under a modeled Galactic potential was determined in Jilinski et al. (2008) as the time elapsed since the NGC 2516 and Mamajek 2 orbital convergence. This dynamical results showed that Mamajek 2 group and the open cluster NGC 2516 may have had a common origin at the age of 135 ± 5 Myr. On the other hand the calculation showed that the α Persei cluster has a completely different past dynamical evolution when compared with Mamajek 2 group.

2. The star HD 158450

One of the stars of Mamajek 2 group, HD 158450, shows a highly peculiar spectrum. This star was included in the list of "the brighter stars of astrophysical interest in the southern sky" by Bidelman & MacConnell (1973) as a peculiar A star of the Sr-Cr-Eu type.

2.1. Observations

We have one high-resolution spectrum of this star obtained at June 2, 2007 (MJD = 54253.31316) with the FEROS spectrograph attached to the 2.2 m telescope of ESO at La Silla, Chile, with a resolution R = 48 000 and a spectral range coverage from 3800 to 8800 Å.

2.2. The Magnetic Field

The analysis of this spectrum indicates the presence of a strong magnetic field resulting in the magnetic splitting of some spectral lines. The most prominent spectral feature is the Fe II 6149.258 Å line (see Figure 1), commonly used for magnetic field strength determination (Mathys 1997). In unpolarized light the profile of this line in the presence of a magnetic field is a simple doublet. The mean magnetic field modulus (the line-intensity weighted average over the visible stellar hemisphere of the modulus of the magnetic vector) can be estimated by the well known formula:

$$\frac{1}{2} \cdot \Delta\lambda_Z = 4.67 \cdot 10^{-13} \cdot g_{\rm eff} \cdot \lambda^2 \cdot \langle H \rangle \,,$$

where $\Delta\lambda_Z$ is the measured Zeeman splitting in Å,

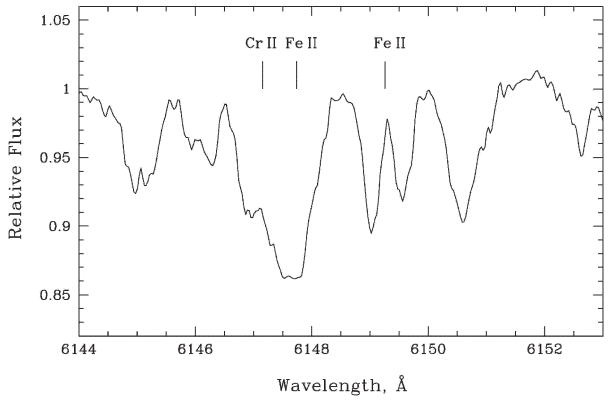

Figure 1: Spectrum of the Ap star HD 158450 showing the lines of Cr II 6147.154 Å, Fe II 6147.741 Å, and Fe II 6149.258 Å. Note the direct magnetic splitting of the Fe II 6149.258 Å line.

$g_{\rm eff} = 1.35$ - the effective Landé factor, λ - the central wavelength of the unshifted line in Å, and $\langle H \rangle$ - the mean magnetic field modulus in Gauss. Thus, the measured mean magnetic field modulus of HD 158450 turns out to be $\langle H \rangle = 11.1$ kG.

The presence of a magnetic field on the surface of this star was recently discovered by Kudryavtsev et al. (2006) from the spectropolarimetric observations of a sample of chemically peculiar stars at the 6-m telescope of the SAO RAS, Russia. These authors found the mean longitudinal component of the magnetic field to be $\langle {B_l}^2 \rangle^{\frac{1}{2}} = 1570 \pm 180$ G, whereas the individual values of the longitudinal magnetic field vary for different dates from -2920 ± 200 to $+810 \pm 240$ G, indicating strong variation of the magnetic field strength with stellar rotation.

2.3. The Stellar Parameters

We used the $B2-G$ Geneva index (Rufener 1988) to estimate the effective temperature of HD 158450. Estimating the reddening of the star as $E(B-V) = 0.31$ (Mamajek 2006) and employing the relation $E(B2-G) \sim E(B-V)$ we find the dereddened index $(B2-G)_0 = -0.477$ which gives, with the calibration of Hauck & North (1993), an effective temperature of $T_{\rm eff} = 8880$ K. Placing the star on the isochrone for a cluster age of 135 Myr (Lejeune et al. 2001), we determine stellar mass $M = 1.96\,M_{\odot}$.

Based on the Schaller et al. (1992) evolution tracks, we estimate that HD 158450 has completed only about 12% of its main-sequence life.

The approximation of the Fe II 6149.258 Å magnetically splitted line by a synthetic spectrum showed that this star has the low projected rotational velocity of $v \sin i = 9 \pm 1$ km s^{-1}. The radial velocity of HD 158450 measured by us is $v_{\rm rad} = -17.3$ km s^{-1}.

3. Discussion and Conclusions

The origin and evolution of the strong magnetic fields of upper- and middle-main-sequence stars continue to be the subject of long debates. Two different theories have been suggested: according to one of them, the stars would acquire their fields at the time of their formation – this is the fossil field theory; according to the other theory, the fields would be generated and maintained by a dynamo mechanism acting inside the star.

The study of the evolution of magnetic fields across the main sequence will provide important observational constraints for testing theoretical predictions. Magnetic field measurements for stars, members of stellar clusters or groups having well-determined ages, are very important. Recent discoveries of stars with strong magnetic fields close to ZAMS may be seen as an argument in favour of the fossil-field theory. Photometric and longitudinal magnetic field monitoring of HD 158450 is needed to determine its rotational period.

It is interesting to mention that Bagnulo et al. (2003) discovered a very strong magnetic field on the surface of the star HD 66318 belonging to the open cluster NGC 2516 which has, as it was shown in Jilinski et al. (2008), a common origin with Mamajek 2 group: the mean field modulus of HD 66318 is $\langle H \rangle = 14.5$ kG. With $T_{\rm eff} = 9200 \pm 200$ K, $M = 2.1 \pm 0.1\,M_{\odot}$, the star HD 66318 is quite similar to HD 158450 in the Mamajek 2 group.

References

Bagnulo S., Landstreet J.D., Lo Curto G., Szeifert T., Wade G.A.: 2003, *A&A*, **403**, 645

Bidelman W.P., MacConnell D.J. 1973, *AJ*, **78**, 687

Jilinski E.G., Ortega V.G., de la Reza R., Drake N.A., Bazzanella B.: 2008, *arXiv: astro-ph/08101198* (to be published in *ApJ*, January 2009)

Hauck B., North P. 1993, *A&A*, **269**, 403

Kudryavtsev D.O., Romanyuk I.I., Elkin V.G., Paunzen E. 2006, *MNRAS*, **372**, 1804

Lejeune T., Schaerer D.: 2001, *A&A*, **366**, 538

Mamajek E.E. 2006, *AJ*, **132**, 2198

Mathys G., Hubrig S., Landstreet, J.D., Lanz T., Manfroid J.: 1997, *A&AS*, **123**, 353

Rufener F. 1988, GENEVA Photometric Catalogue, 4th edition, Observatoire de Genéve

Schaller G., Schaerer, D., Meynet, G., Maeder, A. 1992, *A&AS*, **96**, 269

ABUNDANCES OF COPPER AND ZINC IN STARS OF THE GALACTIC THIN AND THICK DISKS

T.I. Gorbaneva[1], T.V. Mishenina[1], N.Yu. Basak[1], C. Soubiran[2], V.V. Kovtyukh[1]

[1] Astronomical Observatory, Odessa National University
T.G.Shevchenko Park, Odessa 65014 Ukraine, *astro@paco.odessa.ua*

[2] Observatoire Aquitain des Sciences de l'Univers
CNRS UMR 5804, BP 89, 33270 Floirac, France

ABSTRACT. The spectra of studied stars were obtained with the ELODIE spectrograph at the 1.93-m telescope of the Observatoire de Haute Provence (France). The determination of Cu and Zn abundances was carried out in LTE assumption by model atmosphere method, for Cu the hyperfine structure was taken into account. Cu and Zn abundance trends for thin and thick disk's stars are presented.

Key words: Stars: fundamental parameters; stars: Cu, Zn abundances.

1. Introduction

The nucleosynthesis mechanisms and the relative contributions of different sources by Cu and Zn enrichment are still uncertain. The probable sources of enrichment by Cu and Zn are different objects, such as the massive stars, type II and type Ia supernovae and low- and intermediate-mass stars – stars AGB. These sources can give different contribution to enrichment by these elements for thick and thin disks. Therefore, the dependences of elemental abundances [El/Fe] vs. metallicity [Fe/H] for thin and thick disks can differ. In this paper we present the determination of Cu and Zn abundance and the dependences of [El/Fe] vs. [Fe/H] for thin and thick disk's stars for which the separation according to kinematic criteria has been made earlier.

2. Observations and stellar parameters

The spectra of studied stars were obtained on 1.93 m telescope of the Observatoire Haute Provence (France) equiped with echelle-spectrograph ELODIE. A resolving power is 42000, the wavelength range 4400-6800 ÅÅ has used. Spectrum extraction, wavelength calibration and radial velocity measurement have been performed at the telescope with the on-line data reduction software while straightening of the orders, removing of cosmic ray hits, bad pixels and telluric lines were performed as described in Kats et al. (1998). The spectra processing was done through the DECH20 code (Galazutdinov, 1992). Equivalent widths of lines were measured by Gaussian function fitting. The temperatures were determined with the very high level of accuracy using the line depth ratios. The surface gravity log g was determined using the iron ionization equilibrium assumption, where the average iron abundance determined from FeI lines and Fe II lines must be identical. Microturbulent velocities $V_t$were determined by forcing the abundances determined from individual FeI lines to be independent of equivalent width. The parameter's determination and the separation of thin and thick stars on kinematic criterion was made earlier (Mishenina, 2004).

3. Elemental abundances

Elemental abundances were determined from LTE analysis basing on the atmosphere models by Kurucz (1993). **Copper.** Cu abundance was determined for 171 dwarfs by line profile fitting of the synthetic to stellar spectra using the lines 5105.54, 5218.20, 5782.12 ÅÅ and the STARSP code developed by Tsymbal, 1996. We have taken hyperfine structure of Cu I (Steffen, 1985) into account for the profile calculations. **Zinc.** Zn abundance for 65 dwarfs was determined with equivalent width measurements. The log gf-values for these lines were taken from (Kovtyukh, Andrievsky, 1999) and WIDTH9 code developed by (Kurucz, 1993) was used. [Zn/Fe], [Cu/Fe] and [Cu/Zn] vs. [Fe/H] for different populations are shown in Fig.1, Fig.2. and Fig.3. Thick disk stars are marked as filled circles, and thin disk stars as open circles.

4. Results and conclusions

We have determined Cu and Zn abundances for 171 and 65 stars, correspondingly. The metallicities of study stars is in the range -1.2 < [Fe/H] < +0.4.

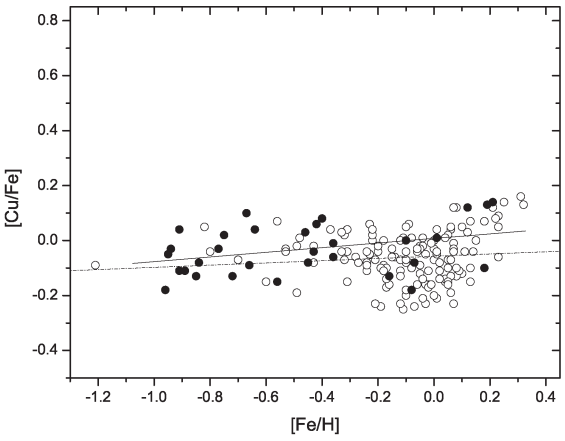

Figure 1: The run of [Cu/Fe] with [Fe/H]. Thick disk stars are marked as filled circles, and thin disk stars as open circles.

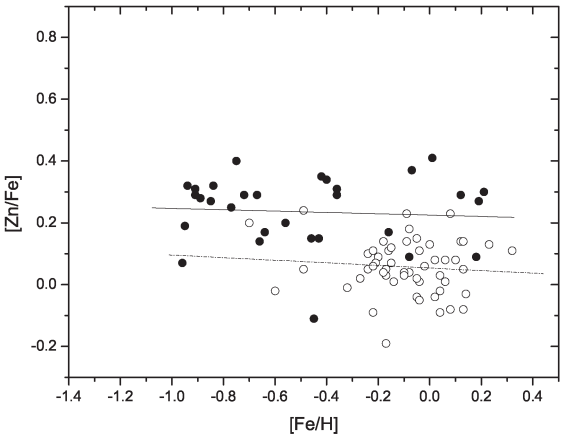

Figure 2: The run of [Zn/Fe] with [Fe/H]. The notation is the same as in Fig.1.

Among them 33 stars belong to thick disk populations according to their kinematics. As see from Fig.1, 2, the Zn abundance shows the higher dispersion than Cu abundance. The dependences of Cu and Zn abundances vs. [Fe/H] are also differ for these elements, that may be evidence of the various mechanisms responsible for production of these elements.

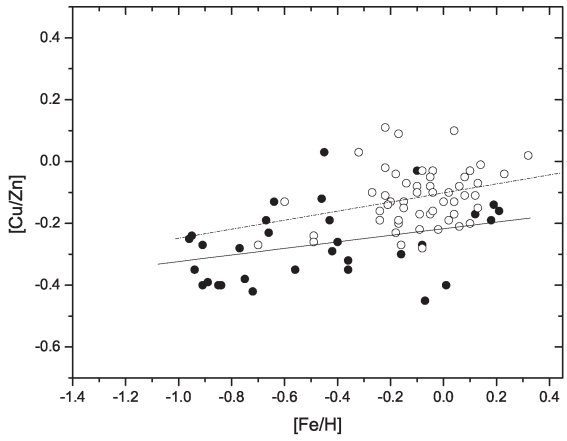

Figure 3: The run of [Cu/Fe] with [Zn/Fe]. The notation is the same as in Fig.1.

References

Galazutdinov G.A.: 1992, *Prepr.SAORAS*, **92**, 28.

Katz D., Soubiran C., Cayrel R., et al.: 1998, *A&A*, **338**, 151.

Kovtyukh V.V., Andrievsky S.M.: 1999, *A&A*, **351**, 597.

Kurucz R.L.: 1993, CD ROM n13.

Mishenina, T.V., Soubiran, C., Kovtyukh V.V., et al.: 2004, *A&A*, **418**, 551.

Steffen M.: 1985, *A&A*, **59**, 403.

Tsymbal V.V.: 1996, *ASP Conf. Ser.*, **108**, 198.

ESTIMATION OF THE MASS AND THE SPECIFIC MOMENT OF ROTATION OF A BLACK HOLE IN THE CENTER OF SPHERICAL CLUSTER M15

A.A. Kisselev, Yu.N. Gnedin, N.A. Shakht, E.A. Grosheva,
M.Yu. Piotrovich, T.M. Natsvlishvili

Central Astronomical Observatory at Pulkovo, St.-Petersburg, Russia

ABSTRACT. Using dispersions of radial velocities of stars, being near to the center of spherical cluster M15, and having applied integral of energy, we have estimated the minimal mass of the central body as 2×10^3 masses of the Sun. The estimation of kinetic energy of outflow of substance of the area surrounding a black hole in M15 also is fulfilled, and the size of the specific angular moment of rotation of a black hole a/M_{BH} is determined.

1. Introduction

Astrometric observations of double and multiple stars and stars with invisible satellites are conducted in Pulkovo observatory for many years on a Zeiss refractor ($D = 65$ cm, $F = 10.4$ m).

Using a technique of determination of orbits and masses of double stars we have taken part in an estimation of mass of the central object in the center of our Galaxy (Kisselev et al., 2007), using those data of observations of stars near to the center which were accessible from publications. The observations of ESO, (VLT) (Genzel et al. (2003) and Keck (Ghez et al., 2005) are available in view.

We managed to show, that with knowing of precise parameters of movement is possible to determine orbital elements and to estimate the mass having not on all visible ellipse, but by means of a small part of an arc. Also using the solution of a problem of two bodies we applied our methods to the estimation of mass of a supermassive black hole in the center of our Galaxy.

In the further in work (Kisselev et al., 2008) we have estimated mass of the central object of spherical cluster M15 by means of astrometric method using the energy integral which has been applied to the value of average space velocity, and also by means of astrophysical data.

2. Determination of mass of central object M15

For the astrometric approach we used radial velocities of 13 stars nearest to the dynamic center of a cluster in the field of $r < 1''$ (see fig.2 in work Kisselev, 2008) which have been received by means of Space Telescope Imaging Spectrograph (STIS) and are published in the article by Gerssen et al. (2002).

We have considered stars with a negative and positive dispersion of radial velocities from the list [5]. The dynamic analysis of these velocities has been carried out on the basis of a problem of two bodies as there were concrete objects with individual velocities for this solution.

We were limited to consideration of movements of stars only in small central area of a cluster ($r < 1''$), because the distribution of stars velocities has come to light in this area appeared not casual.

In the distribution of residual radial velocities

$$\Delta \bar{V}_r = V_r - \bar{V}_r \qquad (1)$$

there is a rotational movement of this group of stars relatively of an axis, whose projection on a picture plane is the axis with positional angle near to 130°.

For more general case (accidental distribution of velocities) we had been used also statistical properties of distribution of movements of stars according to theorem of Kleiber.

In our work (Kisselev, 2008), we used estimations of average distance up to a cluster: Cox et al.(1983); Harris (1996), MacNamara et al. (2004), which give on the average 10 kps.

Recently the study by Lugo et al. (2007) has been published, where the distance is determined by means of V and R photometry on stars RR Lirae available in a cluster. It has appeared equal 8.67 ± 0.41 kps.

Thus, at the account of new distance the area considered by us $r < 1''$ in the center of a cluster was reduced in the linear sizes from 10^4 a.u. up to 8.67×10^3 a.u. Radial velocities and their dispersion have not changed.

Accordingly, we receive following estimations of mass of a black hole in the center of a cluster.

Table 1: Data about spherical cluster M15.

$\alpha_{(2000.0)}$	$\delta_{(2000.0)}$	$l_{(2000.0)}$	$b_{(2000.0)}$	Size
$21^h27^m.6$	$+12°10'$	$65°05'$	$-27°00'$	19'×19'

In the case when the observed dispersions of velocities of stars near the center of a cluster we consider as a projection of the circular movements in a plane, parallel to a line of sight with velocity $V_r = 3.0$ a.u./year, the mass (M) of the central body in the field of $r = 1''$ ($r = 8.67 \times 10^3$ a.u.) is estimated according to integral of energy:

$$V^2 = 4\pi^2 M \left(\frac{2}{r} - \frac{1}{a}\right) \tag{2}$$

$$if\ r = a\ and\ V = V_r\ \ M_1 = \frac{rV^2}{4\pi^2} = 1.98 \times 10^3 M_\odot;$$

$$if\ \rho = 0.''5\ \ M_1 = 10^3 M_\odot \tag{3}$$

In the second case, if observed velocities of stars one can consider as a projection to a line of sight of velocities of stars chaotically moving about the center of a cluster, then according to theorem Kleiber: $|V_r| = 1/2\bar{V}$, $\bar{V} = 6$ a.u./year.

The mass M_2 determined by us for the second case will be equal:

$M_2 = 7.89 \times 10^3 M_\odot$, if $\rho = 1''$

and

$M_2 = 3.95 \times 10^3 M_\odot$, if $\rho = 0.''5$.

Thus, our former estimations of mass of the central body (a black hole) in the center of the cluster M15 received in Kisselev et al. (2008):

1) $M_1 = 2.28 \times 10^3 M_\odot$ and $M_1 = 1.14 \times 10^3 M_\odot$

2) $M_2 = 9.11 \times 10^3 M_\odot$ and $M2 = 4.56 \times 10^3 M_\odot$

have changed only proportionally to change of distance, because the basic observational data for research, namely, the relative radial velocities of stars, expressed in an absolute measure - have not changed.

Thus, if the dispersion of radial velocities $\{\Delta V_r\}$, is real, but it is not consequence of mistakes of measurements, then this dispersion is possible to explain an attraction of a supermassive star in the center of a cluster which mass is estimated according to integral of energy and makes from 1000 up to 8000 masses of the Sun.

It is necessary to notice also, that, the given estimations take place only in the event that observed stars of the central area really belong to cluster M15, but are not projected to a cluster, being placed, thus, on uncertain distance from the observer.

3. Astrophysical analysis

In the given work also we consider the specific angular moment of rotation of a black hole, which is key parameter and criterion of an belonging of an object or to metrics Kerr (if this object is a rotating black hole), or to metrics Schwarzschild (if rotation is absent).

The analysis of available black holes has shown, that the most probable value for a rotating black hole is $a/M_{BH} = 0.5$, however it is accepted to account, that if $a/M_{BH} > 0$ the object also corresponds to metrics Kerr.

Discovery of some supermassive black holes on greater cosmological distances has allowed to consider black holes of intermediate masses as initial stage of supermassive black holes.

Such objects at which mass M is in following limits: $10M_\odot < M < 10^5 M_\odot$ are considered as black holes of intermediate masses. According to new data such objects can be in the central areas of spherical clusters.

Astrophysical research of M15 gives a weak inconsistent results concerning mass of the central object. However authors of these researches recognize, that the black hole can exist in the center of a cluster.

It is revealed now, that in M15 there is no essential X-ray flux, which it would be possible to expect as a result accretion of gas on a black hole. But it does not contradict the possibility of existence of other mechanisms of extraction of energy from a rotating black hole.

The scientific explanation of process of extraction of energy from a black hole is one of the central problems of modern astrophysics.

Straumann (2007) and Blanford (1977) have suggested electromagnetic process of energy extraction from a rotating black hole. Here the essential role plays the magnetic field captured by a black hole amplified by rotation of a black hole near to horizon of being events. As a result of such process from a vicinity of a black hole there is a strong expiration of plasma both in the form of magnetic wind, and in the form of relativistic jet.

Other variant of this process is process of magnetic coupling between the central rotating black hole and a accretion disk surrounding it (see, for example, Blanford, 1999). In this case energy and the angular moment are taken from accretion on a black hole of substance.

We have stopped on last variant. At first the power of energy L_{BZ} from a rotating black hole in view of metrics Kerr has been obtained. Then the strength of magnetic field B_H near to horizon of events according to a relation between the strength of magnetic field B_H on horizon of events and magnitude of mass of central massive black hole M_{BH} by means of following formulas has been obtained:

$$L \equiv L_{BZ} = (1/32)\omega_F^2 B_H^2 R_H^2 c(a/M)^2 \qquad (4)$$

$$\omega_F^2 = \Omega_F(\Omega_H - \Omega_F)/\Omega_H^2 \qquad (5)$$

Here L is the power of energy, Ω_H and Ω_F are angular velocity of rotation of a black hole and magnetic power lines accordingly, $\omega_F^2 = 1/2$.

$$R_H = \frac{GM_{BH}}{c^2}\left(1 + \sqrt{\left(\frac{a}{M_B H}\right)^2}\right) \qquad (6)$$

Following step was determination of the angular moment of rotation a/M_{BH} with use of equality of kinetic energy L_{kin} and L_{BZ}.

It has appeared that $a/M_{BH} = 0.08$. Thus, it is possible to make the conclusion of that the given object can be considered within the limits of Kerr metric.

4. Conclusions

For small sample inside of a cluster ($r \leq 1''$) distribution of radial velocities which can be interpreted as reflection of rotary movement of the given subsystem as the whole is revealed. Having accepted average velocity of the rotation as 14 km/s, (3 a.u./year), the mass of the central kernel of a cluster at the assumptions mentioned above cannot be less than 2.0×10^3 masses of the Sun. The size of the specific angular moment of rotation of a black hole a/M_{BH} in view of value of the mass received by an astrometric method is determined.

Acknowledgements. Our study is supported by Russian grant: Sci.School: 6110-2008.02. Also our research was supported by the RFBR (project No. 07-02-00535a), Program of Prezidium of RAS "Origin and Evolution of Stars and Galaxies", the Program of the Department of Physical Sciences of RAS "Extended Objects in the Universe". This research was also supported by the Grant of President of Russian Federation "The Basic Scientific Schools" NS-6110.2008.2. M.Yu. Piotrovich acknowledges the Council of Grants of President of Russian Federation for Young Scientists, grant No. 4101.2008.2.

References

Blanford R.D., Znajek R.L.: 1977, *MNRAS*, **179**, 433.
Blanford R.D.: 1999, *ASP Conf. Ser.*, **160**, 265.
Cox A.N., Hudson S.W., Clancy S.P.: 1983, *Astropys. J*, **264**, 94.
Genzel R., Schödel R., Ott T. et al.: 2003, *Astrophys. J*, **594**, 812.
Gerssen J., van der Marel R.P., K. Gebhardt et al.: 2002, *Astron. J*, **124**, 3270.
Ghez A.M., Salim S.D., Hornstein S.D.: 2005, *Astrophys. J.*, **620**, 744.
Harris W.E.: 1996, *Astron. J*, **112**, 1487.
Kisselev A.A., Gnedin Yu.N., Grosheva E.A., Shakht N.A., Gorshanov D.L., Piotrovich M.Yu.: "The Supermassive Black Hole at the Center of Our Galaxy: Determination of Its Main Physical Parameters", 2007, *Astronomy Reports*, **51**, # 2, 100.
Kisselev A.A., Gnedin Yu.N., Shakht N.A., Grosheva E.A., Piotrovich M.Yu., T.M. Natsvlishvili: 2008, *Pis'ma v AJ*, **34**, # 8, 585.
Lugo G.G., Ferro A.A., Rosenzweig P.: 2007, *Proc IAU Symp* **240**, 605.
MacNamara B.J., Harrison T.E., Baumgardt H.: 2004, *Astron. J.*, **602**, 264.
Straumann N.: 2007, arXiv:0709.3895.

Non-LTE LINE FORMATION FOR S I

S.A. Korotin
Department of Astronomy, Odessa National University
T.G.Shevchenko Park, Odessa 65014 Ukraine, *serkor@skyline.od.ua*

ABSTRACT. A comprehensive model atom for non-LTE line formation calculations for neutral sulfur in the spectra of F-K stars is presented. All the calculations were made using the 65-level atomic model of S I and Kurucz's atmosphere models with $T_{\rm eff} = 5000 \div 6500$ K, log $g = 2 \div 4$ and $[Fe/H] = -4 \div 0$. It was found that the lines of different multiplets are differently sensitive to the NLTE effects. The NLTE corrections themselves are quite small (about –0.1 dex) for the lines 6543-6557 Å, they increase up to –0.26 dex for 8694 Å line, and achieve –1.1 dex for IR triplet 9212-9237 Å. The atomic model adequacy was checked by modeling of the sulfur lines that belong to the investigated multiplets in the solar spectrum, as well as in the spectra of two main sequence and two giant stars. Good fit between calculated and observed profiles is obtained. It was showed that the rather high sulfur overabundance found in some metal-deficient stars can be explained as a result of neglecting of the strong NLTE effects.

Key words: atomic data - line: formation - star: abundances

1. Introduction

At present time it is not clear whether we have correct knowledge about the sulfur abundance in galactic halo stars. In some works (Nissen et al. 2004, 2007, Ryde and Lambert 2004) it was reported that the stars with metallicity $-3 <$[Fe/H]< -1 sulfur shows systematical overabundance at the level of 0.3 dex, and this is in a good agreement with predictions of the galactic chemodynamical models. The main source of the metals in early Galaxy is SNeII. The ration [S/Fe] decreases at [Fe/H]>–1 because of the iron abundance increase due to SNeIa, At the same time some investigators (Israelian and Rebolo 2001) find the larger sulfur overabundances (up to +0.8 dex) in the stars with [Fe/H]=–2. There is an attempt to explain such overabundances by the shorter time of the mixing, or by the hypernovae explosions.

The sulfur abundance in metal-poor stars is based on an analysis of 8694 Å and 9212-9237 Å lines. As it was showed by Takeda et al. (2005) all these lines are subject of NLTE effects. Authors used photoionization cross sections found in hydrogen-like approximation. Oscillator strengths were taken from incomplete list of Kurucz.

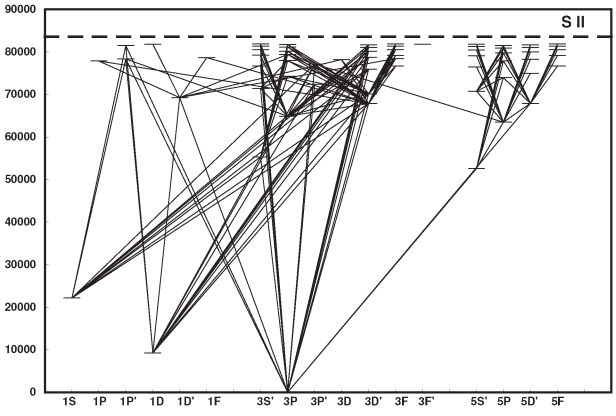

Figure 1: Grotrian diagrams for S I.

2. The S I model atom

In our calculations we used modified program MULTI (Carlsson 1986). The sulfur atomic model consists of 64 lower singlet, triplet and quintet systems of SI and the ground level of SII (Fig. 1). The radiative photoionization rates for all considered levels were calculated using the detailed photoionization cross-sections listed in OP TopBASE. The detailed consideration comprises 137 radiative b-b transitions (allowed and inter-combination transitions). The radiative rates of the other 200 very weak radiative transitions were adopted to be constant and they were calculated in LTE. Oscillator strengths are from OP TopBASE.

In the visual and near IR parts of the spectrum of metal-poor stars there are only a few sulfur lines which are appropriate for the abundance determination. Among them there multiplet 1 (9212-9237 Å), 6 (8694 Å) and 8 (6743-6757 Å). The rest of the lines are very weak or blended.

To check the model we calculated the line profiles for

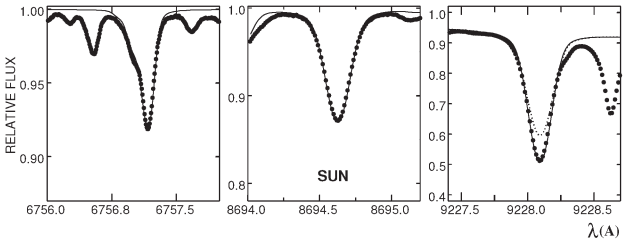

Figure 2: Comparison of the calculated and observed profiles of sulfur lines in a spectrum the Sun. The dotted lines show the LTE and solid lines - nonLTE profiles.

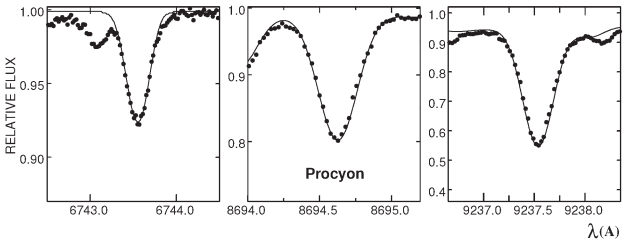

Figure 3: Comparison of the calculated and observed profiles of sulfur lines for Procion.

the different multiplets in the solar spectrum. For the lines of 1st multiplets that are situated in the wing of the hydrogen line we have first calculated with MULTI b-factors and then used these factors in the LTE synthetic spectrum code STARSP (Tsymbal 1996). Thus we calculated LTE synthetic spectrum in vicinity of the sulfur lines, while their own profiles were calculated with NLTE source function.

There is a goof agreement with observed profiles (Fig. 2). The dashed line represents LTE profiles. It is seen that there is significant difference between LTE and NLTE profiles for the lines of 1st multiplet, while the lines of 6^{th} and 8^{th} multiplets are not suffered from NLTE effects. The same test has been performed for the two main sequence stars and two supergiants. Again, a good agreement is seen in Fig. 3.

3. NLTE effects for sulfur lines

We have calculated profiles and equivalent widths of the spectral lines for the grid of the atmosphere models in the range of effective temperatures 5000-6000 K with [Fe/H] from 0.0 to –4.0 and log g from 2 to 4. For the metal-poor stars we have performed calculations with [S/Fe] = +0.3, since in these stars some the alpha-elements have increased abundance. In all the cases LTE abundances of sulfur were larger than those found within the NLTE approximation (Fig 4.).

Table 1: Atomic data of used spectral lines.

λ (Å)	log gf	Γ_{rad}	Γ_{wv}
8694.626	0.08	7.62	-6.98
9212.863	0.42	7.47	-7.37
9228.093	0.26	7.46	-7.37
9237.538	0.04	7.46	-7.37
6743.440	-1.200	7.58	-7.12
6743.531	-0.850	7.58	-7.12
6743.640	-0.950	7.58	-7.12
6748.573	-1.320	7.58	-7.12
6748.682	-0.730	7.58	-7.12
6748.837	-0.530	7.58	-7.12
6756.851	-1.670	7.59	-7.12
6757.007	-0.830	7.59	-7.12
6757.171	-0.240	7.59	-7.12

As one can see the lines of 8^{th} multiplet practically are not affected by NLTE effects, but these lines become very weak to be used at [Fe/H] $<$ –1.5. The same picture is seen for 8694 Å, but this line is much more sensitive to the departure from LTE.

The lines of the 1^{st} multiplet are strongly influenced. There is significant dependence of the NLTE corrections upon log g and $T_{\rm eff}$. Corrections become larger with metallicity increase, achieving maximum value of about 1.1 dex at [Fe/H] = –2, then corrections decrease.

NLTE corrections for the lines of considered multiplets are qualitatively the same but with different values. Fig. 5 shows this difference as a function of $T_{\rm eff}$ for log g = 2 and 4, and [Fe/H] = –2. Fig. 6 shows a dependence of the NLTE corrections as a function of V_t for 1^{st} and 6^{th} multiplets. One can note apparently complicated form of this dependence.

Summarizing one can make a conclusion that calculated grid of the NLTE corrections should be used with a caution, taking into account an influence from the microturbulent velocity, metallicity, temperature, luminosity and individual characteristics of the certain sulfur line. For the more precise determination one needs to perform a direct NLTE calculation of the sulfur line profiles.

References

M. Carlsson: 1986, *Uppsala Obs. Rep.* **33**, 1.
Israelian G., Rebolo R.: 2001, *Astrophys.J.* **557**, 43.
Nissen P.E., Chen Y.Q., Asplund M., Pettini M.: 2004, *Astron. Astrophys.*, **415**, 993.
Nissen P.E., Akerman C., Asplund M. et al.: 2007, *Astron. Astrophys.*, **469**, 319.
Ryde N., Lambert D.L.: 2004, *Astron. Astrophys.*, **415**, 559.
Takeda Y., Hashimoto O., Taguchi H., et al.: 2005, *PASJ*, **57**, 751.
Tsymbal V.V.: 1996, *ASP Conf. Ser.*, **108**, 198.

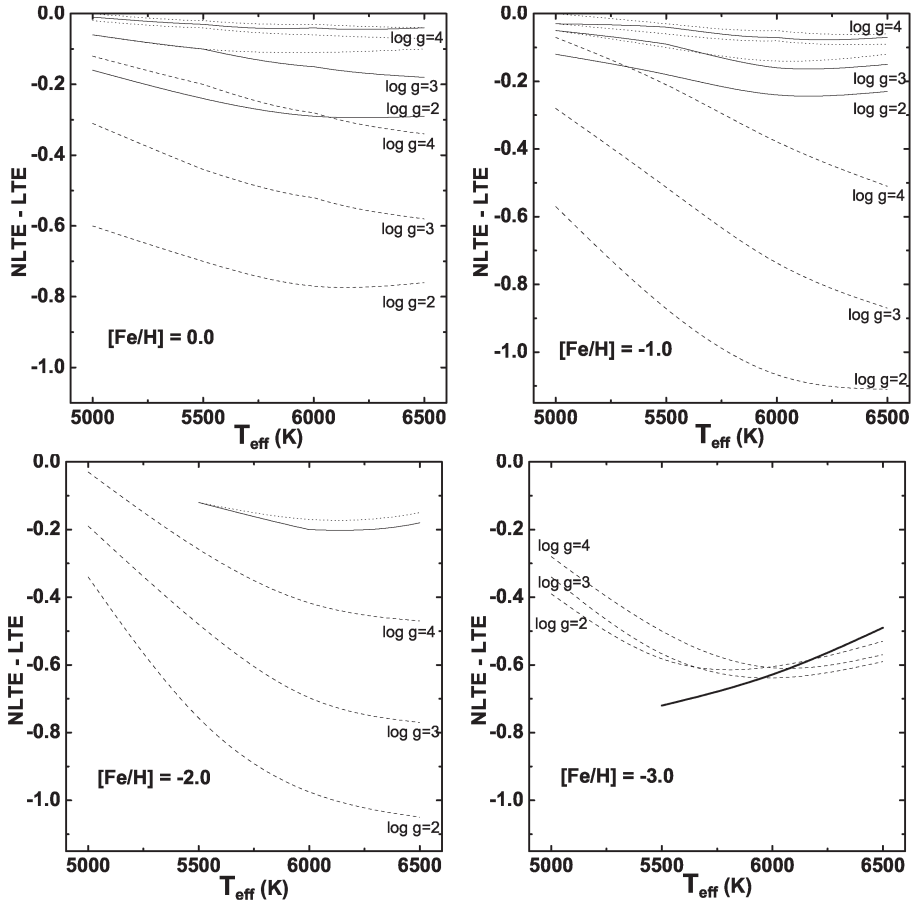

Figure 4: NLTE corrections computed as a function of the temperature and the metallicity of the model. NLTE corrections for lines 9212 Å show dashed lines; for lines 8694 Å - solid lines; and for lines of the eighth multiplets - dotted lines.

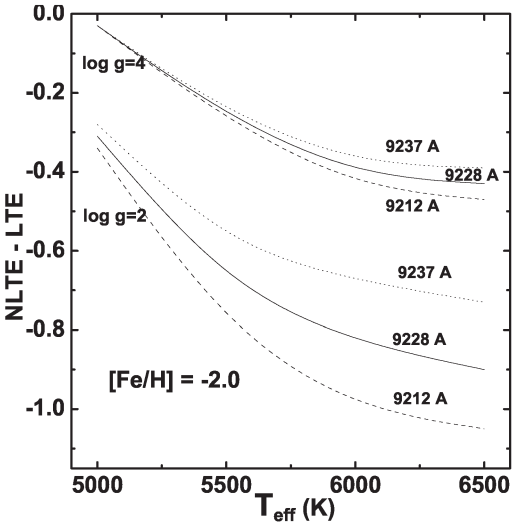

Figure 5: NLTE corrections for three lines of the first multiplets for model atmospheres with log $g = 2$ and 4 and [Fe/H]$= -2$.

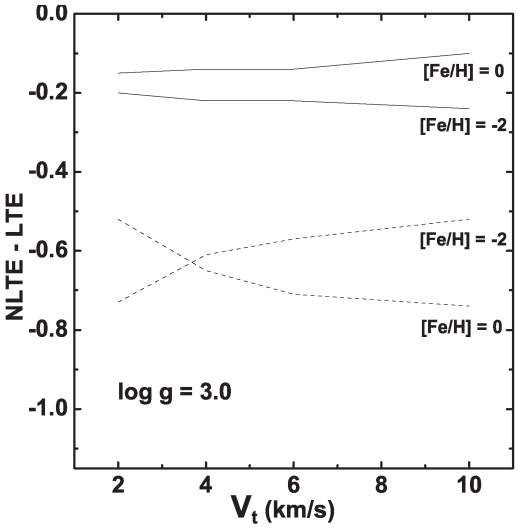

Figure 6: NLTE corrections computed as a function of the $V_{\rm t}$ for lines of the first and the sixth multiplets ($T_{\rm eff} = 6000$ K, log $g = 3$, $[Fe/H] = -2.0$).

EVOLUTIONARY CHANGES OF THE KINEMATICS OF THE GALACTIC THIN DISK STARS IN THE SOLAR NEIGHBOURHOOD

V.V. Koval[1], T.V. Borkova[1], V.A. Marsakov[1]

[1] Southern Federal University
Rostov-on-Don 344090 Russia,
koval@ip.rsu.ru, borkova@ip.rsu.ru, vmarsakov@ip.rsu.ru

ABSTRACT. According to the data of Nordstrőm et al. (2004) catalog is carried out the comparative analysis of the velocity ellipsoid parameters of the galactic disk stars of different metallicity and the character of their change from the age is investigated. It is shown, that dispersions of all three components of spatial velocities increase with age, submitting to the power law $\sigma_i \sim t^{0.26}$, i. e., exponent proved to be beyond the ranges of errors less than previously usually obtained It is discovered a difference in the values of the semiaxes of velocity ellipsoids between stars with the metallicity more and less [Fe/H] ≈ -0.3, which can evidences about a difference in the dynamic state of the matter, from which they were formed. It is established that the form of the velocity ellipsoids of the stars of different metallicity in the course of time does not change – ellipsoid simply increases in the sizes and is turned. After exception of the stars of the moving groups the character of dependences on the age of the velocity ellipsoids parameters did not undergo the significant changes.

Key words: Galactic disk, velocity ellipsoid, moving groups.

Introduction

The observable morphological structure of the thin disk of our Galaxy, as well as any its other subsystem, is obliged to exclusively instantaneous shapes of orbits of the stars entering into it. Therefore the "external" form of the Galaxy can be recreated on the total three-dimensional velocities of the stars located even in the nearest vicinity of the Sun. It is simultaneously possible to attempt to trace the dynamic evolution of the thin disk subsystem on the stars of different age. A research of the dependences of the velocity ellipsoid parameters of nearest stars on the age is the classical method of the extraction of such information.

The properties of velocity ellipsoids can serve as a key for solving of both the problem of stationarity and the relaxation, and also they can shed light to the most important questions of star formation. If in the Galaxy effective relaxation mechanism acts, thus it should lead system to the steady state, in which the form of velocity ellipsoid depends only on rotation curve. But if the relaxation is insufficiently effective, then the relations of the semiaxes of ellipsoid can differ from steady-state values and should depend on the mechanism of relaxation.

Character of dependences between the age and the velocity dispersions in close field stars was investigated in many works on the basis of contemporary astrometric and spectroscopic measurements. In this case the exponent on the different samples of stars occurred within the limits from $\gamma \approx 0.33$ (Binney et al., 2000), to $\gamma \approx 0.5$ (Funch et al., 2001; Holmberg et al., 2007). Unfortunately, in all these works the dependence was built on all close field stars, among which is present a noticeable quantity of stars of the thick disk.

For obtaining the correct results it is necessary to remove stars of so-called Eggen moving groups from the sample of thin disk stars also. It is known, that in the Solar vicinity about third of stars it is possible to identify by members of various moving group. All these streams distort the velocity field of field stars of different age and hamper the extraction of the information, necessary for restoration of dynamic evolution of the Galaxy.

In order to verify, they do have an effect on the values of dispersions existence of the moving groups in the disk, we calculated the values of velocity ellipsoids both according to all field stars and after excluding the stars of the moving groups. In connection with much discussed recently existence of very old and simultaneously metal rich stars we traced also a change in the parameters of ellipsoids for the stars of the thin disk of different metallicity.

As the basic source the Geneva-Copenhagen catalog,

which contains ages, metallicity and kinematics for 14000 F–K- dwarfs (Norstrőm et al., 2004) was used. This catalog contains the stars not only of the thin disk subsystem, but also of the thick disk of the Galaxy. To select the stars of the thin disk it is necessary to use any criterion, however the unique and sufficient criterion there does not exist. The criterion used by us calculates the probabilities of a belonging of star to the thin disk subsystem against the alternative of belonging of it to the thick disk. Procedure of the calculation of the corresponding probabilities, which are based on the values of the dispersions of the components of the three-dimensional velocities $(\sigma_U, \sigma_V, \sigma_W)$ and the average rotational velocities of a subsystems (V_{asym}), is developed in Bensby, et al. (2003). As a result we receive the sample, for which probability of a belonging of stars to the thin disk above probability of their belonging to the thick disk subsystem. Then from the sample were removed the noted in the catalog binary stars, far evolutionized stars $(\delta M_V > 3^m)$ and star uncertainly obtained ages $(\epsilon t > \pm 3$ Gyr), as a result in the our sample remained 5116 single stars of the thin disk. For the account of influence of stars of moving groups on integrated kinematic parameters of stars of the thin disk we have counted sufficient to exclude from the sample of a star of the largest known streams. Such proved to be about 12 % of stars from the entire sample.

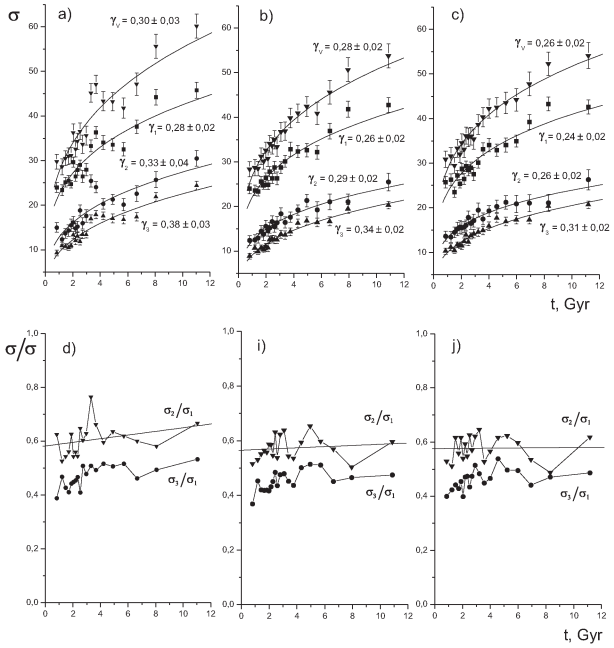

Figure 1: Relation semiaxes values of the stellar velocity ellipsoids (1a,1b,1c) and relationship of semiaxes values (1d,1i,1j) of age.

Results and discussions

Special interest was caused always the dependence of the velocity dispersion of starry populations on their age $\sigma_V(t)$, since by the character of this connection it is possible to judge whether there was a relaxation in the galactic disk and even to specify the mechanism, which increases in this case the peculiar velocities of stars. From the size of an exponent it is possible to judge the character of the heterogeneities of the gravitational potential of the Galaxy, which lead to a continuous increase in the velocity dispersion of the stars which have born simultaneously, that is to their "warming up".

On the panel (a) of Figure **??** are given the dependences of $\sigma_i \sim (t)$ for all close stars, while on the panel (b) – for the selected stars of the thin disk. All dependences by the method of least squares are approximated by the power law of the form of $\sigma_i \sim t^{\gamma}$. One can see well, that although the character of dependences was kept, but sizes of all exponents γ for the similar dispersions have noticeably decreased. And if for all close stars the values of exponents have turned out coincided with obtained usually by other authors and are equal on the average $\langle\gamma\rangle = 0.32 \pm 0.04$, then for the correctly selected stars of the thin disk all indices became somewhat less $\langle\gamma\rangle = 0.29 \pm 0.03$. An additional research showed that the application of a less strict criterion leads only to the small overstating in the oldest groups only of value of major semiaxis, whereas average and minor semiaxes remain in them constant. The exponents of all dependences within the limits of errors also did not change. In Fig. **??** c the age-semiaxes diagram for the thin disk stars without the moving groups are given. From the figure one can see that the exception of star streams has in turn led to the small (again within the ranges of errors) decrease of the values of all semiaxes of the star subgroups of each age – all dependences were simply displaced downward to themselves. As a result the exponents of all dependences still decreased up to the average value $\langle\gamma\rangle = 0.26 \pm 0.03$ and began to differ already beyond the ranges of errors from those receiving on all close stars.

Interest causes also the relation of semiaxes, mainly the ratio of average axis to the large one. In the second row of Figure **??** the dependences on the age of the values of the relations of semiaxes for all close field stars, for the stars of the thin disk and for the thin disk stars without the moving groups are consistently given. From the figure one can see that the values of the relations of semiaxes in the appropriate subgroups of different age practically did not change. Approximation by the direct regressions of variation on the age of these relations did not reveal the statistical significant trend. As a result it is possible to conclude that the form of the velocity ellipsoid of the stars of the thin disk does not depend on age.

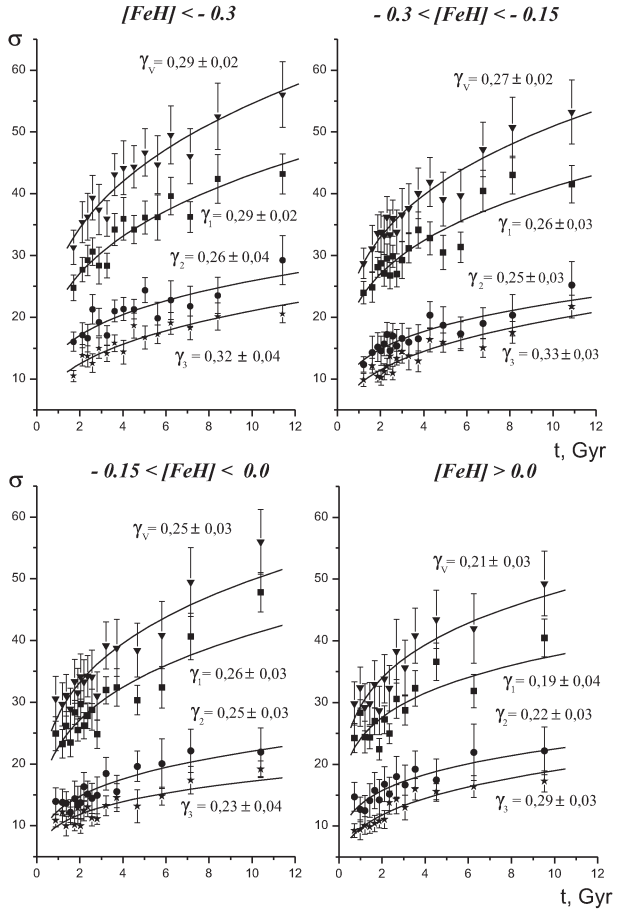

Figure 2: Relationship between the semiaxes values of the stellar velocity ellipsoids of different metallicity and age.

On (Fig. **??**) changes in the values of the semiaxes of the velocity ellipsoids of the stars of different metallicity from age are shown. It is evident from the figures that the behavior of all semiaxes is approximately identical. As well as generally, this change is described by power law with the same exponent $\langle\gamma\rangle = 0.26 \pm 0.06$.

We will note that most metal poor stars demonstrate the greatest sizes of semiaxes at any age. It seems that metal poor stars are formed from the matter of that falling into the galactic plane from the external parts of the Galaxy.

Conclusions

The properties of the velocity ellipsoid parameters of the thin disk stars in the dependence on the age and the metallicity are investigated. It is shown that a change in the course of time in the values of all ellipsoid semiaxes of star of different metallicity, are described by power law with the approximately identical exponent $\langle\gamma\rangle = 0.26 \pm 0.02$. This result contradicts the results, obtained in other works, where the index is located in the range $(0.33 - 0.50)$. It is discovered, that the semiaxes size of the thin disk stars with metallicity [Fe/H] ≤ -0.30 at any age have more than ones of more metal rich stars. Investigating chemical composition in the thin disk, we have found out that among so metal poor stars appears much with the anomalously high relative contents of magnesium (Marsakov, Borkova, 2006). Presence of the metal poor stars with different kinematics and the relative content of magnesium testifies in favor that these stars could be formed from the matter, which fell into the thin disk as a result of accretion from the regions with another history of chemical evolution. In this case the parameters of the velocity ellipsoids of the stars of different metallicity can reflect the state of interstellar medium at the moment of their generation. It is finally shown that the velocity ellipsoids of the thin disk stars are far from on state of equilibrium and depend neither from the age nor from the metallicity – ellipsoids simply vary in the sizes and are turned.

The full text of this report will be published in "Pis'ma v Astronomicheskii Zhurnal".

Acknowledgements. This work was supported by the Federal Agency for Education (projects RNP 2.1.1.3483 and RNP 2.2.3.1.3950)

References

Allen C., Santillan A.: 1991, *Mexicana Astron. Astrophys.* **22**, 255

Assian R., Figueras F., Tjrra J., Chen B.: 1999, *Astron. Astrophys.* **341**, 427

Borkova T.V., Marsakov V.A.: 2005, *Astron. Zh.,* **82**, 453

Borkova T.V., Marsakov V.A.: 2006, *Pis'ma Astron. Zh.,* **32**, 577

Girargi L., Bressan A., Chiosi C., et al.: 2000, *Astron. Astrophys.* **141**, 371

De Simone R.S., Wu X., Tremaine S.: 2004, *Mon. Not. Roy. Astron. Soc* **350**, 627

SPECTRAL LUMINOSITY INDICATORS FOR FGK SUPERGIANTS AND CLASSICAL CEPHEIDS

V.V. Kovtyukh, F.A. Chekhonadskikh

Dpt. of Astronomy and Odessa Astronomical Observatory, Odessa National University
T.G.Shevchenko Park, Odessa 65014 Ukraine, *val@deneb1.odessa.ua, chehonadskih@gmail.com*

ABSTRACT. We have determined 28 relations between M_v, $T_{\rm eff}$ and line depths ratios $R_{\lambda1}/R_{\lambda2}$. These relations have been used for the estimation of the absolute magnitudes M_v of 56 FGK supergiants with an error 0.05-0.30 mag (Table 1). The application range is F0–K0, luminosity classes I and II.

Key words: Stars: fundamental parameters; stars: absolute magnitudes; stars: supergiants.

1. Introduction

FGK-supergiants are very luminous stars and can be seen to large distances. However, being rare stars and residing in the galactic plane, they are are normally severely reddened. This fact presents a serious problem for studying supergiants, in particular when trying to infer their intrinsic luminosities. Cepheid Period–Luminosity (PL) relation remains the primary tool for determination of the distances within the Local Group and to the nearby galaxies. The absolute calibration of this relation relies on the accurate estimates of the distance of the calibrating Cepheids and their interstellar extinction and reddening. For non-periodic variable supergiants, obviously, PL relation is not applicable. Other techniques need to be developed for determination of the absolute stellar magnitudes and luminosities for a wide range of supergiants. In this work we turn to spectroscopy to search for the luminosity-sensitive features.

Calibrations of absolute magnitude from OI 7774 Å data are derived from narrow-band photometry and low dispersion spectroscopy for A0-G2 stars were presented by Arellano Ferro (1993). These calibrations allowed to estimate absolute magnitude with accuracies of 0.6 mag, they were improved (Arellano Ferro, Giridhar & Rojo Arellano, 2002) and then it was achieved accuracies of 0.38-1.5 mag for non-periodic supergiants and 0.42-0.43 mag for Cepheids. But the disadvantage of this method is the difficulty of observing and measuring the equivalent width of the OI 7774 Å feature in faint distant stars.

A further reaching approach is the calibration of the stellar absolute magnitude in terms of the photometric color indices. Arellano Ferro & Parrao (1990) were offered an independent calibration of the *uvbyβ* photometric system to determine absolute magnitudes for luminous F-G supergiants, using as calibrators non-periodic yellow supergiants whose reddenings and absolute magnitudes are believed to be known. The similar and parallel research was presented by Gray (1991).

Andrievsky (1998ab) suggested to use the lines of the BaII to calibrate absolute magnitudes of non-periodic supergiants and low-amplitude Cepheids.

Apart from OI 7771-4 Å and Ba II, other lines in photospheric spectra of supergiants seem to evolve with luminosity. The ion lines behave similar to BaII, and the S I trough is strongest for supergiants with higher luminosity (if $T_{\rm eff}$ is constant). In particular, the ratio of the strengths of the Fe I and Fe II lines, was suggested as a potential luminosity indicator (for example, see Fig.1,2). The ratio Fe II/Fe I depends essentially on the strength of Fe II line, because Fe I line is about constant. In more luminous objects, Fe II is stronger because of a rapidly increasing Fe lI/Fe I ratio. Thus, the correlation between FeI/FeII ratio and luminosity is the effect of ionisation balance and NLTE effects.

Similar correlations are observed between luminosity and others ion line depths (for a given temperature). As example, Fig. 3 shows our measurements of depth of the Fe II 6129.69 Å and Si I 6155.14 Å lines. While the depths clearly increase with decreasing temperature, $R_{\lambda1}/R_{\lambda2}$ is approximately constant in all measurements. The resulting ratio 6129.69 FeII/6155.14 SiI vs Mv as shown in Fig. 4. The value increases towards higher luminosities.

The accuracy of spectroscopic luminosity determination could be improved if additional luminosity indicators were found that rely on species other than Fe. A number of such quantities has already been investigated (TiII/FeI, SI/FeI, FeII/NiI, ScII/FeI, YII/FeI etc). We selected in priority lines belonging to the iron-peak elements (such as Si, Ti, V, Cr, Fe, Ni) because they have a negligible star to star variation in element

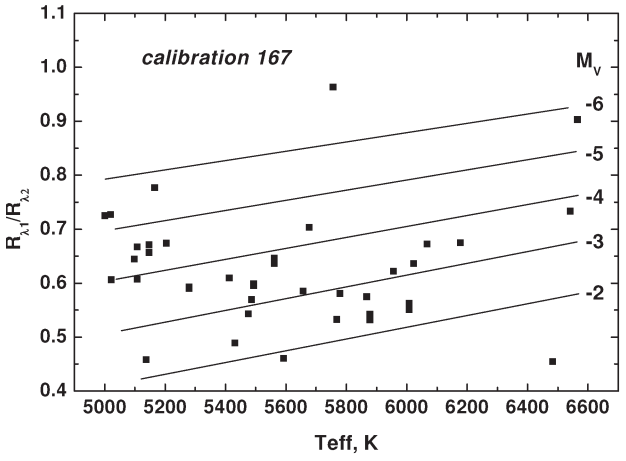

Figure 1: Calibration of the ratio 6129.69 FeII/6055.99 FeI in terms of the absolute magnitude M_v and temperature $T_{\rm eff}$ (calibration 167).

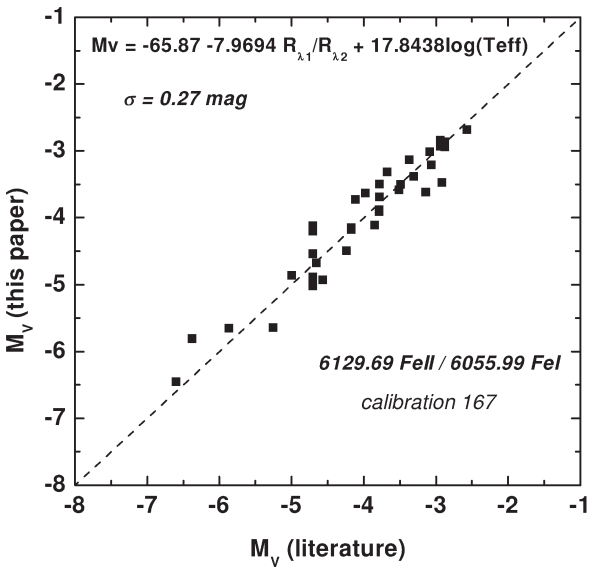

Figure 2: Comparison of our M_v with estimates from the literature for 6129.69 FeII/6055.99 FeI ratio (calibration 167).

abundances.

The aim of this paper is to determine M_v for F, G and K supergiant stars and Classical Cepheids from these new spectroscopic indicators.

2. Observations

The spectra of the FGK supergiants were obtained using the 1.93 m telescope of the Haute-Provence Observatoire (France) equipped with the echelle spectrograph ELODIE (Baranne et al. 1996) and retrieved from its online archive of spectra (Moultaka et al. 2004). The resolving power was R = 42 000 over the wavelength interval 4400-6800 ÅÅ, with a signal-to-noise ratio for each spectrum of S/N>100 (at 5500 ÅÅ). Initial processing of the spectra (image extraction, cosmic ray removal, flat-fielding, etc.) was carried out as described by Katz et al. (1998).

We also made use of spectra obtained with the Ultraviolet-Visual Echelle Spectrograph (UVES) instrument at the Very Large Telescope (VLT) Unit 2 Kueyen (Bagnulo et al. 2003). All supergiants were observed in two instrumental modes, Dichroic1 (DIC1) and Dichroic2 (DIC2), in order to provide almost complete coverage of the wave-length interval 3000-10 000 Å. The spectral resolution is about 80 000, and for most of the spectra the typical S/N ratio is 300-500 in the V band.

For Classical Cepheids we have used our published results (see Kovtyukh et al (2008) and references therein). We have used only phases of maximum radius (radial velocity V_{rad}=0 km s^{-1}) because at the phases of maximum radius (and close phases) an influence from the "dynamical" term on the luminosity indicators should be negligible. During the maximal compression of the Cepheid envelope the strong ther-

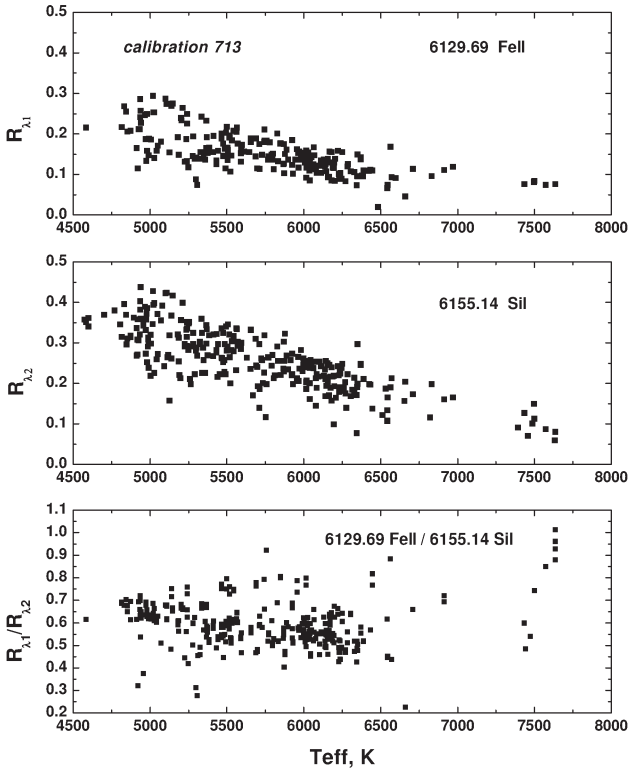

Figure 3: Behavior of depth of the FeII 6129.69 Å and SiI 6155.14 Å lines (calibration 713). See text for comments.

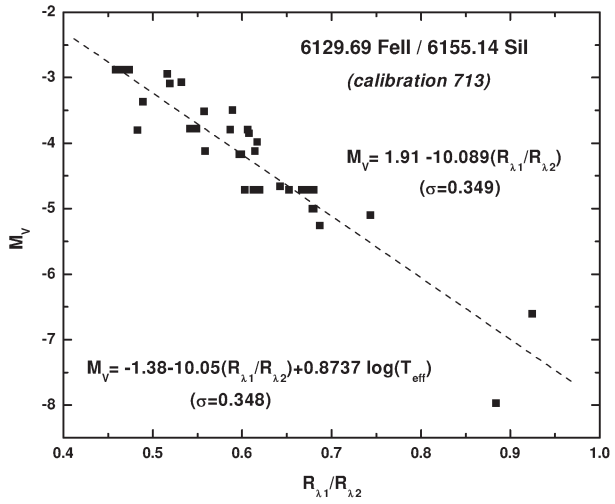

Figure 4: Comparison of our M_v with estimates from the literature for calibration 713 (see Fig.3).

mal and dynamical effects (like shock waves) are expected, while the phases at the maximum radius may be considered as the rather "quiet" ones enabling one to search for some dependencies between the Cepheids' M_v and their spectral luminosity indicators.

The further processing of spectra (continuum level location, measuring of line depths and equivalent widths) was carried out by us using the DECH20 software (Galazutdinov 1992). Line depths R_λ were measured by means of a Gaussian fitting.

3. Results

The next step was to choose the initial M_v for supergiants. This is a very important procedure since it affects the accuracy of the final luminosity scale, namely, the run of the systematic error with M_v and $T_{\rm eff}$. For 25 supergiants from our sample (see Table 1) we based the initial M_v estimates on the following 4 papers: Arellano Ferro & Parrao (1990), Gray (1991), Arellano Ferro (1993), Arellano Ferro, Giridhar & Rojo Arellano (2002). The effective temperature for supergiants has been determined using the calibrating relations from Kovtyukh (2007). These relations combine the effective temperature with a set of spectral line depth ratios. The internal accuracy of the effective temperature determined in this way is rather high in the temperature range 5000 K to 6500 K: typically 150 K or less (standard deviation or 10 to 20 K for the standard error). Another very important advantage of this method (or any spectroscopic method) is that it produces the reddening-free $T_{\rm eff}$ estimates. For 10 classical Cepheids we have used our previously published results (M_v and $T_{\rm eff}$).

Using the least-square method we have obtained 28 relations of the form:

$$M_v = a + b(logT_{\rm eff}) + c(R_{\lambda1}/R_{\lambda2}) + d(R_{\lambda1}/R_{\lambda2})^2,$$

where a,b,c,d – constants. Starting with an published value M_v, the relations are then self calibrated by an iterative process. Our final estimates have been compared to published M_v and show a good agreement (Fig. 5). In Table 1 we report M_v for 56 supergiants derived from our calibrations. Each entry includes the name of the star, $T_{\rm eff}$, mean M_v, error (σ), number of calibrations used, and the error of the mean (σ_{mean}).

The averaging of M_v obtained from 10-25 line ratios significantly reduces the uncertainty from a single calibration. The final precision we achieve is 0.05-0.30 mag (1 sigma), for the spectra of R=42 000, S/N=100–150. This can be further improved with higher resolution and larger S/N. We note that this error budget does not include the possible uncertainties that arise from the individual properties of stars, like rotation, chemical composition, binarity, etc.

4. Discussion

Having clarified the behaviour of observed FeI/FeII values, we now briefly discuss the use of line strengths ratios as luminosity indicators. We have shown that FeII/FeI correlates with luminosity. Thus, FeII/FeI should be the most direct and meaningful luminosity indicator. There are, however, uncertainties even in FeII/FeI as a spectroscopic luminosity indicator. First, the trend in the line is due to the combination of trends that are nonlinear in temperature, luminosity and also in [Fe/H] in the relevant ranges. In order to obtain luminosities from spectra, one has to choose an appropriate functional form (e.g. linear, second or third order) to fit the relation between line strength ratio, temperature and luminosity. Inaccuracies introduced by the use of such a functional form can easily be overlooked or misinterpreted as scatter. Second, intrinsic variations in the supergiants and their spectra limit the precision of spectroscopic luminosity indicators. Differences in the abundance distributions (e.g. He, C, N, O) among equally luminous supergiants are a possible reason for this.

One way to reduce the error would be to use a number of spectroscopic luminosity indicators, because different indicators respond differently to spectral peculiarities. Besides ratios like SiII/SiI, YII/FeI is also worth considering. Supergiants for which spectroscopic luminosity determination is unreliable could be identified if different indicators gave inconsistent luminosities.

Interesting trends have been found for SI 6046.00 Å and SI 6052.68 Å: SI/FeI and SI/SiI ratio correlates with luminosity like FeII/FeI. Sulphur has differ-

Table 1: The computed M_v for 56 supergiants.

HD	T_{eff} K	M_v mag	σ	N	σ (mean)	HD/BD	T_{eff} K	M_v mag	σ	N	σ (mean)
000611	5431	–2.69	0.38	18	0.09	109379	5117	–1.81	0.58	10	0.19
003421	5302	–1.75	0.47	17	0.12	125809	4837	–3.92	0.67	6	0.28
004362	5325	–3.26	0.43	19	0.10	136537	4960	–3.60	0.56	11	0.17
008890	6050	–3.06	0.16	18	0.04	159181	5220	–2.84	0.41	7	0.16
009973	6654	–7.13	0.30	10	0.09	174104	5657	–3.44	0.23	2	0.17
011544	5126	–3.54	0.33	4	0.17	179784	4956	–3.23	0.63	5	0.29
016901	5555	–2.91	0.18	21	0.04	182296	5072	–3.52	0.39	6	0.16
018391	5871	–6.47	0.37	12	0.11	183864	5323	–3.05	0.33	10	0.11
020123	5165	–2.28	0.37	9	0.13	185758	5390	–1.58	0.34	9	0.12
020902	6541	–4.96	0.08	3	0.05	187203	5710	–3.07	0.68	6	0.28
025056	5752	–3.31	0.54	6	0.22	187428	5911	–1.89	0.33	4	0.17
026630	5337	–3.12	0.30	9	0.10	188650	5669	–0.66	0.83	10	0.26
034248	6101	–4.41	0.47	13	0.13	190403	4894	–3.16	0.88	18	0.21
038808	5112	–2.43	0.42	10	0.13	191010	5269	–2.09	0.52	11	0.16
039949	5248	–2.76	0.38	20	0.09	192713	5028	–3.72	0.54	5	0.25
042454	5277	–3.67	0.24	17	0.06	194093	6202	–6.19	0.60	9	0.20
042456	4754	–4.44	0.42	13	0.12	195432	5872	–2.19	0.78	7	0.29
047731	4989	–3.77	0.39	4	0.20	202109	4976	–1.97	0.43	9	0.15
050372	4794	–4.02	0.74	15	0.19	204022	5375	–3.78	0.23	22	0.05
052220	5661	–2.90	0.29	20	0.07	204075	5287	–2.05	0.63	10	0.20
053003	5540	–2.89	0.31	11	0.09	204867	5466	–3.24	0.20	19	0.05
054605	6443	–7.83	0.24	7	0.09	205114	5224	–3.14	0.40	10	0.13
057146	5134	–3.47	0.21	21	0.05	209750	5210	–3.63	0.31	12	0.09
074395	5264	–2.94	0.24	21	0.05	214714	5424	–1.16	0.70	18	0.17
077912	4957	–3.05	0.85	12	0.25	216206	5003	–3.17	0.53	10	0.17
084441	5296	–1.62	0.15	5	0.07	219135	5479	–2.91	0.30	20	0.07
090452	6688	–7.24	0.65	10	0.21	249750	5475	–3.38	0.45	15	0.12
092125	5354	–2.15	0.27	12	0.08	+60 2532	6268	–4.30	0.74	3	0.43

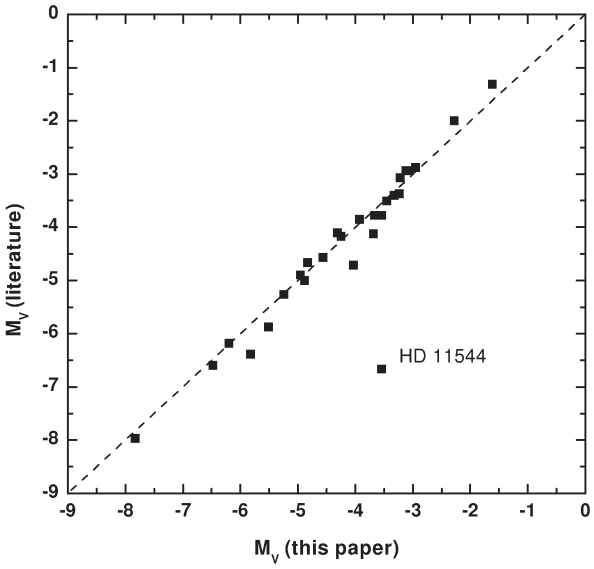

Figure 5: Comparison of our final M_v with estimates from the literature. The supergiant HD 11544 deviates from the least square fit found for FGK supergiants.

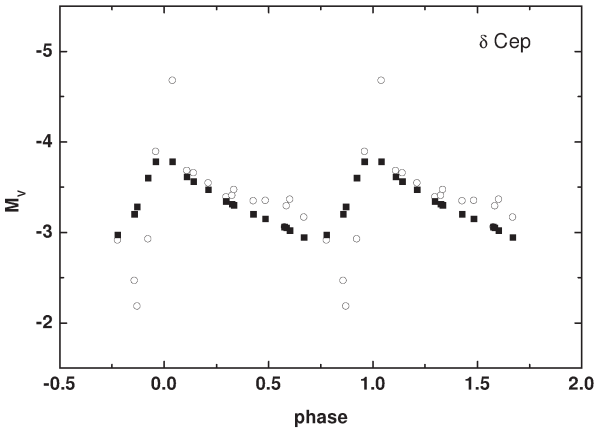

Figure 6: Comparison of our M_v with observed for Classical Cepheid δ Cep: filled squares – observations; open circles – calculations (showed are the individual phases for the Cepheid).

ent level structures and a higher ionisation potential than iron and silicon.

As noted by Andrievsky (1998ab), the Ba II 5853.6 Å and 6141.7 Å strengths could be used as a luminosity indicators for s-Cepheids. However, the relations between luminosity and BaII/FeI line ratios show large scatter.

However, the validity of these potential luminosity indicators still needs to be critically assessed in terms of the physical differences among supergiants with different abundances.

5. Conclusion

We showed that the ratio of the depths of FeII and FeI lines is larger for luminous supergiants (for a given temperature). Accordingly, FeII/FeI ratio could be used as a distance-independent spectroscopic luminosity indicator. Other spectral features (for example, FeII/NiI ratios) have subsequently been suggested as possible luminosity indicators. The BaII/FeI, YII/FeI ratios itself may be the best spectroscopic luminosity indicators for supergiants, but all these indicators show scatter which may be related to abundance distributions. As a result, we found that star HD 11544 can not be a member of a χ and h Per cluster.

Acknowledgements. This work is based on spectra collected with the 1.93-m telescope of the OHP (France) and the ESO Telescopes at the Paranal Observatory under programme ID266.D-5655. Drs. C. Soubiran and R.E. Luck are acknowledged for their help with spectral material.

References

Andrievsky S.M.: 1998a, *Astr.Nachr.*, **319**, 239.
Andrievsky S.M.: 1998b, *IBVS*, **4572**, 1.
Arellano Ferro A., Parrao L.: 1990, *A&A*, **239**, 205.
Arellano Ferro A.: 1993, *AJ*, **106**, 2516.
Arellano Ferro A., Giridhar S., Rojo Arellano E.: 2003, *RMxAA*, **39**, 3.
Bagnulo S., Jehin E., Ledoux C. et al.: 2003, *ESOMessenger*, **114**, 10.
Baranne A., Queloz D., Mayor M., et al.: 1996, *A&AS*, **119**, 373.
Galazutdinov G.A.: 1992, *Prepr.SAORAS*, **92**, 28.
Gray R.O., 1991, *A&A*, **252**, 237.
Katz D., Soubiran C., Cayrel R., Adda M., Cautain R.: 1998, *A&A*, **338**, 151.
Kovtyukh V.V.: 2007, *MNRAS*, **378**, 617.
Kovtyukh V.V., Andrievsky S.M., Belik S.I., Luck R.E.: 2005, *AJ*, **129**, 433.
Kovtyukh V.V., Soubiran C., Luck R.E., Turner D.G., Belik S.I., Andrievsky S.M., Chekhonadskikh F.A.: 2008, *MNRAS* **389**, 1336.
Luck R.E., Kovtyukh V.V., Andrievsky S.M.: 2006, *AJ*, **132**, 902.
Moultaka J., Ilovaisky S.A., Prugniel P., Soubiran C.: 2004, *PASP*, **116**, 693.

HANSKY ALEKSEY PAVLOVITCH

Lemeshchenko N.D., Shevchyuk T.V.
Astronomical Observatory of Odessa National University

ABSTRACT. An essay devoted to A.P.Hansky, a famous astronomer, a graduate of Novorossiysk (Odessa) University.

On 11th August 2008 was a centenary since the tragic death Aleksey Pavlovitch Hansky. He was an outstanding Pulkov astronomer, one of the founders of the Simeiz department of the above observatory, later on becoming the Crimean Astrophysical Observatory.

A.P.Hansky was born on 20th July (on 8th July old style) (Backlund, 1908) 1870 in the family belonging to the gentlefolk's, in Odessa. After graduating from the physical-mathematical faculty of the Novorossiysk (Odessa) University he stayed there preparing for professorship. At that time Professor A.K.Kononovich, an energetic, progressive scientist and a talented educationalist that was the first in Russia to be engaged in studying astrophysics, headed the Odessa Astronomical Observatory. Under his leadership throughout 1894 – 1896 A.P.Hansky was mainly busy with taking the Sun's photographs for the sake of studying the spots. He could not afford to use the most modern instruments; nevertheless he was able to obtain excellent photos by using modest instrumental mean (a 6.5-inch refractor).

In May 1896 the Odessa Observatory was visited by Academician O.A.Backlund – Director of the Main Astronomical Observatory of Russia, and soon Hansky came to Pulkov for further perfection in astrophotography.

An summer of the very year he was invited to the scientific expedition of the Pulkov Observatory for observing the total solar eclipse on the Novaja Zemlja on the ninth of August. This expedition proved to be a success in all respects, and the best possible observational material was obtained. Furthermore, A.P. collected photographs and sketches of the total solar eclipses obtained in different years by many astronomers. After analyzing all the material collected he came to important conclusions about the dependence of the corona form on the quantity of spots on the Sun. When there is a maximum of the solar spots, the corona forms an entire radiance around the Sun. When there is a minimum, the corona stretches more and more along the solar equator, and its brilliance weakens respectively (Hansky, 1897; Perel, 1958). Thus Hansky discovered

Figure 1: A.P.Hansky

the change of the solar corona form with the phase of the 11-year cycle of the solar activity (Sobolev, 1989). His prediction of the corona form for the total solar eclipse 1900 (Hansky & Kostinsky, 1897) was brilliantly corroborated further on by many astronomers. A.P. was the first to accentuate the universality of the 11-year cycle for active physical phenomena taking place in all the layers of the solar atmosphere.

After finishing the expedition work, at the beginning of 1897 Hansky left for Paris. He became a listener of Sorbonne lectures on mathematics, physics and astronomy, at the same time he was busy with taking photos of the Moon under competent direction of Levi. Later on he began working at the Meudon Observatory which was well-known all over the world with their classic methods of taking the Sun's photos. From 1876 the leader of this Observatory was one of the most outstanding French astronomers – P.J.S.Janssen – a pioneer in using photography and spectroscopy in astronomy, when studying the Sun, in particular.

An order to solve the problems of astrophysics, the physics of the Earth and meteorology, he, with the help of his own allocations built in 1893 an observatory at the Mont Blanc summit, the highest mountain of Europe. The work at this Observatory was very complicated because of very hard ascending the mountain and poor climatic conditions at its summit.

With an exceptional persistence A.P.Hansky overcomes these difficulties. All in all he made 9 ascents to Mont Blanc in different years, and staying there for rather a long time he used to make the most valuable observations (Perel, 1958). According to Janssen's er-

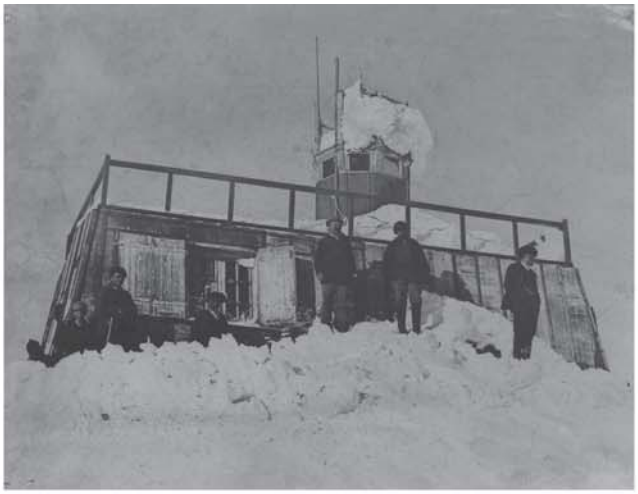

Figure 2: On the Mont Blanc

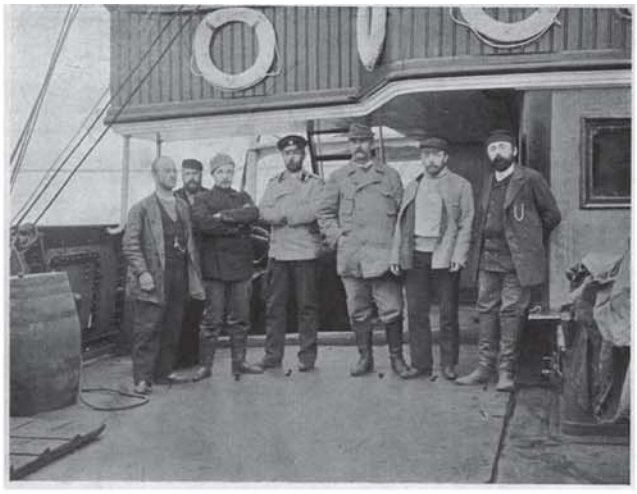

Figure 3: Russian-Swedish expedition in Spitsbergen

rands he studied the Sun's constant with the help of André Crova actinometer (Hansky, 1900). At was here on the Mont Blanc that Hansky carried out great work on finding the methods of taking photos of the solar corona without eclipses. He observed Venus too, made estimations of its period, made gravimetric measurements which also refer to important results obtained on Mont Blanc.

A.P. succeeded with mountaineering, and this fact was noticed in Odessa where the Crimean-Caucasian Mountaineering club, the first in Russia, had already been functioning for 10 years. Hansky took the most active part in the club's life, one of its tasks being the collection of means for teaching excursions. Whit this aim in view it was not once that Aleksey Pavlovitch made reports which were of great interest, narrated the history of conquering Mont Blanc, of creating and working at the Alpine observatory, showed photographs and figures, mainly, made by him self. A 1900 he was been accepted a member of this club. In the same year according to the A.P.Hansky's suggestion, Jules Janssen was accepted as an honorary member of the club. The French scientist had already ascended Mont Blanc three times.

While working in Paris A.P.Hansky did not stop writing his friends from his native town and those from the astronomical society. When answering his letters they expressed their "hope for his not forgetting their farther friends henceforth in spite of the friendship with K.Flammarion, Janssen, Nansen and other luminaries of science and civilization (March 1897) (Archiv, N80)".

A summer 1899 and 1901 Aleksey Pavlovith took part in the Russian-Swedish expedition on the degree's measurement in Spitsbergen. Nearly all the trigonometric and astronomical determinations in the Russian part of the arc were carried out by Pulkov astronomers at the head of Observatory Director O.A.Backlund. Hansky A.P. determined gravities in these expeditions that are he was mainly busy with gravimetry; however he worked as a geodesist, astronomer and photographer too. For his work in the last expedition he was awarded with the Tsar's premium handed on behalf of Russian astronomical society in which he participated from 1896.Further on he will be elected Vice-President of Russian astronomical society.

Her, we see the photo by Hansky in 1899 (Archiv, N59). From the left to the right there stand geodesists judging by his inscription: I.I.Sikora (Derpt Observatory). Then the second – V.V.Akhmatov (AO Petersburg University), the third in the one row stands D.D.Sergieffsky – Expedition Chief, later on Professor, the Academy of General Staff, then Director of Pulkov Observatory O.A.Backlund, Hansky A.P. and A.S.Vasilyev – from Pulkov as will. It is of Novorossiysk University in different years, and in spite of the most modest interest to note that Orbinsky, Hansky and Vasilyev are graduates of the means and resources of the University Observatory Professor A.K.Kononovich and his colleagues – talented lecturers – used to prepare excellent specialists for the astronomical science in the Fatherland.

The end of the XIX-th and the beginning of the XX-th centuries was the period of searching for new ways, methods and technical possibilities in the observational astronomy. French scientists, Janssen and Flammarion, were enthusiasts of astronomical observations from the air balloons, and it happened many times that they themselves flew up in the balloons. Hansky A.P. two times in Paris and one time in Petersburg flew air balls with scientific purposes.

A 1900, all the year round he was in Potsdam working in the astrophysics laboratory belonging to Vogel, one of founders of spectral classification of stars. It was there that he mastered Hartman new method of investigating telescope optics (Hansky, 1904). At the

same time it was at the Potsdam geodesic Institute that Hansky studied the methods which the German scientists used in the gravimetry.

It 1903 A.P.Hansky began to investigate solar granulations, and he continued them throughout his last life years. There were only three astronomers at the beginning of the XXth century, and namely Janssen, Hansky and Chevalier who proved to be unprecedented masters of obtaining the Sun's photographs imprinting the finest details of the solar spots and granulations (Bray & Lowhed, 1966).

The quality of the Sun's photographs and those of formations in it which were taken by Aleksey Pavlovith remained unprecedented till 1959 when the Sun's photo was taken by means of telescopes within the air balls raised up to the stratosphere. Other observers' in ability of repeating such high quality photographs resulted in their doubts about some conclusions drawn by Hansky A.P. from his photographs, for example, on the granules' fragmentation velocity. But life puts everything in its order, and nowadays we can read a note (Kandrashov): "He took the best quality photographs with "a night" instrument – Normal astrograph installed in the Western tower of the Observatory building during the afternoon heat, the photos of such a quality which the Pulkov astronomers failed to obtain even with the specialized solar telescopes equipped with automatics and an electronic analyzer for the image quality sixty years later. Besides Hansky obtained not separate "record" photographs but steady series of photos upon which one could follow the biography of each granule. For the analogous work in the 70-ies of the XX-th century it was necessary to set up The Stratosphere Solar Observatory, with the weight as high as 8 tons, heaved with a helium balloon to the 20.5 km altitude".

An 1905 A.P.Hansky ascertained that the average longevity of separate granules equals to 2 – 5 minutes, thereafter they disintegrate and are substituted by the new ones. These results were published in Pulkov and Paris (Hansky, 1905, 1906 and 1908). Nowadays these data are published in all the text-books an astrophysics, unfortunately, without any reference to his works.

On the 23-rd of September 1904, in Saint Luis (at USA), a constituent Congress of the International Union on the Sun investigation took place under the chairmanship of George E.Hale who became its first President. The striving for cooperation was caused by practical importance of constant and comprehensive research of the Sun. The Director of the Pulkov Observatory O.A.Backlund was a delegate from the Petersburg Academy of Science. And on the third of January 1905 The Russian Department of this union was based and named Commission on the Sun's investigation with A.A.Belopolsky as a head. A.P.Hansky was elected a Secretary (Gnevychev, 1984). On the day of creating The Russian Department, Aleksey Pavlovitch made a very important report in which he suggested creating Alpine solar observatory (Gnevychev, 1984). Hansky was the first astronomer in Russia to realize the necessity of organizing the Heliophysical Observatory in the south. He himself worked out the project, made up estimates of building the future observatory, and in his articles of that time he noted the possibility of building it in the Crimea, the Caucasus or even in the Pamir (Hansky, 1905).

An 1904 A.P.Hansky was awarded with the medal after P.J.S.Janssen by the Paris Academy of Sciences. The second of the Russian astronomers who was awarded with the very medal in 1907 was A.A.Belopolsky.

Figure 4: The medal after P.J.S.Janssen

On the 8th of April (old style) 1905 he began to work on the staff of the Pulkov Observatory as the adjunct-astronomer. Two expeditions were sent off by Pulkov Observatory to observe the total solar eclipse on the 30th of August in 1905 – one to Spain under the competent direction of Hansky A.P. and another to Egypt under the leadership of Okulich. Hansky's elder brother Peter, a famous painter helped the astronomer to draw this eclipse, by the way Peter painted J.Janssen's portrait for the Pulkov Observatory in 1904. A.P.Hansky arrived at important conclusions from the results of this expedition, and namely, that the forms and directions of the solar corona rays depend upon the forms and directions of protuberances. Thus, once more, the interaction of diverse physical phenomena occurring in the Sun was convincingly grounded (Hansky, 1907).

An May 1906 A.P.Hansky and G.A.Tikhov appealed to the Academy Of Sciences with a proposition of arranging an expedition to the Crimea in order to investigate the zodiacal light and to study the qualities of images. The scientific results from this trip were insignificant (Tikhov, 1959) but it was in Simeis wherein Hansky A.P. came across the N.S.Maltsev's private Observatory, and it might be its best luck. It is a well-known history of this observatory becoming the Simeiz department of the Pulkov Observatory.

At the beginning of 1907 Hansky A.P. left for his last expedition for observing the total solar eclipse in Turkestan. The Pulkov astronomers were unlucky be-

cause of the bad weather on the eclipse day, however Hansky A.P. succeeded in observing the zodiacal light.

On the 20th of January (the old style) in 1907 A.P.Hansky and Slovak astronomer Milan Stefanic after returning together from the expedition visited L.N.Tolstoy in Yasnaya Polyana. The great writer after talking with them wrote in his diary:"The astronomers are interesting".

During the last two years A.P.Hansky made a number of observations of the Jupiter's surface. And his talents for drawing did him a good turn in this case. However, the results of these observations are not treated completely.

At the beginning of summer 1908 A.P.Hansky left Odessa for Simeiz for installing telescopes and setting at the Observatory. After a month's active work on setting the Tseiss astrograph and after obtaining the first test photos A.P.Hansky perished tragically.

G.A.Tikhov (Tikhov, 1959) and G.N.Neuimin, two astronomers, have noted the fact of obtaining the first astronomical photos in the Simeiz Observatory by A.P.Hansky. Thus, we are given the right of calling Hansky the first astronomer – observer of the Simeiz, later on, the Crimean Observatory.

The astronomers in commemoration of the outstanding investigator Hansky gave his name to:

The year 1928 – minor planet 1118 (discovered by Belyavsky S.I.)

The year 1970 – crater on the far side of the Moon (selenographics coordinates – + 97°, -10°)

The glacier on the Spitsbergen is called after his name too. Its coordinates are 78°40' of northern latitude and 20°30' of eastern longitude. In Simeiz there is a street of a name A.P.Hansky.

References

Archive RAS, The Fund 543, Inventory 11, No. **59, 80**.

Backlund O. *A.P. Hansky*, Transactions of Russian astronomic society, XIV, part 7, December 1908, p. 232.

Bray P., Lowhed R.: 1966, *The Solar Spots*, Moscow, pp. 22-23.

Gnevychev M.I.: 1984, *The History of the Sun Service*, Historical-astronomic investigations, Moscow, **XVII**, pp. 161-184.

Hansky A. *Total solar eclipse on the 9^{th} of August, 1896*, St. Petersburg, 1897.

Hansky A. et Kostinsky *L'éclipse totale de Soleil du 27 Jullet 1896*, Bulletin de l'Academie des Sciences, St. Petersbourg, 1897.

Hansky A.P. *The Observatory on the Mont Blanc*, The Notes of the Crimean Mountain Club, Part 4, 1900.

Hansky A.P. *The Investigation of the 30-inch objective of the Pulkov Observatory by the Hartman methods*, Izvestiya Imper. Acad. Nauk, 1904, vol. **20**, N 2.

Hansky A. *Photographies de la granulation solaire faites à Poulkovo*: 1905, Pulkovo Mitt., **1**, 81.

Hansky A. *On the Sun's observations and on the basis of Heliophysical Observatory in the south of Russia*, St. Petersburg, 1905.

Hansky A. *Photographies de la solaire*: 1906, Bull. Soc. Astr. France, **20**, 178.

Hansky A. *Observations de l'éclipse totale de Soleil du 30 août 1905 faites par l'expédition de l'Observatoire de Pulkovo..., Mitteilungen der Nikolai–Hauptsternwarte zu Pulkovo*, 1907, Band I, N 10, Seite 121-135.

Hansky A. *Mouvement des granules sur la surfage du Soleil*, Pulkovo Mitt., 3, 1, 1908.

Kandrashov Edward V. (Internet)

Perel Yu.G. *Jubilees of Fatherland and World Astronomy in 1958*, Astronomic Calendar – 1958, Moscow, 1957, pp. 275-278.

Sobolev V.M., Vitinsky Yu.I., Rubashev B.M. *Investigations of the Sun in the Pulkov Observatory* in: *150 years of Pulkov Observatory* /ed. V.K.Abalakin, "Science", 1989, pp. 153-181.

Tikhov G.A. *Sixty years long at the telescope*, Moscow, 1959.

CHEMICAL COMPOSITION AND EVOLUTIONARY STATUS OF SPECTRAL BINARY STAR 12 PER

V.V. Leushin[1,2], M.K. Kuznetsov[2,3]

[1] Special Astrophysical Observatory
Nizhnij Arkhyz, Zelenchukskij region, Karachai-Cirkassian Republic 369167 Russia
admsao@sao.ru

[2] Southern Federal University
105 Bolshaya Sadovaya Str., Rostov-on-Don 344006 Russia *rectorat@mis.sfedu.ru*

[3] Institute of Astronomy of the Russian Academy of Sciences Department in Terskol
IC AMER Terskol Observatory, Kabardino-Balkaria Republic, 361605 Russia
admin@terskol.com

ABSTRACT. The star 12 Per is known as a spectroscopic and interferometeric binary. The high resolution spectra in 3700−8000 Å band were obtained with the 2 m telescope at Peak Terskol. A detailed analysis of the atmosphere of system's components was carried out using the collected data.

Key words: stars: binary: spectroscopic and interferometric binary; stars: individual: 12 Per.

1. Introduction

The study of binary systems with large orbital eccentricity (e>0.6-0.7) is a topical problem in the formation and evolution of multiple stars. In general evolutionary status of components and systems can be obtained if we have accurate parameters of stars in the system, including the abundance of their atmospheres. It is important for the stars with chemical features which star 12 Per has, as its components have heightened metallicity. (Barlow et al., 1998, Gardiner et al., 1999). System 12 Per (HD 16739; HIP 12623; HR 788) is the spectral and speckle-interferometric binary. Star of the systems are on the main sequence. Their spectral classes are estimated as F8 V and G1.5 V. There is one notable feature of this star: it has relative small period (P=330.^{d}98) when its eccentricity is big enough (e=0.663). And the system often can be observed with separated spectral liens of the components.

2. The general parameters of components and characteristics of atmospheres

The luminosity of each component and the system as a whole is determined by the distance to it and, consequently, the value of parallax. We used the value of parallax from the work Bagnuolo et al., (2006): π=41.19 mas, which corresponds with the distance to the system at 24.28 pc. Effective temperature of the stars according to Barlow et al., (1998) are as follows: 6125±80K and 5800±70K. Estimates of temperature from photometric measurements confirm these values. The values of photometric measurements are taken from SIMBAD. On the other hand, the study of hydrogen lines and the full flow of radiation (Smalli et al., 2002) leads to a temperature of the components: T_{eff}(A)=6371±176K, T_{eff}(B)=6000±143K. Our calculations for the ionization equilibrium Iron show that the temperature of components are within these limits and T_{eff}(A) = 6195±200K, T_{eff}(B)=6000±200K. Total luminosity of the system is $L/L_\odot$=5.15. Based on analysis of studies made by other authors we have chosen m=0.51 (Bagnuolo et al., 2006). Then, $L(A)/L_\odot$ =3.17 and $L(B)/L_\odot$=1.98. These luminosities and effective temperatures component led to radii: R(A)=1.55 $R_\odot$ and R(B)=1.31 $R_\odot$. Calculated radii and masses of component of M(A)=1.382±0.019 $M_\odot$ and M(B)=1.240±0.017 $M_\odot$ (Bagnulo et al., 2006) provide an acceleration of gravity on surfaces:
log g(A)=4.20±0.10 and log g(B)=4.30±0.10.

3. Observations

Spectral observations of 12 Per were occured in 2005–2007 with eshelle spectrometr in kude's focus 2–m telescope TF INASAN on the mount Terskol. Fig.1 shows a part of the spectrum near H_α lines for different phases. The lines of metals are well separated, and it is allowing to examine each compo-

nent separately. However, the relative radial velocity of components for each of the observed phases is insufficient to deform the contour lines H_α significantly. As light detector was used CCD camera 1242x1152 pixels from the company Write (Great Britain). The spectra were obtained in the spectral range 3500-8000 Å with a spectral resolution R=45000.

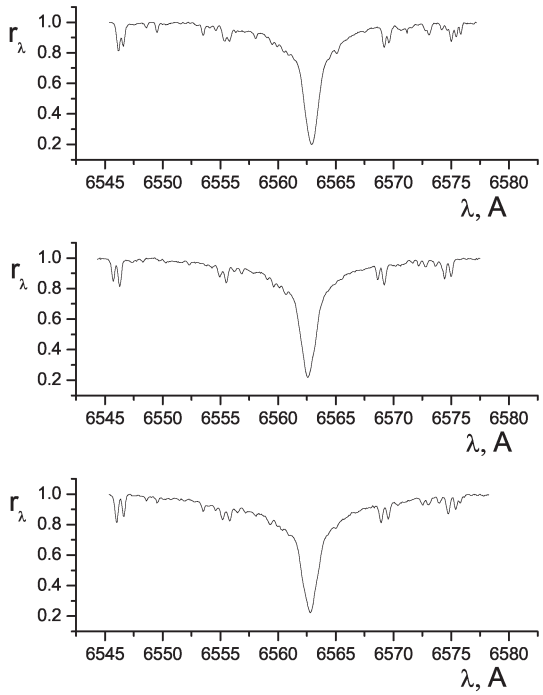

Figure 1: Spectrum 12 Per near H_α for different phases.

4. Models of atmospheres

For further analysis of component, we calculated several models of atmospheres with temperature range T_{eff} (A)=6371±176K and T_{eff} (B)=6000±143K. For each temperature, based on the values of luminosity and mass written above, their value acceleration of gravity on the surface was determined. For 6195K and 6000K log g was 4.20 and 4.30 respectively. The calculations were carried out on the program LLmodels (Shuliak et al. 2004), taking into account all the absorption lines.

Table 1: Parameters of models of atmospheres for components 12 Per

Component	T_{eff}K	log g	V_t,km/s	$V_{sin(i)}$,km/s
A	6195	4.20	1.6	8.0
B	6000	4.30	2.3	8.0

These models were used for calculating the contours of hydrogen lines on the program SintVA (Tsimbal, 2002), then contours for the first and the second component were summarized and compared with observed. Parameters of the model with the best match of theoretical and observed spectra are shown in the table. 1.

5. The content of iron and microturbulences in the atmospheres of components 12 Per

To the determine the iron content in the atmosphere of components of the system we measured the equivalent width of lines FeI and FeII in the summary spectrum of the system. Equivalent width of the spectra of components with its full division, are determined with the help of the observed values of the equivalent width and equation: W(A)=W_{obs}(A)(1-1/n) and W(B)=W_{obs}(B)(1-n). Here: W(A) and W(B) - equivalent width of the absorption lines in the spectra of the first and the second component. W_{obs}(A) and W_{obs}(B) - observed values of equivalent width of lines of the first and the second components, n=L(A)/L(B) - ratio of luminosity of relation component. In our case, m=0.51, n=1.6. The calculations were carring out using the program KONTUR (Leushin, Topilskaya. 1985). According to the results of determine logN (Fe) for different values microturbulences V_{obs} give linear regression were constructed logN(Fe)=lgN(Fe)$_0$+k W_λ ,which allow you to set V_{turb} for atmospheres of stars (by k=0). Obtained coefficients suggest that microturbulences in the atmospheres of components 12 Per are equal V_{turb}(A)=1.60 km/s and V_{turb}(B)=2.30 km/s for the first and the second components, respectively.

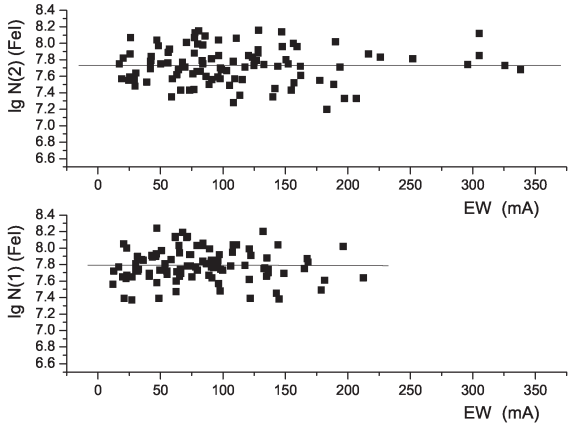

Figure 2: The dependence of the content of Fe I from equivalent width component A and component B

Lines FeI with these values of velocity give the content of iron in the atmospheres of components equal: A logN(Fe)=7.79±0.15, B logN(Fe)=7.73±0.15. The average value of iron content received with help of the lines of FeII, for each of the components are: A

logN(Fe)=7.79±0.15, B logN(Fe)=7.78±0.15.

6. The contours of lines of iron

Fig. 3 shows a comparison of some theoretical and observed contours of lines FeI and FeII. Synthetic contours were constructed for three different contents (solar content, the content of the sun - 1 dex and solar content + 1 dex). Microturbulent velocity are V_{turb}(A)=1.60 km/s and V_{turb} (B)=2.30 km/s, respectively, for the first and the second component. The rotational velocity of stars in the models were taken V_{rot}=8 km/s for both components. Synthetic spectrum built using KONTUR (Leushin, Topilskaya, 1985).

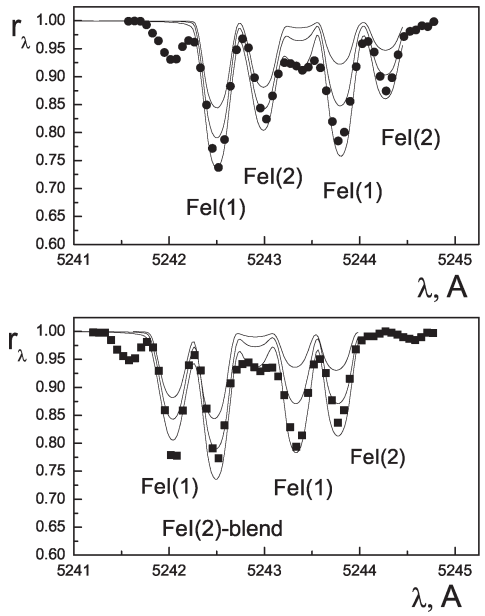

Figure 3: Comparison of synthetic and observed the spectrum of 12 Per for different phases. Points - observed spectra, lines - synthetic spectra for different content Fe.

Analysis of the contours of spectral lines FeI and FeII shows significant excess of iron in the atmosphere of component, is comparison with the solar content. This confirms the results obtained by equivalent width.

7. Conclusions

A detailed analysis of the chemical composition of the atmosphere of each component of the system 12 Per was carried out. The fundamental parameters of stars were precised. Received data on the content of iron in the atmosphere components 12 Per indicate high metallicity system: the value of [Fe]≥0.35. Using refined luminosities (L(A)=3.02$L_\odot$ and L(B)=1.86$L_\odot$) and effective temperature improved (T_{eff}(A)=6195K and T_{eff}(B)=6000K) of the components, we calculated the evolutionary status of the system. In our opinion, its age is 1.12 billion years. The components are are being in the process hydrogen's burning near the main sequence.

References

Bagnuolo W.G., Taylor J.S.F., McAlister H.A., et al.: 2006, *Astron.J.,* **131**, 2695.

Barlow D.J., Scarfe C.D., Fekel F.S.: 1998, *Astron. J.,* **115**, 2555-2560.

Gardiner R.B., Kupka F., Smalley B.: 1999, *Astron. Astrophys.,* **347**, 876-890.

Leushin V.V., Topilskaja G.P.: 1985, *Astrofizika,* **22**, 121.

Shulyak D., Tsymbal V., Ryabchikova T., Stutz Ch., Weiss W.W.: 2004 *Astron. Astrophys.,* **428**, 993.

Smalley B.. Gardiner R.B.. Kupka F.. Bessell M.S.: 2002, *Astron. Astrophys.,* **395**, 601.

Tsinbal V.V.: 2002, *priv. comm.*

POPULATION OF THE Be STARS IN THE YOUNG OPEN CLUSTERS

S.L. Malchenko[1,2]

[1] Crimean Astrophysic Obseratory, Nauchniy, Crimea, Ukraine

[2] Tavrida National University, Vernadskogo ave., 4, Simferopol, 95097, Ukraine

Svetlana_mal@ukr.net

ABSTRACT. Both high and medium resolution spectroscopy of the Be stars and binary stellar systems in the young open clusters (e.g., NGC 869 & 884, NGC 6913, NGC 6871, NGC 7160 and NGC 7419) were carried out. High resolution spectroscopy of 100 stars in the Hα region and 42 stars in the region of 4400–4960 Å with the medium resolution were obtained. The spectra of 52 B and 48 Be stars were studied. T_{eff}, $log\, g$ and $V \sin i$ were determined by using the medium resolution spectra. One new Be star was found, one star showed complex variability of the Hα line profile, which is characterized as a close binary system. A few demonstrate long - term V/R variability of the emission peaks that can be easy described by the one arm oscillations in theirs envelopes. Our clusters survey approved that classical Be stars mostly appeared at age of 10 Myr, and reached the maximum abundance in the age of interval 12-20 Myr.

Key words: Clusters: yuong open clusters: individual clusters: NGC 869 & 884, NGC 6913, NGC 6871, NGC 7160 and NGC 7419; Stars: Be stars.

1. Introduction

The phenomenon of Be stars has been known for over a century. The fact that at least 20% of B stars have an emission spectrum supports that the definition that this phenomenon is not special but it is rather typical from a large group of objects at a certain stage of evolution. The vagueness of the concept of the Be phenomenon suggests that this definition encompasses a broad group of objects near the main sequence that includes binary systems with different rate of mass exchange. Thus, the hypothesis that all Be stars are the consequence of the evolution of binary systems is still current. On the other hand, most classical Be stars are probably individual objects and the formation, at rotational velocities far from critical of the disks surrounding them requires a separate explanation.

One way of solving this problem might be to study the properties of Be stars in young open stellar clusters. In the 1980's a number of photometric (Mermilliod, 1982) and spectral (Slettebak, 1985) studies were undertaken which showed that clusters with ages of 14-25 millions years contain the maximum number of Be stars. Fabregat et. al (2000) interpreted their results in a sense that the Be phenomenon is an evolutionary effect and proposed that it could be related to the main the structural changes that had been happing at this evolutionary phase.

In this paper we study and compare population of Be stars in some young open stellar clusters (e.g., NGC 869 & NGC 884, NGC 6871, NGC 6913, NGC 7160 and NGC 7419), which have differentness but have similarities because of close age. The goal of this work is to find new Be stars with a faint emission in the Hα line and a binary star in these clusters. To study long-term spectral variability of the emission spectrum of the Be stars and possible binary some of them, was used the high resolution spectroscopic observations.

2. Observation

Spectral observations of the B and the Be stars in all of the open stellar clusters were carried out at the Crimean Astrophysical Observatory from 1997 to 2007 by using the Coudé focus of the 2.6-m ZTSh telescope. The spectral resolution was about 30000. The signal-to-noise ratio for most of the spectra was about 100. A total of 125 spectra were obtained for 52 B and 48 Be stars in the Hα line region from six young open stellar clusters (e.g., NGC 869 & 884, NGC 6871, NGC 6913, NGC 7160 and NGC 7419).

In 2000 - 2002 years spectral observations of the B and Be stars were made over wavelengths of 4400-4960 Å , in addition to the Hα observations. These spectra were obtained at the Nesmith focus of the 2.6-m ZTSh telescope with a moderate resolution of 2.5 Å and a signal/noise ratio of about 100. The Hβ line, a number of the HeI lines, and several metal lines lie within this spectral range. In all, 32 spectra were obtained for 27 Be stars and 15 spectra for 12 B stars in the region of

4400-4960 Å .

3. h/χ Per

The binary open cluster h/χ Per (NGC 869 and NGC 884) has been well studied by many authors. The distance to the cluster is about 2.3 kpc with a distance modulus of $11^m.4$ - $12^m.0$. Strömgren photometry yields different estimates for the ages of h and χ Per, *logt* = 7.0 and 7.3, respectively, which slightly differe from ages of the clusters remains an open question to this day. The clusters are rich in Be stars, context of Be stars in young clusters are variously estimated form 25 to 50% of the overall number of B stars (Fabregat et. al 2000).

From 1997 to 2002 we obtained 90 spectra for 48 stars in the early spectral class B0-B3 which are members of the h/χ Per cluster. We found no traces of emission in the Hα line in the spectra of 28 of the stars. Several objects which were previously identified as or suspected of being Be stars showed no traces of the emission in the Hα line profile during our observations. These include the stars Oo146, Oo566, Oo717, Oo922, and Oo1268. (Here and in the following the numbers stars for the h/χ Per follow the Oosterhoff catalog (1937).)

An emission Hα line profile was obtained for 20 stars in the h/χ Per cluster. In addition, one new Be star, Oo2296, was observed and it is possible that Oo992 also has a faint emission in the wings of the absorption profile (fig. 1). It can be seen there that faint emission is definitely present in the wings of the photospheric Hα line of Oo2296. The presence of the faint emission in the Hα line is less evident in Oo992 as can be seen in Fig. 1, the Hα line profile for this star is asymmetric and varies in time.

Three Be stars, Oo1161, Oo2242, and Oo2371, manifested significant variability in the emission profile of the Hα line during the time of our observations. The variability in the Hα profile for Oo1161 (fig. 2) and Oo2242 are similar and show up as a change in both the intensities of the blue and red emission components with a characteristic time of hundreds of days and in slow variations in the equivalent width of the line. This type of variability in the emission spectrum is fairly widespread among Be stars and is customarily explained by the one arm oscillations in the circumstellar disk.

Oo2371 (BD $+58^0578$, V622 Per) was observed in more details during 1997-2002 the spectra revealed a regular variability in the Hα line profile (fig. 3). This variability indicates that the star is a binary with an orbital period of about 5.2 days. Both components can be seen in their spectrum. This star appears to have passed through the phase of active mass exchange and little emission in the Hα line wich is been currently

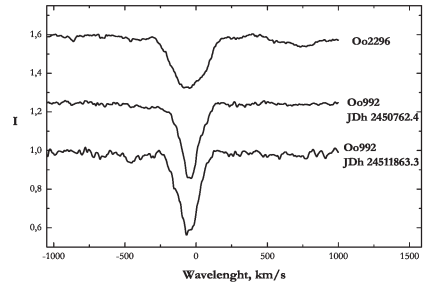

Figure 1: Profiles of the Hα line for the stars Oo2296 and Oo992, from the cluster h/χ per. (The Julian date of the observation is indicated for each star.)

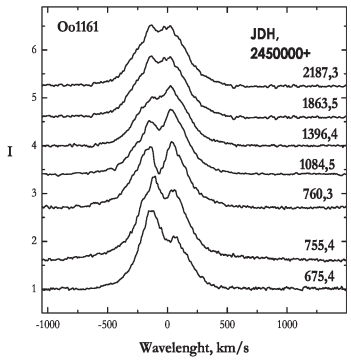

Figure 2: The variability in the Hα profile for Oo1161, member of the cluster h/χ Per.

observing.

In addition to the spectral observations of the Hα line, the moderate resolution spectra were obtained in the range of 4400-4960 Å for a number of the B and Be stars. The Hβ line falls in this range together with the Hα line it manifests signs of emission in most Be stars. In some of the Be stars that were observed the Hβ line profile is in absorption (e.g., Oo1268, Oo2262, Oo2371, and Oo2649). Other stars manifested a weak emission in the Hβ line, e.g., Oo2402, Oo2242, Oo2088, Oo2138, or a bright single component structure (e.g., Oo309, Oo1261, Oo1926, Oo2284, Oo2563). Probably, the last group of objects has more extended and optically thicker disks, unlike the first group, which disks are optically thin, so that emission does not show up in the Hβ line.

4. NGC 6913

This young open cluster in the Cyg OB1 association, is also know as M29, contains a large number of luminous stars with spectral types around B0. An extreme variation of extinction is found by Wang et. al (2000) across the young open cluster NGC 6913, extinction in

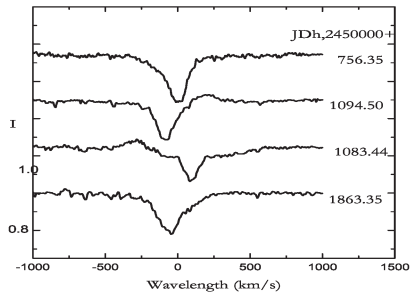

Figure 3: Selected Hα profiles for the Be star Oo2371, the member of the cluster h/χ per.

the cluster center is relatively homogeneous, but very large. The north and south of this cluster have the largest extinction. The eastern and western parts are seem to be low reddening region. The average value of the E(B-V) is 0.71±1.82. A mean distance modulus of 10.17±0.14 mag is derived for the cluster by Wang et. al (2000), which corresponds to a distance of 1.08 kpc. From the UBV photoelectric photometry, Joshi et. at (1983) obtained distance modulus as 10.85±0.15 mag. The estimated ages of a stars in the cluster span from 0.3 - 1.75 Myr (Joshi et.al, 1983) and 10 Myr.

We observed 10 spectra for 7 B stars and one known Be star in the blue region. The spectra of the two stars (1 and 9 (named from Hoag A.A. et. al 1961)) have characteristically the profiles of a more cool star and probably they do not the members of the cluster, but Boeche (2004) these stars found as binaries. For the Be star V1322Cyg (HD 229221) obtain tree spectra in the Hα region. The star has a stronger emission in the Hα and Hβ lines, there are some variability of the profiles from the Hα line. Two spectra in the Hα region were taken for the B star HD 229227, which was determined as a possible Be star; however there are no traces of an emission in the Hα line in time of the our observations.

5. NGC 6871

NGC 6871 is a rather extended open cluster, which boundaries are not well defined. It is believed to be the core of the Cyg OB3 association. The estimates of its distance and age vary relatively from the large amounts to different authors. From isochrone fitting by Massey et. all (1995) was derived from ages of 2-5 Myr for the stars with M $\leq$ 25M$_\odot$, Reimann (1989) estimated an age of 12 Myr and distance modulus 11.9 mag. The difference between two ages suggests that a large age spreads among the cluster numbers, the contamination of the nearby stars in the local spiral arm, or the large uncertainties in the ages approximately derived from optical photometry. Massey et. al (1995) notes that the cluster contains 15M$_\odot$ stars with main sequence of the lifetimes of 11 Myr.

The brightest star in the cluster is the O9.5I+WN4 binary HD190918. Recent searches of emission - line stars by Bernabei et. al (2001) and Balog et. al (2002) detected several faint Be stars and some pre-main-sequence objects. In the period from 1998 to 2002 years were observed a 11 spectra for 7 B stars and 6 spectra for two Be stars in the region of the line Hα. It was also observed a binary V1676Cyg (HD190918). HD 227611 is known as a Be star with strong emission in the Hα line, from period of the our observation profiles of the Hα, it was not shown a variability. The second Be star, which had been obtained, BD +35^{0}3956 has changed from the single absorption to the duplicity emission profile of the Hα line in about 10 days (fig.4). For the stars HD227586 and HD227621 were obtained some spectra, but profile changes of the Hα did not found (see fig.4). Other stars have the clear absorption profiles.

The moderate resolution spectra were obtained in the region 4400-4960 Å for 5 the B and 2 Be stars. The Be star V1676Cyg has a strong emission in the Hβ line and in the other lines such as HeI4471 Å and HeI4712 Å. Line profile of the Hβ for BD +35^{0}3956 is absorption, all lines from this region for the star are broad and this is likely to be group due to the fast rotation. However, the shape of the metallic lines strongly suggests that it is a double-lined spectroscopy binary star (Negueruela, 2008). The star HD 227630 from this region, which is also as in the region of the Hα line, has typically the spectra for cool stars and it is not a member of the cluster.

6. NGC 7419

NGC 7419 is a small, young open cluster in the Cepheus, with unusual presence of gigant and super giants. Form a photometric observation by Bhatt et. al (1993) was found a differential reddening of 1.54 to 1.88 mag with a mean value of 1.71 mag, a cluster distance of 2.0 kpc and the age about 40 Myr. Beauchamp (1994) estimated a younger age of 14±2 Myr and a distance of 2.3 ± 0.3 kps.

Based on a CCD photometric observation of 327 stars in UBV passabands Subramaniam et. al (2006) estimated the cluster parameters as a reddening (E(B-V)) = 1.65 ± 0.15 mag and the distance 2.9 kpc. The turn-off age of the cluster was estimated as 25 ± 5Myr by using isochrones fits. The isochrones fits to pre-MS stars in the optical color-magnitude diagram showed that the turn-on age of the cluster is 0.3 - 3 Myr. This indicates that there has been a recent episode of star formation in the vicinity of the cluster.

From CCD photometry in narrow Hα band, R and I filters, were identified 31 Be stars, that constitute 36 ± 7 % (Pigulski et. al, 2000). With Nesmith

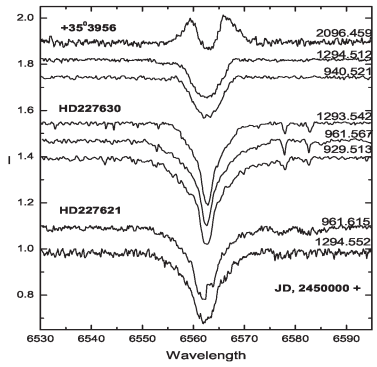

Figure 4: Profiles of the Hα line for the Be and two B stars in the NGC 6871

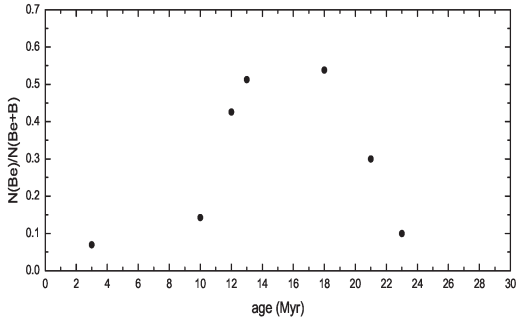

Figure 5: Dustribution of the Be stars as a function of age

spectrograph were observed 30 spectra for 25 Be stars and 11 spectra for 10 B stars in the Hα region. All spectra were taken with a low resolution (about 6-8 Å). The four stars (e.g., 290, 318, 451, 458 and 967, numerous for the stars from NCG 7419 as in Beauchamp et. al (1994)), which previously identified as Be stars, showed weak emission in the profile of the Hα line or absorption profiles of the Hα line during our observations. In the blue region were taken 11 spectra for ten Be stars and one for B star. In the same nights spectra for 7 stars were obtained in both regions. It allows us to see the spectra into the region 3700 - 7850 Å, and to study the emission in the Hα, Hβ and for few stars in the Hγ lines.

7. Results and conclusion

In total, we studied about 140 profiles of the Hα line and 47 spectra in the region of the Hβ for more than 100 stars in the young open stellar clusters. One (possibly two) new Be stars were discovered by mean of the high resolution spectra. The finding of the study especially a small number of new Be stars with faint emission, was unexpected. Given that, up to now this clusters has been observed with a much lower resolution. Some stars manifested a significant long-term variability in the Hα line. It was found that the binary Be star V622Per, which previously had been suspected of being a Be star, is indeed that, with an orbital period of 5.2 days.

The Hα and Hβ lines demonstrated a weak emission or a bright single component structure for the Be stars and a completely absorption profile for some of them.

We used data from the both our observations and literature in order to determine the distribution of the relative fraction of a Be stars in a clusters with an age. This distribution has been show on the fig.5. Data for the clusters, which we studied are marked on fig.5. We can conclude, that the classical Be stars appear in the clusters with age 10 Myr and they are absent or appear very rare in the clusters with age more than 100 Myr. As it seens from fig.5 the maximum content of Be stars are in clusters with age 12-20 Myr. The decrease of the Be abundance with the age after 25 Myr is underlined the dependence of the Be stars abundance from the spectral type. Zorec et. al (1997) found that the maximum abundance occurs in the spectral type of B1-B2. Clusters that are older than 25 Myr have their turnoff at type B3 or late.

Acknowledgements. The authors are grateful Tarasov, A.E. for helping, comments and suggestion during the development of this paper.

References

Balog Z., Kenyon S.J.: 2002, *AJ*, **124**, 2083.
Beauchamp A., Moffat A. F.J. and Drissen L.: 1994, *Asrtoph. J. Suppl. Ser.*, **93**, 187.
Bernabei S., Polcaro V.F.: 2001, *AA*, **366**, 817.
Bhatt B.C., Pandey A.K., Mohan V., et, al.: 1993, *Bull. Astr. Soc. India*, **21**, 33.
Boeche C., Munari U., Tomasella L. and Barbon R.: 2004, *Astron. Astrophys.*, **415**, 145.
Bragg A.E., Kenyon S.J.: 2002, *Astrophys.J.*, **124**, 3289.
Fabregat J., Torrejon J.M.: 2000, *Astron. Astrophys.*, **375**, 451.
Joshi U.C., Sanwal B.B., Sagar R.: 1983, *PASJ*, **35**, 405.
Hoag A.A., JohnsonH.L., Iriate B.: 1961, *Publ.U.S. Naval Obs. Ser. 2*, **17**, 343.
Massey P., Johnson K.E. and DeGioia-Eastwood K.: 1995, *Ap.J.*, **454**, 151.
Mermilliod J. C.: 1982, *Astron. Astrophys.*, **109**, 48.
Negueruela I.: 2008, *Astron. Nachr.*, **325**, 380.
Oosterhoff P.T.: Ann. Sterrewacht Leiden, 17, part 1, 1937.
Pigulski A. and G.Kopacki: 2000, *Astron. Astrpys. Suppl. Ser.*, **146**, 465.
Reimann H.-G.: 1989, *Astron. Nachr.*, **310**, 273.
Slettebak A.: 1985, *Astrophys. J.Suppl.Ser.*, **59**, 769.
Subramaniam A., Mathew B. Bhat B.Ch., et al.: 2006, *MNRAS*, **370**, 743.
Wang J.-J., J.-Y.: 2000, *Astron. Astrophys.*, **356**, 118.
Zorec J., Briot D.: 1997, *AA*, **318**, 443.

OMEGA CENTAURI: GLOBULAR CLUSTER, STELLAR STREAM – DWARF GALAXY

V.A. Marsakov, T.V. Borkova
Southern Federal University
Rostov-on-Don 344090 Russia,
vmarsakov@ip.rsu.ru and borkova@ip.rsu.ru

ABSTRACT. Data from our compiled catalogs of the spectroscopic determinations of the abundances of α-elements in the stars of field and globular clusters of the Milky Way are used to investigate the chemical evolution of the ω Cen globular cluster and of the same name moving group. It is established that the dependences of the relative abundances of α-elements on the metallicity for the stars of both the ω Cen moving group and the globular cluster coincide, which with the great probability testifies as genetic connected and belonging both to dwarf galaxy-satellite galaxy, the decomposed under the action of tidal forces of the Galaxy. It is simultaneously discovered that the metallicity functions of the stream and globular cluster demonstrate identical spread, but the positions of the maximums of distributions are spread to Δ[Fe/H]≈ -0.5 (with the peak on the smaller metallicity in globular cluster). The following conclusions are made: 1. The descending branch of the "[Fe/H] – [α/Fe]" dependence of the ω Cen globular cluster is formed by the young metal-rich stars, which was captured from the parental dwarf galaxy. 2. The stars of the ω Cen globular cluster are absent in the same name moving group – are there located only the stars of their parental galaxy. 3. The star formation rate in the ω Cen dwarf galaxy was always considerably lower than in the our Galaxy, about which they testify the small metallicity of characteristic knee ("break point") to [Fe/H]≈ -1.3 and steeply incidence in the relation [α/Fe] with further increase in the metallicity.

Key words: stellar chemical composition, the ω Cen globular cluster, the Centauri stellar stream, dwarf galaxy evolution.

The present situation

The ω Cen globular cluster is the most massive ($\approx 5 \cdot 10^6$ M$_\odot$) and the most uncommon cluster from approximately hundred sixty ones, which belong at present to our Galaxy. It occupies the area considerably more than lunar disk – a tidal radius is equal to 57′. This cluster proves to be sufficiently old dynamically (value of central concentration $c = 1.61$), although with so large mass and sizes the time of two-body relaxation in it is one of the large for the globular clusters and is compared with Hubble time. The distributions of star density and velocities of stars along cluster radius cluster testify about the high probability of existence in its nucleus of such exotic object as black hole with a mass on the order of $4 \cdot 10^4$ M$_\odot$, characteristic, faster, for the nuclei of galaxies. All these qualities, and also described below chemical and kinematical properties, make to assume that this cluster was in the past the nucleus of dwarf galaxy-satellite, captured by our Galaxy and destroyed by the action of its tidal forces.

In system with the large initial mass, such as is observed in the ω Cen globular cluster, it is possible to assume sufficiently prolonged chemical evolution. And actually, the distribution of cluster stars on the photometric metallicity revealed not only the clearly expressed peak near [Fe/H]≈ -1.6 but also the long tail, which is stretched up to [Fe/H]≈ -0.5 with the possible peak in the environment [Fe/H]≈ -1.2. Studies showed that the stars of metal rich tail occur $\approx 20\,\%$, moreover they more strongly are concentrated to the cluster center and prove to be kinematically colder, than the bulk of more metal-poor stars. Simultaneously, the most metal-poor population demonstrates well known anomalously high ellipticity in the direction East-West, while more metal-rich stars, on the contrary, occupy the volume, elongated in the direction North-South. Moreover, if star with [Fe/H]< -1.2 reveal the distinctly observed rotation, the more metal-rich stars is not noted rotation. The proper motions of more metal-rich stars also indicate the dynamics different from the bulk of the cluster stars. The described shape and kinematic differences difficult to pack in the framework of hypothesis about the formation of all stars of this system from united isolated proto-cloud. Therefore, became completely popular hypothesis assuming that the extremely metal-rich ([Fe/H]> -0.8) population, which comprises is less than $5\,\%$ all stars

of cluster, completely it can prove to be the separate captured cluster. From other side, some authors assume that the model of heterogeneous chemical evolution with three flashes of star formation can explain a variation in the chemical composition in the cluster also.

Photometric data for more than 220 000 ω Cen stars demonstrate the very wide red giant branch, which indicates the significant spread of ages among the cluster stars. The ages of the chosen on metallicity stellar groups ($\langle$ [Fe/H] $\rangle \approx -1.6$, -1.2 and < -0.5) proved to be equal to 15 ± 3, 13 ± 3 and 8.5 ± 2 Gyr, respectively. The spread of ages can come out, in particular, as a result of indicated above scenario of the capture of the small metal-rich cluster (however then it becomes obscure – as where it could be formed so metal-rich globular cluster), so also as a result the prolonged evolution of the united isolated system.

The analysis of the detailed chemical composition of cluster stars gives additional information. At the present time the different authors determined the abundances of different chemical elements (as a whole of approximately 20) more than for two and one-half hundred red giants of the ω Cen. The greatest number of determinations is obtained for α-elements, since precisely they contain the most significant information about the early stages of formation and evolution of stellar system. In particular, it is shown that the relative α-elements abundances among the ω Cen stars do not change with an increase in the metallicity up to [Fe/H] ≈ -1.0 and are equal to [α/Fe] ≈ 0.3. Then is observed the "characteristic break" of the dependence and the [α/Fe] relations begin to systematically decrease approximately to the solar value up to [Fe/H] ≈ -0.5. Specifically, this dependence must come out in the case of the closed model of chemical evolution. Actually, according to contemporary ideas the α-elements are formed practically exclusively in the stars with masses > 8 $M_\odot$, being exploded after characteristic time on the order of 30 Myr as a second type supernovas. With the explosions the same stars eject a small quantity of iron atoms. However, the basic mass of the elements of iron peak is produced with the flashes of the close pairs of the smaller mass stars, which are exploded as supernovas of the type SNe Ia after the characteristic time ≈ 1 Gyr. When an epoch of this type supernova explosion begins in the system, the relative abundance of α-elements begins to decrease in the interstellar medium (and in the young stars). The presence of the characteristic knee ("break point") in the dependence [α/Fe] $-$ [Fe/H] among the ω Cen stars evidences about the sufficiently large duration of the evolution of this system.

The Omega Centauri globular cluster not is lonely in its orbital motion around the Galactic center – the Centauri moving group, which consists of the field stars, accompanies it. As now they assume, there are several types of the moving group, which are distinguished by their origin. In particular, the results of the numerical simulation showed that the orbits of sufficiently massive satellite galaxies constantly decrease in the sizes and are moved into the Galactic plane by dynamic friction (Abadi et al., 2003). In the course of time such galaxies, after acquiring very eccentric orbits, the practically parallel to the Galactic disk, begin be intensively destroyed with the tidal forces of the Galaxy with their each passage of peri-galaktic distance, losing stars with the clearly determined orbital energies and the angular momentum. Therefore, if observer is located between apo-galaktic and peri-galaktic radii of this orbit, then tidal "tail" from the destroyed galaxy will be observed as a stellar "moving group" with the small vertical velocity components and the wide, symmetrical and frequently bimodal distribution of the radial velocities. In our recent work we (Marsakov and Borkova, 2006) isolated the stars of the Centauri moving group from the author's compiled catalog of the spectroscopic determinations of the magnesium abundances (representative of α-elements) in ≈ 800 close field F–K-dwarfs (Borkova and Marsakov, 2005). It turned out that revealed 18 stars of moving group actually demonstrate the sufficiently narrow sequence [Mg/Fe] $-$ [Fe/H], characteristic for the genetically connected stars. Moreover the position of the "break point" of the relative magnesium abundance to [Fe/H] ≈ -1.3 indicate that star formation rate in their parental galaxy was lower than in the Milky Way. Moreover star formation in this galaxy continued so for long, that its most metal-rich stars reached the value of the relation [Mg/Fe] < 0.0, i. e., even are less than in the Sun.

Thus, the variation of the relative magnesium abundances on the metallicity in the stars of globular cluster and moving group ω Cen is sufficiently similar, but to make the statistically significant conclusion about their genetic connection is impossible because of the low statistics for the stars of the moving group and small number for them of uniform determinations of the abundances of other α-elements, except magnesium. Furthermore the question remains open: are the moving group stars the remainders of the dwarf galaxy or only its nucleus, i. e., ω Cen globular cluster? Therefore the purpose of this work is the refinement of fine structure of both diagrams and fulfillments their comparative analysis on the basis of the created summary catalogs of the spectroscopic determinations of the abundances of four α-elements separately for the stars of the cluster and the moving group.

The observational data

To investigate the moving group we used the yet not published new version of our compiled catalog of

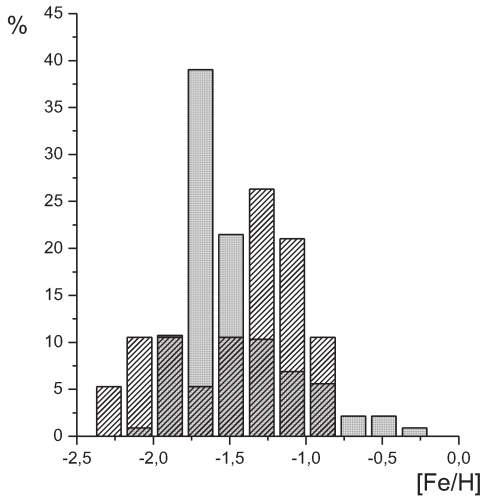

Figure 1: Distributions of stars of the Omega Centauri globular cluster grey column and the Centauri moving group (shaded column) according to the iron abundance.

the spectroscopic determinations of α-elements (magnesium, silicon, calcium and titanium) abundances, obtained by the different authors for the close field stars. In the work is used the three-pass iterative averaging procedure of the reduction of the atmospheric parameters, abundances of iron and elements of α-process with assignment of a weight both to each primary source and to each individual determination. As a result the greatest weight obtained determinations in the best way coincided with the majority of other determinations. With the determination of the atmospheric parameters and abundances of iron are used about 4700 determinations from 136 publications. The relative abundances of α-elements were obtained for $\approx$ 2000 stars on the basis of approximately 2800 determinations for each element from 81 publications. The estimated completeness for data sources with the volume is more than 5 stars to April 2008 exceeds 90 %. The internal errors in determination of the parameters the following: εT_{eff} = 60° K and 140° K; ε(log g) = 0.12 and 0.24; ε[Fe/H] = 0.06 and 0.09 for the stars with the metallicity [Fe/H] is more and less than −1.0, respectively. For the relative abundances of magnesium, calcium and silicon the corresponding values are equal to 0.07 and 0.10, whereas for titanium error in entire range of metallicity is equal to 0.15. Distances and components of space velocities for all stars are determined according to the data of contemporary high-precision astrometric and spectroscopic observations. Furthermore, for the catalog stars are calculated the elements of galactic orbits on the basis of the three-component model of the Galaxy, which consists of the disk, bulge and the massive extended halo.

For investigating the chemical composition of globular clusters we composed the compiled catalog, which uses all published spectroscopic determinations of the abundances of different chemical elements in the accessible globular clusters stars. The abundances of four α-elements and iron for more than two and one-half hundred giants of the ω Cen globular cluster were published in 4 papers. For each investigated star the atmospheric parameters and abundances of chemical elements are determined, as a rule, only once; therefore almost all given in our final list data are initial, i. e., undergone no correction. The internal accuracy of the determination of the relative abundance of each α-element we estimated by equal to $\approx$ 0.18, and the average relative abundances of all measured α-elements – $\approx$ 0.12.

Analysis of stellar chemical composition of the Centauri flow and of the Omega Centauri globular cluster

Let us compare the metallicity functions of Omega Centauri globular cluster and Centauri moving group, which arose by the hypothesis from the same destroyed dwarf galaxy. We isolates the stars of the Centauri moving group, being based on recommendations Mesa et. al., (2004), from our compiled catalog of spectroscopic determinations of α-elements abundances in field stars on the azimuthal and vertical components of their space velocities ($-50 < \Theta < 0$ km s^{-1} $|W| <$ 65 km s^{-1}, respectively). In our catalog such stars was located with 19. From the [Fe/H] − [α/Fe] diagram (Fig. 3) it is evident that all stars were arranged along the sufficiently narrow strip, which with the small metallicity ([Fe/H] ≤ -1.3) demonstrates the approximately constant quantity of the relation [α/Fe] $\approx$ 0.35, but then, with an increase in the metallicity beginning from this point, is observed a sharp drop in the relative abundance of α-elements up to the Solar one (more detail see below). This behavior is very similar to the expected dependence of the [α/Fe] on [Fe/H] relation, obtained in the closed model of chemical evolution, what is the independent evidence in favor of the genetic connection of the chosen stars. The distribution of the ω Cen globular cluster stars according to the spectroscopic determinations of the iron abundances into them and analogous distribution for the moving group stars are given in Fig. 1, where for convenience in the comparison of the distributions of different number scale along the Y-axis is given in the percentages of the total number of stars in the appropriate sample. From the comparison of distributions it is evident that the metallicity function of one object is the mirror image of another. In this case the ranges of metallicity completely coincide, whereas the maximums of distributions are spread according to the [Fe/H] scale almost by an order, i. e., far beyond the ranges of the errors in

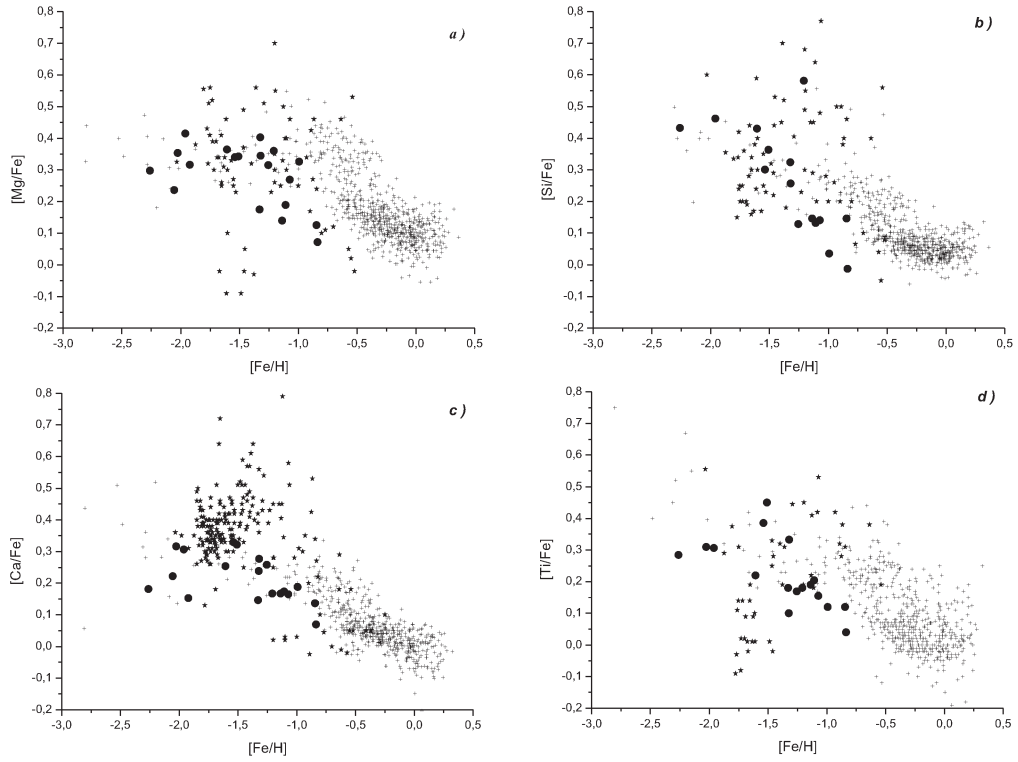

Figure 2: Metallicity – relative abundances of α-elements diagrams for magnesium (a), silicon (b), calcium (c) and titanium (g), where the star of the Centauri stream – filled circles, the ω Cen globular cluster – filled asterisk and the genetically connected field stars of the Galaxy – small crosses.

determination of this value.

The diagrams of a change in the relative abundances of four α-elements (magnesium, silicon, calcium and titanium) with an increase of the metallicity in the moving group stars and globular cluster stars are consecutively given on the panels of Fig. 2. For the comparison on all diagrams the genetically connected (i. e., formed from the matter of the united proto-galactic cloud) stars of our Galaxy are also substituted. They are selected from our compiled catalog on the local standard of rest velocity ($V_{LSR} < 240$ km s^{-1}). Stars with the higher velocities possess very high orbital energies, besides most of them demonstrates retrograde orbits, whereas precisely opposite direction of the rotation of objects around the Galactic center appears, as they assume, by the most convincing evidence against their formation from the united proto-galactic cloud. This selected stars of the Galaxy on the diagrams [Fe/H] – [α_i/Fe] of Fig. 2 for each investigated chemical element demonstrate the distinct and very similar sequences, identical special feature of which is the presence of characteristic knee in one and the same place – in the environment [Fe/H] ≈ -1.0.

The stars of the Centauri moving group in the same figure along all four α-elements also demonstrate sufficiently narrow dependences, with the clear tendency of the decrease of the relative abundance of each element with an increase in metallicity, confirming the conclusion about their genetic link. Moreover in the [Fe/H] ≈ -1.0 environment [α_i/Fe] relations in the stars of moving group they occur on the average noticeably lower than in the stars of the Galaxy - means moving group "break point" is located on the smaller metallicity. Because of a small quantity of chosen stars of the moving group and completely natural spread in the stars of the abundance of each element, is more reliable the "break point" position of group to determine an averaged abundance of all measured α- elements.

In spite of the sufficiently large number of the chemical elements abundance determinations in the atmosphere of the stars of the globular cluster ω Cen, each element on the diagrams of Figure 2 demonstrate not only disproportionately large spread, but also systematic displacement relative to the abundances of the same element in the stars of both the Galaxy and the moving group. We assume that this, it is most likely, caused by the very large distance to the cluster and by the impossibility to build the adequate models of the atmosphere for its giant stars. In favor this conclusion testifies the systematic differences in the relative abundance of titanium, obtained along the lines of ionized and neutral titanium. In order somewhat to get rid of this uncertainty, further analysis of the behavior of the dependences [α/Fe] – [Fe/H] of moving group and

cluster is carried out in the averaged abundances of α-elements in their stars, moreover only three – magnesium, silicon and calcium, after excluding the abundances of titanium, the error in determination of which, as we see, much more.

In Fig. 3 different marks represented the [Fe/H] – [⟨Mg, Si, Ca⟩/Fe] diagrams for the stars of moving group, globular cluster and genetically connected stars of the Galaxy. Averaging over three chemical elements noticeably decreased the thicknesses of all three sequences, which increased the justifiability of assumption about the genetic connection of stars inside each object. Now it is distinctly evident that the characteristic "knee" for the stars of moving group begins somewhere in the environment [Fe/] ≈ -1.3, i. e., much earlier than in the Galaxy, where it is located at the point [Fe/H] ≈ -1.0. In this case the descending section of the sequence completely proved to be lying in the range with the smaller metallicity, where the genetically connected stars of the Galaxy practically be absent. This will agree with our result (Marsakov, Borkova, 2006), obtained on the basis of a study of the distribution only of one representative of α-elements – magnesium.

The picture is not so clear for the stars of globular cluster. Group of intermediate metallicity 11 stars with the anomalously high relative abundances of the α-elements (they are marked out in the figure with the being differed marks) mixes the uniqueness of interpretation. Such high relations ($[\alpha/\mathrm{Fe}] > 0.4$) for the stars of this metallicity are uncharacteristic. The analysis of the determinations of the chemical elements abundances in these stars did not reveal the systematic preferences, which facilitate their unjustified overstating; therefore status of these stars for us remains incomprehensible. It is not possible to exclude the probability that this group of stars has another origin, in any event additional studies be required for them. The remaining stars of cluster on the diagram can be conditionally divided into two parts. The first - this bulk of metal-poor stars with the high relations of $\langle[\alpha/\mathrm{Fe}]\rangle \approx 0.33$, and the second demonstrates the systematic decrease of this relation with an increase in the metallicity, beginning from [Fe/] ≈ -1.3. As a result, if we do not take into consideration of 13 stars with anomalously high relative abundances of α-elements, it is possible to note the very good agreement of all components of the discussed sequences of moving group and cluster.

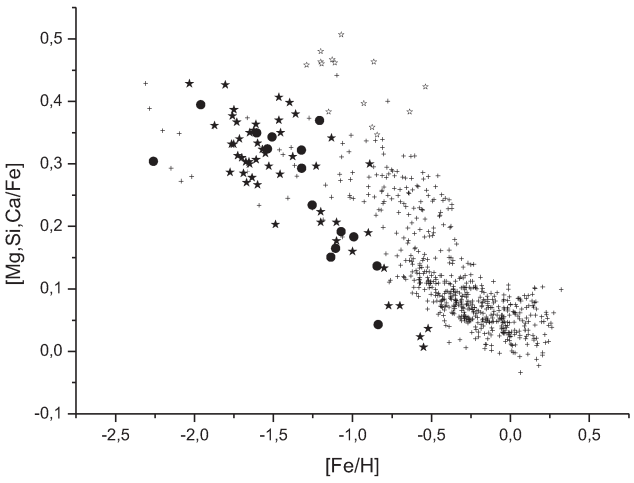

Figure 3: Metallicity – average relative α-element abundances (Mg, Si, Ca) diagram for the stars of the Centauri moving group, the ω Cen globular cluster and genetically connected field stars of the Galaxy. Designations are as in Fig. 2. Stars of globular cluster with the anomalously high relations [⟨Mg, Si, Ca⟩/Fe] are additionally isolated.

Discussion

Thus, the behavior of the [α/Fe] – [Fe/H] dependence for the ω Cen globular cluster indicates that with the great probability both most metal-poor and most metal-rich stars can prove to be genetically connected. Hardly the stars of high metallicity could in it appear as a result the captured of small cluster, since then it is very difficult to explain in them the trend of the relation [α/Fe] from the metallicity. Actually, according to contemporary ideas this trend can arise only as a result of continuous star formation in the a starry-gas system, when begin to predominate the supernova explosions of the 1a type, which enrich interstellar medium exclusively with the elements of iron peak and therefore relative abundances of α-elements systematically reducing in it. To more natural assume this process in the massive stellar system (such it is ω Cen globular cluster), than in the cluster twenty times, as they assume, smaller mass. However, here apparently possibly and another explanation - precipitation to the center of the dwarf galaxy of its younger stars, irregularly caused by the tidal forces of our Galaxy. In this case it is possible to explain not only the being differed kinematics of metal-rich stars, but also another three-dimensional configuration of the volume occupied by them. (By the way, last observant fact cannot be understood within the framework the hypothesis of the formation of all stars of cluster from one proto-cloud – already only existence of correlation between the velocities dispersion and the metallicity inside the globular cluster (Norris et al., 1996; Sollima et al., 2005) some authors (Ferraro et al., 2002; Panchino et al., 2003) interpret as evidence of the accretion events, proceeding inside the parental system ω Cen.) In this case only stars of metal-poor bulk are strictly the initial population of globular cluster, which, as in all known globular

clusters, it does not reveal the noticeable dispersion of chemical composition, which exceeds the errors of its determination.

The conclusion about the genetic link of the stars of moving group means that they all in the past belonged dwarf galaxy-satellite, center of which was the globular cluster ω Cen. Moreover to precisely parental galaxy, but not to globular cluster, since the cluster first of all must delegate into the stellar stream its very high velocity stars, but such, as show observations, appear most metal-poor. In the stream, as can be seen from Fig. 1 c, vice versa – are the surplus of most metal-rich stars. Observed in Fig. 3 very good agreement of the descending branches of the sequences [α/Fe] from [Fe/H] of stream and cluster, beginning from the point "knee", assumes the identical star formation rate both in the parental galaxy and in the cluster, which is highly improbable. This surprising agreement is additional evidence of in favor expressed above hypothesis about the possible capture by the central globular cluster of stars of the parental dwarf galaxy. (Certainly, for an increase in the ponderability of this assumption one should fulfill the numerical simulation of the dynamic processes, proceeding with interaction of galaxies.) The observed on the metallicity function of the moving group significant scarcity of metal-poor stars most likely could come out as a result the sufficiently continuance of interaction of the galaxy-satellite with our Galaxy, during which in the initial stages of this interaction it lost first of all its oldest, kinematically hot, i. e. metal-poor stars, which we do not observe from the Earth as a stellar stream because of a change in the course of time in its orbit. And only the slow stars of the dwarf galaxy is most gravitationally attached to the central globular cluster in essence proved to be the components of the moving group, observed now in the environments of the Sun. However, the stars of very globular cluster in this stellar stream most likely thus far be absent.

Proposing now that the united sequence [α/Fe] from [Fe/H] of stream and cluster reflects the chemical evolution of their parental galaxy, let us try to restore some of its moments. In particular, judging by the agreement of the average relative abundances of α-elements in the metal-poor stars of the Galaxy and the ω Cen dwarf galaxy, the parameters of the ejections of second type massive supernovas in these objects were not differed from each other. Further, the "break point" position of the dependence [α/Fe] on [Fe/H] with the smaller than in the Galaxy metallicity testifies that the initial star formation rate in it was substantially lower than in our Galaxy. Completely rapid reduction in the relation [α/Fe] after the "break point" evidences, that subsequently the star formation rate remained in it sufficiently low. The linearity of this drop indicates the invariability of this low star formation rate; therefore hardly correctly to speak about several flashes in it of star formation (as, however, and in the cluster itself). And finally the absence in it of stars with the metallicity [Fe/H] > -0.5 testify about the early exhaustion in it of interstellar gas, most probably because of the loss it as a result of interaction with our Galaxy.

The full text of this report will be published in "Pis'ma v Astronomicheskii Zhurnal".

Acknowledgements. This work was supported by the Federal Agency for Education (projects RNP 2.1.1.3483 and RNP 2.2.3.1.3950)

References

Borkova T.V., Marsakov V.A.: 2005, *Astron. Zh.,* **82**, 453.

Borkova T.V., Marsakov V.A.: 2006, *Pis'ma Astron.* Zh., **32**, 545.

Meza A., Navarro J.F., Abadi M.G., Steinmetz M.: 2005, *Mon. Not. Roy. Astron. Soc.*, **359**, 93.

Norris L., Freeman K.C., Mighell K.J.: 1996, *Astrophys. J.*, **462**, 241.

Panchino E., Seleznev A., Ferraro F.R., Bellazzini M., Piotto M.: 2003, *Mon. Not. Roy. Astron. Soc.*, **345**, 683.

Suntzeff N., Kraft R.: 1996, *Astron. J.,* **111**, 1913.

Sollima A., Panchino E., Ferraro F.R., et al.: 2005, *Astrophys. J.*, **634**, 332.

Ferraro F.R., Bellazzini M., Panchino E.: 2002, *Astrophys. J.*, **573**, L95.

Abadi M.G., Navarro M.G., Steinmetzand M., Eke V.R.: 2003, *Astrophys. J.,* **597**, 21.

FORMATION OF SMALL-SCALE STRUCTURES IN THE INTERSTELLAR MEDIUM

E.E. Matvienko[1], E.O. Vasiliev[2,3], Yu.A. Shchekinov[1,4]

[1] Department of Physics, Southern Federal University
Rostov-on-Don 344090 Russia, *ematvien@mail.ru, yus@phys.rsu.ru*
[2] Institute of Physics, Southern Federal University
Rostov-on-Don 344090 Russia, *eugstar@mail.ru*
[3] Institute of Astronomy, Russian Academy of Sciences
Moscow 119017 Russia
[4] Special Astrophysical Observatory, Nizhny Arkhyz
Karachai-Cherkesia Russia

ABSTRACT. We consider formation of small scale structures in the process of interstellar cloud destruction by shock waves. We calculate statistical properties of HI column densities, optical depth and brightness temperature in 21 cm line. We discuss possible relation of the small-scale structures found in numerical models to the so called "low-N(HI)" clouds observed recently in the interstellar medium.

Key words: interstellar medium, neutral hydrogen, shock waves.

1. Introduction

Physical properties of the neutral atomic gas are of great importance for the star formation and overall dynamics of the interstellar medium (ISM). The sizes of structures in the neutral component of the ISM vary from several AU (tiny scale atomic structures) to several parsecs (standard HI clouds) (Kulkarni & Heiles 1987, Dickey & Lockman 1990, Heiles & Troland 2003, 2005). Recently a possibly new population of HI clouds has been discovered (Braun & Kanekar 2005, Stanimirović & Heiles 2005). Such structures have HI column densities among the lowest ever detected for cold neutral medium, $\sim 10^{18}$ cm^{-2}; these structures are called "low-N(HI)" clouds (Stanimirović et al 2007).

Formation of "low-N(HI)" clouds can be associated with various dynamical processes taking place in the interstellar medium. For instance, Hennebelle & Audit (2007) have described turbulent atomic gas formed by colliding flows, which reproduce observational features of turbulent HI flows resonably well. Such dynamical processes as destruction of interstellar HI clouds by shock waves, stellar wind, or cloud collisions seem to produce similar structures. During the interaction of shock wave with a cloud its external layers become turbulent due to Kelvin-Helmholtz instability, form vortices and filaments which finally leave the cloud (Klein et al 1994, Vietri et al 1997);such filaments can appear as isolated HI structures. Their size depends on the size of a detroyed cloud and in general varies in a wide range.

Here we consider a possibility of formation of small scale HI structures in the process of interstellar cloud destruction by shock waves.

2. Model

In our model a spherical homogeneous cloud of the density $n = 1$ cm^{-3} and the radius $a = 2$ pc is immersed under pressure equilibrium into a homogeneous intercloud medium with the temperature $T = 10^4$ K and the density $n = 0.1$ cm^{-3}. At initial time, $t = 0$, a planar shock wave (assumingly from a distant supernova) encounters the cloud with the Mach number $\mathcal{M} = 10$. The computational zone of size 60×10 pc is a cylinder with 1200 grids in z-direction, and 200 radial grid points. Numerical simulations were performed with using ZEUS-2D code (Stone & Norman 1992). Energy losses include the cooling by collisional exitation of atomic hydrogen, CII and OI fine-structure transitions (Hollenbach & McKee 1989).

To compare our simulations with observational features of interstellar structures we calculate synthetic spectrum and optical depth of the 21 cm line. We find the spin temperature for each elememt of neutral gas ($T \leq 10^4$ K). We consider only collisional excitation of the 21cm line by HI atoms and electrons (Field 1958). Collisional de-excitation rates by hydrogen atoms and electrons are taken from Kuhlen et al (2005) and Liszt (2001). We take the electron fraction in

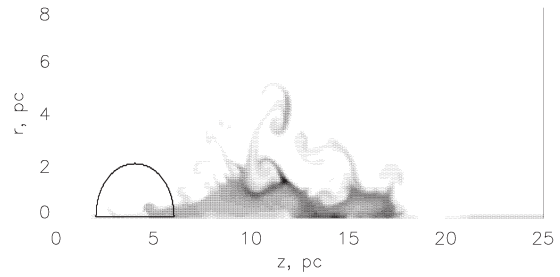

Figure 1: Density disribution in the computational domain for time 8×10^{13} s.

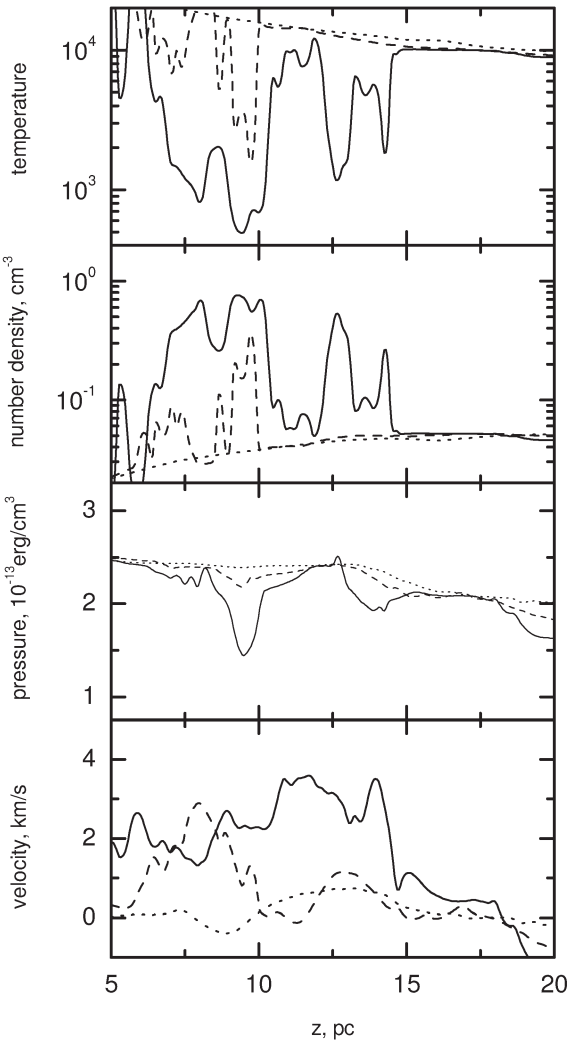

Figure 2: Temperature, density, pressure and velocity distributions for time 8×10^{13} between 5 and 20 pc along lines of sight at the distance from the axis of symmetry 1, 3 and 5 pc are depicted by solid, dashed and dotted lines, correspondingly.

neutral gas 10^{-3}, however, the influence of electrons on the brightness temperature is negligible. The velocity resolution of the spectra calculated here is 1 km s^{-1}. To calculate the total spin temperature along line of sight we find average harmonic value for each velocity interval (e.g. Kaplan, Pikel'ner 1963).

3. Results

Figure 1 presents the distribution of density at $t = 8 \times 10^{13}$ after the shock wave encounters the cloud. The cloud is destroyed onto many filaments stretched along the axis of symmetry. In most dense filaments n reaches ~ 1 cm^{-3}.

Figure 2 shows the disributions of temperature, density, pressure and velocity along three lines of sight (LOS) at distance 1, 3 and 5 pc from the axis of symmetry. The first LOS is rather close to the symmerty axis and crosses many filaments including cold and dense clumps. One can find a region with minimum temperature $\sim$ 500 K and density ~ 1 cm^{-3}. The pressure in the region is quite low, so that this clump will be further contracted in the direction of the line of sight. The more distant LOS passes through the postshocked medium with a small fraction or even without material from cloud, therefore we can distinguish features of the disrupted cloud from the postshock gas.

Figures 3 and 4 depict the 21 cm syntethic spectra and optical depth for the three lines of sight. For time $t = 8 \times 10^{13}$ s the brightness temperature and optical depth have clear maximum only for the first LOS. Indeed, this line crosses a group of clumps seen around $z = 10$ pc in Fig. 2. The velocity of the group is close to 3 km s^{-1}. Although the group reveals a complexity of the structure, the spectral features are relatively smooth. The largest parameters of spectral lines are: the brightness temperature is about 9 K, the extinction is ~ 0.006, the width of the line is ~ 5 km s^{-1}. These numbers are very similar to typical numbers for the so called "low-N(HI)" clouds (Braun & Kanekar 2005, Stanimirović & Heiles 2005). At later time $t = 1.2 \times 10^{14}$ s the brightness temperature and the extinction value decrease about half, while the line becomes wider, ~ 10 km s^{-1}. For the other two LOS the line is sufficiently broad without obvious spectral features. These LOS represent the postshock gas with a limited number of filaments.

We calculate column densities along one hundred lines of sight parallel to the axis of symmetry, with the velocity resolution 1 km s^{-1}. Figure 5 presents the simulated distributions for N(HI) along the whole set of lines of sight in all velocity intervals. The sample of the LOS is sufficiently complete in the sense that this distribution is stable against variations of the number of LOS. For $t = 8 \times 10^{13}$ s the number of spectral features decreases with column density sharply, so that

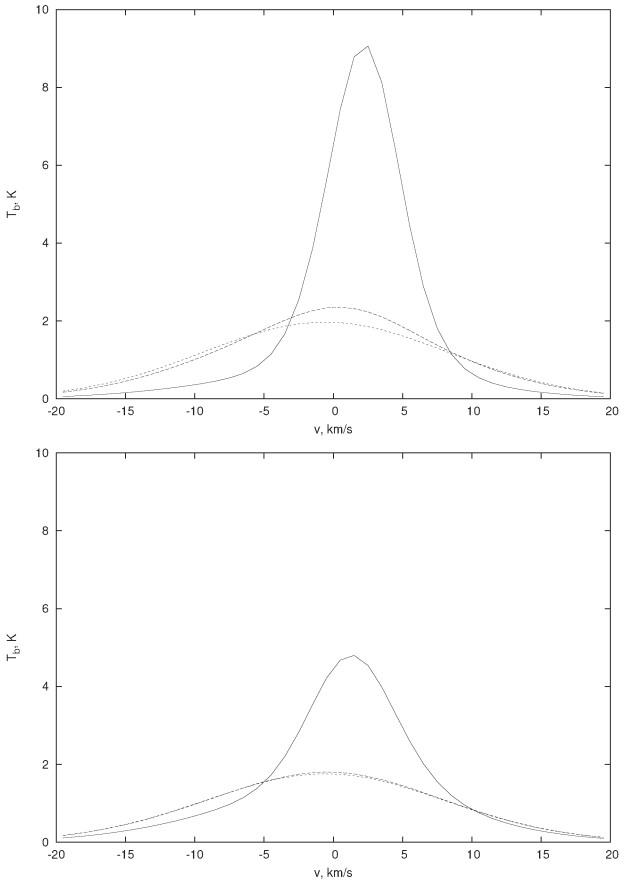

Figure 3: Brightness temperature along lines of sight at the distance from the axis of symmetry 1, 3 and 5 pc is depicted by solid, dashed and dotted lines, correspondingly. Upper panel is for $t = 8 \times 10^{13}$ s , lower – for $t = 1.2 \times 10^{14}$ s .

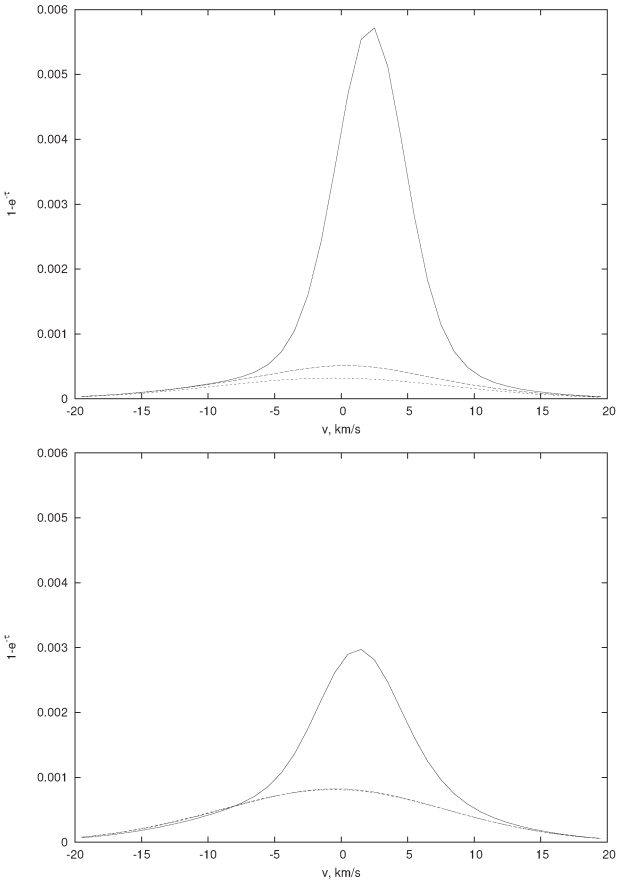

Figure 4: Optical depth along the same lines as in Figure 3.

the most probable column density is $\sim 10^{18}$ cm^{-2}. At later time one can observe two well pronounced peaks in the N(HI) distribution; the average column density remains still close to the value at earlier times. This value almost coincides with the typical column density for "low-N(HI)" clouds Stanimirović & Heiles 2005. It is worth noting that the average column density weakly grows in time, however the increase over several cloud disruption times is rather small.

4. Conclusion

In this contribution we considered the physical and statistical properties of filaments formed during destruction of an interstellar homogenious cloud by a shock wave. We found that:

- small scale structures form during disruption of interstellar clouds by shock waves;
- the 21 cm line profiles of small scale structures are close to the observed in the ISM at the lower end of column densities;
- the simulated column densities at intermediate times (a few dynamical times) are very close to the observed HI column densities in low-N(HI) clouds.

We can assume thus that the formation of small scale structures is a common feature of dynamical processes in the interstellar medium, and recently observed low-N(HI) clouds may be attributed to interstellar cloud destruction by shock waves from SNe.

Acknowledgements. This work is supported by the RFBR grant 08-02-91321, the Federal Agency of Education grant RNP 2.1.1.3483. EOV is supported by the RFBR through the mobility programme grant 08-02-90706, YuS acknowledges support from RFBR through the grant 08-02-00933.

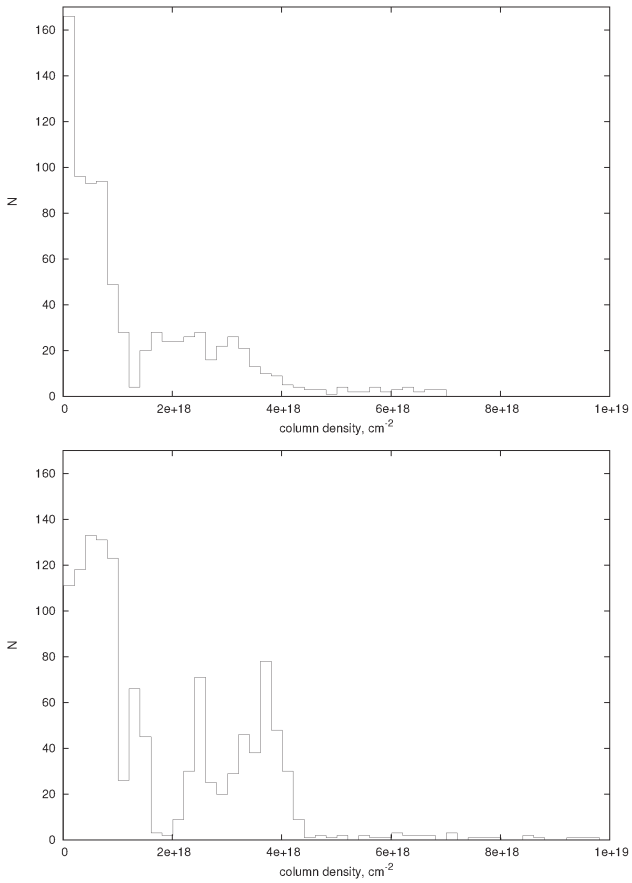

Figure 5: The distribution N(HI) for all line of sight for $t = 8 \times 10^{13}$ (upper) and $t = 1.2 \times 10^{14}$ (lower).

References

Braun R. & Kanekar N.: 2005, *Astron. Astrophys.,* **436L**, 53.

Dickey H. and Lockman F.: 1990, *Ann. Rev. Astron. Astrophys.,* **28**, 215.

Field G.B.: 1958, *Proc. IRE,* **46**, 240.

Heiles C., Troland T.: 2003, *Astrophys. J.,* **586**, 1067.

Heiles C., Troland T.: 2005, *Astrophys. J.,* **624**, 773.

Hennebelle P., Audit E.: 2007, *Astron. Astrophys.,* **465**, 431.

Hennebelle P., Audit E., Miville-Deschenes M.-A.: 2007, *Astron. Astrophys.,* **465**, 445.

Hollenbach D., McKee C. F.: 1989, *Astrophys. J.,* **342**, 306.

Kaplan S. A., Pikel'ner S. B.: 1963, *Mezhzvezdnaya sreda*, Moscow, *in Russian.*

Klein R.I., McKee C.F., Colella P.: 1994, *Astrophys. J.,* **420**, 213.

Kuhlen M., Madau P., Montgomeri R.: 2006, *Astrophys. J.,* **637L**, 1.

Kulkarni S. R., Heiles C.: 1987, *Interstellar processes*, /ed. Hollenbach D., Thronson H.

Liszt H.: 2001, *Astron. Astrophys.,* **371**, 698.

Stanimirovic S., Heiles C.: 2005, *Astrophys. J.,* **631**, 371.

Stanimirovic S., Heiles C., Kanekar N.: 2007, *ASP Conf. Ser.,* **365**, 22.

Stone J.M., Norman M.L.: 1992, *Astrophys. J.,* **390**, L17.

Vietri M., Ferrara A., Miniati F.: 1997, *Astrophys. J.,* **483**, 262.

DESTRUCTION OF THE INTERSTELLAR CLOUDS BY THE SHOCK WAVES

E.E. Matvienko[1], Yu.A. Shchekinov[1,2]

[1] Department of Physics, Southern Federal University
Rostov-on-Don 344090 Russia, *ematvien@mail.ru, yus@phys.rsu.ru*
[2] Special Astrophysical Observatory, Russian Academy of Sciences
Nizhnij Arkhyz, Karachai-Cherkess Republic 369167 Russia

ABSTRACT. We study the influence of the interstellar cloud structure irregularity on the dynamics of its destruction by a supernova shock wave. It is shown that irregular clouds are destroyed twice quickly as the spherical ones. Subject to that the fragments of the clouds sustain high-density and do not mix with the intercloud gas.

Key words: interstellar medium, shock wave, cloud destruction.

1. Introduction

The issue of the interaction of the shock waves with the interstellar clouds is one of the fundamental ones in the space gas dynamics. Usually the phase homogeneity of the medium is implicitly assumed in ISM dynamic processes considerations. However, recently there were performed several studies, where the effects of the multiphase ISM are explicitly taken into account. The system of the clouds is treated in several ways: a) a dynamically constant background (Hartquist et al 1986, Shchekinov 1996, Lizano et al 1996), b) as a dynamically independent component described as a set of the point objects (Cowie et al 1981), c) as an independent gas dynamic subsystem (Kamaya & Shchekinov 1997). In all cases the functions describing the exchange of the mass, the momentum and the energy between the phases are based on the simplified estimates of the dynamic destruction efficacy of the clouds, or on the calculations of the spherically symmetric vapour of the clouds by the heat transfer from the surrounding hot gas. We study destruction dynamics of the clouds by a shock wave from the point of view of chaotic movements excited in it and in terms of the conversion efficacy of a part of the shock wave energy to the kinetic energy of the fragments of a cloud. We especially pay attention to the influence of the cloud surface structure irregularity on the dynamics of destruction.

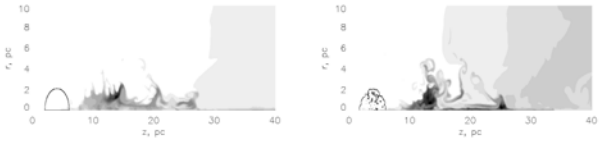

Figure 1: Density distribution after the interaction with the shock wave (left panel – spherical cloud, right – irregular cloud).

2. Description of the model

We consider the dynamics of the spherical and quasi-spherical clouds after the interaction with shock wave. Initially the clouds are in dynamic equilibrium with the background gas. In our main model, we study the temperature of the intercloud medium – $T_i = 10^4$ K, the density $n_i = 0.1$ cm^{-3}; in the cloud at undisturbed state $T_c = 10^3$ K, $n_c = 1$ cm^{-3}. We examine two cases for cloud: cloud with spherical surface of the radius $a_0 = 2.5$ pc and quasispherical cloud with irregular surface and average radius a_0. In the calculations we neglect gravity, the effects of the heat conduction and radiation losses taking the ideal gas state equation with a factor of an adiabatic $\gamma = 5/3$.

The calculations were conducted on a fixed cylindrical grid $[z, r] = 1200 \times 200$ of cells with a spatial resolution of 0.05 pc that corresponds to the physical size of the entire computational zone 60 pc $\times$ 10 pc. The detailed desription of the model can be found in (Matvienko & Shchekinov 2007).

3. Results

Fig. 2 shows with the mosaics the distribution of the cloud density contrasts by the mass depending on time; it is shown with the shades of the gray tones the mass of the calculated cells with a density contrast (with respect to the background value) at a given interval with

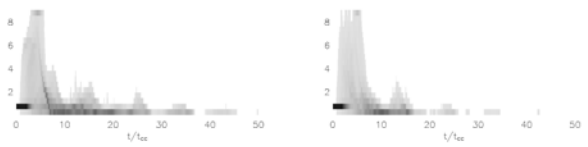

Figure 2: Histograms of the density distribution (left panel – spherical cloud, right – irregular cloud).

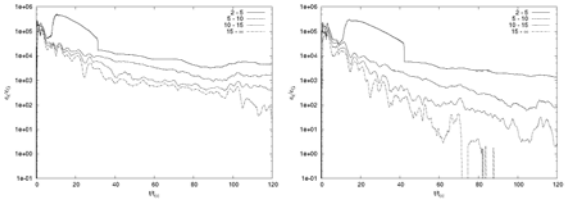

Figure 3: Average kinetic energy of the cloud fragments to the original gravitational energy per unit of volume (left – spherical cloud, right – irregular cloud).

darker areas corresponding to the larger mass involved in the computational zones. It should be noted that a cloud with an irregular border shows faster evolution, it overcomes a smaller number of oscillations of the cells number with the high contrast of the density and it disappears.

Fig. 3 shows the ratio of kinetic energy per unit of volume of the cloud fragments chaotic motions (for the spherical and quasispherical cases) with different values of the density contrasts to the original gravitational energy per unit of volume of the spherical cloud.

Another quanity characterized the random motions of cloud fragments is the velocity autocorrelation function. Fig. 4 shows the autocorrelation functions for several time moments. The autocorrelation function for velocities of the chaotic motions shows the coherence of the motions in z direction and in perpendicular direction to it. The autocorrelation function for velocities of the chaotic motions shows the coherence of the motions in direction of the initial blast spread and in perpendicular direction to it.

4. Conclusions

In this paper we examined the dynamics of destruction of the interstellar clouds with an irregular border. We have shown that:

- The destruction of the clouds with irregular shape by the shock waves is more effective - such clouds are destroyed with the time twice less than the time of a spherical cloud.
- The proportion of the energy of a shock wave that falls on the cloud and converts to the kinetic energy of the chaotic movements of the fragments in case of the irregular cloud is half times more. Stimulation of the starburst by the action of the shock waves on the clouds is difficult, particularly if we take into consideration that fact that the real clouds have irregular shape.
- The autocorrelation function for velocities of the chaotic motions shows the coherence of the motions in direction of the initial blast spread and in perpendicular direction to it.

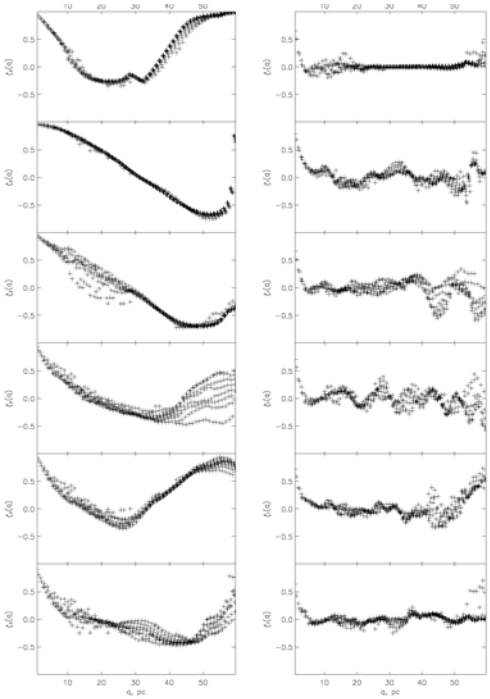

Figure 4: The velocity correlation functions in z (left column) and r (right column) directions for several time moments.

Acknowledgements. This work is supported by the RFBR grant 08-02-91321, the Federal Agency of Education grant RNP 2.1.1.3483.

References

Cowie L.L., McKee C.F., Ostriker J.P.: 1981, *Astrophys. J.,* **247**, 908.

Hartquist T.W., Dyson J.E., Pettini M., Smith L.J.: 1986, *Month. Not. Roy. Astron. Soc.*, **221**, 715.

Kamaya H., Shchekinov Yu.A.: 1997, *Astrophys. J.*, **486**, 840.

Lizano S., Canto J., Garay G., Hollenbach D.: 1996, *Astrophys. J.*, **468**, 739.

Matvienko E.E., Shchekinov Yu.A.: 2007, *Astron. Rept.*, **84**, 128.

Shchekinov Yu. A.: 1996, *Astrophys. Geophys. Flu. Dyn.*, **82**, 69.

THE LOCAL DWARF GALAXIES:BUILDING BLOCKS OF MASSIVE ONES? I.THE FORNAX DWARF GALAXY

T.V. Nykytyuk

Main Astronomical Observatory
Ak. Zabolotnoho St. 27, Kyiv 03680, Ukraine, *nikita@mao.kiev.ua*

ABSTRACT. A chemical evolution of the Local Group dwarf galaxy Fornax is considered in the framework of the merger scenario. We suppose a galactic stellar halo to be formed as separate fragments which then merge; thus, we can calculate the set of such the fragments to reproduce the observed metallicity distribution function of a galaxy. Accordingly, if dwarf galaxies were such the systems, which, once merged, have formed massive galaxies, we need to obtain only one fragment to reproduce the observed metallicity distribution function of a dwarf galaxy. To test this assumption, the stellar metallicity distribution functions of Fornax was calculated in the framework of the merger scenario. The more than one fragment was obtained for galaxy under consideration; thus, it is unlikely the systems similar to Fornax to be building blocks of massive galaxies.

Key words: galaxies: merger; galaxies: Local dwarfs; Fornax: metallicity distribution function.

1. Introduction

The theory of hierarchical clustering of galaxies considers the formation of massive galaxies by merger of smaller ones. As it shown in our previes works (Nykytyuk, 2004; 2008), massive spiral galaxies in Local Group could be formed by merger of individual fragments; two of them (M31 and M33) were formed by merger of 2 fragments only. It is natural to suppose the systems like Local dwarf galaxies to be building blocks of massive ones.

The Fornax dwarf galaxy is one of the most massive and luminous of the dwarf galaxy satellites of our Galaxy. The Fornax stellar population is quite metal-rich as for a dwarf galaxy; Pont et al. (2004) found a metallicity distribution of Fornax centered at [Fe/H] = - 0.9 with metal-rich population reaching [Fe/H]=-0.4. Thus, the system like Fornax galaxy could be building blocks for M31 and M33 galaxy formation.

Our goal is to analyze a possibility for Fornax dSph to be a fragment for formation of more massive galaxies and to study the chemical evolution of this galaxy.

2. The merger scenario

We suppose that the halo stellar population is composed of a mixture of stars that were formed in fragments originally evolving independently from the main protogalactic cloud and/or from each other. Hence, there should be a set of fragments whose total stellar populations reproduce the observed stellar halo metallicity distribution.

The mass of fragments from which the halo is formed, to equal the sum of the masses of their stellar population and the gas fallen onto the disk up to the present epoch. The star formation process in different fragments can begin at different times. A fragment can evolve up to a given astration level s before falling onto a protogalaxy.The stars formed up to this moment replenish the halo stellar population, and the gas falls onto the galactic disk. Fragments can be captured by a protogalaxy before a stellar population is formed, i.e. fragments composed completely by gas can be captured.

Let a_j - number of stars finding in a range of metallicities Z_j, $Z_j + \Delta Z_j$ in a fragment with mass m. Then an observable amount of halo stars finding in a range of metallicities Z_j, $Z_j + \Delta Z$ will be represent an total amount of stars $N_{Z_j} = a_j \sum_{i=1}^{n} m_i$ of a given metallicity Z_j from all fragments whose the maximum metallicity exceeds Z_j. For given set of metallicities we have

$$\begin{aligned} a_1 \cdot m_1 + a_1 \cdot m_2 + a_1 \cdot m_3 + \ldots + a_1 \cdot m_n &= and N_{Z_1} \\ a_2 \cdot m_2 + a_2 \cdot m_3 + \ldots + a_2 \cdot m_n &= and N_{Z_2} \\ \vdots \qquad\qquad & \vdots \\ a_n \cdot m_n &= and N_{Z_n} \end{aligned} \tag{1}$$

Thus, the fragment with the high astration level s determines a number of stars a_n with the greatest value of a metallicity Z_n. Having solved a set of equations (1), it is possible to obtaine masses of fragments with maximum metallicities of stars from Z_1 up to Z_n (i.e. number of fragments falling on given Z_j and responsible for halo stars with such metallicity). Thus, using observed metallicity distribution of halo stars and

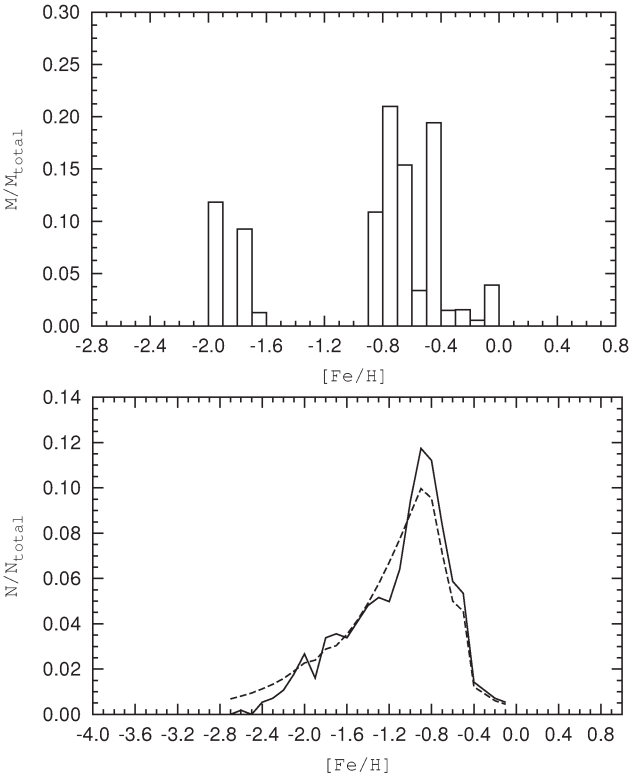

Figure 1: The masses and metallicities of merging fragments(top panel); the comparison of observed (solid line, Battaglia et al. 2006) and modelled (dashed line) halo metallicity distribution functions of Fornax (bottom panel).

model of evolution of a single fragment we shall obtaine a value of an total mass of all fragments evolved up to each given value of astration level s. The chemical evolution of a fragment is described in details in the paper of Nykytyuk (2008).

In order to compare the calculated and observed metallicity distribution functions, we have used the Kolmogorov - Smirnov criterion of convergence of two distributions. The significance level σ denotes the coincidence level of two distribution: a small values of σ indicates that the data samples have different probability distributions.

3. The results: merger vs. monolitic evolution

We suppose that the halo stellar population is the sum of stellar populations of separate fragments. If using the observed metallicity function for Fornax under solving the set of equations (1) we would obtain one fragment only, this means that the systems like Fornax could be building blocks of Local Group massive spirals.

But our results show that the Fornax metallicity distribution function can be reproduced by merger of

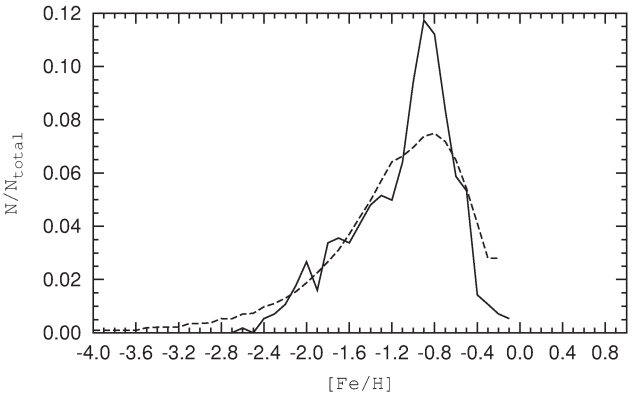

Figure 2: Monolitic evolution: the comparison of observed (solid line, Battaglia et al. 2006) and modelled (dashed line) halo metallicity distribution functions of Fornax.

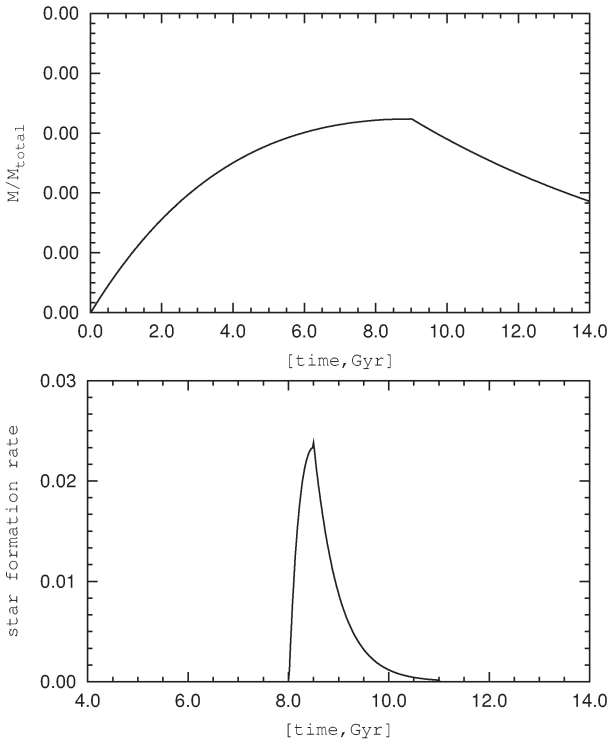

Figure 3: The star formation rates: the case of merger (top panel) and monolithic evolution (bottom panel).

twelve fragments, Fig.1; metallicity dispersion of the obtained set of fragments rather high. The shape of the metallicity distribution function of a halo stellar population depends on the characteristics of the fragments which have formed the halo of Fornax. The evolution of fragments before merger is considered in the framework of closed model of chemical evolution with SNIa yields. The star formation history in a single fragment before merger is shown in Fig.3. In the case of merger scenario the criterion of convergence ~ 0.93.

For comparison, we have investigated monolithic evolution of the Fornax dwarf galaxy, Fig.2. The metallicity distribution function have been obtained in the framework of closed chemical evolution model without SNIa yields. In this case we have no need to use the SNIa yields in our model because the star formation passes during 3 Gyr only; thus, SNIa has no enough time to contribute the main mass of iron into interstellar medium of Fornax. The star formation history in the case of monolitic evolution is shown in Fig.3. In this case the criterion of convergence ~ 0.74.

Thus, one can see that the merger scenario better reproduces the observed metallicity distribution function of Fornax than the monolitic scenario; the using of the latter don't allow to reproduce the central part of the observed metallicity distribution function quite well, Fig.2. Battaglia et al. (2006) found a different kinematic behavior of metal-rich and metal-poor stars. They interpreted this fact as recent capture of external material by Fornax. Authors argue that part of the object accreted by Fornax must have been dominated by stars more metal poor than [Fe/H] < -1.3.

4. Main results

The Fornax metallicity distribution function can be reproduced by merger of more than one fragment; I.e. the systems like Fornax could not be building blocks of massive galaxies. Probably, the merger did play role in the formation of the Fornax dwarf galaxy; the merger scenario represents the observed metallicity distribution function better than the monolitic scenario. To reproduce the observed metallicity function of the Fornax, it need the twelve fragments evolved as closed systems. To reproduce the metallicity distribution function in the framework of monolitic scenario, it's enough to use the closed box model as in the merger scenario.

References

Battaglia G., Tolstoy E., Helmi A. et al.: 2006, *A&A*, **459**, 423.
Nykytyuk T.: 2004, *KFNT*, **20**, 489.
Nykytyuk T.: 2008, *NewAst*, **13**, 340.
Pont F., Zinn R., Gallart C. et al.: 2004, *AJ*, **127**, 840.

ON THE CORRELATION OF IR AND OPTICAL VARIABILITY IN NGC 4151

V.L. Oknyanskij, V.M. Lyuty, O.G. Taranova, E.A. Koptelova, V.I. Shenavrin

Sternberg Astronomical Institute, Moscow State University
Universitetsky prospect, 13, Moscow 119992, Russia, *oknyan@mail.ru*

ABSTRACT. We combine all published and new unpublished yet NIR (near infrared) photometrical observations of NGC 4151 which can be used for determination of time delays between optical and NIR variations. In previous study we have found that the values of time delay in NIR filters are not the same for different states of the luminosity. Here we consider the new photometrical data for the deep minimum in 2003-2007 following the very high state of the nucleus. We conclude that after sublimation in high state of nucleus the dust particles were recovering during at least several years.

Key words: galaxies: AGNs: dust: IR: variabilty; AGNs: individual: NGC 4151.

1. Light curves

Our past results about NIR time delay in NGC4151 as well as other AGNs were published mostly at Oknyanskij (1993) [1], Oknyanskij et. al. (1999, 2006) [2, 3], Oknyanskij and Horn (2001) [4]. Here we take into account new photometrical data for NGC 4151 obtaned during 2003-2007. The combined light curves at filters K and U presented at Fig.1. See details in [1-4].

2. Cross-correlation analysis

We are using the same method for time delay determination **MCCF** as in the past papers. The cross-correlation function for new data in 2003-2006 time interval is presented at Fig.2 As it is seen the time delay between the variations in U and K is about 40 days.

3. Results and summary

We combine all, published [1-4] and new results about the NIR time delay determinations at the Tab.1. It was found before for a sample of 10 AGNs with $z \leq 0.165$ that the distance from the central source to the NIR (dust) regions increases with UV luminosity as ${L_{UV}}^{0.5}$ [4]. Our investigations of NGC 4151 during more than 30 years show that the time delay in filter K is variable but not following exactly to the relation delay $\sim {L_{UV}}^{0.5}$. Possible explanation of this result may be connected with sublimation of the graphite grains during high level of UV continuum. According to our result the dust recovering or recreation time should be at least several years.

Table 1: Results of NIR-to-Optical time delay determinations.

Time delay in days (1 from 2)	filter 1(2)	Time interval	References
18 ±6	K(U)	1968-1980	[1]
24 ±6	L(U)	1968-1980	[4]
35 ±8	K(U)	1985-1998	[2]
8 ±4	H(U)		
97 ±10	L(U)		
104 ±10	K(U)	1998-2003	[3]
94 ±10	H(U)		
105 ±10	L(U)		
41 ±5	K(U)	2003-2006	this paper
41 ±5	H(U)		
105 ±5	L(U)		
94 ±10	L(J)		
37 ±5	K(U)	2003-2007	

One of the possibilities is that the dust particles (graphite grains) can survive during the powerful outbursts in deep places of gas clouds and then need some time to move closer to cloud's surfaces can be needed.

Alternative explanations can be anisotropy of radiation field, shielding of the central source on the light of sight and also special orientation of the dust region, as well as real physical changes in the NIR emission region during the period of our study.

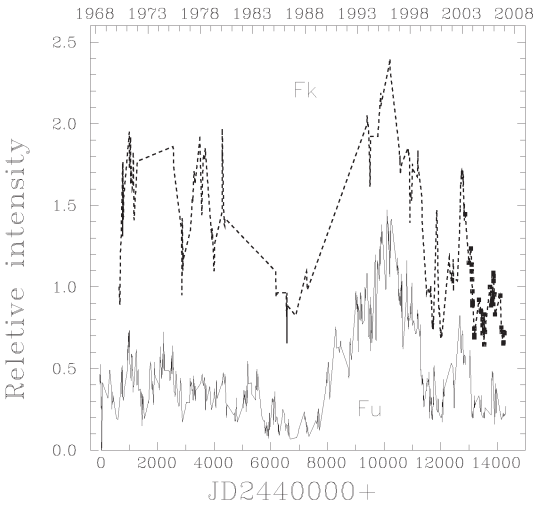

Figure 1: Observed light curves of the nucleus of NGC 4151 over 1968-2007 in relative intensities. Dashed line intensity in K, boxes - new data for 2003-2007, solid line intensity in U.

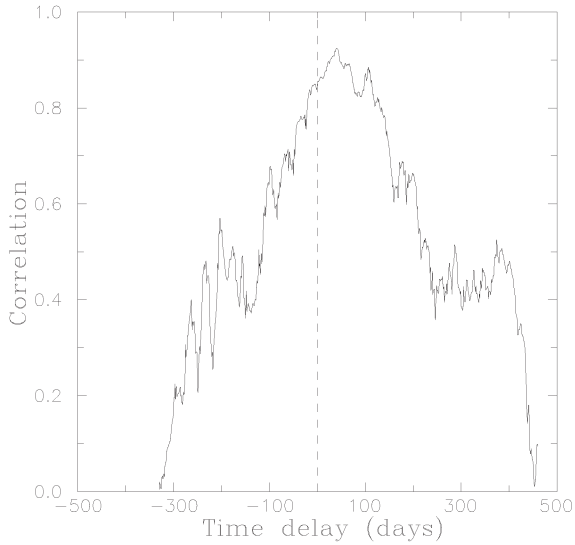

Figure 2: Cross-correlation of K and U flux variations of NGC 4151 over 2003-2006.

References

Oknaynskij V.L.: 1993, *Astron. Lett.*, **19**, 416.

Oknyanskij V.L., Lyuty V.M., Taranova O.G., Shenavrin V.I.: 1999, *Astronomy Letters*, **25**, 483.

Oknyanskij V.L., Lyuty V.M., Taranova O.G., Shenavrin V.I.: 2006, *ASP Conf. Ser.*, **360**, 75.

Oknyanskij V.L., Horn K.: 2001, *ASP Conf. Ser.*, **282**, 330.

СТАНОВЛЕНИЕ И РАЗВИТИЕ НАЗЕМНОЙ СПЕКТРОСКОПИИ

Панчук В.Е.

Специальная астрофизическая обсерватория РАН

РЕЗЮМЕ. Перечислены основные этапы развития технических средств мировой и отечественной астрономической спектроскопии.

Первые сто лет астрономической спектроскопии ознаменованы следующими этапами. В 1802 г. В.Г.Волластон, используя щель и призму (этот эксперимент можно считать зарождением спектроскопического приборостроения), обнаружил в спектре Солнца семь темных линий, которые счел границами естественных цветов. В 1814 г. И.Фраунгофер наблюдал уже около 600 линий, половину из которых нанес на карту спектра. Начиная с 1817 г., Фраунгофер визуально сравнивал спектры Солнца, планет и ярких звезд, в 1823 г. убедился, что спектры звезд различны. В 1842 г. Х.Доплер высказал предположение, что характер светового луча изменяется в зависимости от скорости перемещения источника света относительно наблюдателя. В 1859 г. Г.Р.Кирхгоф установил закономерности поведения линейчатого (абсорбционного и эмиссионного) и непрерывного спектров (зарождение спектрального анализа). Первый солнечный спектр был опубликован Кирхгофом в 1861 г. В 1868 г. в спектре хромосферы обнаружена желтая линия, отождествленная с линией гелия, открытого на Земле в 1895 г. В 1868 г. Локьер обнаружил смещения и искривления линий хромосферного спектра, что интерпретировал как проявление эффекта Доплера. В 1863 г. Секки начал использовать призму прямого зрения, и в 1868 г. опубликовал результаты первых попыток спектральной классификации звезд (четыре типа: водородные, металлические и два типа молекулярных). В 1886 г., в память Г.Дрепера, основателя «конвейерного производства» в астроспектроскопии – метода с предобъективной призмой, – было начато составление обзора спектров звезд северного неба (руководил – Пикеринг, работала, в основном, – А.Кэннон, выполнившая классификацию спектров для 360 тысяч звезд). В 1890 г. Килер (Ликская обсерватория) выполнил первые надежные визуальные измерения лучевой скорости по спектру Арктура. В 1888 г. Фогель (Потсдам) начал фотографические измерения лучевых скоростей, методику изучили и развивали Фрост (Йеркская обсерватория) и А.А.Белопольский (Пулково). На Лике фотографическую спектроскопию развивал Кэмпбелл. В 1897 г. А.С.Мори опубликовала различия в ширинах и интенсивностях линий, которые в 1905 г. Герцшпрунг проинтерпретировал как эффекты светимости. В 1900 г. Белопольский экспериментально подтвердил принцип Доплера. Итак, за первое столетие составлен атлас спектра Солнца, в спектрах выделены основные эффекты (эмиссия, абсорбция, сдвиг линий), созданы методы фотографической спектроскопии, проведено накопление звездных спектров с последующей классификацией, начаты массовые измерения деталей в спектрах (интенсивности, ширины и сдвиги линий). В конце XIX века спектроскопия высокого разрешения (достигая R=30000), была связана с применением крупнейших телескопов того времени.

Становление астроспектроскопии в России обусловлено следующими обстоятельствами. Астрофизика зародилась на астрономических обсерваториях, последние можно разделить на два типа: приморские и придворные. Каждая придворная обсерватория (Франция, Англия, Россия) рассматривалась, прежде всего, как политический проект (например: «Пулково должно обладать лучшими в мире инструментами»), климатические соображения отступали на второй план. Климат южных приморских обсерваторий был не намного лучше. Первые полстолетия стратегия развития Пулкова определялась иностранными учеными. Астрофизические наблюдения в России были начаты на университетских обсерваториях, скромное оборудование которых уступало превосходной оснащенности Пулкова. Особенности этого этапа спектроскопии были персонифицированы, т.к. работало всего около дюжины специалистов. Темпы развития были высокими, например, для большого пулковского рефрактора (стоимостью 300 тыс.руб.), за 2 года был изготовлен 76-см объектив (стоимостью 32 тыс. долларов). В первой декаде XX века уже все 14 обсерваторий России (Дерпт, Харьков, Николаев, Москва, Пулково, Киев, Одесса, Ташкент, Санкт-Петербург, Казань (2), Львов, Дубоссары, Симеиз), – обладали оборудованием, пригодным для выполнения астрофизических исследований. Российских обсерваторий было в 10 раз меньше, чем в Западной Европе, и в 3 раза меньше, чем в Соединенных Штатах. Но по степени оснащенности оборудованием, предназначенным для астрофизических работ или пригодным для таковых, – Россия находилась в числе лидеров.

Второе столетие астроспектроскопии можно характеризовать следующими техническими этапами: 1) создание первой астрофизической лаборатории (Хэйл); 2) создание спектрографа фокуса кудэ, R=70000 (Адамс, 1911); 3) совершенствование техники изготовления дифракционных решеток, длина нарезанной части от 110 мм в 1935 г. до 304 мм в 1952 г. (Вуд); 4) изобретение катадиоптрических светосильных камер (Шмидт, Максутов); 5) увеличение угловой дисперсии решетки за счет перехода в высокие порядки дифракции (Гаррисон, Герасимов, Копылов, Стешенко); 6) массовое применение малошумящих светоприемников; 7) создание специализированных спектроскопических телескопов.

В 1935 г. половина всех публикаций в ApJ была посвящена исследованию звездных спектров, а к 1975 г., когда практически все спектрографы неподвижного фокуса кудэ были построены, эта доля снизилась до 1/7. Обнаружение объектов новой природы, или новых свойств у известных объектов, привело к смене приоритетов в астрофизике, что неизбежно отразилось на развитии техники звездной спектроскопии во второй половине XX века. «Золотой век» звездной спектроскопии завершился.

Выделим концептуальные приборы этого столетия. А) Универсальный призменный спектрограф 1.8-м рефлектора, Виктория, конец 20-х. Линзовая фотографическая камера устанавливалась после одной, двух или трех призм, что расширяло набор вариантов наблюдений. Б) Спектрограф фокуса кудэ 2.5-м телескопа Маунт Вилсон, ценность которого подчеркивается высказыванием Мак-Лафлина, 1956: «Если даже с помощью 200-дюймового телескопа и не сделают новых открытий, он полезен тем, что освободит 100-дюймовый телескоп для решения многих задач». В) Спектрограф фокуса кудэ 1.9 м рефлектора обсерватории Верхнего Прованса, – щель, коллиматор, дифракционная решетка, и 4 камеры спектрографа были заключены в объем постоянного давления и температуры. Г) Корреляционный фотоэлектрический измеритель лучевых скоростей CORAVEL. Д) Эшелле спектрограф 1.4-м телескопа ЕЮО – первый прибор высокого разрешения, работавший каждую ясную ночь в течение почти двух десятков лет, в т.ч. и в режиме дистанционных наблюдений. Е) Эшелле спектрограф фокуса кудэ 3.9-м телескопа AAT, где эффективно внедрены резатели изображения и принцип перезаполнения эшелле. Ж) Эшелле спектрограф с оптоволоконным сочетанием ELODIE, одна из первых схем белого зрачка.

Памятные даты отечественной астроспектроскопии полезно сравнить с соответствующими зарубежными вехами (указаны в скобках). Призменный спектрограф на рефракторе – 1891, Белопольский. Дифракционный спектрограф на рефракторе – 1897, Белопольский. Призменный спектрограф на рефлекторе – 1926, Альбицкий, Шайн. Солнечный спектрограф – 1924, Белопольский, (1908, Хэйл). Интерферометр Фабри-Перо – 1960, (1937, Франция). Спектрограф фокуса кудэ – 1962, ЗТШ, (1919, Маунт Вилсон). Небулярный спектрограф 1955?, КрАО, (1939, Мак Дональд). Звездный спектрограф с эшелле 1963, КрАО, (1967, США). Корреляционный измеритель скорости 1984, ГАИШ, (1967, Гриффин). Картину дополняет почти полувековое наше отставание в применении Фурье-спектрометра (начало 60-х, Конн), и отсутствие у нас спектрографов с оптоволоконным сочетанием, (1986, США).

В годы становления спектроскопии наше отставание определялось: отсутствием отечественного точного приборостроения; сосредоточением основных средств наблюдений в местах, малопригодных для астрофизических работ; бедностью университетов. Затем начали сказываться частые послереволюционные реформы системы образования и резкий рост числа научных организаций (последнее увеличило нагрузку на отечественную оптико-механическую промышленность). В послевоенный период отставание определялось, в основном, состоянием технологии производства приемников излучения.

Становление оптической промышленности в довоенный период. В Ленинграде активно развивались научные основы технологии варки оптического стекла, контроля его однородности и измерения оптических характеристик. В Государственном оптическом институте (ГОИ) за короткий срок удалось освоить промышленное производство оптического стекла, и в 1927 г. прекратить его импорт. Наличие стекла основных марок позволило развернуть работы по расчетам оптических систем и разработке приборов различного назначения. С созданием необходимой промышленной базы оптики и инженеры А.А.Чикин, Д.С.Рождественский, Д.Д.Максутов, Н.Г.Пономарев, В.П.Линник, Г.Г.Слюсарев, – приступили к развитию отечественного телескопостроения и приборостроения. Например, Д.Д.Максутову было поручено изготовление объектива для 82-см рефрактора. После подготовительных работ две пары заготовок отличного качества были успешно отлиты и отожжены в 1934 году. Изготовление пары стекол хорошего качества для ахроматического объектива такого размера остается до настоящего времени одной из труднейших задач оптического стекловарения. При непосредственном участии Н.Г.Пономарева на заводе оптического стекла были проведены опыты по изготовлению зеркал облегченной (сотовой) конструкции методом спекания отдельных прессованных и обработанных элементов. Одна из таких заготовок диаметром 98 см была обработана спустя много лет. Регулярный выпуск астрономических приборов начат на ГОМЗ в 1935 году, под руководством Н.Г.Пономарева. До 1941 г. среди выпускаемых заводом ГОМЗ астрономических приборов главное место занимали приборы для наблюдения Солнца.

Солнечный телескоп Пулковской обсерватории (1941г.), имел 50-см целостат и 65-см дополнительное зеркало. Главное параболическое зеркало имело фокусное расстояние 17 м и отверстие 50 см. По проектам Н.Г.Пономарева были созданы рефлектор с зеркалом 33 см для Абастуманской обсерватории, спектрогелиограф Харьковской обсерватории и другие приборы.

Развитие системы астрономических организаций. В довоенный период в СССР было организовано шесть обсерваторий и станций: Полтавская, Китабская, Иркутская, Абастуманская, Сталинабадская, Свердловская, и расширены возможности существующих обсерваторий. Деятельность ведущих астрофизиков (В.В.Стратонов, В.Г.Фесенков), по организации Главной Российской АстроФизической Обсерватории (ГРАФО), завершилась лишь объединением столичных астрономических учреждений и основанием Абастуманской астрофизической обсерватории, последняя своей работой подтвердила целесообразность устройства астрофизических учреждений в горах. Создание Абастуманской и Сталинабадской обсерваторий явилось также первым звеном в политике формирования национальных астрономических учреждений.

Итоги войны и послевоенной изоляции. Оборудование, полученное из Германии по репарациям, послужило для развития Крымской астрофизической обсерватории (1.2-м телескоп), Пулковской обсерватории (большой рефрактор) и Бюраканской обсерватории (1-м Шмидт), создания Кисловодской Горной станции ГАО и развития Астрофизического института в Алма-Ате (внезатменные коронографы). В условиях начинающейся холодной войны был поставлен и решен вопрос об оснащении обсерваторий исключительно отечественным оборудованием. На территории вновь построенной Пулковской обсерватории было установлено два десятка телескопов. Решение о строительстве крупнейших оптических телескопов послужило основанием для создания новых промышленных мощностей.

Создание отечественных спектрографов. В довоенный период в СССР были построены солнечный спектрограф (Пономарев) и светосильные спектрографы с камерами Шмидта (Леонтовский). На 1-м симеизском рефлекторе использовался призменный спектрограф швейцарского производства. Однопризменный спектрограф конструкции Альбицкого использовался на 1.2-м рефлекторе Крымской астрофизической обсерватории. Крупнейший из семейства менисковых телескопов системы Максутова, 70-см АС-32, (Абастумани, 1955), был оснащен предобъективной призмой. Для спектроскопии протяженных объектов строились небулярные спектрографы с камерами сверхвысокой светосилы (от 1:1 до 1:0.6), работающие без телескопа. В ГОИ и на ГОМЗ были разработаны два типа небулярных спектрографов, в т.ч. небулярный спектрограф АСИ-1. В 1948 г. был создан серийный бесщелевой спектрограф АСИ-5, состоящий из параболического 25-см рефлектора, призмы Корню и кварцевого объектива F:6. В 1960 г. на Бюраканской астрофизической обсерватории был смонтирован АЗТ-10 (диаметр отверстия 100 см, фокусное расстояние 2.13 м, диаметр главного зеркала 125 см, светосила 1:2.3, угловое поле по стороне фотопластинки 4°10'). Этот телескоп системы Шмидта, создание которого было начато еще в фашистской Германии, снабжен тремя сменными объективными призмами – из крона с преломляющими углами 1.5° и 3°, и из флинта с углом 4°. Для 1.25-м телескопа ЗТЭ ГАИШ были изготовлены: 1) АСП-3 – двухпризменный спектрограф фокуса Кассегрена. Коллиматор с отверстием объектива 60 мм, две призмы из легкого флинта с преломляющими углами 63°, две камеры с фокусными расстояниями 175 и 520 мм. Дисперсия 59 и 19 Å/мм при 4341 Å соответственно. 2) Кварцевый однопризменный спектрограф с дисперсией 240 Å/мм при 4046 Å, устанавливаемый в фокусе Кассегрена. 3) Однопризменный бесщелевой спектрограф для системы Ньютона. Для проверки принципов работы при переменных значениях окружающей температуры и положении в пространстве, разработан экспериментальный дифракционный спектрограф, установленный на 1.2-м телескопе КрАО. Спектрограф имеет зеркальный коллиматор типа Кассегрена, дифракционную решетку 140х150мм (1200 штр/мм), камеру Шмидта (F=185мм). Дисперсия 36 и 15 Å/мм (в 1 и 2-ом порядках спектра). Имеется линзовая камера и сменная дифракционная решетка (300 штр/мм), для работы в ИК-диапазоне. В комплект 2.6-м рефлектора ЗТШ входили два бесщелевых дифракционных спектрографа с линзовой оптической системой: СП79 имеет положительный коллиматор и предназначен для диапазона 3300-4000А, дисперсия 180 Å/мм, светосила камеры – 1:4.7. СП80, для диапазона 4000-6500А, дисперсия 250 Å/мм, имеет отрицательный коллиматор и камеру со светосилой 1:3.8. Поле одновременно исследуемых объектов у обоих спектрографов равно примерно десяти минутам дуги. Спектрограф СП72 устанавливался в фокусе Нэсмита ЗТШ. Оптическая схема включает зеркальный коллиматор типа Кассегрена, дифракционную решетку (90х100 мм, 600 штрихов/мм), и две камеры Шмидта, светосилой 1:1 и 1:2. Обратная линейная дисперсия 160 Å/мм и 80 Å/мм соответственно. АСП-14, спектрограф фокуса кудэ ЗТШ, был оснащен решеткой, изготовленной в ГОИ, (600 штр/мм на площади 280х300мм). Концентрация энергии (на 4400 Å в 3-ем порядке), составляла 40%. Создание подобной решетки представляло рекорд для начала 60-х. (В спектрографе кудэ 5-м рефлектора Хэйла была установлена решетка почти такого же размера, но составленная из четырех отдельных 15-см решеток, собранных в общей оправе). Камеры АСП-14: F=0.7, 1.35 и 3.35 м (внеосевая), линейные дисперсии соответственно 12, 6 и 2.4 Å/мм во 2-ом порядке и 8, 4 и 1.6 Å/мм – в 3-ем. Длина фотографического спектра составляла 12, 22 и 53 см, соответственно. Итак, к началу 60-х в оптико-механической промышленности были разработаны и выпускались астрономические спектрографы всех типов, причем часть из них – небольшими сериями.

Серьезная загрузка оптико-механической промышленности другими заказами, не позволяла (начиная с конца 70-х), развивать астрономическое приборостроение по концептуально новым идеям. Уже с 60-х в ряде астрономических учреждений астрономические спектрографы создавались самостоятельно. Распространение получила схема Сейя-Намиока, в которой угол между линиями, соединяющими вогнутую решетку и щели, а также расстояния до щелей, – постоянны. В качестве примера приведем спектрофотометр на 50см рефлекторе Герца (1:22) АФИ АН Казахской ССР. Использовалась решетка 600штр/мм, 46х50 мм, R=500 мм, результаты наблюдений записывались на магнитную ленту. В Одессе на основе 43см (F:10) катадиоптрического телескопа системы

Аргунова был создан оригинальный сканер с предобъективной 7-градусной призмой. Сканирование спектра осуществлялось путем небольшого рассогласования режима сопровождения объекта.

Первое поколение спектроскопического оборудования 6-метрового телескопа БТА, ориентированное на применение фотографической регистрации и электронно-оптических преобразователей (ЭОП), было создано промышленным образом. Последующие два поколения спектроскопической аппаратуры БТА созданы непосредственно астрономами САО, а промышленности заказывались только дифракционные решетки и некоторые компоненты светоприемных комплексов. Детали этого процесса можно найти в монографии «САО РАН. 40 лет». Нижний Архыз, 2006.

Эффективность использования спектроскопической аппаратуры в значительной мере определяется астроклиматическими характеристиками. Темпы послевоенного создания новых обсерваторий были высокими, опережая выполнение программ поиска мест для установки нового оборудования. В 40-х было создано 7 обсерваторий и станций, в 50-х – 10, в 60-х – 8, и в 70-х – 4. Становление астроклимата как экспериментального научного направления проходило в конце 60-х – начале 70-х, так что большинство новых пунктов наблюдений было выбрано без длительных предварительных исследований. После создания обсерватории систематические исследования астроклимата, как правило, прекращались.

Другим фактором, повлиявшим на развитие астрономической спектроскопии, явилась инерционность системы подготовки специалистов. Уже в 70-е обозначились признаки кризиса в отечественной практической астрофизике. Обострились проблемы оснащения университетских обсерваторий и кафедр современным лабораторным и научным оборудованием, вычислительной техникой. Учебники и учебные пособия по практической астрофизике также не отражали разнообразие новых научно-технических методов. В это же время происходил расцвет теоретических школ, значительная часть молодежи устремилась в новые астрофизические направления. Ежегодно университетами СССР выпускалось более сотни астрономов, но вакансий в институтах и на обсерваториях было на порядок меньше.

Системный кризис, завершившийся распадом СССР, нанес урон научным исследованиям. Особенно пострадали направления, деятельность которых определялась территориальным распределением экспериментальных и технических баз: обсерваторий, полигонов, заповедников, средств средств запуска космических аппаратов и контроля космического пространства. Была свернута деятельность конструкторских бюро, работавших в области астрономического спектроскопического приборостроения.

Пути развития астрономической спектроскопии в нашей стране – не просматриваются, хотя бы потому, что сегодня нет внятно сформулированной программы развития наземной астрономии оптического диапазона. Многие годы в концепции нашего развития преобладал соревновательный тезис: «достичь того, чего другие еще не достигли». Сегодня ситуация такова, что мы уже не в состоянии соревноваться, но еще в состоянии понимать то, что сегодня происходит в астрономическом приборостроении за рубежом.

О ПОЛЬЗЕ НЕКЛАССИЧЕСКИХ ПРЕДСТАВЛЕНИЙ АСТРОНОМИЧЕСКИХ СПЕКТРОВ

Панчук В.Е., Сачков М.Е., Якопов М.В.

Институт астрономии РАН

РЕЗЮМЕ. Рассмотрены некоторые пути повышения эффективности астрономической спектроскопии высокого разрешения на крупных оптических телескопах.

1. Три способа модуляции спектра

В классическом спектрографе детектируемый сигнал пропорционален интенсивности света в данном интервале длин волн. В призменных и дифракционных спектрографах калибровка шкалы длин волн осуществляется в отдельных точках, соответствующих положению линий спектра сравнения. Принцип действия таких приборов аналогичен способу амплитудной модуляции в радиоэлектронике.

Частота колебаний сигнала на выходе Фурье-спектрометра обратно пропорциональна длине волны. Метод спектроскопии, основанный на преобразовании Фурье, аналогичен способу частотной модуляции в радиоэлектронике. Запаздывание внедрения метода определялось его зависимостью от развития цифровых вычислительных средств, (тогда как в классических спектрографах долгое время достаточным было аналоговое представление сигнала, – например, фотографирование спектра). Поэтому спектрометрия с преобразованием Фурье считалась «весьма трудоемким *косвенным* методом изучения спектров» (Mertz, 1965).

Если излучение объекта искусственно поляризовать по известному закону, то появляется возможность использовать поляриметрическую калибровку по длинам волн, что аналогично способу фазовой модуляции в радиоэлектронике. При поляриметрической калибровке спектра фаза синусоидальной модуляции интенсивности сигнала на выходе – обратно пропорциональна длине волны искусственно поляризованного света.

В эпоху одноканальных приемников лидеры практической астрофизики иногда использовали Фурье-спектрометры и даже поляризационные спектрометры (Serkowski, 1972). Внедрение многоканальных приемников породило мнение, что о мультиплексных методах можно забыть. Сегодня, когда технические ресурсы дифракционных спектрографов представляются нам «выработанными», нелишне вспомнить некоторые моменты истории спектроскопии с одноканальными приемниками.

2. Пределы дифракционной спектроскопии

Несмотря на то, что в фурье- и поляризационных спектрометрах калибровка по длинам волн осуществляется для каждой точки спектра, в астрономической спектроскопии по-прежнему популярен первый из трех способов модуляции – т.е. представление сигнала в форме «интенсивность в функции длины волны (частоты)». Этот консерватизм в известной мере обусловлен относительной доступностью и традициями изготовления спектральной аппаратуры, а также наглядностью соответствующих методов спектрального анализа. Определенную роль сыграло и то обстоятельство, что классический спектрограф позволил выявить структуру энергетических уровней атомов и молекул раньше, чем это было сделано при помощи интерференционных методов. Впоследствии интерферометрические методы сыграли основную роль в лабораторной атомной спектроскопии, когда потребовалось измерять положения спектральных линий с высокой точностью и(или) со спектральным разрешением, недоступными для дифракционных спектрографов.

В астрономической спектроскопии преимущество интерферометров перед дифракционными спектрографами (выигрыш Жакино), в значительной мере скомпенсировано (Panchuk et al., 2007), достижениями технологии изготовления дифракционных решеток с большой заштрихованной площадью. Для крупнейших телескопов построены десятки спектрографов высокого разрешения, но один из основных параметров этих приборов – геометрическая светосила $L=A\omega$ – уже близок к пределу. (Здесь A – площадь зрачка системы, заполняемая под телесным углом ω). Например, у двух самых крупных эшельных спектрографов высокого разрешения (HIRES Keck и HDS Subaru), диаметр коллимированного пучка d=30см, у НЭС БТА – d=24см, еще около десятка приборов имеют d=20см. Увеличение d позволяет пропорционально уменьшить угол ω, минимальное значение последнего ограничивается состоянием атмосферы и качеством оптики телескопа. Спектроскопия высокого разрешения на больших телескопах является случаем, когда диаметр изображения звезды β больше ширины щели ω. Поэтому выигрыш в проницающей способности наблюдений пропорционален не квадрату, а первой степени диаметра D зрачка телескопа. Следовательно, необходимо искать методы, альтернативные увеличению D. Перспективным является сочетание дифракционного спектрографа с адаптивной оптикой телескопа, (см., например, Ge et al., 2002), но этот подход не является достижением собственно спектроскопии.

3. Дифракционные приборы с фильтрацией пространственных частот

В радиотехнике известно, что для получения максимальной величины отношения сигнал/шум следует проводить оптимальную согласованную фильтрацию сигнала, причем до устройства, принимающего решение о наличии или отсутствии сигнала. В оптическом диапазоне согласованная фильтрация временных частот сигнала невозможна, и заменяется фильтрацией частот модуляции сигнала. В одноканальном сканирующем спектрометре реализован простейший случай фильтрации частот амплитудной модуляции (на выходную щель последовательно проецируются соседние участки спектра). Для увеличения светосилы метода можно применять системы входных и выходных щелей (или более сложные двумерные конфигурации, т.н. растры), т.о. дополнительно к фильтрации частоты модуляции используется фильтрация пространственных частот в изображении. В растровом спектрометре модулируется та длина волны, для которой в данный момент времени изображение входного растра в точности совпадает с выходным растром. Требование идеального совпадения изображения входного растра с выходным растром ограничивают интервал сканирования длин волн. Интервал сканирования может быть увеличен в несколько раз за счет выбора закона модуляции (см., например, Горский и др., 1970). Широкая составляющая аппаратной функции прибора с растром функционального типа ограничивала применение приемников, шумы которых зависели от уровня сигнала. Были предложены различные методы учета (устранения) паразитной засветки приемника, технически простым оказался метод модуляции потока излучения путем периодического перемещения входного растра на величину, определяемую наиболее узким элементом растра. В астрофизике спектрометры с растрами Жирара применялись преимущественно в инфракрасном диапазоне, где шумы приемника не зависели от уровня сигнала. Принцип двойного мультиплексирования (на входе и на выходе спектрометра) позволяет реализовать выигрыш Фелжета и, одновременно, приблизить светосилу дифракционного спектрометра к таковой для интерференционного. Было показано (Harwit et al., 1970), что, по светосиле и шумовым характеристикам, схема двойного мультиплексирования с бинарным циклическим кодированием, – приближается с интерферометру Майкельсона. Однако технически спектрометр с кодирующими масками (например, строками матрицы Адамара), изготовить и эксплуатировать гораздо проще, чем сканирующий интерферометрический прибор. Спектрометры с преобразованием Адамара применялись в бортовых астрофизических экспериментах. Метод кодирования спектра был распространен и на панорамную спектроскопию, путем кодирования изображений (Harwit, 1971; 1973). Главный недостаток растровой спектроскопии состоит в высоких требованиях к качеству изображения спектра и к неизменности этого изображения при сканировании спектра. Эта проблема, как и проблема изготовления мелких растров, может быть решена, если в качестве растров использовать кольца интерференции (Girard, 1960), в работе (Тарасов & Гуд, 1974) для этой цели использовались эталоны Фабри-Перо. Применение интерференционных растров позволит увеличить разрешение и светосилу (последнее из-за того, что в качестве коллиматора и объектива могут использоваться светосильные объективы). Применение многоэлементных приемников, шумы которых не зависят от уровня сигнала, открывает новые возможности для схем с фильтрацией пространственных частот. На больших телескопах, где диаметр турбулентного диска звезды намного превосходит ширину щели спектрографа высокого разрешения, применение кодирующих масок может обеспечить многократный выигрыш в светосиле.

4. Интегральные характеристики спектра

Спектр звезды обладает характеристиками двух типов. Первый тип относится преимущественно к свойствам атомов, ионов и молекул – это число и интенсивность линий различных химических элементов. Второй тип характеризует макроскопические свойства среды, в которой эти элементы находятся – это температура, плотность, и различные формы движения: осевое вращение, турбулентность, радиальные и нерадиальные пульсации, перемещение звезды в пространстве. В оптическом диапазоне спектр атмосферы холодной звезды представлен преимущественно линиями элементов железного пика, так что различия во влиянии атомного веса на параметры теплового уширения «среднестатистической» линии незначительны. Измерение макроскопических свойств среды при классическом способе модуляции – интенсивность в функции длины волны – является трудоемкой процедурой. В спектрограмме необходимо измерить характеристики (положения, форму профилей, полуширины, асимметрию) большого числа линий, чтобы затем определить средние (для большинства линий) характеристики. Например, с целью точного определения средней лучевой скорости необходимо измерить положения 200ч300 линий. При этом для измерения фотографических спектров иногда применялись осциллоскопические компараторы (Антропов, 1972), т.е. положения отдельных линий измерялись методом автокорреляции. Таким образом, по фрагменту спектра выполнялось необходимое функциональное преобразование. Этот же метод может быть применен непосредственно при наблюдениях, без регистрации собственно спектра или его фрагментов. Так, если в спектрографе в фокальной плоскости установить щель, а изображение спектра перемещать поперек щели, то фотоэлектрический приемник зарегистрирует корреляционную функцию, положение и ширина которой охарактеризуют спектральную линию, находящуюся вблизи щели. Светосилу метода можно увеличить, установив систему щелей, положения которых

согласованы с положением спектральных линий. Метод фотоэлектрического корреляционного измерения лучевых скоростей, обоснованный в (Fellgett, 1955) и впервые реализованный в (Griffin, 1967), явился первым примером создания анализатора, осуществляющего представление излучения в виде удобного функционала, параметры которого содержат искомые характеристики спектра. Этот подход, когда необходимое интегральное преобразование осуществляется непосредственно в схеме прибора, оказался достаточно эффективным в эпоху одноканальных приемников и маломощных вычислителей. В настоящее время, когда корреляционная функция может быть вычислена непосредственно по спектру, зарегистрированному многоканальным приемником, преобладает точка зрения, что естественный путь определения интегральных характеристик – это вычисление их по классическому спектру.

В фотоэлектрическом измерителе лучевых скоростей, операция разложения излучения в спектр все же выполняется, и выигрыш состоит только в реализации принципа многоканальной спектроскопии на одноканальном приемнике, обладающим относительно высоким квантовым выходом, но имеющим шумы «неудобной» природы. В Фурье-спектрометре выигрыш Фелжета реализуется только при использовании приемника с шумами тепловой природы, а при использовании приемника с шумами квантовой природы – не реализуется вообще. Показано (Лебедев, 1978), что если построить гипотетический специализированный прибор, в котором операция определения первого момента контура линии выполняется автоматически, в реальном времени, то вместо выигрыша Фелжета ($N^{1\backslash 2}$ для теплового приемника), будет реализован более высокий выигрыш (N для теплового и $N^{1\backslash 2}$ для фотонного приемников). Таким образом, интегральный способ измерения обобщенных характеристик спектров оказывается эффективнее классического, спектрального способа. Внимание привлекли оптические схемы, осуществляющие интегральное преобразование спектра, без разложения спектра по длинам волн.

5. Интерферометры

Основным способом представления случайных процессов, помимо функций распределения, является описание при помощи средних и моментов. Существует и другой подход – описание случайных величин и процессов с помощью кумулянтов (семиинвариантов) и кумулянтных функций. Преимущества такого описания отмечены в (Малахов, 1978). Проводя аналогию между контуром спектральной линии и статистической функцией распределения, авторы (Кожеватов и др., 1995) показали, что кумулянты (семиинварианты) спектрального распределения можно получить в интерферометре Майкельсона, реализующем как выигрыш Фелжета, так и выигрыш Жакино. В (Кожеватов и др., 1995) также отмечено, что чувствительность интерферограммы к семиинвариантам разных номеров зависит от разности хода интерферирующих лучей. Поэтому для оптимального измерения избранных семиинвариантов было предложено применять интерферометрические схемы с различной разностью хода. Метод был реализован при наблюдениях лучевых скоростей на поверхности Солнца (Дидковский и др., 1986), затем для измерения четырех семиинвариантов, (три из которых идентичны первым трем центральным моментам), были использованы два интерферометра Майкельсона, с оптимально подобранной разностью хода (Кожеватов, 1983). Сочетание классических интерференционных схем с многоэлементными приемниками позволяет обойти проблему точного перемещения оптических элементов, примеры соответствующих решений приведены в (Panchuk et al., 2007). Измерения пространственно фиксированной интерферограммы позволяет определить интегральные характеристики спектра в приборе, не имеющем перемещаемых элементов.

6. Выводы

Звездная спектроскопия становится все более массовой, в смысле статистики объектов. Астрономы уже оперируют тысячами измерений лучевых скоростей, очередь за массовыми измерениями турбулентных характеристик и других движений в атмосферах. Здесь могут сыграть свою роль как методы кодировки изображений, так и интегральные методы, причем последние не сводятся только к двухлучевым интерферометрам.

Литература

L.Mertz: 1965, *Transformations in Optics*. J.Wiley & Sons, Inc. NY. (Русск. перевод: Мерц Л.: 1969, *Интегральные преобразования в оптике*, М.: Мир, 181с.).

K.Serkowski: 1972, *PASP*, **84**, 649.

V.E.Panchuk, V.G.Klochkova, D.S.Nasonov: 2007, *Odessa Astron. Publ.*, **20**, 103.

J.Ge, J.R.P.Angel, B.Jacobsen, N.Woolf, R.Q.Fugate, J.H.Black, M.Lloyd-Hart: 2002, *PASP*, **114**, 879.

С.М.Горский, В.А.Зверев, Г.К.Иванова: 1970, *Новая техника в астрономии*, **3**, 67.

M.Harwit, P.G.Phillips, T.Fine, N.J.A.Sloane: 1970, *Appl. Opt*., **9**, 1149.

M.Harwit: 1971, *Appl. Opt*. **10**, 1415.

M.Harwit: 1973, *Appl. Opt*. **12**, 285.

A.Girard: 1960, *Optica Acta*, **1**, 81.

К.И.Тарасов, В.В.Гуд: 1974, *Изв. вузов. Приборостроение,* **17**, 106.

Ю.Ф.Антропов: 1972, *Новая техника в астрономии*, **4**, 75.

P.B.Fellgett: 1955, *Optica Acta*, **2**, 9.

R.F.Griffin: 1967, *ApJ*, **148**, 465.

В.П.Лебедев: 1978, *Оптика и спектроскопия,* **45**, 222.

А.Н.Малахов: 1978, *Кумулянтный анализ случайных негауссовых процессов и их преобразований*, М.: Советское радио, 376 с.

И.Е.Кожеватов, Е.Х.Куликова, Н.П.Черагин: 1995, *Оптика и спектроскопия*, **78**, 536.

Л.В.Дидковский, И.Е.Кожеватов, Н.Н.Степанян: 1986, *Изв. КрАО*, **74**, 142.

И.Е.Кожеватов: 1983, *Исследования по геомагнетизму, аэрономии и физике Солнца*, **64**, 42.

THE ROLE OF POOR GALAXY CLUSTERS FOR STUDYING SUPERCLUSTER STRUCTURE

E.A. Panko[1,2]

[1] Department of Astronomy, Odessa National University
T.G.Shevchenko Park, Odessa 65014 Ukraine, *tajgeta@sp.mk.ua*
[2] Astronomical Observatory of Nikolaev State University,
Nikolskaya, 24, Nikolaev, 54030 Ukraine.

ABSTRACT. The distribution of galaxy clusters is analyzed in regions of 6 galaxy superclusters with both measured and estimated redshifts. The positions of ACO and APM galaxy clusters in the regions are compared with the positions of galaxy clusters and groups from a new catalogue based on the Muenster Red Sky Survey. The locations of galaxy clusters and groups are shown on $10^\circ \times 10^\circ$ maps of the fields. A comparison is made between maps that include all galaxy clusters and groups, rich and poor clusters, and only rich clusters. The resulting large-scale structure in the regions is described in detail on the basis of both rich and poor clusters, and a new catalogue is produced that is convenient for further study of galaxy superclusters.

Key words: large-scale structure; galaxy supercluster; galaxy clusters: individual: SCl 16, 37c, 38c, 190, 199, 212c.

1. Introduction

The large-scale distribution of galaxy clusters as a reflection of initial density variations in the universe has attracted considerable attention during the past decade. Shapley (1933) used the term "supercluster" in his research into galaxy distributions, and identified the first 25 galaxy clusters. At present the study of networks of supercluster-voids is based upon observations in both visual and other spectral regions. Einasto et al. (1997, 2001, 2002) created catalogues of superclusters of galaxies using visual data samples from the ACO (Abell, Corwin & Olowin, 1989) catalogue of rich clusters of galaxies and from APM rich clusters of galaxies (Dalton et al., 1997). The main goal of this paper is to compare the distribution of ACO and APM clusters of galaxies with a new catalogue of galaxy clusters and groups compiled by Panko & Flin (2006, hereafter PF), and to demonstrate its usefulness for studying the supercluster-void network. We also quantify cluster richness, which is needed for future research. Note, Einasto et al. (2002) provided a list of additional superclusters of non-Abell X-ray clusters; the PF catalogue can include useful information in the optical range for such superclusters.

2. Input data

The PF catalogue of galaxy clusters and groups was based on the analysis of a homogeneous portion of the Muenster Red Sky Survey (MRSS, Ungruhe, Seitter & Duerbeck, 2003). It includes 6188 structures, both clusters and groups, with at least ten galaxies in the field of each structure. Moreover, the additional listing of galaxies in each structure field provided an opportunity to construct detailed galaxy cluster maps. A comparison of the PF catalogue with the ACO and APM catalogues made it possible to calibrate distances for the PF structures using the $z - m_{10}$ relation, where m_{10} is the brightness of the tenth brightest galaxy in the structure. The maximal redshift z for this calibration is 0.18. We selected 6 regions (listed in the Table 1) for this work, using such criteria as:

1. The region does not oincide with a large supercluster.
2. Superclusters are present in the ACO supercluster list, but are absent in the APM catalogue.
3. Superclusters must have both measured and estimated redshifts.

3. Large-scale structures in the 6 regions

The large-scale galaxy cluster distribution is show in Fig. 1. The size of each identified field was $10^\circ \times 10^\circ$. In all cases, excluding SCl 199, long elongated structures were interpreted as superclusters. PF catalogue clusters and groups contain both filaments, as chains of PF objects, and voids. The positions of such groups in the

Table 1: Selected regions parameters.

RAJ2000	DEJ2000	SCl	$N_{members}$	Dist, (h^{-1}Mpc)	z_{est}
$00^h\ 52^m$	-63^o.9	16	4	207 (204)	0.07
02 00 (02 16)	-36.3 (-40.1)	37c	2(5)	318 (296)	0.11 0.10)
02 02	-26.3	38c	4	330	0.11
21 57 (21 54)	-30.4 (-30.6)	190	5	256 (252)	0.09
22 40 (22 37)	-33.9 (-34.2)	199	3	174	0.06
23 35 (23 33)	-68.7 (-69.1)	212c	3	296 (285)	0.10

where:
RAJ2000, DEJ2000 are coordinates (J2000) of the supercluster centers;
SCl - is the supercluster number (Einasto et al., 1997), "c" denotes superclusters with estimated z;
$N_{members}$ - is the number of ACO clusters in the supercluster;
Dist - is the distance in h^{-1}Mpc;
z_{est} - is the estimated z according to the preceding column;
Bracketed data were obtained from Einasto et al.(2002).

ACO an APM catalogues are frequently not congruous, although we find a significant number of cluster congruities from both catalogues with the positions of the PF catalogue objects. For example, SCl 37c has three ACO clusters of five supercluster members with analogues in the APM and PF, one supercluster member has an analogue only in the PF catalogue, and one does not have analogues in either the APM or PF. However, for SCl 16, all four ACO clusters form a chain with analogues only in the PF. At the same time, at least three ACO clusters and one PF structure can belong to the same chain. For the PF catalogue we can estimate z, so PF0097-6680 and its ACO cluster analogue S112 may also be a member of SCl 16. PF0097-6680 R.A.=0.^{h}97621, Dec.= $-66°.79035$) is a rich cluster with 190 galaxies in the cluster field, 73 in the magnitude range $m_3, m_3 + 3^m$. The estimated redshift z is 0.062, while S112 has $z = 0.066500$ according to NED. Both values show good agreement with the estimated z for SCl 16 in Table 1 and this cluster can superslucter member too.

Additional maps were constructed for supercluster 16 (Fig.2). In this map only PF galaxy clusters with $N > 30$ (upper panel) and with $N > 50$ (lower panel) are shown. In the upper panel of Fig. 2 some details are lost, but a common type of large-scale structure remains. As in Fig 1, we can see the usual forms in detail, such as chains along filaments. The lower panel map displays significant differences relative to the Fig. 1 map: three ACO supercluster members do not have corresponding PF structures. The PF structures contain 29, 35, and 45 galaxies in the magnitude range $m_3, m_3 + 3^m$. At the same time we see a chain of five PF clusters with estimated redshifts z from 0.07 to 0.12, crossing the supercluster 16 chain.

Table 2: Tne number of galaxy cluster in six regions

SCl	ACO	APM	PF (all)	PF ($N > 30$)	PF ($N > 50$)
16	46	15	113	60	34
37c	43	22	123	70	28
38c	51	4	134	70	32
190	22	15	98	56	26
199	39	19	95	51	29
212c	58	12	118	66	32

The other 5 fields display similar results. The number of ACO, APM, and PF galaxy clusters in every region is listed in Table 2. As one can see from Table 2 and Fig 2, poor galaxy clusters are important in the reconstruction of large-scale structure. It is obligatory to take into consideration PF structures with $N > 30$ in our future work.

4. Conclusions

The present paper studies the large-scale distribution of galaxies in six supercluster regions. The distribution of galaxy clusters from three catalogues (ACO, APM, PF) are different; the PF clusters of galaxies trace compact high-density regions - the skeleton of the large-scale structure - in detail. Poor PF objects with $N > 30$ must be included in supercluster structure reconstruction.

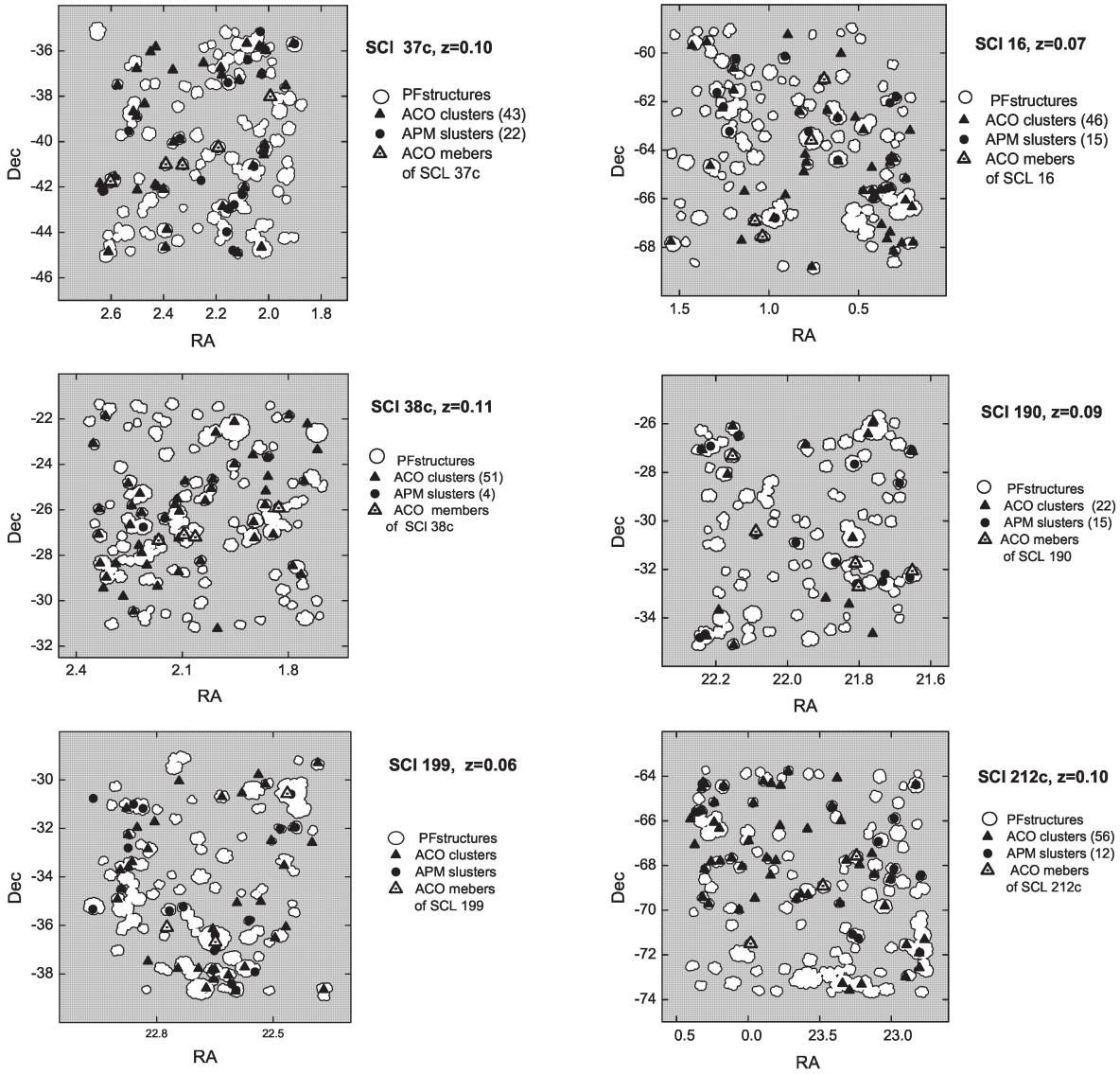

Figure 1: The distribution of galaxy clusters in the studied supercluster region. White regions represent PF structures; the number of ACO and APM clusters for each field is noted in brackets.

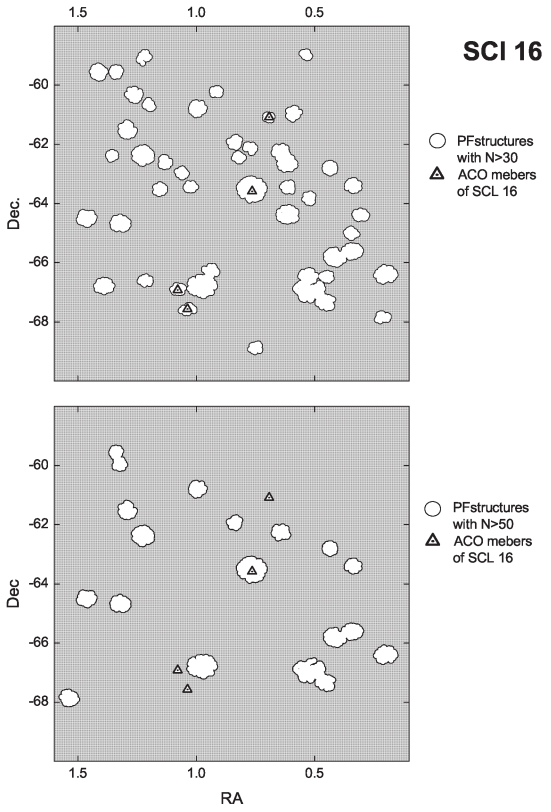

Figure 2: The distribution of PF galaxy clusters with $N > 30$ (upper panel) and with $N > 50$ (lower panel) along with ACO supercluster members in the SCl 16 region.

Acknowledgements. For this research we have used NASA's Astrophysics Data System and the NASA/IPAC Extragalactic Database (NED) which is operated by the Jet Propulsion Laboratory, California Institute of Technology, under contract with the National Aeronautics and Space Administration.

References

Abell G.O., Corwin H.G., Olowin R.P.: 1989, *Astrophys. J. Suppl. Ser.,* **70**, 1.

Einasto M., Tago E., Jaaniste J. et al.: 1997, *A&A. Suppl.,* **123**, 119.

Einasto M., Einasto J., Tago E. et al.: 2001, *AJ,* **122**, 2222.

Einasto M., Einasto J., Tago E. et al.: 2002, *AJ,* **123**, 51.

Dalton G.B., Maddox S.J., Sutherland W.J. et al.: 1997, *MNRAS,* **289**, 263-284.

Panko E. & Flin P.: 2006, *J. Astron. Data,* **12**, 1.

Shapley H.: 1933, On the Distribution of Galaxies. *Proceedings of the National Academy of Sciences of the United States of America,* **19**, 389.

Ungruhe R., Seitter W.C., Duerbeck H.W.J.: 2003, *J. Astron. Data,* **9**, 1.

MODEL ATMOSPHERES OF PECULAR CARBON GIANTS

Ya.V.Pavlenko[1], L.A.Yakovina[2]

Zabolotnogo 27, Main astronomical observatory
of National academy of scienses of Ukraine, Kiev, Ukraine
[1]*yp@mao.kiev.ua*, [2]*yakovina@mao.kiev.ua*

ABSTRACT. We calculated 240 model atmospheres f carbon giants of high carbon abundances (2800 ≤ T_{eff} ≤ 3400 K, 0.06 ≤ log(C/O) ≤ 2.7). The set f models was calculated in process of analysis by pectral synthesis of spectral energy distribution of he evolved carbon star DY Per shown photometric eatures of R CrB type stars. The majority of these nodels are metal deficient (-3.5 ≤ [Fe/H] < 0), part f them are calculated with hydrogen deficiency (1/9 ≤ H/He < 9/1). Model atmosphere calculations were arried out in the framework of classical approaches ith account of the relevant opacity sources in carbon tars. The opacity sampling method was used to alculate the opacity due to atomic and molecular line bsorption.

Introduction

Recently Yakovina et al. (2009) using spectral ynthesis technique determined the atmosphere arameters of DY Per - carbon giant shown some hotometric features of R CrB type stars. We t computed fluxes calculated with high carbon bundances, metal deficient and hydrogen deficient nodel atmospheres to the observed SED of DY Per.)ur model atmospheres are outside the known and ccessible grids of model atmospheres for carbon tars (Johnson, 1982; Eriksson et al., 1984; Harris t al., 2003). Model atmospheres of carbon giants ith such high values C/O, [N/Fe], low [Fe/H] and ith the deficiency of H were not calculated by other uthors at all. We consider that they can be useful to ther researchers of carbon stars for the similar studies.

Model atmosphere calculations

We calculated model atmospheres of carbon giants n the classic assumptions by the program SAM12 Pavlenko, 2003) which is a modification of the AT-LAS12 (Kurucz, 1999). SAM12 allows to calculate nodel atmospheres for stars with the peculiar chemical compositions. Bound-free absorption by CI, NI and OI (Pavlenko & Zhukovskaya, 2003) is added to the sources of continuous absorption included in ATLAS12. We account CIA (Collisional-Induced Absorption) - the absorption by the molecular complexes He-H_2 and H_2-H_2 induced by collisions. It becomes the important source of opacity in the atmospheres of cool metal deficient stars (Borysow et al., 1997). The opacity sampling method was used to calculate the opacity due to atomic and molecular line absorption.

For most models we set "non solar" abundances not only of C but of H, He and N too. We vary parameters C/O, H/He and [N/Fe]. We set solar abundances from (Gurtovenko & Kostik, 1998) for other elements and adopt the microturbulent velocity V_t =3 km/s.

Results

We present 240 model atmospheres of carbon-rich red giants of the effective temperatures 2800 ≤ T_{eff} ≤ 3400 K and carbon abundances 0.06 ≤ log(C/O) ≤ 2.7. Majority of model atmospheres were computed for log g = 0.0, but 32 models were calculated for log g= -1, -0.5, 0.5 or 1. Some calculated model atmospheres are metal deficient (-3.5 ≤ [Fe/H] < 0), 83 models are hydrogen deficient (1/9 ≤ H/He < 9/1). All our model atmospheres are given in the ATLAS12-like format. Models and short description are available on the web:

ftp://ftp.mao.kiev.ua/pub/users/yp/Cmod/cmod.pdf (description),
ftp://ftp.mao.kiev.ua/pub/users/yp/Cmod/hsol.htm (models of "solar" H/He),
ftp://ftp.mao.kiev.ua/pub/users/yp/Cmod/hdef.htm (models of "not solar" H/He).

The model columns contain the next parameters:

RHOX - $\rho_x = \int_0^x \rho(z) * dz$ (g/cm^2) is mass of matter above 1 cm^2 of atmosphere on the geometrical depth

z, $\rho(z)$ is a density of matter on the depth z;

T - T_e, electronic temperature of level (K);

P - P_g, gas pressure (dyne/cm^2);

XNE - n_e, electronic density (1/cm^3);

ABROSS - $\kappa_{\rm ross}$, rosseland opacity (cm^2/g);

ACCRAD - $a_{\rm rad}$, acceleration due to radial pressure (cm/s^2);

VTURB - $V_{\rm turb}$, turbulent velocity (km/s);

FLXCNV - $F_{\rm conv}$, energy flux that bear a convection (erg/cm^2/s);

VCONV - $V_{\rm conv}$, convective velocity (km/s);

Tauross - $\tau_{\rm ross}$, rosseland optical depth;

FluxErr - ΔF, difference of fluxes in two last iterations (in percents from a flux in last but one iteration);

DELTAT - ΔT, correction to the temperature after last iteration;

DeltaRx - $\Delta\rho_x$, correction to ρ_x after last iteration;

FluxRatio - $F_{\rm conv}/F_{\rm total}$, relation of convective flux to the total one.

The convergence of models can be seen in the column FluxErr. For most our models FluxErr < 1 % at all depth levels. It is evidence of good convergence. Sometimes we assumed the small exceeding above 1 % in the deepest layers of model and consider it possible because these layers show very little impact on the calculated stellar spectra.

As a example, we show a fit of the computed spectrum for model atmosphere with $T_{\rm eff}$/log g/[Fe/H] = 3000/0/-1.5, H/He=5/5, log(C/O) =0.8, [N/Fe]=0.5 to the observed fluxes of DY Per. We computed synthetic spectrum by the program WITA6 (Pavlenko, 1997). The same continuum opacity sources and V_t were used as in model atmosphere calculations. We account atomic lines from VALD (Kupka et al., 1999) and molecular lines from database (Kurucz, 1993-1994), CD-ROM N18.

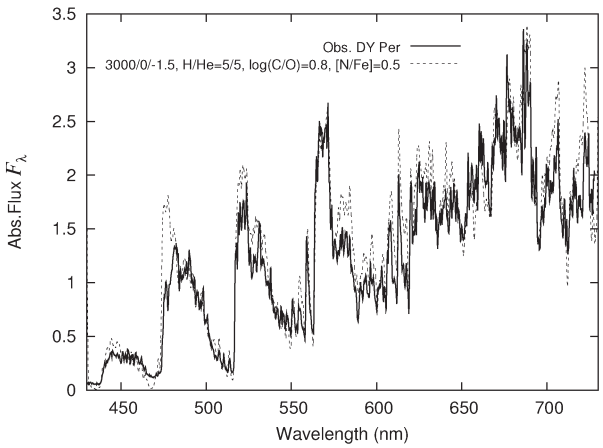

Figure 1: Fit of the theoretical spectral energy distribution of DY Per to the observed one for the model atmosphere {3000/0/-1.5, H/He=5/5, log(C/O) =0.8, [N/Fe]=0.5}.

Discussion and conclusions

Our model atmospheres of C-giants were computed in the framework of the classical assumptions. We believe that they are suitable for qualitative and quantitative analysis of the spectra of C-giants. Moreover, we obtain a good fit of the theoretical spectra computed with our subgrid of model atmospheres to observed SED of the peculiar C-giant DY Per.

At one hand, our models can be used at least for investigation of the peculiar DY Per-like stars.

On the second hand, they can be used as a starting model atmospheres to be improved in the future. No doubt, we need more sophisticated procedures accounting more complete sets of opacity sources, 3D convection, stellar wind and dusty phenomena, etc.

Acknowledgements. Authors thank A.F.Pugach for the observed spectrum of DY Per.

References:

Borysow A., Jorgensen U.G., Zheng C.: 1997, *Astron. Astrophys.*, **324**, 185.

Eriksson K., Gustafsson B. et al.: 1984, *Astron. Astrophys.*, **132**, 37.

Gurtovenko E.A., Kostik R.I.: The system of solar oscillator strengths, preprint MAO-98-3E, Main astronomical observatory NAS Ukraine, Kyiv, 1998, 63 p.

Harris G.J., Pavlenko Ya.V., Jones H.R.A., Tennyson J.: 2003, *MNRAS*, **344**, 1107.

Johnson H.R.: 1982, *Astrophys. J.*, **260**, 254.

Kupka F., Piskunov N., Ryabchikova T.A., Stempels H.C., Weiss W.W.: 1999, *Astron. Astrophys.* Suppl., **138**, 119.

Kurucz R.L.: 1993-1994, Data Bank – CD-ROM NN 1-22.

Kurucz R.L.: 1999, http://kurucz.harvard.edu.

Pavlenko Ya.V.: 1997, *Astrophys. Space Sci.*, **253**, 43.

Pavlenko Ya.V., Zhukovskaya S.V.: 2003, *KFNT*, **19**, N1, 28.

Pavlenko Ya.V.: 2003, *Astron. Rep.*, **47**, 59.

Yakovina L.A., Pugach A.F., Pavlenko Ya.V.: 2009, *Astron. Rep.*, 1, in press.

GENERAL MAGNETIC FIELD OF THE SUN AS A STAR AS INDICATOR OF MASSIVE STREAMS FLOWING ON THE SUN

S. Plachinda[1], D. Baklanova[1], I. Han[2], K.-M. Kim[2], P. Reegen[3], G. Valyavin[2], W. Weiss[3]

[1] Crimean Astrophysical Observatory, Nauchny, Crimea, 98409, Ukraine
[2] Korea Astronomy and Space Science Institute, 36-1 Whaam-dong, Yuseong, Daejeon, Korea 305-348
[3] Institut fur Astronomie, Turkenschanzstrasse 17, 1180 Vienna, Austria

ABSTRACT. The behaviour of the General Magnetic Field of the Sun as a Star (GMFSS) is characterized by the change of amplitude of oscillations with the eleven-year cycle of activity. In maximum of activity GMFSS reaches its maximal values, and in a minimum reaches minimal values. The values of active frequencies vary from cycle to cycle of sunspots activity. Each peak of GMFSS power spectrum is widened by the number of active frequencies. From observations of GMFSS the velocity of solar photosphere movements deviates from the speed of the differential rotation of the Sun more than 5 ms^{-1} as it follows from gelioseismology. For 40 years of direct observations (two solar magnetic cycles) resulting magnetic field of GMFSS is non equal to zero. GMFSS demonstrates properties of a real large-scale field because there is a balance of positive and negative magnetic fluxes, i.e. the magnetic tubes are closed.

Key words: Sun: magnetic fields

1. Introduction

The first results of the magnetic field measurements of the Sun as a star were published by Severny (1969). It is the General Magnetic Field of the Sun as a Star (GMFSS). The General Magnetic Field (GMF) is averaged value of the longitudinal component of magnetic structures and weighted by stellar surface brightness distribution. Observations of the Suns GMF were obtained mainly at four observatories: Crimean Astrophysical Observatory (CrAO), since 1968 on the present time; Mount Wilson Observatory (MWO), since 1970 until 1982; Wilcox Solar Observatory of Stanford University (WSO), since 1975 on the present time (see Solar Geophysical Data); and the Sayan Observatory (Russia), since 1982 on the present time. GMF as the large-scale magnetic field is absent in the Babcock and Leighton phenomenological magneto-kinematic model of the solar cycle and in terms of standard $\alpha - \Omega$ dynamo theory. There are only two main components of large-scale magnetic field on the Sun: toroidal magnetic field and axisymmetric poloidal field. Both toroidal (strong) and poloidal (weak) fields change its polarity with the period of 22 ys.

The main properties of GMFSS are:

1. The strength of GMF versus rotational period shows both sign and shape variations. Both dipole, as dominant, and quadrupole components of the field are detected in the observations.

2). The amplitude of variations of GMF varies with the period of sunspots cycle: GMF is strongest during peaks in spot activity, reaching values of about 1 - 2 G (see Fig. 1).

3). During four decades of direct observations, for mean GMFSS excess of the positive magnetic flux is concentrated on the one side of the Sun, and excess of the negative flux is concentrated on the opposite side (Plachinda and Tarasova, 2000; Haneychuk et al., 2003). Therefore, GMF of the Sun as a star not reverses its polarity with the 22 yr of the solar cycle period.

4). The ratio of the positive to negative magnetic flux of GMF $\Delta_+/\Delta_- \sim 1.0$ in agreement with Maxwell equation $\vec{\nabla} \bullet \vec{B} = 0$ (the tubes of the induction $\vec{B}$ are closed in the atmosphere of the Sun) (Plachinda & Tarasova, 2000; Plachinda et al., 2008).

What do we know about GMF on solar-like stars?

The presence of weak GMF (up to some dozen Gausses) for 21 convective stars (F9-M3 spectral types and I-V luminosity classes) is detected (Plachinda, 2004a). For two solar-like stars variations of GMF as a function of the stellar rotation has been determined for more active and more young star than the Sun ξ Boo A (G8 V) with $P_{rot} \sim 6.2$ days, and for old solar-like star 61 Cyg A (K5 V) with $P_{rot} \sim 36.6$ days

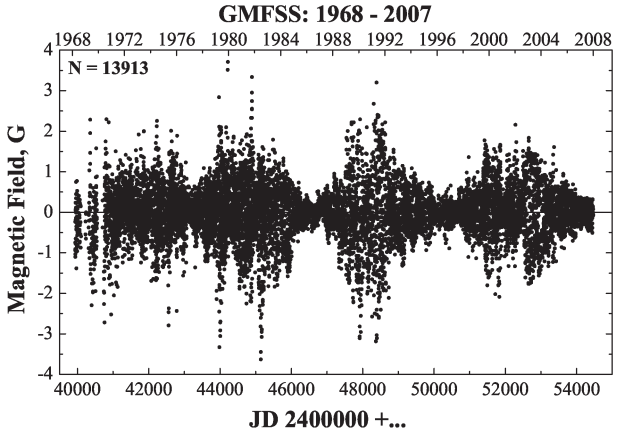

Figure 1: Scatter-plot diagrams for individual GMFSS measurements during the last 40 years. Picture represents combined data for three observatories - CrAO, MWO and WSO. CrAO and MWO data were normalized to WSO data (Kotov et al., 1998).

(Plachinda & Tarasova, 2000; Plachinda, 2004b; Petit et al., 2005).

What the nature of GMFSS phenomenon?

1. The first point of view: we measure magnetic disequilibrium of the Sun. (Haneychuk et al., 2003).
2. Plachinda & Tarasova (2000) have come to a conclusion that GMFSS together with known toroidal and poloidal fields can be the third large-scale component of a magnetic field of the Sun formed as a result of penetration on a surface of a global magnetic field from a radiative zone.
3. Livshits & Obridko (2006), analyzing the time series of GMFSS and surface magnetograms of the Sun, have come to a conclusion that GMFSS it is a product of a dynamo mechanism operations.

This article presents some aspects of the frequency analysis of GMFSS with using softwares 'SigCpec' (Reegen, 2007) and 'Period04' (Lenz, & Breger, 2005).

2. General magnetic field of the Sun as a star

As it was above mentioned the amplitude of GMFSS varies with the eleven year sunspots cycle. In addition, in the upper layers of the Sun the differential rotation and torsion fluctuations of the solar plasma are present. Furthermore, the picture of the distribution of the velocities of torsional oscillations depends on the phase of the cycle of the activity (Howe et al., 2004).

Therefore, due to the frozenness of the magnetic field lines into the plasma, the obtained measurements of the GMFSS must include modulation by the differential rotation, whose rate depends on latitude and falls to the pole of rotation, and to contain modulation as a result of existence of torsional oscillations, i.e., to contain modulation by surface flows with the different speed of the motion of plasma relative to the smooth curve of differential rotation. From the aforesaid it follows that the observed variability of GMFSS must be described by the large set of active frequencies.

We calculated power spectrum of the all Stanford data (N = 9664 dates during the last 33 years) for the wide frequency range using software SigSpec (Reegen, 2007). In the range of periods (synodic) from 25.7 to 30.8 days the observed picture of GMFSS variability is satisfactorily described by beating the collection of 50 frequencies the alarm probability of which does not exceed 10^{-5} (see Fig. 2).

In Fig. 3 we show the region of the power spectrum with highest peak, which corresponds to the Sun's rotation with a value at 26.88596 ± 0.00086 days. The half-width of peak (0.0759 days) by two orders exceeds the period error (0.00086 days) as this is marked in the figure. It is obvious that the series of observations GMFSS contains the large number of active frequencies, and each of the peaks is composite and is widened by the collection of frequencies.

The values of active frequencies of prominent peaks of power spectrum significantly vary from the cycle to the cycle of activity. Thus, for the cycle of activity since 1975 until 1986, which is overlapped by Stanford observations, for two most powerful peaks in the spectrum of power P_{prim} = 26.8715 ± 0.0022 and P_{sec} = 27.0800 ± 0.0027 days, for the observations of the cycle of the activity since 1987 until 1997 P_{prim} = 26.9169 ± 0.0025 and P_{sec} = 27.1426 ± 0.0031 days, and for the observations of the cycle of the activity since 1998 until 2008 P_{prim} = 26.5770 ± 0.0030 and P_{sec} = 27.1888 ± 0.0027 days.

Fig. 4 demonstrates the decrease of the value of periods calculated according to the GMFSS observations with respect to the smooth fitting curve of differential rotation. In this figure the closed marks show the synodic (triangles) and sidereal (circles) periods of the maximum peaks of the power spectrum under conditional envelope, which was carried out on the tops of peaks in the selected frequency range (see Fig. 3). Dashed line and open triangles are helioseismology periods of the differential rotation of the Sun surface in synodic reference frame (left Y axis, sun latitudes). Solid line and closed triangles are magnetic field periods in synodic reference frame (right Y axis, power spectrun amplitudes). Dashed line and open circles are helioseismology periods of the differential rotation of the Sun surface in sideral reference frame (left Y axis). Solid line and closed circles are magnetic field periods in sideral reference frame (right Y axis). The above mentioned facts convince us that:

first, *both the differential rotation of the Sun and torsion fluctuations as well as the dependence of behavior GMFSS and torsion fluctuations on the phase of solar activity actually makes the picture of*

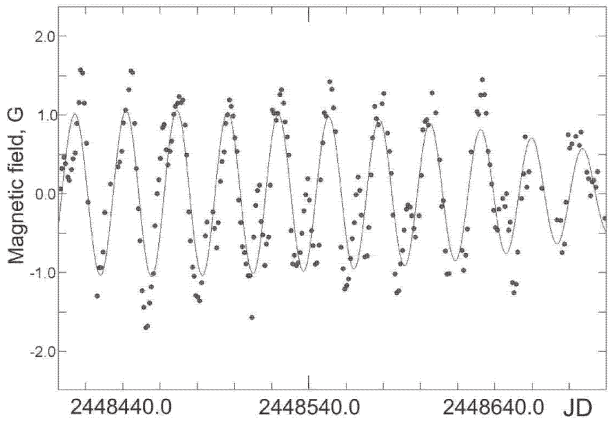

Figure 2: Example of GMFSS behavior in the maximum of solar activity.

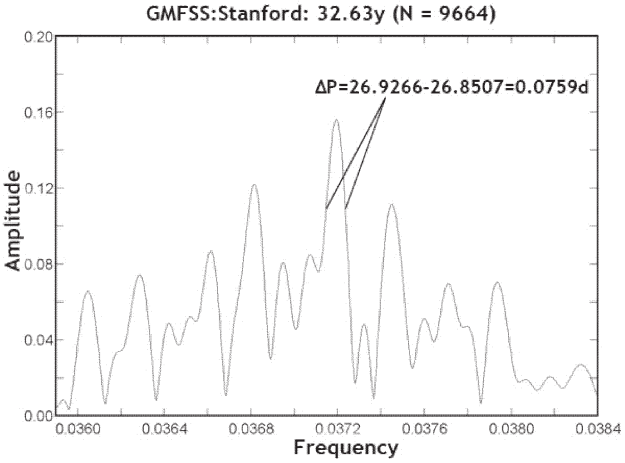

Figure 3: Power spectra.

the behavior GMFSS of complex;
second, *an additional shortward displacement between the observed and calculated periods for the smooth curve of differential rotation is presented.*

The expected shift between the observed periods and those calculated for the smooth curve of differential rotation, according to the data of helioseismology, must be $\sim 5\ ms^{-1}$. This corresponds to the difference in the periods of $\sim$ 0.1 days for the solar equator. One can see from Fig. 4 that the difference between the obtained periods and expected values noticeably greater than 0.1 days. I.e., in the case of GMFSS observations we record additional to the differencial rotation speed of plasma motions in the photosphere of the Sun large than $5\ ms^{-1}$.

Acknowledgements. D. Baklanova and S. Plachinda acknowledge support from the Ukrainian Fundamental Research State Fund (M/364); S.Plachinda acknowledges support in part from the Austrian Science Fund (P17890).

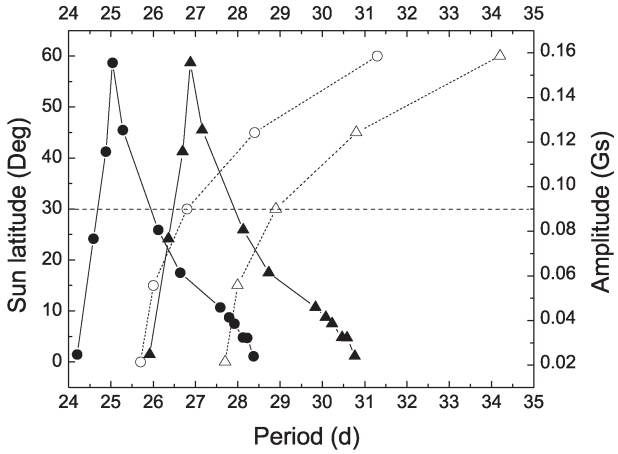

Figure 4: Period diagram

References

Haneychuk V.I., Kotov V.A., Tsap T.T.: 2003, *A&Ap*, **403**, 1115.

Howe R., Komm R.W., Hill F., Christensen Dalsgaard J., Haber D.A., Schou J., Thompson M.J.: 2004, in: *Proc. of the SOHO 14/GONG 2004 Workshop "Helio- and Asteroseismology: Towards a Golden Future"*, ESA SP-**559**, 472.

Kotov V.A., Scherrer P.H., Howard R.F., Haneychuk V.I.: 1998, *ApJSS*, **116**, 103.

Lenz P., Breger M.: 2005, *Comm. in Asteroseismology*, **146**, 53.

Livshits I.M., Obridko V.N.: 2006, *AstRep*, **50**, N11, 926.

Petit P., Donati J.-F., Auriere M., Landstreet J.D., Lignieres F., Marsden S., Mouillet D., Paletou F., Toque N., Wade G.A.: 2005, *MNRAS*, **361**, 837.

Plachinda S.: 2004a, NATO Science Series, **161**, 351.

Plachinda S.: 2004b, in: *Multi-Wavelength Investigations of Solar Activity, IAU Symp.*, **223**, 689.

Plachinda S.I., Tarasova T.N.: 2000, *ApJ*, **533**, 1016.

Plachinda S., Baklanova D., Han I., Kim K.-M., Reegen P., Valyavin G., Weiss W.: 2008, *BCrAO*, in press.

Reegen P.: 2007, *A&Ap*, **467**, 1353.

Severny A.B.: 1969, *Nature*, **224**, 53.

ACTIVIVE PHENOMENA OBSERVED IN ATMOSPHERIC LINES OF THE HERBIG AE STAR HD163296

M.A. Pogodin[1], M.M. Guimaraes[2], S.H.P.Alencar[2], W.J.B.Corradi[2], S.L.A.Vieira[3]

[1] Pulkovo Observatory, St.Petersburg 196140, Russia, *pogodin@gao.spb.ru*
[2] UFMG, Belo Horizonte 30123-970, MG, Brazil
[3] Centro Univeritario UNA, Belo Horizonte 30455-590, MG, Brazil

ABSTRACT. We present new results of a high-resolution spectroscopic investigation of the young Ae Herbig star HD 163296. Nineteen spectra of this object had been obtained on May 8 - 10, 2002 at the ESO with the FEROS high-resolution echelle spectrometer (R=48000) installed at the 1.52m telescope. We have revealed a variability in a number of atmospheric lines of some ionized metals. This variability correlates with spectral parameters connected with the accretion process. In the night on May 8 a correlation of the atmospheric activity with the intensity of the outflowing matter was also observed. An interpretation of these phenomena is considered in the framework of several model.

Key words: Stars: pre-main sequence: circumstellar matter; stars: spectroscopy; stars: individual: HD 163296

1. Introduction

A study of active phenomena in the Herbig Ae star HD 163296 was carried out using new data obtained with the high-resolution FEROS echelle-spectrometer installed at the 1.52m telescope of ESO (La Silla, Chile). Nineteen spectra of the object have been registered on 8 - 10 May, 2002.

We addressed the following questions: a) spatial structure of the stellar wind; b) existence of interrelation between the accretion onto the star and the matter outflow, and c) existence of atmospheric activity in HD 163296.

The first stage of our investigation was devoted to solving the first two problem. The results of this investigation was published in Pogodin et al. (2007), where the used instrument was described and the collection of all spectra was presented. Nineteen high-resolution (R=48000) spectra have been obtained on May 8-10, 2002 with the echelle-spectrometer FEROS installed at the 1.52m telescope ESO (La Silla, Chile).

As it has been concluded in Pogodin et al. (2007): a) the model of the disk stellar wind is the most appropriate for HD 163296; b) it is likely, that the stellar wind zone contains layers of preferential generation of dense outflowing gas, and c) noticeable correlation exists between processes of accretion and stellar wind.

The study presented here was aimed at an investigation of active phenomena observed in atmospheric lines of HD 163296.

2. Results

Fig. 1 displays a fragment of the spectrum of HD 163296 containing a number of atmospheric lines. The synthetic spectrum is also given for comparison, which was calculated using the SYNTH+ROTATE code (Piskunov 1992) and model parameters taken from Guimaraes et al. (2006): T_{eff} = 9400 K, $\log g$ = 4.1, [Fe/H] = 0.5, and $V \sin i = 130\,km\,s^{-1}$.

Some blends are in good agreement with the model fit, but several lines of ionized metals demonstrate notable discrepacies. Moreover, depth and velocity positions of these lines at minimum intensity were different in different dates (bottom box of Fig. 1).

In contrast to the absorption line HeI 4471, originating in the accreted flow and demonstrating in all cases only positive positional shift, the ionized metal lines were shifted toward both negative and positive radial velocities.

Therefore, a source of these variations cannot be placed directly in the infalling gas. It cannot be situated in the stellar wind either, because of rather small radial velocity shefts of MgII, TiII anf FeII lines in comparison with velocities observed in the wind. According to Pogodin et al. (2007), all features, originating in the outflowing gas, are observed at $V_r <$ -25 $km\,s^{-1}$ (Fig. 3 in Pogodin et al., 2007), and the wind cannot be responsible for distorting atmospheric line profiles at smaller negative velocities.

We tried to investigate a character of the variability observed in the metal lines and constructed the residual spectra by subtraction of the mean spectrum from each individual one (Fig. 2).

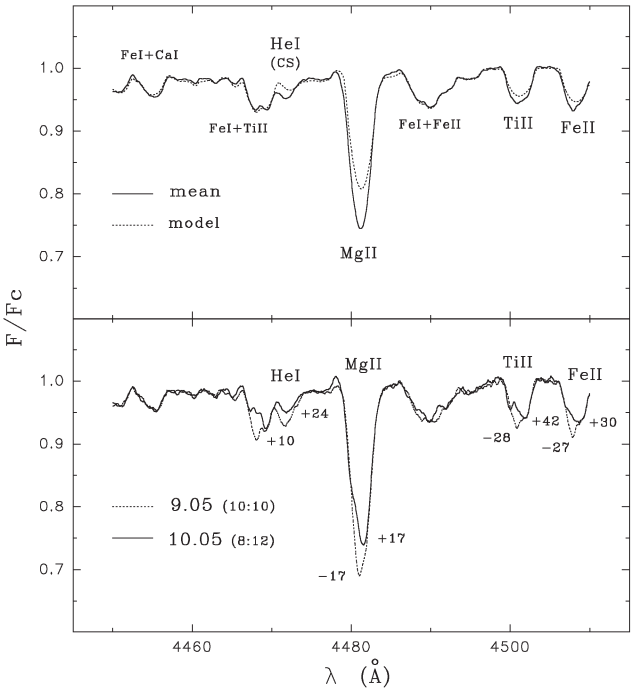

Figure 1: **Top:** Atmospheric lines in the spectrum of HD 163296 in comparison with the synthetic spectrum. **Bottom:** Variability of atmospheric lines of ionized metals.

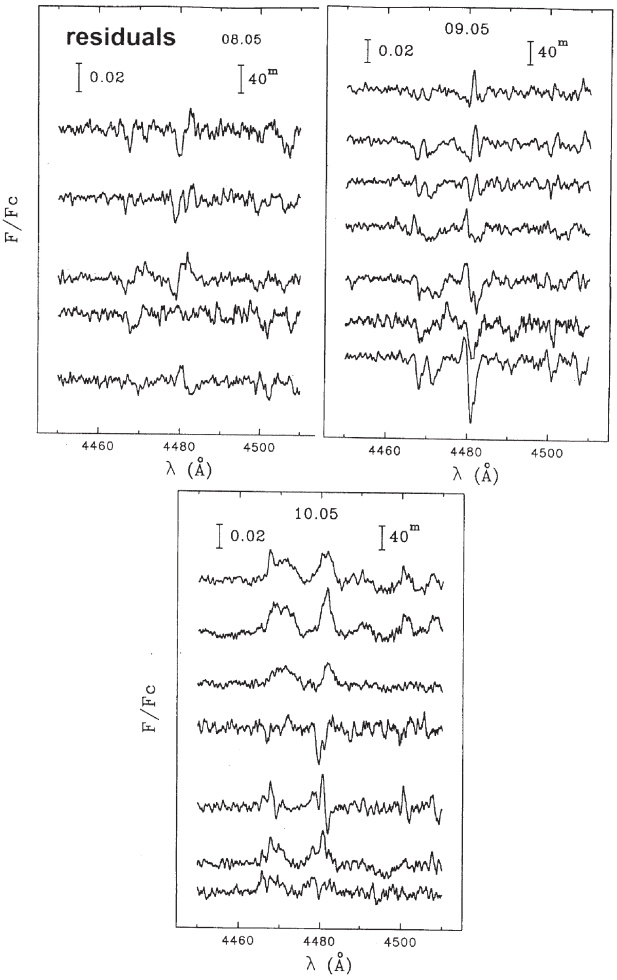

Figure 2: Residual spectra in the region of atmospheric lines. Shift between neighboring spectra is proportional to the time interval between expositions (time increases from top to bottom).

One can see that the character of variability is rather complex. Sometimes the neighboring spectra are rather similar, sometimes the changes are very significant and rapid.

In late 80's Baade & Stahl (1989) revealed a short-term variability of some atmospheric lines in the spectrum of HD 163296. They tried to establish periodicity of these variations, but had no success and assumed that a multi-harmonious non-radial pulsations (NRP) could take place in the stellar atmosphere. But actually, the question on a nature of the variations remains an unresolved one.

We tried to find a possible relation between the activity, observed in atmospheric lines and the processes in the circumstellar (CS) matter: accretion and stellar wind. With this aim, we chose several parameters, connected with these three processes, which could serve as their quantitative characteristics. These parameters are as follows: a) intensity in the red wing of the HeI 5876 line profile at radial velocity, corresponding to its maximum (or minimum) is a characteristic of the rate of accretion onto the star and designated as "HeI(red)"; b) the same intensity, but in the red wing of the CaII K line profile after subtracting the synthetic atmosphere component – "CaII(CS,red)"; c) the same as b), but for the blue wing, as a parameter, connected with the rate of gas outflow – "CaII(CS,blue"; d) another parameter of the rate of wind – the asymmetry index of the emission Hα profile "Q(Hα", determined as the relation of (EW_+ - EW_-) and (EW_+ + EW_-), where EW_+ = EW ($V_r > 0$) and EW_+ = EW ($V_r <$ 0). This index Q is zero for a symmetric profile and becomes close to 1 for a classical PCyg II-type profile with a deep blue absorption.

The bisector radial velocity of an atmospheric line at the 0.7 F_c level (V_r) was accepted as a characteristic of the atmospheric activity.

Fig. 3 presents the temporal run of radial velocities of atmospheric lines MgII 4481 and FeII 4508 in comparison with temporal variations of the Q index for the Hα line (upper boxes). One can see, that a correlation between these parameters and the Q index was observed only during the first night (on May 8). This fact is well illustrated by the diagram in the bottom box, constructed using data, obtained for the MgII line. Points for different nights, marked by different symbols, are

divided into three separate groups.

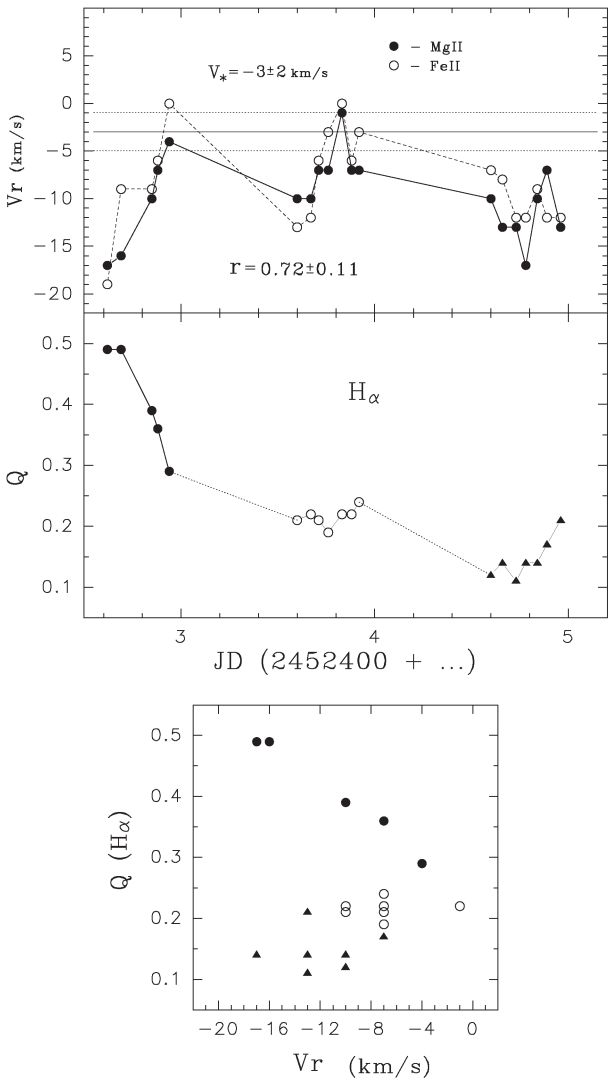

Figure 3: Correlation between the radial velocities of atmospheric lines and the index Q(Hα), characterising the rate of stellar wind (all designations are explained in the text).

A quite different relation is observed between the radial velocity of the MgII 4481 line and two parameters, chosen as characteristics of the accrertion process. One can see, that points in the diagrams, corresponding to different nights, are not separated into different groups, but form a common single dependence with noticeable correlation coefficient, which is very similar for these two parameters. This fact allows us to assume, that a real physical relation exists between the atmospheric activity and the process of accretion onto the star.

We assume, that a cause of this relation can be processes in the internal part of the accretion disk, partly screening the sellar limb, provided the disk is situated close to the star.

We cannot also exclude a possibility, that the accreted streams, exciting equatorial region of the stellar surface, stimulate the observed atmospheric activity.

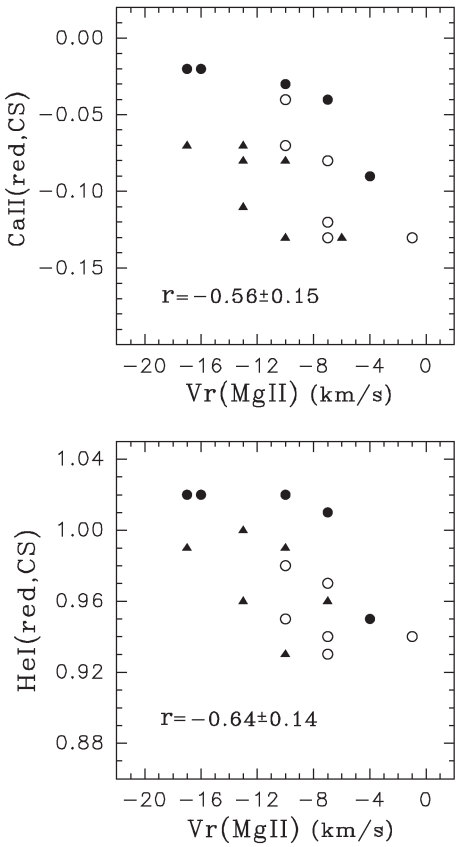

Figure 4: Correlation between the radial velocity of the atmospheric MgII line and parameters, characterising the rate of accretion (all designations are the same as in Fig. 3).

Forthcoming collecting the observational data as well as a development of theoretical models will allow to construct a rigorous theory of this interrelation.

Acknoledgements. M.Pogodin would like to remark that his contribution to this work was sponsored by the Program of the Presidium of the RAS No 4, OFN RAS Rrogram No 10104, RFBR (grant No 07-02-00535a) and Sci.Schole No 6110.2008.2. Brasilian co-authors aknowledge support from FAREMIG (EDT-1883/03 and CEX-96/04). We also thank Dr.Herman Hensberge for help with the reduction of FEROS data.

References

Baade D., Stahl O.: 1989, *A&A* **209**, 268.

Guimaraes M.M., Alencar S.H.P., Corradi W.J.B., Vieira S.L.A.: 2006, *A&A*, **457**, 581.

Piskunov N.E.: 1992, *Stellar Magnetism*, 92.

Pogodin M.A., Guimaraes M.M., Alencar S.H.P., Corradi W.J.B., Vieira S.L.A.: 2007, *Odessa Astron. Publ.*, **20**, 182.

THE MODELLING OF THE MASS–METALLICITY RELATION FOR THE LOCAL GROUP DWARF GALAXIES

M.V. Ryabova[1], Yu.A. Shchekinov[1,2]

[1] Southern Federal University, Rostov-on-Don, Russia, *rgyaf@yandex.ru*
[2] Special Astrophysical Observatory, Nizhnyi Arkhyz, Russia, *yus@phys.rsu.ru*

ABSTRACT. We present results of modelling of the mass-metallicity relation for the Local Group dwarf spheroidal (dSph) galaxies. In this work, we use a single-zone chemo-dynamical model. Our model is based on the scheme suggested by C. Firmani and A. Tutukov (1992). The behaviour of the dark-to-visible mass ratio has been taken from M.-M. Mac Low & A. Ferrara (1998). We have considered two classes of models: open and closed. The obtained mass-metallicity relation for the open model shows that the galaxies can be divided into two distinct classes: low-mass ($M_{tot} < 10^8 M_\odot$) and high-mass ($M_{tot} > 10^8 M_\odot$) groups which agrees with observation data.

Key words: Dwarf galaxy, local group, mass–metallicity relation.

1. Introduction

One of the fundamental problems, connected with chemical evolution of stellar systems including globular clusters and galaxies, is the problem of dependence of stellar system average metallicity on its mass. The solution of this problem is not trivial because the mass-metallicity relation can be determined by many factors, in particular, by exchange of material with an environment. It seems that the more massive self-enriched systems should have more metals. For low-mass systems the situation can change, because only those systems where the total energy from SNe is smaller than their binding gravitational energy can survive, otherwise they are destroyed and cannot be observed as separate stellar units.

To investigate this problem we carried out the modelling of the mass-metallicity relation for low-mass stellar systems – dwarf galaxies.

2. The model

We have applied a standard set of the integro-differential equations describing an exchange of mass between the stellar and gas components, the elemental abundances, and also the dynamic equation connecting the supernovae (SNe) explosion energy and dynamic characteristics of the system (Firmani & Tutukov 1992).

It is known that dwarf galaxies contain dark matter determining the gravitational potential of the system. In our calculations we used the empirical dark-to-visible mass ratio $M_h/M_g = 34.7 \cdot (M_g/10^7 M_\odot)^{-0.29}$, where M_h is the total halo mass, M_g is the baryon mass (Mac Low & Ferrara 1999).

3. Mass–metallicity relation

Two classes of models have been considered: the open and closed. In open model the fraction of mass which can be ejected from galaxy as a function of the total number of SNe is given by

$$\delta = \begin{cases} 1, & N_t < 100 \\ 1.76 - 0.165 \ln(N_t), & N_t > 100 \end{cases}$$

The ejection is inhibited for galaxy's mass above certain value $10^9 M_\odot$ (Ferrara et al. 2000).

Two important issues have to be mentioned: first, the increase of the total galactic mass increases its gravitation potential. Second, while the galactic mass increases star formation becomes less coherent through the galactic area and the energy from SNe dissipates in the surrounding interstellar gas.

The results of calculations for closed and open models are shown on Fig. 1. For closed models, we have obtained an obvious result: the metallicity reaches constant value when the galactic mass increases. For open models a nonmonotonous dependence in the range of mass from $5 \cdot 10^6$ to 10^9 is observed. The obtained mass-metallicity dependence allows to distinguish the whole range of masses on to two intervals with a completely different behaviour: $M_{tot} < 10^8 M_\odot$ and $M_{tot} > 10^8 M_\odot$.

In the work by Tamura et al. (2001) the massmetallicity relation among the Local Group dSph galaxies has been examined. It was noticed that dSph galaxies

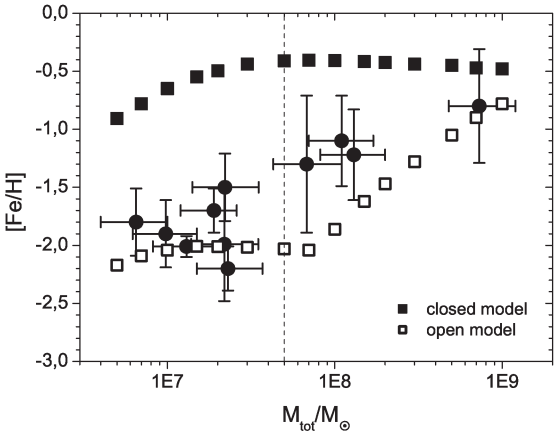

Figure 1: The mass-metallicity relation for closed and open models. Circles are the observed mass-metallicity relation for the Local Group dSph galaxies (Tamura et al. 2001).

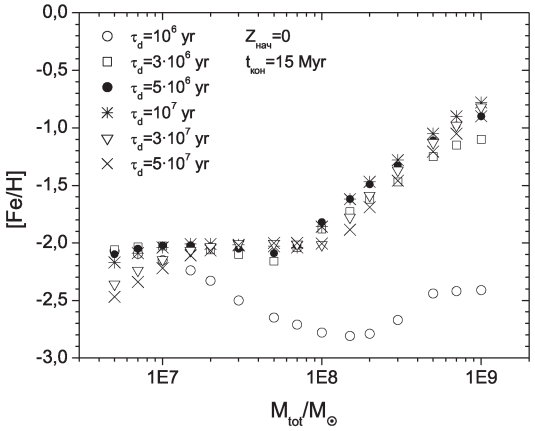

Figure 2: The mass-metallicity relation for open models with variations of dissipation time.

can be divided by mass on to two groups: low mass and high mass galaxies (vertical dash line on Fig. 1 indicates the boundary between the groups).

It is easy to see that the modelled mass-metallicity relation for the open model is in a quite good agreement with the observed dependence.

The numerical calculation within the frameworks of a single-zone scheme depends on several free parameters. One of such a parameter is the dissipation time estimated phenomenologically. The dependence of the mass-metallicity relation on dissipation time has been investigated. The results of calculations for the open model are shown on Fig. 2. As can be seen that the mass-metallicity relation for small dissipation time greatly differs from all other obtained dependencies (especially by its anticorrelation for low masses $M_{tot} < 10^8 M_\odot$). In the range $M_{tot} > 10^8 M_\odot$, the metallicity grows with the galactic mass independently of dissipation time. Such a behaviour is observed in dSph galaxies, which still remains unexplained. Our simulations allow to conclude that it is determined by the mass exchange with an environment and by the corresponding metal losses. The decrease of metallicity with mass in the range of low masses can be explained by that the gravitational potential in this case is small in comparison with SNe explosion energy. The subsequent increase of galactic mass leads, on the one hand, to increase of the gravitational binding energy, and on the other hand, to desynchronization of SNe explosions followed by considerable energy loss in the interstellar gas.

We also have investigated the dependence of the mass–metallicity relation on the age of system. It was found that in the low mass range the metallicity decreases when the age decrease. In the high mass range the metallicity values are independent of the age.

3. Summary

The obtained results allow to draw the following conclusions:

- The gravitational potential (dark matter) essentially influences on the mass-metallicity relation.
- The observed nonmonotonous behaviour of mass-metallicity relation for low-mass dwarf galaxies represents a transition from the systems with weak gravitational potential to the systems with high potential.
- The observed mass-metallicity relation in the low mass end can be described by the dissipation time 10^7 yr, while in the high mass range by the dissipation time $> 10^7$ yr.
- In high mass galaxies $M_{tot} > 10^8 M_\odot$ enrichment takes place on a short timescale.

Acknowledgements. This work was supported by the Federal Education Agency (project code RNP 2.1.1.3483).

References

Firmani C., Tutukov A.V.: 1992, *Astron. Astrophys.*, **264**, 37.

Mac Low M.-M., Ferrara A.: 1999, *Astrophys. J.*, **513**, 142.

Ferrara A., Pettini M., Shshekinov Yu.A.: 2000, *Mon. Not. R. Astron. Soc.*, **319**, 539.

Tamura N., Hirashita H., Takeuchi T.T.: 2001, *Astrophys. J.*, **552**, 113.

THE SEQUENTIAL STAR FORMATION IN GLOBULAR CLUSTERS

M.V. Ryabova[1], Yu.A. Shchekinov[1,2]

[1] Southern Federal University, Rostov-on-Don, Russia, *rgyaf@yandex.ru*
[2] Special Astrophysical Observatory, Nizhnyi Arkhyz, Russia, *yus@phys.rsu.ru*

ABSTRACT. The results of [O/Na] abundance modelling in globular clusters NGC 2808 and NGC 6752 are presented. The evolutionary scenario allowing to reproduce characteristic observed features of [O/Na] distribution function has been suggested. Slow winds from massive rotating stars are assumed as a producer of chemical anomalies. It is shown, that the abundance pattern in globular clusters can be explained within a model with a limited mixing of stellar wind and surrounding interstellar gas. This means in other words that the second generation stars are born in a vicinity of individual massive stars of the first generation from the heterogeneously distributed material ejected by these stars.

Key words: Globular clusters: individual (NGC 2808, NGC 6752), stars: abundances.

1. Introduction

Usually it is considered, that stars of the globular clusters (GCs) are formed simultaneously from chemically homogeneous material. In other words, GCs are considered as "simple stellar population".

However, there is a growing number of observational facts which challenge this traditional view. Since the eighties we know that GCs show a peculiar pattern in their chemical abundances (Gratton *el al.* 2004 for a review). While they are generally homogeneous insofar Fe-peak elements are considered, they often exhibit large anticorrelations between the abundances of C and N, Na and O, Mg and Al. Moreover, there are direct observational evidences of the presence of more than one stellar population in some GCs.

At present the several hypotheses are suggested for interpretation of chemical anomalies observed in GCs. Most of them are based on the assumption that stars of GCs are originated from material, enriched at previous stages of stellar evolution inside GCs — it is the self-enrichment hypothesis. Arguments for the self-enrichment hypothesis are based on observational O-Na anticorrelation. Indeed, the necessary high temperature ($> 10^7$ K) for CNO-cycle and NeNa-chains is not reached in stars near a turnoff and a subgiants branch for which O-Na anticorrelation is observed. This means, that the Na, O and He abundance anomalies was already present in the material the observed stars have formed from. However, the assumption that Na and O were already present in GCs material before formation of its stars, can be refused, because it means highly efficient mixing of elements of CNO-cycle, on the one hand, and elements of NeNa-chain on the other. It is worth noting that the self-enrichment scenario in modern understanding differs from "classical" self-enrichment scenario, where GCs are assumed to form from pristine gas (Fall & Ress 1989).

At present there is no physically proved self-consistent evolutionary scheme of GCs which would allow to explain the observed abundance pattern. In the present work we are attempting to construct the evolutionary scheme able to reproduce this pattern.

2. Numerical model

For the computing we used a single-zone model based on the standard system of equations describing evolution of the gases mass and the elemental abundances of star forming system (Matteuchi *et al.* 1989, Firmani *et al.* 1992, Shustov *et al.* 1997). In the present work the evolution of GCs is considered within the framework of self-enrichment scenario.

Following Decressin *et al.* (2007), we consider the slow wind from massive rotating stars as a producer of chemical anomalies in GCs.

2.1 Model 1

A detailed description used single-zone model of chemical evolution is given in previous works (Kasjanova & Shchekinov 2005, Ryabova & Shchekinov 2008). In all considered models we assume variations of the initial mass function (IMF) (Kasjanova & Shchekinov 2005).

In the assumption, that all material injected by stars is fully mixed with the interstellar medium, it

is not possible to reach the high helium abundance in gas before formation of next stellar generation even if only the massive rotating stars (the main source of helium) are born at the first episode of star formation (SF). At full mixing of the injected material with the gas primordially contained in the protocluster the helium fraction in gas will increase only by $\Delta Y = (\Delta M_{He} - Y \cdot \Delta M)/(\Delta M + (M - M_*)) \sim 2 \cdot 10^{-3}$.

In order to avoid full mixing, we will consider that the slow wind material ejected by massive rotating stars is redistributed not over the whole volume of the system, but only over its part where further SF takes place — the area of active SF. Technically realization of such a model is carried out by the control of gaseous mass in this area. Initially this mass coincides with the total mass of the system since the first generation stars are assumed to born through the whole volume of the system. By the moment when the second generation stars are formed this mass should become essentially small, so that its helium abundance would be appreciable. For this purpose in the equation for gaseous mass in active SF area we add the term $-\zeta M_g$ in comparison with the equation for the total mass of the system. The value of ζ is considered distinct from zero over time interval Δt. As a result the gas mass involved in further SF, decreases by factor $e^{\zeta \Delta t}$, which can correspond, e.g., to mass loss forced by energy injection from SNe explosions or stellar wind; ζ and Δt are considered as free parameters. Actually this means, that at $\zeta \Delta t >> 1$ the next generations of stars are born mostly from the material injected by slow wind of massive stars while the gas primordially filled the protocluster leaves the area of active SF. This prescription allows to formalize partial mixing (where the enriched material is mixed with the limited mass of primordial matter) in a single-zone scheme.

Transformation of gas in active area is described by the equation

$$\dot{M}'_g = -\Psi + \int_{M_{min}}^{M_{max}} \Psi(t-\tau_M)\varphi(M, t-\tau_M) M_{\rm ej} dM - \zeta M'_g, \quad (1)$$

while for the whole volume the transformation rate of gas is equal to

$$\dot{M}_g = -\Psi + \int_{M_{min}}^{M_{max}} \Psi(t-\tau_M)\varphi(M, t-\tau_M) M_{\rm ej} dM. \quad (2)$$

Here star formation rate is

$$\Psi = f\rho^2 \upsilon,$$

where $\rho = M_g/V$ — the gas density and $\upsilon = M'_g V/M_g$ — the volume of active SF area.

An example of calculation of such a model is presented on Fig. 1. From Fig. 1 one can see, that the

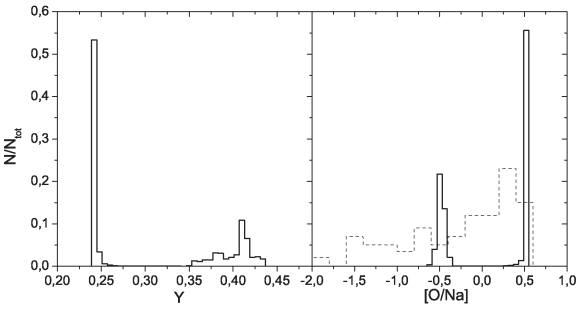

Figure 1: An example of He and [O/Na] distributions in model 1 (solid line). Dash line shows the observed [O/Na] distribution function in NGC 2808.

suggested model with partial mixing really describes formation of the stellar population with a high helium abundance. However, within the framework of such a model it is not possible to reproduce observed behaviour of [O/Na] function. The distribution shows a failure in the interval of -0.3¡[O/Na]< 0.4. The variation of free parameters of model, such as SF efficiency, the minimal mass of forming stars in the first episode, parameter ζ, changes only the number of stars in the vicinity of peaks. It is caused by the fact that the ejected matter from stars of different mass with various O and Na abundance is mixed in the active area and new stars are born from material with the average abundance of chemical elements. Apparently, it is possible to prove, that observed [O/Na] distribution function evidences of the absence of mixing in the area of active SF.

2.2 Model 2

In order to exclude mixing of chemical elements injected by stars of different masses into the SF area, it is necessary to assume the presence in system of several active areas disconnected with each other. Each such an area should include chemical elements from individual stars or stars in some mass interval.

The description of mixing process within the frameworks of a single-zone models is always schematic, and can be carried out "by hands" only. Technically realization of such a scenario of the partial mixing was carried out as follows. Stars with mass from 20 to $100 M_\odot$ which produce anomalies, have been divided onto groups by mass with an interval ΔM. For each interval of stellar masses which are born in the first episode, the independent set of equations (1) – (2) was solved. The transition time to standard IMF within the frameworks of this model was equal for each group to the life time of a star of the greatest mass (i.e. to minimal time that stars stay on the main sequence for a given group). The obtained abundance distributions for each independent case were summed taking into

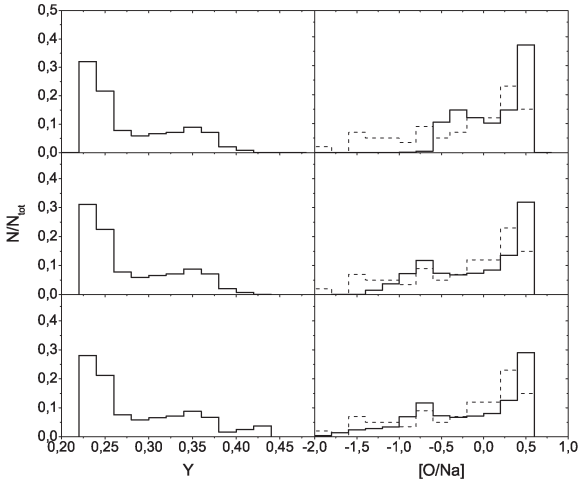

Figure 2: An example of calculations in model 2 (solid line). On right panels dash line shows the observed [O/Na] distribution function in NGC 2808.

account the fraction in the IMF from 20 to $100M_\odot$ occupied by the given group of stars.

An example of calculations in model 2 with mass spacing $\Delta M = 2M_\odot$ is presented on Fig. 2 (the top panel). It is easy to see, that the model with a limited mixing allows to reproduce the observed distribution function in the range of [O/Na]> -1, limited by the minimal value of [O/Na] available in a used database(Decressin *et al.* 2007). On the middle panel the [O/Na] distribution for [Z]$=-1.75$ is shown. This value of metallicity allows to obtain the stars with low value of [O/Na]. However, it is evident, that in the range of [O/Na]< -1 the number of stars obviously smaller than the observed. Using a more flat IMF corrects this situation: on the bottom panel of Fig. 2 the distribution is presented for the same parameters of model as on the middle panel, but for the slope of the IMF equal to -0.35 .

2.3 Model 3

The results obtained in models 1 and 2 allow to draw a conclusion that the pattern chemical abundances in GCs can be explained by assumption of the limited mixing of metals injected from stars. More specifically this means, that stars of the next generation are born from material, enriched by an individual (i.e. isolated) star. In such a scenario the [O/Na] distribution reflects the contribution of regions, enriched by all set of massive stars with metals ejected into their local interstellar medium. One of the opportunities of realization of such a scenario is the mechanism of stimulated SF. Further development would be the model in which the degree of mixing of the metals ejected even by an individual star turns to be incomplete, i.e. metals can be distributed inhomogeneously in a vicinity of an isolated star. Below we describe model in which such a scenario is realized.

Technically this scenario is carried out as follows: it is supposed, that up to the time $2.6 \cdot 10^6$yr (corresponding to the first SN explosions) the massive rotating stars with masses from 20 to $100M_\odot$ are born. The star formation rate is described by a Schmidt law with a constant $f = 6 \cdot 10^{-10}\mathrm{pc}^3 M_\odot^{-1}\mathrm{yr}^{-1}$. This value of the SF efficiency is by two orders less than the one accepted normally for spiral galaxies (Shustov *et al.* 1997). The necessity of a variation of parameter f in evolution of GCs was shown in (Kasjanova & Shchekinov 2005).

For each interval of time $\Delta t \sim 10^4$ $(0 < t < 2.6 \cdot 10^6\mathrm{yr})$ and the mass interval $\Delta M \sim 0.01M_\odot$ in the whole range $20 < M < 100M_\odot$ the number of the born massive stars $\Delta N = \Psi(t)\varphi(M)\Delta M \Delta t$ is calculated. Further on stars of small masses $(0.1M_\odot < M < 1M_\odot)$ are born from the material ejected by slow wind in the vicinity of each star of the first generation. The chemical abundance of second generation stars is determined not only by the ejected material from massive stars, but also by its mixing with the primordial protocluster gas. Note that here we understand mixing as a dilution of the material injected by massive stars with the surrounding primordial gas. The matter ejected by massive star is mixed inhomogeneously with the primordial gas, which leads to variations of the [O/Na] abundance in the second generation stars born in the vicinity of a parent massive star.

Let M^{SW} is the mass of matter injected by one massive rotating star. This matter is redistributed through over an area of a given mass with the initial chemical composition. Let M_{cloud} is the cloud mass per one star where the injected material is redistributed. The mass transformed into stars of the second generation is equal to $\eta(M^{SW} + M_{cloud})$, where $\eta \leq 1$ is the SF efficiency.

In the model 3 we characterize the degree of mixing $0 \leq \xi \leq 1$ such that matter with the mass $M_{ej} + \xi M_{cloud}$ contains homogeneously distributed products of stellar nucleosynthesis, while the remained cloud mass $(1-\xi)M_{cloud}$ has the initial abundance. Masses of ith chemical element confined into stars of the second generation in these two regions are determined as $\eta(M_{ej}^{(i)} + \xi Z_i M_{cloud})$ and $\eta(1-\xi)Z_i M_{cloud}$ correspondingly. The value $\xi = 0$ corresponds to the absence of mixing, while $\xi = 1$ described full mixing of the injected material through over the part of the cloud belonging to the star.

For each individual star the parameter ξ takes a fixed value, however for the whole stellar system we treat this parameter as a random variable. In such an approach we introduce the function $p(\xi)$ which characterizes the probability that in the vicinity of a star the degree of mixing lies in the interval $[\xi, \xi + \Delta\xi]$.

On Fig. 3a the resulting [O/Na] distribution is presented for the following parameters of the model:

[Z]=−1.5, $M_{cloud} = 200M_{\odot}$ and $p(\xi) \sim 1/(\xi + C)$, $C = 0.001$. The dash line corresponds to the observed distribution function for NGC 2808. It is readily seen, that the modelled distribution is in a good agreement with observation for [O/Na]> −1. However, as well as in the model 2 the interval [O/Na]< −1 contains no stars.

The value of initial metallicity [Z]=−1.75 allows to obtain stars with low [O/Na] (Fig. 3b). For the normal slope of the IMF the number of such stars remains still smaller than found in observations. However, for a more flat IMF (the slope equal to −0.35) the similarity of the modelled distribution and the observed one is obvious (Fig. 3c). On Fig. 3d the observed [O/Na] distribution function in NGC 6752 is shown by dash line. Despite the fact that this cluster and NGC 2808 have similar metallicity, they present distinct shapes for their [O/Na] distribution function. In order to reproduce the behaviour of the [O/Na] distribution function for NGC 6752 we have assumed the following parameters of the model: [Z]=−1.75, $M_{cloud} = 40M_{\odot}$ and $p(\xi) \sim 1/(\xi + C)$, $C = 0.003$, and in addition we assumed that stars do not form from the remaining mass of the cloud with the chemical composition. The result is presented on Fig. 3d by solid line. It is easy to see that the obtained distribution looks similar to the observed one not only qualitative, but also quantitatively.

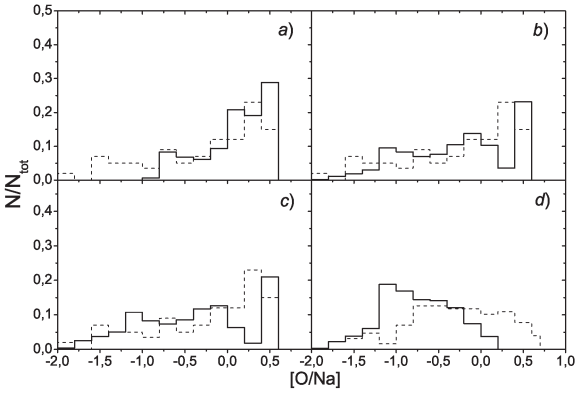

Figure 3: Examples of calculation of model 3 for probability density law $p(\xi) \sim 1/(\xi + C)$ (solid line). Dash line shows the observed [O/Na] distribution function in NGC 2808 (a,b,c) and NGC 6752 (d). Parameters of model:) [Z]=−1.5, $M_{cloud} = 100M_{\odot}$, $C = 0.001$; b) [Z]=−1.75, $M_{cloud} = 100M_{\odot}$, $C = 0.001$; c) the same as on the Fig. 3b, but the slope of the IMF equals to −1.35; d) [Z]=−1.75, $M_{cloud} = 40M_{\odot}$, $C = 0.003$.

3 Conclusions

The results of modelling of chemical evolution of GCs within the frameworks of a single-zone models allow to draw the following conclusions:

1) The excess of helium abundance in GCs NGC 2808 and NGC 6752 can be reached assuming that the first generation stars remove out of the protocluster an essential part (∼ 90%) of its baryon mass.

2) The [O/Na] distribution functions in GCs NGC 2808 and NGC 6752 reflect incomplete mixing of the stellar wind and the surrounding interstellar gas. In other words, the [O/Na] function indicates that the next stellar generation is born in the vicinity of an individual parental star. It can be understood as a stimulation of SF by stellar wind.

Acknowledgements. This work was supported by the Federal Education Agency (project code RNP 2.1.1.3483).

References

Gratton R. *et al.*: 2004, *Astron. Astrophys.*, **369**, 87.
Fall M., Rees M.: 1985, *Astrophys. J.*, **298**, 18.
Matteucci F., Greggio L.: 1989, *Astron. Astrophys.*, **154**, 279.
Firmani C., Tutukov A. V.: 1992, *Astron. Astrophys.*, **264**, 37.
Shustov B. M., Wiebe D. S., Tutukov A. V.: 1997, *Astron. Astrophys.*, **317**, 397.
Decressin T. *et al.*: 2007, *Astron. Astrophys.*, **464**, 1029.
Kasjanova M. V., Shchekinov Yu. A.: 2005, *Astron. Rept.*, **82**, 11.
Ryabova M. V., Shchekinov Yu. A.: 2008, *Astron. Rept.*, **85**, 398.

THE LARGE SKY LENS

R.B. Shatsova, G.B. Anisimova

Southern Federal University
Rostov-on-Don 344090 Russia,
gozha_marina@mail.ru

ABSTRACT. The attention is paid to the lens between the radioloop II and III and to the peculiarities in the disposition of the objects, observed through this lens.

Key words: stellar chemical composition, the ω Cen globular cluster, the Centauri stellar stream, dwarf galaxy evolution.

The sky region between the spur shells (radioloops) II and III ($l \approx 90 - 15°$), having the diameter about 60° and small axis twice and a half smaller, we name the Lens (L) (Fig. 1). Apparently, the shells' intersection also takes place in the space (Fig. 1 in the article Shatsova and Gozha in this volume) at the distances about $100 - 250$ pc. L is turned to us by its edge, located in the Gould belt (GB). The centre of the L-equator proved to be the ascending node of GB on the Milky Way (MW). The spur circle S', connecting the radioloops $I - IV$ centres and perpendicular to GB, according to Shatsova and Anisimova (2002), also passes nearby. A and B vertexes in Fig. 1 are the antipodes of the Loop I centre and the point of its shell, that is the nearest one to the Doradus shell (over GB). The main planes of Perseus and Virgo supergalaxies pass through the same points.

So, L connects the structures of the Galaxy, the Local System and the system of spurs.

The cosmic Lens is irregular. It consists schematically of two spherical layers (of II and III shells), three almost flat intersecting layers (of GB, MW and S') and the gaps between them. The thickness of each layer is several degrees. The layers are filled in by the electron gas, the neutral and ionized hydrogen, natrium, etc, the dust and the stars. One can see it over the radiation and polarization in many frequencies from γ to radio diapasons.

The theoretical examination of the optical features of such conglomerate would be of great interest, if the lensing is effective. It seems to us, it really takes place for the system of objects, observed through L. Here are the examples:

1. The Perseus arm has only one bright region at $l = 90° - 150°$. The light absorption here is even larger, then in the neighbouring regions: $A_V = 0.7$ and 1.2 m kpc^{-1} in comparison to 0.5 and 0.6 according to Efremov (1989). The mean density of stars, having $V < 9^m$ and point IRAS sources at $\lambda = 100\mu$ and 60μ is also 1.5 times larger according to Shatsova and Anisimova (2001). The outlines of the arm region and L coincide in the celestial projection.

2. Near the L centre the supernova Tycho is surrounded by the ring of 10° in radius, consisting of 4 SN, burst out in 369, 902, 1181 and 1667. It means, that 5 from 12 historical SN found themselves near the projection of L centre at the area < 0.7 % of the sky. At the same time, the chain, consisting of SN 902 and SN 1181 together with the supernova remnants (SNR) HB3 and G110.3+11.3, is stretched along the upper edge of L, according to Green (2006). Light passes through the diameter of the lens (nearby 150 pc) for 500 years. The interval between dates of registration of flares at pairs (SN 369 – SN 902) and (SN 1181 – SN 1667), and also (SN 1054 – SN 1572) and at a number of others is approximately same. Probably not flares and their reflections by the lens are observed. SNR G 292.0+1.8 and SN 1667 are antipodes on the sky and analogues by the toroidal structure of the escape matter, and also by prevalence of oxygen and neon lines in their spectra (Lozinskaya, 1986).

3. The centres of four OB-associations (Cep OB 3, Cas OB 2, Cas OB 6, Cas OB 8) are situated at the same ring between SN, and four else (Cas OB 1, Cas OB 4, Cas OB 5, Cas OB 7) are inside the ring. The number of stars in six of them is about 20, Humphreys (1978). The most rich complex is Per OB1 at the side of A vertex, and some smaller is the number of stars in Cep1 together with Cep2, near vertex B.

4. The remote open clusters also demonstrate the symmetry elements in a sector of inclined L, according to Dias, Alessi et al. (2002): the ring around the centre and the chains along the projection of shells II and III.

5. The attention was paid to the cepheids – the "twins" on coordinates, periods and velocities (Efremov, 1989).

6. The group of large molecular clouds over Huang, Thaddeus (1986) inscribes into L.

7. The three peak distributions of both 21 cm line

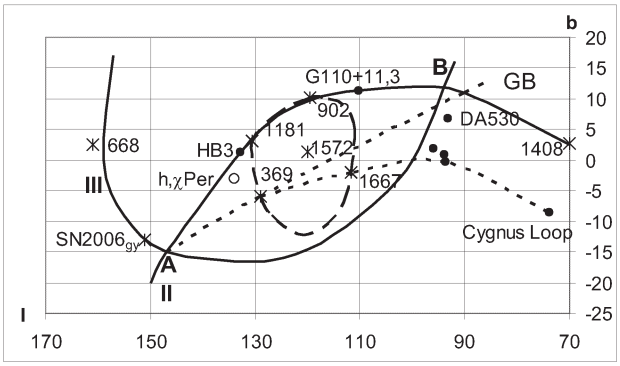

Figure 1: The SN ring around SN Tycho and other objects, observed through the lens L

profiles and the stellar velocity are similar inside L and different outside it, Humphreys (1970).

8. The chain consisting of 8 sources of WMAP catalogue and galaxies of local group NGC 6789, And VII and the pairs (NGC 147 and 185), (And V and X) is stretched along the lower L edge. There is only IC 10 near the centre on the whole L area. The tens of γ-bursts were observed along the whole L perimeter and 4 were inside SN ring, according to Lipunov (2005). Their distances are unknown.

9. Only one extragalactic supernova is near the L centre and about 20 are situated along the perimeter, the majority of them are near A and B points. The lens is projecting on the avoidance zone of galaxies, this only intensify the situation. It is also interesting, that A and B points are situated on the intersection of the zone's border and the main planes of Virgo (B) and Perseus (A) supergalaxies. By the way, the most powerful SN burst was near A point in 2006.

10. The sky cells (3°, 3°), having the largest number of point IRAS sources at the latitude b are situated along the same SR ring, in the centre and along the L perimeter. It shows the places of dust concentration, having the $1.5 - 3$ times contrast.

Perhaps, the number of almost symmetrical images in the mentioned above examples exceeds the number of real objects. It may be the result of the light reflection and refraction in the lens L.

One can also see the other lenses in the sky.

Many notions, based on the observations, can be cardinally changed if we'll take into consideration the lensing in such great scales.

References

Dias W.S., Alessi B.S., Moitinhond A., Lepime J.R.D.: 2002, *Astron. Astrophys.*, **389**, 871.

Efremov Y.A.: 1989, "Sites of star formation in galaxies", M.

Green D.A.: 2006, A-catalogue of galactic SNR (Version VI).

Huang Y.-L., Thaddeus P.: 1986, *Astrophys. J*, **309**, 804.

Humphreys R.M.: 1970, *Astron. J.*, **75**, 602.

Humphreys R.M.: 1978, *Astrophys. J. Suppl. Ser.*, **38**, 309.

Lipunov V.M.: 2005, *Physica cosmosa*, **34**, 110, Ekaterinburg

Lozinskaya T.A.: 1986, "Supernova Stars", M.

Shatsova R.B., Anisimova G.B.: 2001, *Astrofisika na rubezhe vekov*, 298.

Shatsova R.B., Anisimova G.B.: 2002, *Astrofisika*, **45**, 535.

RADIO LOOPS IN ZONE OF AVOIDING OF OPEN CLUSTERS

R.B. Shatsova, M.L. Gozha

Southern Federal University
Rostov-on-Don 344090 Russia,
gozha_marina@mail.ru

ABSTRACT. New catalogues have confirmed the existence of open clusters avoiding zone in the Sun's vicinity. Originally the zone has been found out by Shatsova & Anisimova in 1990. The zone is filled with the radio loops I - IV, the loops opened later and HI areas. Probably the system of open clusters forms a spatial lattice of the density waves. Internal parts of the loops are inside its cells. Shells are limited by the crests of waves.

Introduction

Distribution of open clusters (OC) is used for studying of Galaxy structure and kinematics for a long time. Areas of the increased density of OC are notable. So Platais et al. (1998) studying distribution of 93 OC according to Hipparcos at $r \leq 0.5$ kpc have noted a layer of ≈ 0.1 kpc thickness inclined to the galactic plane like the Gould Belt. Areas of the lowest density represent not smaller interest. In article of Platais et al. (1998) in a projection (x, y) round the Sun almost empty area of 0.5×0.25 kpc^2 is visible. It is a lot of OC on borders of this area. Authors have not noticed this fact for some reason.

But in 1990 Shatsova & Anisimova have paid attention to this area when there were 52 OC in the same volume at their disposal. Here there would be tens OC at uniform distribution in a layer. It is impossible to explain this emptiness by neither casual fluctuations, nor errors of distances and absorption of light around the Sun, nor any selection. Shatsova & Anisimova (1990a, 1990b) have assumed that anticorrelation of OC with known radio loops $I - IV$ in the same area can clear the situation. The physical and dynamic factors connected with high energy loops could create the avoiding zone of OC.

Several years ago we have checked up and have confirmed the results of works of 1990 with 104 OC from Dias et al. (2002) catalogue. The studied area has been expanded to $r \leq 0.6$ kpc. 80 OC are closer than 0.5 kpc. But there are no clusters in the space of the loops. This result has not been published.

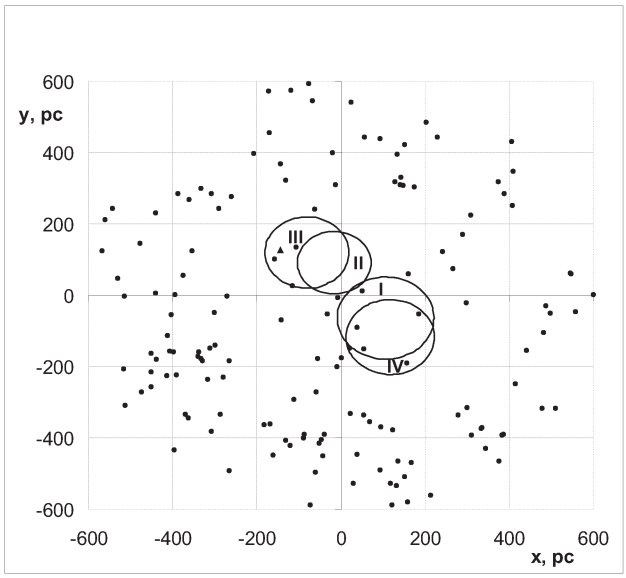

Figure 1: The projections of OC and loops $I - IV$ on the galactic plane

Zone of avoiding of OC

New, more detailed, examination is passed under Kharchenko et al. (2005) catalogues. They contain 148 OC in area with $r \leq 0.6$ kpc. Fig. 1 represents distribution of projections of OC on the galactic plane in coordinates (x, y), where x coordinate is directed towards the galactic centre, y – to galactic rotation. Projections of four radio loops according to Berkhuijsen (1973) are also shown. Similar representations of this system were given by Landecker & Wielebinski (1970) and Spoelstra (1972). 8 OC are only projected on the loops, their z-coordinates are out the loops. Only one of them – Platais 3 ($x = -144$, $y = 127$, $r = 161 - 200$ pc) as possible, but the yet not confirmed cluster, is in the Loop III (a triangle in Fig. 1).

Fig. 1 confirms a reality of OC avoiding zone near the Sun and specifies its borders: on $|x|$ and $|y|$ to $200 - 300$ pc, on $|z|$ – in tens pc. All large loops, small shells according to Hu (1981) and infrared loops from Könyves et al. (2007) catalogue are in this vol-

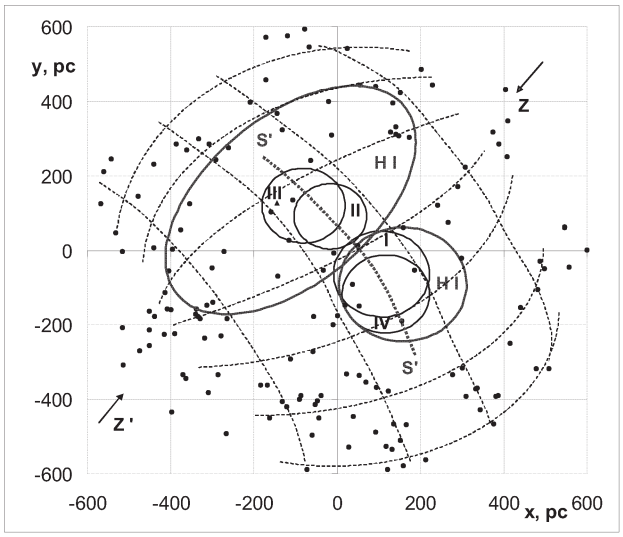

Figure 2: The (x, y)-projections of OC, the loops $I - IV$, H I shells and a variant of the density waves net (dashed lines)

ume. Fig. 1 confirms the anticorrelation OC – radio loops. However the avoiding zone is essentially larger than total volume of the loops. H I shells according to Davelaar et al. (1980) (basically in the fourth quadrant, including the Loops I and IV) and according to Olano (1982) or Lindblad ring (2000) (in the others quadrants, mainly in the second, with the Loops II and III) have the sizes greater than the loops.

Projections (x, z) and (y, z) show that OC fill rather thin layer ($\sim$ 0.1 kpc) inclined to the galactic plane at angle typical for the Gould Belt ($\sim 20°$). But the avoiding zone is not visible on these projections and on a projection to celestial sphere because of forward and far background.

The net of density waves in OC distribution

Long chains of OC in the Gould Belt layer serve as opposite display of non-uniformity of distribution. They also can be link to the system of loops. Shatsova & Anisimova (2002) have shown that the centers of four loops are located on a small circle of sky S' (dotted line in Fig. 2). Circle S' is the middle line of the Spur Belt. S' is perpendicular to one of axes of Local system - ZZ' (longitudes of poles $l = 48°$, $228°$; latitudes $b = \pm 21°$).

Narrow chains of OC are stretched along meridians of axis ZZ'. One of them passes as "corridor" between the Loops I and II. Two other chains touch with these loops outside. One more chain (at $y > 0$) passes on border of large H I area of Lindblad ring. The chain symmetric to it (at $y < 0$), probably, too outlines H I area, but greater than Davelaar et al. (1980) consider. Wide chains (or ridges) of OC are stretched along parallels of axis ZZ'. One pair covers from both sides of the Spur Belt. Another one is more close to poles Z and Z'. But drawing of such chains is less precisely because of ridge width and the greater errors of distances. The greatest OC density near Z' links to Eridanus complex.

The length of the chains is limited by the sizes of area. In total they form the net from two aggregates of the density waves with approximately identical wavelength equal to diameter of the loops ($\sim$ 200 pc). Probably, the density waves of smaller length are available in the third direction – perpendicular to the Gould Belt. Then it will be a spatial wave lattice.

So the crests of waves coincide with contours of some structures in the Sun vicinities: with loops, H I clouds, areas around poles. The troughs of cells coincide with their internal parts. Anticorrelation OC – loops is represented as a combination of the crests and the troughs of the net (lattice) of the density waves.

The geometrical picture of Fig. 2 is clearer than the physical one. But other interpretations of the loops (supernovae, stellar wind and collisions of clouds) are not clearer.

Table 1: Approximate parameters of the elements of the density waves net and the examples of projections of peculiar velocity of OC belonging to these elements. Units: x_i, y_i in pc; v_x, v_y in km s^{-1}.

i	x_i	y_i	N	OC Name	v_x	v_y
Meridians						
1	-460	430	10-15	NGC 752	-2.0	-5.3
				Stock 2	-13.6	-11.6
2	-330	240	10-15	Platais 2	2.2	3.5
3	30	-30	10-15	NGC 1977	-8.5	-2.6
				IC 4665	8.7	0.9
4	330	-240	5-10	Platais 10	-22.3	-1.6
				Alessi 21	-25.1	-4.0
5	460	-430	10-15	Alessi 5	-12.1	-5.4
				Vel OB 2	-12.4	2.5
Parallels						
1	-70	-170	10-15	Melotte 22	3.8	-11.6
				NGC 1901	-0.6	-19.1
2	170	220	10-15	Platais 12	-11.7	12.7
3	430	530	10-15	Roslund 5	4.4	-3.8
				NGC 6281	-7.2	7.4

Parameters of the elements of the density waves net and the examples of projections of peculiar velocity of OC belonging to these elements are given in Table 1. Here x_i, y_i are coordinates of intersections of the meridians and the parallels with coordinate axes, N – number of OC in the net element. There is an uncertainty in calculation of OC for which there is no data for v_r in areas near to intersection of the meridians and the parallels. Examples of projections v_x and v_y of peculiar velocity of OC belonging to the corresponding elements of the net are given in two last columns. Names of these OC are shown in the fifth

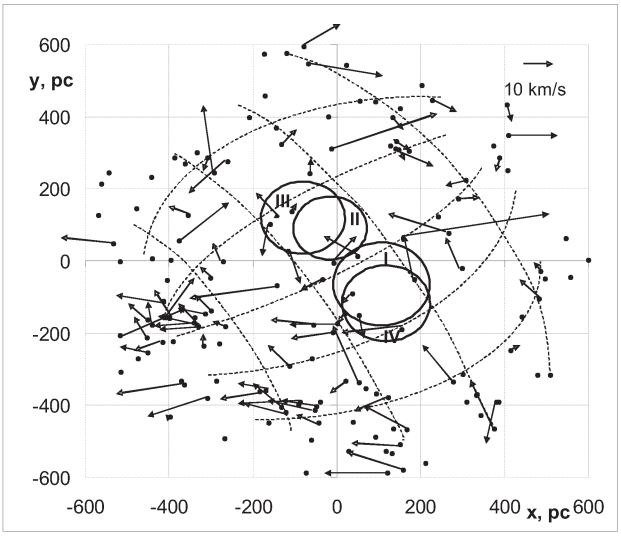

Figure 3: The (x, y)-projections of spatial peculiar velocity vectors of OC

column.

Kinematics of OC

The density waves net would be short-lived if peculiar motions of OC are chaotic. Therefore it is important to know their real motions. Platais et al. (1998) have offered motions relative to the Sun, basically reflecting motion of the Sun towards the apex. Shatsova & Anisimova (2002) have shown that the solar apex coincides with the Local system pole Z.

The Fig. 3 gives picture of peculiar motions in the (x, y)-plane for 2/3 of OC with known Vr. Primary motions along narrow meridian chains have greater values than in wide chains along parallels, where the disorder of velocity directions is more. It is difficult to separate the general expansion suspected in a number of articles from these features.

So the kinematics is compatible to wave structure of OC system. They should be considered together at the decision of all problems connected both with radio loops and with star clusters.

References

Berkhuijsen E.M.: 1973, *Astron. Astrophys.*, **24**, 143.
Davelaar J., Bleeker J.A.M., Deerenberg A.J.M.: 1980, *Astron. Astrophys.*, **92**, 231.
Dias W.S., Alessi B.S., Moitinho A., Lépine J.R.D.: 2002, *Astron. Astrophys.*, **389**, 871.
Hu E.M.: 1981, *ApJ*, 248, 119.
Kharchenko N.V., Piskunov A.E., Rőser S., et al.: 2005, *Astron. Astrophys.*, **438**, 1163.
Könyves V., Kiss Cs., Moór A., et al.: 2007, *Astron. Astrophys.*, **463**, 1227.
Landecker T.L., Wielebinski R.: 1970, *Austral. J. Phys. Astrophys. Sup.*, **16**, 1.
Lindblad P.O.: 2000, *Astron. Astrophys.*, **363**, 154.
Olano C.A.: 1982, *Astron. Astrophys.*, **112**, 195.
Platais I., Kozhurina-Platais V., van Leeuwen F.: 1998, *Astron. J*, **116**, 2423.
Shatsova R.B., Anisimova G.B.: 1990, in *Voprosy neb.mekh.*, Alma-Ata, 160.
Shatsova R.B., Anisimova G.B.:1990, *Astron. Tsyrc.*, **1546**, 13.
Shatsova R.B., Anisimova G.B.: 2002, *Astrofizika*, **45,** 535.
Spoelstra T.A.Th.: 1972, *Astron. Astrophys.*, **21**, 61.

LITHIUM SPOTS IN THE NORTHERN roAP STAR HD 12098

A.V.Shavrina[1], Yu.V.Glagolevskij[2], N.A.Drake[3], N.S.Polosukhina[4], Ya.V.Pavlenko[5], D.O.Kudryavtsev[6]

[1] Main Astronomical Observatory of National Academy of Sciences of Ukraine, *shavrina@mao.kiev.ua*
[2] Special Astrophysical Observatory of Russian Academy of Sciences, *glagol@sao.ru*
[3] Sobolev Astronomical Institute, St. Petersburg State University, Russia , *drake@on.br*
[4] Crimean Astrophysical Observatory, Nauchnyi, Crimea, Ukraine, *polo@crao.crimea.ua*
[5] Main Astronomical Observatory of National Academy of Sciences of Ukraine, *yp@mao.kiev.ua*
[6] Special Astrophysical Observatory of Russian Academy of Sciences, *dkudr@sao.ru*

1. Introduction

The realization of the international project "Li in magnetic CP stars" (Polosukhina et al. 2005) permitted us to discover the variability in intensity and position of the Li I 6708 A line in the spectra of some chemically peculiar A-type stars (Ap-CP stars): HD 83368, HD 60435, and HD 3980. These variations can be interpreted as the existence of two lithium spots on the surfaces of these stars (Polosukhina et al. 1999, Shavrina et al. 2001, Kochukhov et al. 2004, Drake et al. 2004). The synchronism of the variations of the Li I line profile, light curve and magnetic field strength can be explained in terms of the oblique magnetic rotator model.

2. The star HD 12098

Spectral observations of a number of chemically peculiar stars with the echelle-spectrometer NES and the 6 m BTA telescope of SAO RAS allowed us to discover several Ap stars with abnormally high lithium abundance. Among these stars special interest deserves the star HD 12098 - the first rapidly oscillating (roAp) star found on the northern hemisphere (Girish et al., 2001). The rotational period of this star, P = 5.460 +/- 0.001 d, was obtained by Ryabchikova et al. (2005) by determining the mean longitudinal magnetic field.

3. Observation data and treatment

The spectra used in this study are obtained with 6-m telescope of Special Astrophysical Observatory of Russian Academy of Sciences (SAO RAS) and the Nasmyth Echelle Spectrometer (NES, Panchuk et al. 2002) with the resolution of about 42000 in the range 5550-7035 Å. The signal/noise ratio for this spectra was 110-190. The SAO spectra were reduced using REDUCE package of Piskunov and Valenti (2002).

4. The atmospheric parameters and magnetic field modelling

The atmospheric parameters of HD 12098 were estimated in Ryabchikova et al. (2004) who found $T_{\rm eff}$ = 7800 K, log g = 4.3, vsin $v \sin i = 10 \pm 2$ km/s , and magnetic field modulus $B_s = 6.5$ kG. We checked these stellar parameters by means of spectral synthesis in the spectral region 6135 - 6152 Å that contains the Fe I and Fe II lines. The rotational velocity estimate is a difficult task because of the spotted distribution of chemical elements on the surfaces of roAp stars. At the same time, the value of B_s , derived from magnetic lines, dramatically depends on the adopted vsin i value.

For the analysis of HD 12098 spectra we used the code ROTATE of Tsymbal (1996), which permits to calculate synthetic spectra taking into account a spot structure at the stellar surface for different rotation phases, and the code SYNTHM (Khan, 2004) which takes into account the splitting of spectral lines in the magnetic field. The calculation of the non-magnetic Fe I line at 5576.090 A results in the value of $v \sin i = 13 \pm 1$ km/s. Using this parameter we calculated spectral synthesis in the region 6135 - 6152 A with the set of model atmospheres of Kurucz (1993) and the VALD atomic line list (Kupka et al., 1999). The comparison of model spectra with observed spectrum reveals many absorption lines in observed spectrum, which are not included in VALD list, therefore we calculated additional to VALD lines of rare earth elements (REE) on the base of NIST energy levels (http://physics.nist.gov). These additional REE line

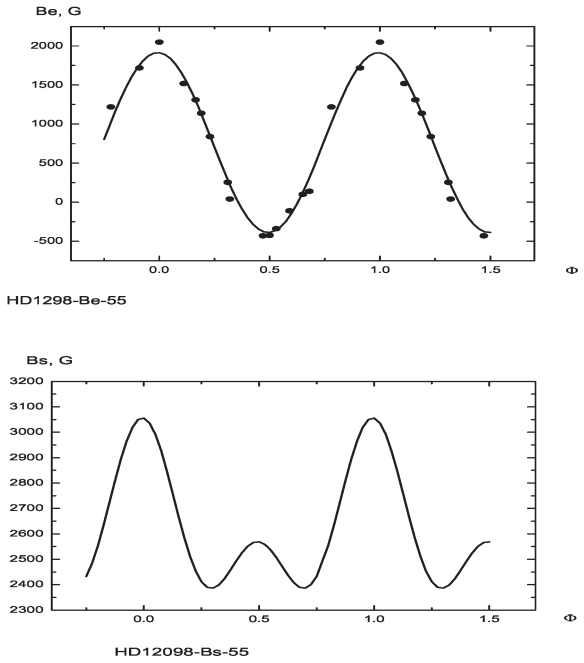

Figure 1: Measurements of effective magnetic field (Ryabchikova et al. 2005) and central dipole model values B_e (upper figure) and B_s (lower figure) for i=55^o .

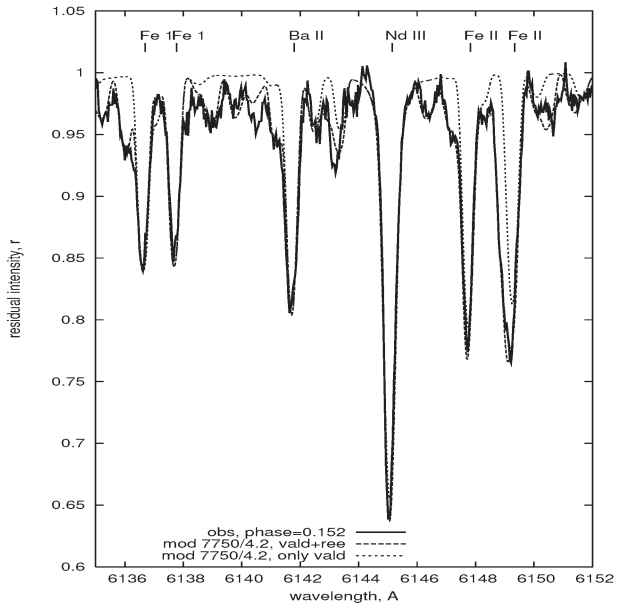

Figure 2: Observed and synthetic spectra of HD 12098 in the 6135 - 6152 ÅÅ spectral region. The additional to VALD lines of the rare-earth elements (REE) permitted us to fit calculated spectrum to observed one rather well.

permitted us to fit better model and observed spectra. The best model was 7750/4.0 with B_s =2700 G. Using this T_{eff} =7750 K and evolutionary tracks from Shaller et al. (1992) we determined mass of star as 1.7 $M_\odot$ and log $L/L_\odot$ =0.978. Using the formulas from the paper Bagnulo and Kochukhov (2003), we have got the radius of star R = 1.71$R_\odot$ and log g = 4.2. From the formula R = 50.613 * V_{rot}/P_{rot} with value P_{rot} = 5.460 d (Ryabchikova et al., 2005) we estimated the value V_{rot} = 15.85 km/s, that results in the angle of inclination of rotational axis to the line of sight i=55^o (with vsini=13 km/s).

For the study of the surface magnetic field of the star we used a model of spatially distributed magnetic charges (Gerth & Glagolevskij, 2000) and measurements of effective (longitudinal) magnetic field from the work of Ryabchikova et al. (2005). A central dipole model for surface magnetic field has been assumed which permit us to fit sufficiently well model values of longitudinal magnetic field B_e to measured ones with i=55^o and the inclination angle of dipole axis to rotational axis $\beta = 65^o$. We obtained the values of magnetic field on the poles +- 4050 G and the mean surface magnetic field 2720 G, which were used for calculation of synthetic spectra taking magnetic splitting of spectral lines (SYNTHM code) into account in the range of lithium line 6708 Å(assuming location of Li spots on the magnetic poles, i.e. B_s = 4050 G) and for the range of Fe I and Fe II lines 6135-6152 Å(assuming concentration of Fe I and Fe II between polar areas, B_s = 2720). For final calculations we used the model 7750/4.2, which was calculated by the code SAM12 (Pavlenko, 2003) with abundances of Przybylski's star (Shavrina et al., 2003).

Table 1: Li spot parameters

N	Longitude	Latitude	R	ϵ(Li)
1	10^o	25^o	70^o	4.0
2	175^o	-25^o	90^o	0.8

5. Lithium spots on the surface of HD 12098

The modelling of magnetic field based on measurements of longitudinal field of Ryabchikiva et al (2005) specified the location of poles of magnetic dipole on the surface of star: 353^o of longitude and 25^o of latitude for one spot, 173^o of longitude and -25^o of latitude for another spot. The location of lithium spots on the surface of HD12098 and abundance of lithium in these spots were found with the help of Tsymbal's code ROTATE which makes it possible to calculate spectra taking a spotted surface structure of a star into account for different rotational phases. We obtained the lithium abundances in the photosphere ϵ(Li) =3.05 dex for all phases and the values of ϵ(Li) = 4.0 and 0.8 dex for two lithium spots (see Table 1).

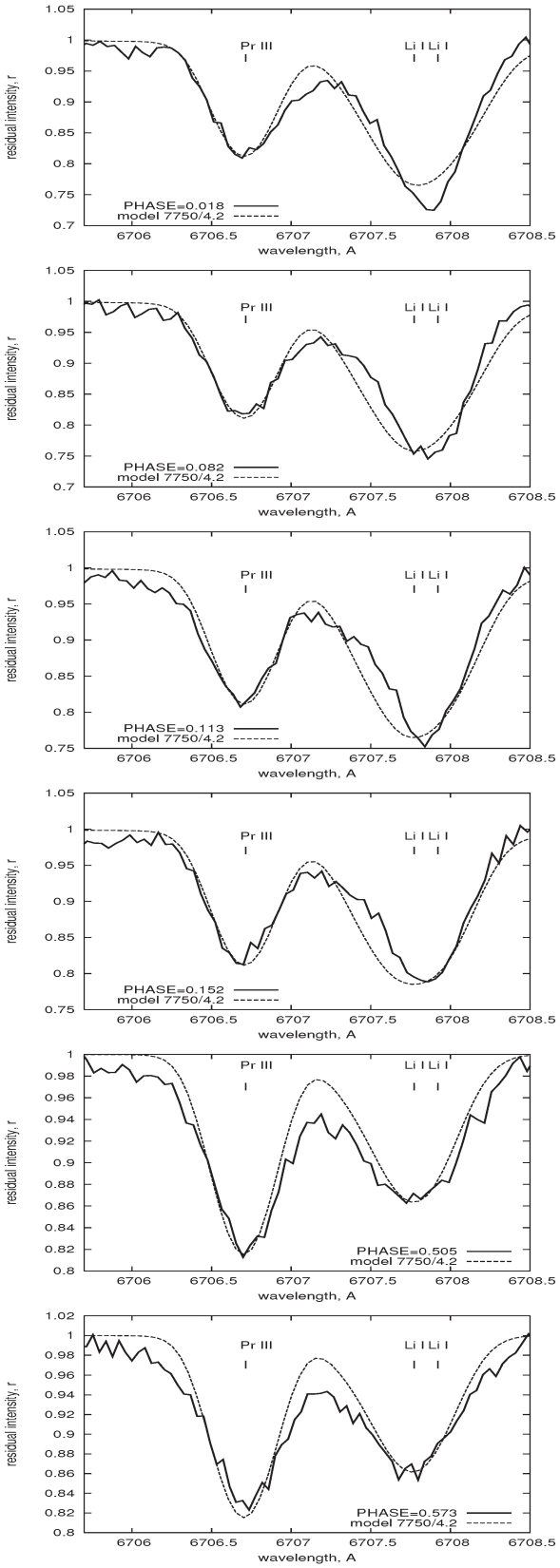

Figure 3: Spectra of HD 12098 in the 6705.5 - 6708.5 ÅÅ spectral range obtained at the phases 0.018, 0.082, 0.113, 0.152, 0.505, and 0.573 and modeled with ROTATE code spectra for parameters of Table 1. Note the strong variations of the Li I 6708 Å line.

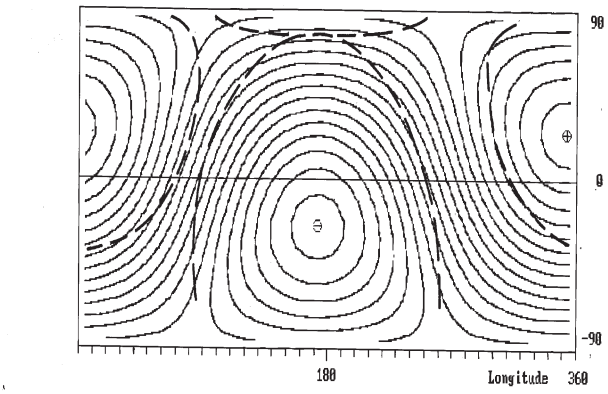

Figure 4: Location of lithium spots on Mercator's map of modelled surface magnetic field for HD 12098 note,the Li abundance in the big spot around 180^o of longitude on 3.dex lower then in the smaller spot around 0^o .

6. Discussion and Conclusions

HD 12098 is a new roAp star with the lithium spots on the surface. For available rotation phases, including phases of maximal and minimal intensities of the Li I 6708 Åline, we calculated synthetic spectra and determined the lithium abundance in the spots and the photosphere, which revealing an anomalously high Li abundance in comparison with the "cosmic" Li abundance (the lithium abundance in T Tau stars is ϵ(Li) = 3.20 +/- 0.2 dex). Our modelling of the Li distribution on the stellar surface points to the existence of two spots located close to magnetic poles of the modeled dipole (see fig.4). A considerable difference, of more than 3 dex, in lithium abundance in two opposite rotational phases (0.018 and 0.573) corresponding to different two spots on the star surface was found. For future analysis we need new spectra of HD 12098 corresponding to the phases 0.2 - 0.4 and 0.7 - 0.9 in order to obtain better phase coverage.

Aknowledgement. We appreciate V. Tsymbal and S. Khan for the possibility to work with their codes ROTATE and SYNTHM. This work was partially supported by the Microcosmophysics program of National Academy of Sciences and National Space Agency of Ukraine.

References

Drake N.A., Polosukhina N., de la Reza R., Hack M.: 2004, in *A-Star Puzzle, Proc. of IAU Symp.,* **224,** 692.

Girish V., Seetha S., Martinez P., et al.: 2001, *A&A*, **380**, 142.

Gerth & Glagolevskij: 2000, mfcp.proc., Eds.: Yu.V. Glagolevskij, I.I. Romanyuk, 151.

Khan S.: 2004, *J. Quant. Spectr. and Radiat. Transf.*, **88**, 71.

Kochukhov O., Drake N.A., Piskunov N., de la Reza R.: 2004, *A&A*, **424**, 935.

Kurucz R.L.: Data Bank - CD-ROM NN 1-22 (1993-1994).

Kupka F., Piskunov N., Ryabchikova T.A. et al.: 1999, *A&AS*, **138**, 119.

Panchuk V., Piskunov N., Klochkova V., Yushkin V., Ermakov S.: 2002, *Preprint SAO*, **169**.

Piskunov N.E., Valenti J.A.: 2002, *A&A*, **385**, 1095.

Polosukhina N., Kurtz D., Hack M., et al.: 1999, *A&A*, **351**, 283.

Polosukhina N., Shavrina A., Drake N.A., et al.: 2005, in *From Lithium to Uranium: Elemental Tracers of Early Cosmic Evolution, Proc. of IAU Symp.*, **228**, 108.

Ryabchikova T., Nesvacil N., Weiss W., et al.: 2004, *A&A*, **423**, 705.

Ryabchikova T., Wade G.A., Auriere M., et al.: 2005, *A&A*, **429**, 55.

Pavlenko Ya.V.: 2003, *Astron. Rept.*, **47**, 59.

Shavrina A., Polosukhina N., Zverko J., et al.: 2001, *A&A*, **372**, 571.

Shavrina A., Polosukhina N., Pavlenko Ya., et al.: 2003, *A&A*, **409**, 507.

Tsymbal V.: 1996, in: *Model Atmospheres and Spectrum Synthesis*, eds. S. J. Adelman, F. Kupka, W. W. Weiss, *ASP Conf. Ser.*, **108**, 198.

SPOTS STRUCTURE AND STRATIFICATION OF SOME CHEMICAL ELEMENTS IN THE ATMOSPHERE OF He-WEAK STAR HD 21699

A.V.Shavrina[1], Yu.V.Glagolevskij[2], J.Silvester[3], G.A. Chuntonov[4], Ya.V.Pavlenko[5], V.R. Khalack[6]

[1] Main Astronomical Observatory of National Academy of Sciences of Ukraine, *shavrina@mao.kiev.ua*
[2] Special Astrophysical Observatory of Russian Academy of Sciences, *glagol@sao.ru*
[3] Department of Physics, Queen's University and The Royal Military College of Canada, *james.silvester@rmc.ca*
[4] Special Astrophysical Observatory of Russian Academy of Sciences, *chunt@sao.ru*
[5] Main Astronomical Observatory of National Academy of Sciences of Ukraine, *yp@mao.kiev.ua*
[6] Département de Physique et d'Astronomie, Université de Moncton, *viktor.khalak@umoncton.ca*

1.Introduction

HD 21699 (HR 1063) was initially classified by Roman and Morgan (1950) as B8IIIvar star. Molnar (1972) has performed analysis of its spectra and determined that helium was extremely deficient (by factor of 5). Therefore, he classified this star as a He-weak type. Shore et al. (1987) refer to HD 21699 as He-weak silicon star (sn class - with broad and diffuse He I lines).

Extremely reduced helium abundance in HD 21699 results in the incorrect spectral classification. The MK classification gives Sp = B8. Abt et al. (2002) suggest a spectral class B8IIIpMn, that corresponds to T_{eff} = 12000 K, while Glagolevskij (2002) has derived T_{eff} = 16100 K from the analysis of color indices. Using the spectra obtained with 6-m telescope, the parameters T_{eff} = 16000 K, lg g = 4.15, V_t = 0.8 km/s are derived by Glagolevskij et al. (2005) from analysis of the H_δ line.

Period of the axial rotation for HD 21699 is P = $2^d.4765$ (Brawn et al. 1985). The relation between the equatorial velocity, period and stellar radius ($V = 50.613 * R/P$) and the measured value of v sin i= 35 km/s yields the inclination angle $i = 32°$ (Glagolevskij & Chuntonov, 2007). The positive maximum of effective magnetic field occurs at the phase $\phi = 0$, and the negative extremum occurs at $\phi = 0.4$ according to the ephemerides of Glagolevskij & Chuntonov (2007) for initial phase:

JD = 2445595.529 + $2^d.49246$

2. Magnetic field model

A one-spot model for helium and silicon surface distribution has been shown by the work of Stateva (1995) to fit observed periodic variations of equivalent widths of He I lines and Si II lines. One large He-weak spot is situated around the positive magnetic pole, while Si II spot is located at the negative pole. A central dipole model for surface magnetic field has been assumed in this work. Analysis of the equivalent widths of helium and silicon lines shows that the peaks of their plots do not coincide in phase, rather they are opposite. Usually, in a case of central magnetic dipole the abundances of the same element are equal in the vicinity of both magnetic poles.

UBV photometry (Percy, 1985) shows only a single wave of the light curve during the rotational period, while stars with a magnetic field of centered dipole always have a double wave. In the work of Shore et al. (1987) it is mentioned that a similar behavior in the photometric data is seen in two other He-weak sn stars: HD 5737 and HD 79158.

Brown et al. (1985) has reported discovery of magnetically controlled stellar mass outflow in HD 21699 basing on IUE observations of the C IV resonance doublet, which is variable on the rotational time-scale of about 2.5 days. He has found only one jet from the only one magnetic pole.

An additional study of the surface magnetic field for this star has been performed by Glagolevskij & Chuntonov (2007) using a model of the spatially

distributed magnetic charges (Gerth & Glagolevskij, 2000) . The measurements of H_β line with the Zeeman polarimeter (Brown et al., 1985) have been employed to reconstruct the magnetic field model.

It is shown that a better agreement between the observed and calculated curves of the equivalent widths of He I and Si II lines for HD 21699 can be reached with a model where the dipole is displaced across its magnetic axis from the stellar center by a factor $a = 0.4 + 0.1$ of stellar radius. Therefore, the magnetic poles appear to be close to one another on the stellar surface (they are separated by 55°, not by 180° as it would be in a case of central dipole). The big "strong" helium spot coincides with the average position of the two magnetic poles, while the "weak" spot is located in the opposite side of the star (Glagolevskij & Chuntonov, 2007).

Phase dependence of the equivalent widths of He I and Si II lines shows extreme values at phases that correspond to the passage through visible meridian of zero magnetic field between the magnetic poles. The intensity of helium lines reaches its maximum at the magnetic poles, while the intensity of silicon lines reaches here its minimum. Silicon abundance is maximal in the regions where magnetic field is predominantly tangential to the stellar surface.

The behavior of atomic diffusion does not depend on the sign of magnetic field nor does the abundance of chemical species in a magnetic spot depend on the field' sign. Observed data show that despite of the intensities of helium lines are weakened in all rotational phases, they still are unmistakably increased in the magnetic spot. On the contrary, silicon lines are more weak in the spot than on the opposite part of stellar surface. Due to averaging over the visible hemisphere and owing to the close location of both magnetic poles to each other, the only one wave of intensity variation in spectral lines is observed for the investigated chemical species. For the same reason we observe the only one wave for the variability of photometric light curve and of average surface magnetic field Bs. Respectively, only one jet of stellar wind, common from both poles, is observed.

3. Variability of He I and Si II line's intensity with rotational phases

HD 21699 is a unique star due to the nature of the surface magnetic field distribution. Due to close location of positive and negative magnetic poles to each other, the common "magnetic spot" are situated on one-half of stellar surface with predominantly vertical magnetic field lines (Glagolevskij & Chuntonov, 2007). Meanwhile, on the other hemisphere the magnetic field lines are horizontal. Such a configuration of the magnetic field is convenient to perform analysis of abundance surface distribution for those chemical species which are concentrated around the magnetic poles (He I and others) and those which are concentrated in the area with the horizontal magnetic field lines (Si II and others). It provides also a unique opportunity to study the variability of mean abundances with rotational phase and the vertical distribution (stratification) of chemical species in stellar atmosphere depending on the structure of magnetic field.

HD 21699 is very suitable star for studying the atomic diffusion of chemical species in the atmospheres of CP stars because its surface can be simply divided on two parts: one where the magnetic field lines are horizontal to the stellar surface and another where they are predominantly vertical.

4. Observation data and treatment

The spectra used in this study are obtained with the 6-m telescope of Special Astrophysical Observatory of Russian Academy of Sciences (SAO RAS) with the main stellar spectrograph (MSS) equipped by slicer of 14 cuts and have spectral resolution R = 15000. The signal-to-noise ratio is 2000. Ten spectra in the region 3900-4300 A cover uniformly the whole rotational period. One more spectrum has been registered with Nasmyth Echelle Spectrometer (NES) for the resolution of 40000 in the range 4500-5900 A (the phase=0.687). The signal-to-noise ratio for this spectrum is 400. SAO spectra are reduced using MIDAS procedures.

Additionally we used spectra obtained with the MuSiCoS spectropolarimeter which is installed on the 2-m Bernard Lyot telescope at the Pic du Midi Observatory in France. MuSiCoS is a table-top cross-dispersed echelle spectrograph which is fed by two optical fibres from the polarimeter, mounted in the cassegrain focus, with resolution R = 35000 and wavelength coverage from 4500 to 6600 A (phases=0.118, 0.322, 0.525). For the MuSiCoS spectra signal-to-noise ratio is about 400 per pixel.

A complete Stokes V exposure is made up of 4 subexposures in which the retarder is rotated by 90 degrees and back. By switching the beams within the instrument, in principle any first order spurious polarization signatures are suppressed to an acceptable level. The MuSiCoS spectra are reduced using the ESPRIT data reduction package (Donati et al., 1997).

5. The spectra modeling and results

Synthetic spectra for HD 21699 are calculated with the code SYNTHM of S.Khan (2004) and SYNTHV of V.Tsymbal (1996). We use Kurucz' model atmosphere with parameters $T_{\rm eff}$ =16000 K and $\log g$ =4.0 as well as Pavlenko' model atmosphere with reduced He abundance. The atomic lists of VALD and

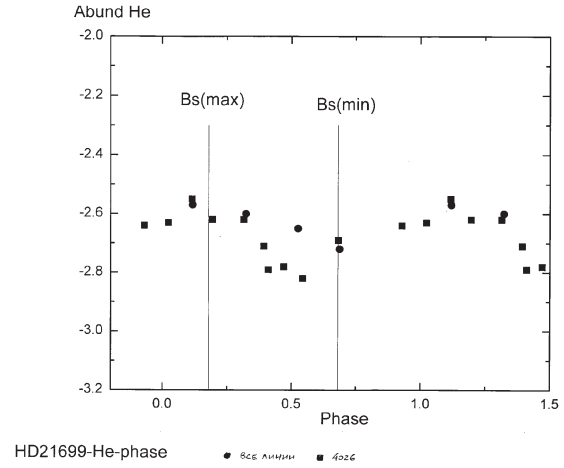

Figure 1: Variability of the helium abundance (log N(He)/N(H)) with rotational phase. The circles present averaged abundance deduced from analysis of He I lines (see Table 1), while the squares stand for abundance deduced from analysis of He I line 4026A. Mean error for all abundance estimates is about ± 0.1dex.

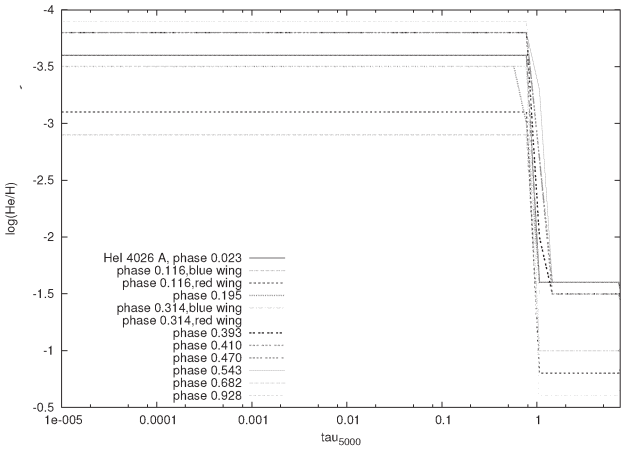

Figure 2: Helium vertical stratification (in the frame of two-step model) from the analysis of He I 4026A line for various rotational phases (in phases 0.928, 0.023, 0.116, 0.195, 0.314 helium abundance is close to its maximum, while in phases 0.393, 0.410, 0.470, 0.543, 0.682 helium abundance is close to its minimum).

Castelli (http://wwwuser.oat.ts.astro.it/castelli/) are employed to simulate the spectra. Average abundance of chemical species (assuming no vertical stratification) is determined with the help of SYNTHV code (no magnetic splitting) and SYNTHM code (Version-04, that takes into account magnetic splitting of lines). Stratification of elements is determined from the best fit of calculated by SYNTHM (Version-05) line profiles (wings and cores) to observed ones. Previously, we have determined the contribution function for each line using the code WITA (Pavlenko, 1997).

HELIUM: The helium lines are weakened in the spectra of HD 21699. Osmer and Peterson (1974) and Vauclair (1975) have shown that formation of He-weak or He-rich stars depends on the wind power in their atmospheres. If we define that VW is a velocity of flux relative to wind and VD is the velocity of diffusion inside a star, then He-weak stars are formed when VD > VW. It is clear from Fig. 1 that on the whole surface of HD 21699 helium appears to be deficit. Nevertheless, in the area of "magnetic spot" the helium abundance is comparatively higher, than that derived for the opposite side.

For those parts of stellar surface, where magnetic lines are horizontal, only He I (not He II) vertical diffusion can be efficient. There the abundance of helium must be higher than on the magnetic poles, where the field lines are vertical, because there is no resistance to the diffusion of He I and He II atoms. The fact that intensity of He I lines on the magnetic poles is higher than on the opposite side supports the idea of a sufficiently strong wind on the magnetic poles. The observed data justify presence of a powerful wind from the "magnetic spot" of HD 21699 (magnetically structured jets, Brown et al. 1985).

We have assumed the two-step approximation for vertical stratification of chemical species in the atmosphere of HD 21699 (see, for example, Ryabchikova et al., 2005). In Fig. 2 we show vertical stratification of helium for 10 phases, derived from analysis of He I 4026 A line profiles (for the lower layers the abundance is derived from line wings, while for the upper layers it is derived from line cores).

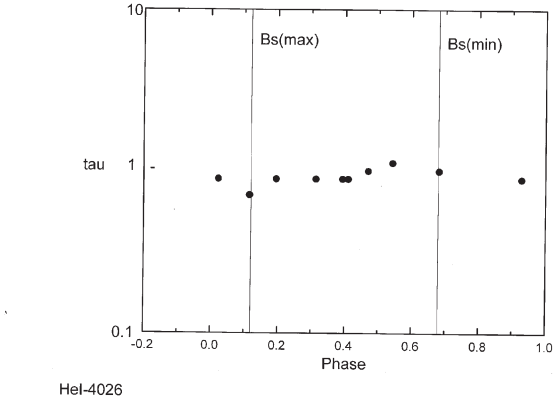

Figure 3: Optical depth τ_{5000} of the abundance jump versus rotational phase for the line He I 4026 A.

The results shown at Fig. 2 confirm theoretical prediction of Vauclair et al. (1991) about enhancement of helium abundance towards the deeper optical depth. We can see in Fig. 3 that optical depth τ_{5000} of the abundance jump does not vary with the rotational

Table 1: Variation of Si II mean abundance with rotational phase (MuSiCoS and NES spectra)

line (A)	E"	log N(Si)/N(H)			
	phase	0.118	0.322	0.525	0.687
6347	8.12	-5.12	-4.92	-4.02	-
6371	8.12	-5.12	-4.92	-4.12	-
5041	10.07	-4.87	-4.67	-4.02	-4.25
5055	10.07	-5.15	-4.99	-4.55	-4.50
4673	12.84	-3.87	-3.82	-3.52	-3.70
5669	14.21	-4.15	-4.05	-3.55	-3.75
5202	16.35	-3.75	-3.80	-3.20	-3.70

phase.

SILICON: In Table 2 we show estimates of silicon abundance derived from MuSiCoS and NES spectra for seven Si II lines with various excitation energies (in the range of 8-16 eV) of the lower transition level for 4 rotation phases. It is easy to track an apparent increase of the derived silicon abundance with the rise of excitation energy (i.e. towards the deeper atmosphere). This tendency supports the idea of vertical stratification of silicon abundance, which was announced by Vauclair et al. (1979).

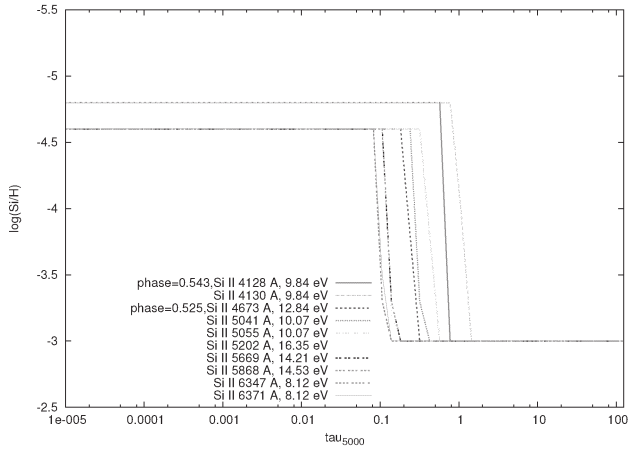

Figure 4: Vertical stratification of silicon for the phase 0.525, where Bs reaches its minimum and Si II abundance rise to its maximum.

Table 2 shows combination of the aforementioned data with the silicon abundances derived from Si II lines 4128 A and 4130 A for ten rotational phases using the MSS spectra. Taking into account the level -4.49 dex of solar abundance for silicon (Grevesse et al 2007), it appears that the lines with low excitation energies show abundance deficit, while the lines with high excitation energy show excess of silicon for phases with maximal Bs (0.118 and 0.322). It is remarkable that the abundance estimates derived from analysis of the lines with low excitation energies are in good agreement between themselves for all available spectra (MuSiCoS, NES and MSS). For the phases with minimal Bs (0.525 and 0.687) all the lines show an excess of silicon. Nevertheless, the lines with higher excitation energies still result in higher abundance.

Table 2: Variation of mean silicon abundance log N(Si)/N(H) (without stratification) with rotational phase (including MSS spectra): * 8-10 eV - lines 6347, 6371, 5041, 5055 A are taken from MuSiCoS spectra lines 5041, 5055 A - from NES SAO spectra; ** 12-16eV - lines 4673, 5202 and 5669 A are taken from NES spectrum (phase 0.682).

Phase	mean 4128, 4130A	mean eshelle (MuSiCoS & NES)		
		9.837 eV	8-10eV*	12-16eV**
0.023	-4.90			
0.116	-4.95	0.118	-5.06	-3.92
0.195	-5.15			
0.314	-4.80	0.322	-4.88	-3.87
0.393	-4.50			
0.410	-4.35			
0.470	-4.35			
0.543	-4.35	0.525	-4.16	-3.42
0.682	-4.15	0.687	-4.37	-3.72
0.928	-4.70			

Fig. 4 shows enhancement of silicon abundance towards the deeper atmospheric layers, as it was predicted by Vauclair et al. (1979). In the Fig. 5 we can see dependence of optical depth τ_{5000} at the Si II abundance jump from rotational phase. The case of non-uniform silicon distribution on the surface of magnetic stars is discussed in the works of Vauclair et al. (1979), Alecian and Vauclair (1981) and Megessier (1984). Silicon is usually accumulated in the places where magnetic field lines are predominantly horizontal and they oppose the gravitational settling of ionized silicon. In the case of a shifted magnetic dipole, as for HD 21699, the side opposite to the magnetic poles has a large area with horizontal magnetic field lines, where silicon should be concentrated. Meanwhile, it has to be weakened around the magnetic poles.

From the Tabl. 1, 2 and Fig. 4 it appears that our results confirm the predictions of Vauclair et al. (1979), Alecian and Vauclair (1981) and Megessier (1984). In the atmosphere of HD 21699 silicon is enhanced in the area where the field lines are horizontal to stellar surface. The optical depth of abundance' jump for silicon (as for helium) is approximately the same for the all rotational phases ($\tau_{5000} = 1$, see Fig. 5).

Abundance stratification due to diffusion processes acting in the atmospheres of chemically peculiar stars is studied in the recent work of Monin & LeBlanc

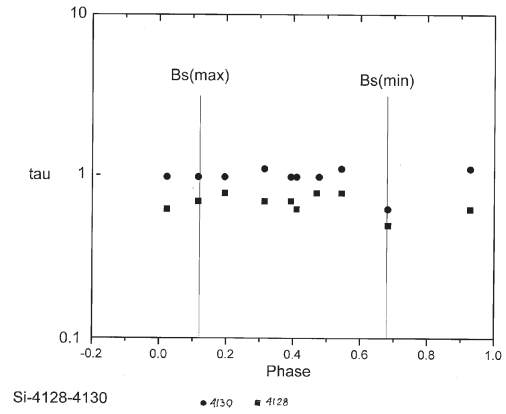

Figure 5: Optical depth τ_{5000} of the abundance jump versus rotational phase for the Si II lines 4128 A and 4130 A.

(2007). Their self-consisting models show that elements such as Fe, Cr, Si and Ca indeed accumulate at large optical depths, while they are dramatically underabundant in the upper atmosphere. The transition zone for iron in their models is located around optical depth $\tau_{5000} = 1$.

7. Basic conclusions

– For the first time the chemical element abundances in the atmosphere of HD 21699 are obtained during the whole rotational period, not only for a one phase.

– Silicon is accumulated in the part of star, where the magnetic field lines are predominantly horizontal, as it was predicted by Vauclair et al. 1979, Alecian & Vouclair 1981 and Meggessier 1984.

– Silicon abundance determined from lines with low excitation energies (8-10eV) appears to be lower in the area of magnetic poles and is approximately solar in the region with horizontal magnetic lines. The lines with high excitation energies (12-16eV) also show enhancement of silicon abundance for the region with horizontal magnetic lines, but this abundance is everywhere significantly higher than the solar one.

– Silicon abundance is lower in the outer parts of the atmosphere and higher in the deeper layers.

– Helium abundance is weakened on the whole stellar surface, which is usual for He-weak stars. Nevertheless, helium has higher abundance in the region of "magnetic spot" due to the influence of stellar wind, which elevates it to the outer layers of stellar atmosphere (Vauclair et al. 1991).

– The optical depth of abundance' jump (in two-steps model) is approximately $\tau_{5000} = 1$.

– The optical depth of abundance' jump for He and Si does not change during the period of stellar rotational.

– Our results support theoretical prediction of Vauclair et al. (1991) that helium abundance should increase with optical depth in the atmospheres of He-weak stars.

Aknowledgements. We appreciate V. Tsymbal and S. Khan for their codes SYNTHV and SYNTHM. This work was partially supported by the Microcosmophysics program of National Academy of Sciences and National Space Agency of Ukraine.

References

Alecian G., Vauclair S.: 1981, *Astron. Astrophys.*, **101**, 16.

Briquet M., Hubrig S., De Cat P., Aerts C., North P., Scholler M.: 2007, *Astron. Astrophys.*, **466**, 269.

Brown D.N., Shore S.N., Sonneborn G.: 1985, *Astrophys. J.*, **90**, 1354.

Castelli F.: http://wwwuser.oat.ts.astro.it/castelli/

Glagolevskij Yu.V., Leushin V.V., Chuntonov G.A., Shulyak D.: 2006, *Astron. Lett.*, **32**, 54.

Glagolevskij Yu.V., Chuntonov G.A.: 2007, *Astrophysics*, **50**, 362.

Grevesse N., Asplund M., Sauval A.: 2007, *Sp. Sci. Rev.*, **130**, Issue 1-4, 105.

Donati J.-F., Semel M., Carter B.D., Rees D.E., Cameron A.C.: 1997, *MNRAS*, **291**, 658.

Khan S.: 2004, *J. Quant. Spectrosc. Radiat. Transfer.*, **88**, 71.

Kurucz R.L.: Data Bank - CD-ROM NN 1-22 (1993-1994).

Kupka F., Piskunov N., Ryabchikova T.A. et al.: 1999, *A&AS*, **138**, 119.

Megessier C.: 1984, *Astron. Astrophys.*, **138**, 267.

Molnar M.R., Stephens T.C., Mollama A.D.: 1978, *ApJ*, **223**, 185.

Monin D., Leblanc F.: 2007, in *Phis. Magnetic Stars*, /Eds. I.I.Romanyuk, D.O.Kudryavtsev, SAO RAN, 360.

Osmer P.S., Peterson D.M.: 1973, *ApJ*, **187**, 117.

Panchuk V., Piskunov N., Klochkova V., Yushkin V., Ermakov S.: 2002, *Prep. SAO*, **169**.

Pavlenko Ya.V.: 1997, *Ap&SS*, **253**, 43.

Tsymbal V.: 1996, in: *Mod. Atmosph. Spectr. Synt.*, /eds. S.J.Adelman, F.Kupka, W.W.Weiss, ASP Conf. Ser., **108**, 198.

Percy J.R.: 1985, *PASP*, **97**, 856.

Vauclair S.: 1975, *AA*, **45**, 233.

Vauclair S., Hardorp J., Pederson D.M.: 1979, *Astrophys. J.*, **227**, 526.

Vauclair S., Dolez N., Gough D.O.: 1991, *AA*, **252**, 618.

Shore S.N., Adelman S.J.: 1974, *ApJ*, **191**, 165.

Shore S.N., Brown D.N., Sonneborn G.: 1987, *Astron. J.*, **94**, 737.

SPECTROSCOPIC MONITORING OF NOVA VULPECULAE 2007 (V458 Vul)

T.N. Tarasova

Crimean Astrophysical Observatory
Nauchny, Crimea, 98908 Ukraine, *taya@crao.crimea.ua*

ABSTRACT. We present results of the spectroscopic monitoring of the peculiar nova V458 Vul during eleven months. At the early decline of the brightness the nova transformed from Fe II to the He/N type. The profiles of the HI and the HeI lines showed the variability connected with the rebrightening. At the final decline of the brightness the nova displays a fast variability (within a day) of the forbidden iron line profiles. The spectral features of V458 Vul allow classifying it as a hybrid "neon" nova.

From the AAVSO light curve we obtained some photometric parameters, the mass of 458 Vul and the distance to the object. The nova showed a fast decline of the brightness (t_2=7, t_3=18 days). It reached M_v= -9.0 mag at the maximum of the brightness. The distance to the nova is in the range d=10.1-12.8 kpc. The reddening E(B-V)=0.59 towards the star is derived using the colour index of the nova at the maximum and the Balmer decrements. The white dwarf mass was derived about 1.1–1.2 $M_\odot$

Key words: Stars: binary: novae; stars: individual: V458 Vul.

1. Introduction

Nova Vulpeculae 2007 was discovered by Hiroshi Abe on 2007 August 8.54 UT (Nakano, 2007). A progenitor B=18.2 was found by Henden & Munari (2007). The nova was named V458 Vul (Samus, 2007). After the rapid decline during a day more then by one magnitudes, the nova underwent two abrupt increasing of brightness about 1.5 mag. The spectra acquired near the maximum showed the Balmer and the FeII (multiplet 42) lines in a emission with the P Cyg profile and the HeI lines in the absorption. The nova was classified as FeII type (Williams, 1991; Williams, 1992). After the rapid decline of the brightness the nova spectrum changed towards the He/N type. Therefore it was classified by us as a hybrid nova (Tarasova, 2007).

In the time of the principal and the second maxima the Balmer, the FeII and the HeI lines had the P Cyg type profiles. Just after the decline of the brightness the intensity and the profiles of the Balmer and the HeI lines changed: the HeI profiles became a saddle shape and the Balmer lines were seen as a complex P Cyg profile. After the rebrightening the profiles of the HI and the He I lines demonstrated an almost flat topped form. The early spectral evolution of V458 Vul was described by Tarasova (2007) and Poggiani (2008). In this work we analysed the subsequent spectral evolution of the V458 Vul and also derived the distance to the nova, the reddening and the Balmer decrement.

2. Spectral evolution

2.1. Observations

The spectral observation was carried out at the Crimean Astrophysical Observatory with the 2.6m Shajn telescope. The low resolution spectra with the dispersion of 2 Å/pix, were observed in the wavelength ranges 3700-6190 Å and 5600-7600 Å. The medium resolution spectrum, obtained on Aug 17^{th}, had the dispersion of 0.75 Å/pix and covers the spectral range 4200-5300 Å. In Fig.1 we presented all our spectral observation.

2.2. Early decline phase: 9^{th}–25^{th} day after the outburst

17.8, 18.8 Aug 2007 (t=+9, 10). The broad emission HI, FeII (27, 28, 37, 38, 42, 49, 74 multiplets) lines and the HeI 5876, 6678, 7065 lines dominate in the nova spectrum . The expansion velocity (FWHM) is about 2700 km s^{-1} for the HI and about 3100 km s^{-1} for the HeI lines.

21.8 Aug 2007 (t=+13). The spectra have been obtained after second rebrightening. Spectra show that V458 Vul evolved towards the He/N class. The N III 4640 and the He II 4686 lines form the broad blend centered at 4670 Å. The line profiles differ noticeably from the previous observation. The HI, FeII lines have a complex P Cyg type profile, while the HeI line profiles have an asymmetric saddle shaped form. The flux of the Balmer lines sharply decreased, while the

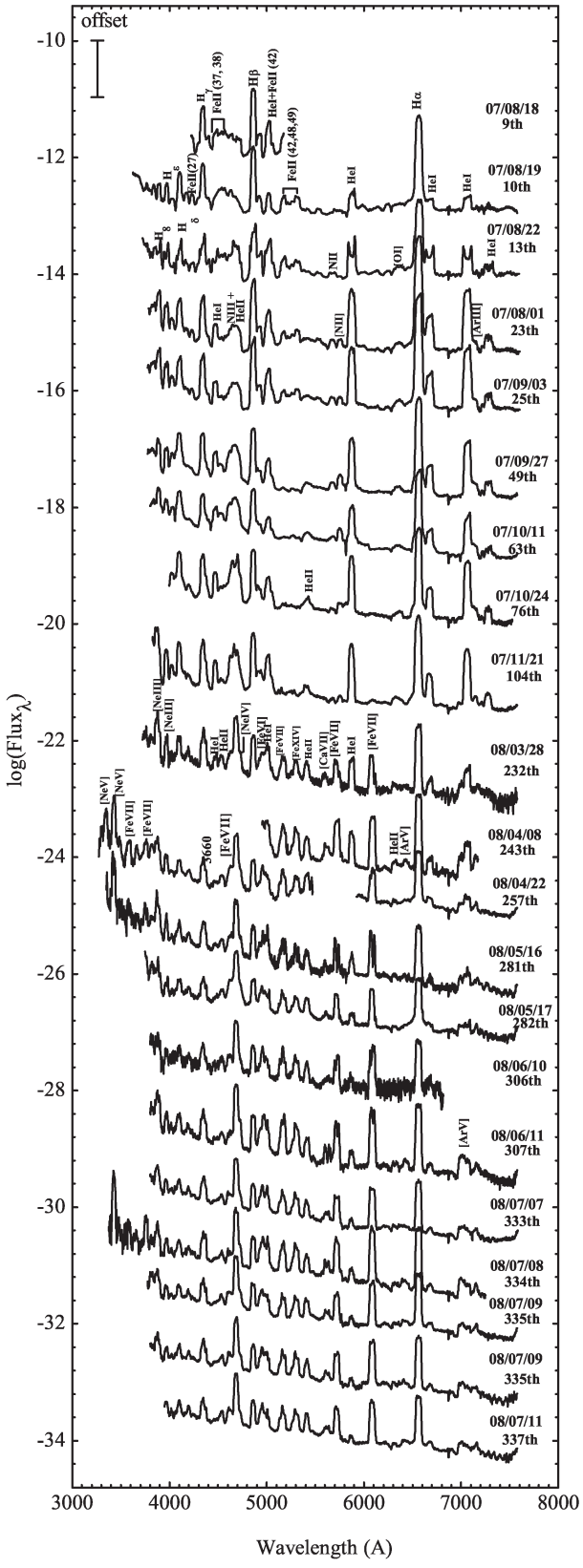

Figure 1: Dereddened spectra of V458 Vul. Fluxes are given in logarithmic scale to show the less intence lines. The spectra are separated vertically by the constant offset.

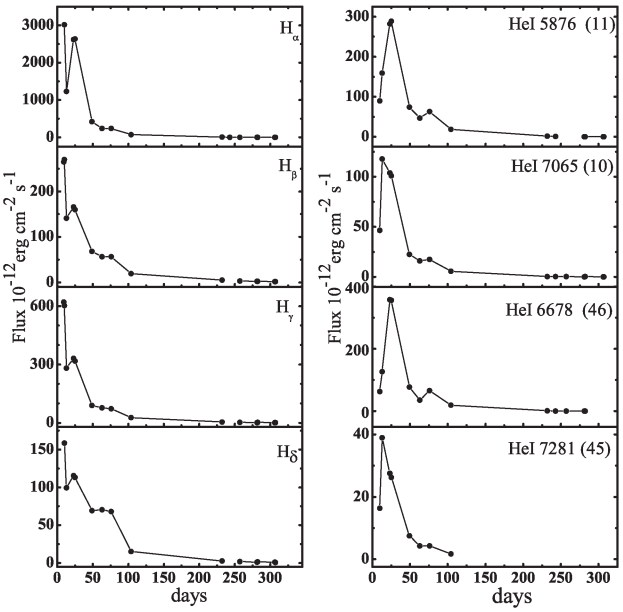

Figure 2: The variability of the HI and HeI line fluxes.

flux of the HeI lines either continues to increase (HeI 5876 (11 multiplet), 7065 (10 multiplet)) or reaches the maximum (HeI 6678 (46 multiplet), 7281 (45 multiplet)) (Fig.2). The noticeable increasing of the velocity of the HI and the HeI lines occurs after the re-brightening. The distance between emission peak of the HI lines is about 3300 km s^{-1}, of the HeI lines is about 3500 km s^{-1}. The line profiles exhibit the complex structure indicating at the asymmetric outburst. The profiles of the various potential ionization lines are diverse.

31.8 Aug, 2.8 Sept 2007 (t=+23, 25). The FeII lines faded, while the HI and the HeI lines intensified. The HeI lines (with exception for the H$_\alpha$ lines) dominate in the nova spectrum. The width (FWHM) of the HI, HeI lines diminished and became about 2700 km s^{-1}, 3000 km s^{-1} respectively.

2.3. Transition phase: 49^{th}–104^{th} day after the outburst

27.4 Sept, 10.8, 23.7 Oct 2007, 20.6 Nov (t=+49, +63, +76, +104). The reduction of the flux in the HI and the HeI lines by one order of a value is observed. The FeII lines disappeared, but the HeII lines became stronger. The width (FWHM) of the HI lines was not changed, but the HeI lines decreased by one third. The HI and HeI lines have the weak P Cyg components on the 49^{th} day and on the 63^{th} day after outburst. They disappeared on the 76^{th} day. The brightness on the light curve oscillated at this time and besides the nova was detected as a supersoft X-ray source (SSS) by Swift XRT on Oktober 17 (Drake, 2008). On of the explanation of that is a outflow of the matter from

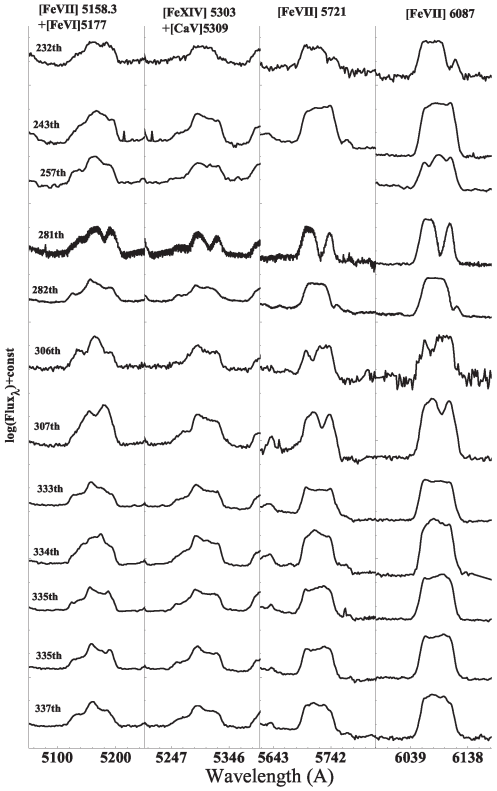

Figure 3: The profile variability of the [FeVII] 5159, 5721, 6086 and [FeXIV] 5303 lines

a surface of the white dwarf. It is provided by the continued thermonuclear reactions on a white dwarf surface.

2.4. Nebular phase: 232th–337th day after the outburst

28.1 Mar, 8.1, 22.0 Apr, 16.0, 17.0 May, 11.0 Jun, 7.0, 7.9, 8.8, 10.9 Jul (t=+232, 243, 257, 282, 307, 333, 334, 335, 337). The spectrum is rich with the [FeVII] (3586, 3759, 5159, 5721, 6086) lines and the HeII (4542, 4686, 5412, 6311) lines. There are [FeXIV] 5303, [CaVII] 5619, [ArV] 6435 and 7006, [NeIII] 3869, 3968, [NeV] 3426, 3346 lines. The [NeV] 3346, 3426 lines stand out against the other lines in the spectra. The strength of these lines qualifies V458 Vul as a "neon" nova. The profiles of the high ionization forbidden iron lines demonstrate a fast variability. The noticeable changes occur within a day (see Fig. 3).

3. Light curve

The light curve has been constructed using the observation of the AAVSO group (Henden, 2007) and the observation published in the IAU Circulars. The light curve of V458 Vul is shown in Fig.4. The striking features of the light curve of V458 Vul are the presence

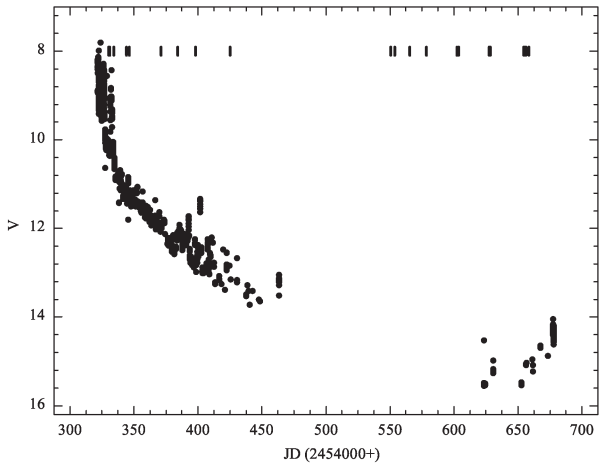

Figure 4: Light curve of V458 Vul based on the AAVSO data. The vertical bars indicate the time of our spectral observations.

of two strong post maximum peaks with the amplitude of about 1.5 mag. The duration of the first and the second peaks is about 3 and 4 days, respectively, and the time between them is about 3 days. The oscillations of a brightness are also seen during the transition phase. The light curve indicates that the maximum V_{max}=8.14 was reached on JD_{max}=2454321.9. A smooth fit of the light curve gives the following: i) the magnitude on the 15th day after the maximum is V_{15}=10.87; ii) the time of the decline through 2 mag is t_2=7 days; iii) the time of the decline through 3 mag is t_3=18 days. Thus V458 Vul is a fast nova according to Payne-Gaposchkin classification (Payne-Gaposchkin, 1957).

The absolute magnitude of the nova at the maximum was estimated using the various $M_{V,max}$, t_n (n=2,3) - relations (Schmidt 1957; de Vaucouleurs 1978; Cohen 1988; DellaValle 1985; Downes & Duerbeck 2000). The absolute magnitude ranges from M_v=–8.8 to M_v=–9.2.

4. Reddening, distance and mass

The reddening towards the nova is calculated using the colour index of a nova at the maximum and 2 mag below the maximum (Van Den Berg & Younger 1987). We defined $(B\text{-}V)_{max}$=0.76 and $(B\text{-}V)_{t_2}$=0.65 from the photometric data of AAVSO group (Henden, 2007). This leads to E(B-V)=0.53 mag and E(B-V)=0.65 mag, respectively.

The reddening was derived also using the flux of the H_α/H_β ratio (Fig.5). During our observations the H_α/H_β ratio varied between 3.3 and 15. The theoretical H_α/H_β ratio was found to be in the range of 2.8-3.0. To calculate the reddening we took the Balmer decrement close to the theoretical. The color excess E(B-V) calculated from the H_α/H_β ratio is 0.42. The average

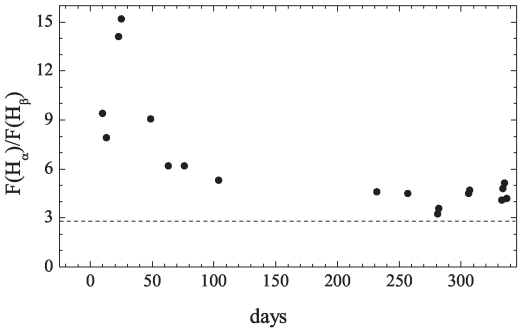

Figure 5: H_α/H_β ratio versus time after maximum (in days)

reddening E(B-V) was found to be 0.59.

The mass of a white dwarf M_{wd} in a nova is given by Livio(1992):

$$M_B^{max} \sim M_V^{max} = -8.3 - 10 \lg \frac{M_{wd}}{M_\odot} \qquad (1)$$

The white dwarf mass is about 1.1-1.2 $M_\odot$. Using the relation:

$$m_v - M_v = 5 \lg d - 5 + A_v \qquad (2)$$

and the absolute magnitude on the 15^{th} day after the initial maximum (Buscombe & de Vaucouleurs 1955; Cohen 1985a; van den Berg & Younger 1987; Capaccioli et al. 1989; Downes & Duerbeck 2000) we estimated the distance to a nova in the range d=10.1–12.8 kpc.

5. Conclusions

The spectral evolution of the V458 Vul allows to classified it as a hybrid "neon" nova according to Williams classification. The general picture of the spectrum evolution is similar to that of V2214 Oph (Nova 1988) (Williams, 1991). But in contrast to Nova Oph 1988 the spectra of V458 Vul exhibit a dramatic change in the early decline phase of the brightness connected with the rebrightening and a fast variability of the forbidden lines on the final decline.

We calculated the fluxes and the widths (FWHM) of the HI and HeI lines and showed that in the time of the rebrightening change not only the profile but also the flux and the width of this lines. At the same time the flux of the HeI lines increased and the HI lines diminished. The width (FWHM) of the HI and the HeI lines rised in the time of the rebrightening and then declined at the following phases.

We revealed the fast variability (within days) of the forbidden iron profiles of the high ionization potential lines during the nebular stage. We believe, that the cause of this variability can be a variable flux of a radiation triggered by the continued thermonuclear reactions on a surface of the white dwarf. Indeed the nova was detected as a supersoft X-ray source (SSS) by Swift XRT in this time (Drake, 2008).

Using the light curve of the V458 Vul we get the parameters t_2=7 d and t_3=18 d and conclude that it is a fast nova according to Payne-Gaposchkin (1957) classification. We estimated the absolute magnitude at the maximum with the various MMRD relations. We believe that the values of M_v range from -8.8 to -9.2. The reddening E(B-V)=0.59 is derived using the colour index of a nova at the maximum and 2 mag below the maximum and the H_α/H_β ratio. The nova distance is in the range d=10.1-12.8 kpc. The white dwarf mass is about 1.1-1.2 $M_\odot$.

Acknowledgements. This work was partially supported by the Ukrainian Fund of Fundamental Research F25/238-2008. I acknowledge with thanks the variable star observations from the AAVSO International Database contributed by observers worldwide and used in this research.

References

van den Berg S., Younger P.F.: 1987, *Astron. Astrophys. Supl. Ser.*, **70**, 125.
Buscombe W., de Vaucouleurs G.: 1955, *Obs*, **75**, 170.
Capaccioli M., et al.: 1989, *Astrophys. J.*, **97**, 1622.
Cohen J.G.: 1985, *Astron. J.*, **292**, 90.
Cohen J.G.: 1988, *ASP Conf. Ser.*, **4**, 114.
Della Valle M., Livio M.: 1995, *Astrophys. J.*, **452**, 704.
Drake J.J. et. al: 2007, *ATel* 1246.
Drake J.J. et. al: 2008, *ATel* 1603.
Downes R.A., Duerbeck H.W.: 2000, *Astron. J.*, **120**, 2007.
Henden A.A.: 2007, Observations from the AAVSO, priv. comm.
Henden A., Munari U.: 2007, *Inform.Bul.Var.Stars*, 5803.
Livio M.: 1992, *Astrophys. J.*, **393**, 516.
Nakano S.: 2007, *CBET*, 1027.
Payne-Gaposchkin C.: 1957, *Science*, **126**, 1350.
Poggiani R.: 2008, *Astrophys. Space Since*, **4**, 77.
Samus N.N.: 2007, *IAUS*, 8863.
Schmidt T.Z.: 1957, *Z. Astrophys*, **41**, 182.
Tarasova T.N.: 2007, *Inform. Bul. Var. Stars*, 5807.
de Vaucouleurs G.: 1978, *Astron. J.*, **223**, 351.
Williams R.E., Hamuy M., Phillips M.M. et al.: 1991, *Astrophys. J.*, **376**, 721.
Williams R.E.: 1992 *Astron. J.*, **104**, 725.

QUASISYNTHETIC PHOTOMETRY

Tsymbal V.[1,2]

[1] Tavrian National University
Vernadskiy's Avenue 4, Simferopol, Crimea, 95007, Ukraine, *vadim@starsp.org*
[2] Institut für Astronomie
Universität Wien, Türkenschanzstrasse 17, 1180 Wien, Austria

ABSTRACT. The brief description of new ideas for the flux calibration of stellar spectra are presented. Described approach lets us to produce a lot of reference stars both for ground and space observations. The metodology also opens possibilities to determine the angular diameters from high resolution stellar spectra and analyze the interstellar medium in the direction of a star.

Key words: Stars: absolute spectrophotometry: angular diameters; stars: individual: Vega, Procyon.

1. Introduction

One of the problems in stellar observational astrophysics is the calibration of observed quantities into physical energy units. The usual approach to make this is to choose the set of the reference stars, calibrate their magnitudes or spectra and use these quantities for calibration of other observed stars. The main problem here is a calibration of reference stars. For the first time this was done using Vega as a primary reference star for ground-based observations while observing the secondary reference stars. But such way is impossible in preparation of the set of reference stars for GAIA project, for instance, because the satellite cannot observe stars brighter than magnitude 10. To calibrate the observed stellear spectra from the ground with high resolution we need to have the flux spectra with same one. The basic idea of the proposal is not totally new. Similar approach is being used in so-called Synthetic Photometry (see, for example, Colina et.al., 1996). In this approach one can use the synthetic spectra for given stellar atmosphere model with calibrational purposes. But in this case we have a lot of problems with accuracy of this data: atmosphere models differ from the real stellar atmospheres, the spectral lines data are incomplete and not accurate either etc.

In this article I propose a simple way to eliminate all those problems: 1) we use the high dispersion, continuum normalized spectra of reference stars; 2) in a usual way we determine for these spectra T_{eff}, log g and [A]; 3) using stellar atmosphere model we calculate the continuum flux spectrum; 4) multiplying a theoretical flux spectrum by the observed normalized one we receive the energy flux spectrum coming from the stellar surface; 5) using this spectrum we calculate the photometric colors, compare them with so-named zero-point observed colors and receive the stellar angular diameter. Comparison of the angular diameters at different colors can help us to estimate the effect of reddening and find the dependence of the radius on wavelengths (for cool giants); 6) having the angular diameters we can tie (move) energy flux spectrum to the orbit of Earth. This proposal based on that we know: 1) the depth of stellar continuum formation differs negligibly for different atmosphere models; 2) in visible spectral region continuum fluxes depend practically only on effective temperature; 3) in visible region the theoretical description of stellar continuum (opacity sources) is well-studied; 4) all this cannot be said about usual Synthetic Photometry.

2. Approach testing

Recently I have tried to perform this procedure for two stars: Vega (HD 172167) and Procyon (HD 61421).

2.1. Vega

For the basic observations I used normilized high resolution Vega atlas (Takeda et.al., 2007). This spectrum was multipled by the theoretical continuum of a synthetic spectrum, computed using Kurucz's model atmosphere for Vega (*http* : *//kurucz.harvard.edu/*). After this I have calculated the B color from surface flux spectrum that comes from the Vega and compared it to the observed B magnitude, using zero-point from (Colina et.al., 1996). In this way I received the angular diameter of Vega $\theta = 3.24$ mas, what number is close to the observed value $\theta = 3.202$ mas (Absil et.al., 2008). Using calculated value, I reduced quasi-synthetic spectrum to the orbit of Earth and compared with Vega energy flux spectrum, compiled by Hayes (Hayes, 1985).

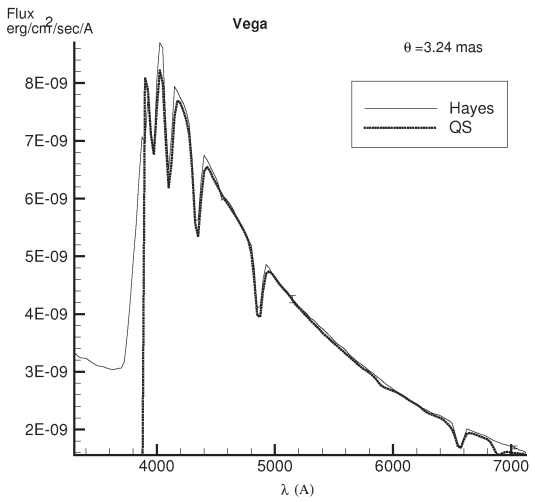

Figure 1: Quasi-synthetic spectrum of Vega, compared with flux spectrum from (Hayes, 1985).

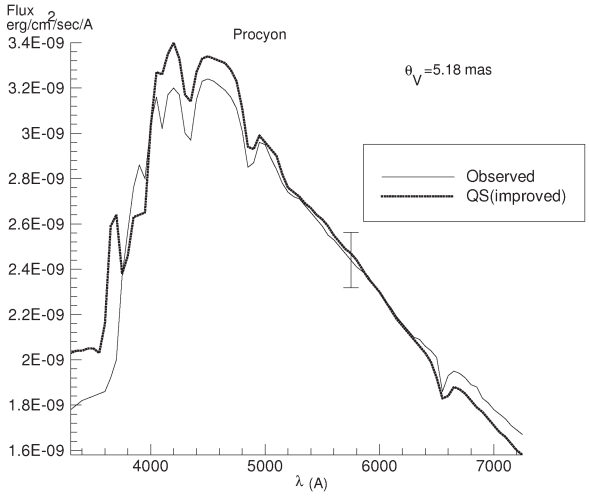

Figure 2: Quasisynthetic spectrum of Procyon, compared with flux spectrum from (Komarov et.al., 1979).

For comparision purposes Vega's quasi-synthetic spectrum was convolved with Gaussian of resolution R = 110. The result is shown on Fig.1.

As we can see, agreement of both flux spectra is perfect, excluding the cores of Hydrogen lines. This is caused by the rough description with the instrumental profile. The small features in the red part of QS spectrum are blends of telluric lines in Vega atlas.

2.2. Procyon

For this star I took the famous Procyon atlas of Griffin (Griffin, 1979), did all what is described above and compared obtained highly dispersed flux energy spectrum of Procyon, convolved with the Gaussian instrumental profile (R=52) with observed flux spectrum from (Komarov et.al., 1979) catalogue. Results are presented on Fig.2 below. The error bar indicates the authors estimated accuracy of observed flux spectrum in region V (5%). This estimated accuracy is degrading (up to 10%) towards the end of the spectrum. The same will happen if one tries to compare the data from different catalogues. There is one distinction in procedure: comparision of Griffin atlas with synthetic spectrum of Procyon shows that continuum normalization of atlas in Hydrogen lines regions, especially in a region of the Balmer jump, was done badly. More than, since the wavelength region of high resolved spectrum of atlas is wide, the telluric spectrum starts influecing strongly the results in a red part of the spectrum. I have roughly corrected the Procyon atlas both for continuum and telluric lines.

For this star the agreement between QS and observed flux spectra still inside error bars. The difference is caused by continuum normalization of atlas and telluric features, which was not removed completely. The angular diameter of Procyon, found from comparision the QS and observed V magnitudes - $\theta = 5.18$ mas is close to the values from interferometric measurements (see table in article Kervella et.al.,2003). For example, the angular diameter at wavelength 7400 Å is: $\theta = 5.19 \pm 0.04$ mas.

3. Discussion

The idea of proposed method is very simple and can be realized very easy. But possible results look very promissing. Let me briefly describe the possible projects. 1) The catalogue of flux spectra for reference stars in visible region both for space and ground-based observations. Practically all stars for which we have high resolution spectra can be used. 2) The measurement of angular diameteres for all stars observed with high resolution. In combination with known parallaxes we can even determine the radii of these stars. 3) From comparison of the QS and observed colors at different wavelengths we can analyze the structure of interstellar medium. 4) The flux calibrated high dispersion spectra open new horizons in the field of stellar atmospheres analysis. For example, we can develop new approaches, based on the Vertical Inverse Problem (VIP) solutions. The reason is that we can directly use the formal solution of transfer equation instead of the LSQ technique that is being used now.

Acknowledgements. The author kindly acknowledges the support from the Austrian Fonds zur Forderung der wissenschaftlichen Forschung (FWF, project The Core of the HR diagram, P17580-N02) and Ukrainian Fundamental Research State Fund ($F25.2/074$).

References

Colina L., Bohlin R., Castelli F.: 1996, *Instr. Sci. Rep., CAL/SCS* – 008.

Takeda Y., Kawanomoto S., Ohishi N.: 2007, *Publ. Astron. Soc. Japan,* **59**, 245.

Absil O., di Folco E., Merand A., et.al.: 2008, $arXiv : astro - ph/0604260v1$.

Hayes D.: 1985, *Calibration of Fundamental Stellar Quantities, Proc. of IAU Symposium No.111, /ed. D.S.Hayes, L.E.Pasinetti, A.G.Davis Phillip (Reidel, Dordrecht),* 225.

Griffin R.E., Griffin R.: 1979, *R. and R. Griffin, publishers, Cambridge, U.K.* .

Komarov N., Karamysh V., Dragunova A., et.al.: 1979, *Photometric and spectral catalogue of the bright stars: Kyiv, Naukova dumka.*

Kervella P., Thevenin F., Morel P. et.al: 2003, $arXiv : astro - ph/0309148v1$.

STELLAR INVESTIGATION IN THE OPEN CLUSTER OF POLARIS

I.A. Usenko[1], A.S. Miroshnichenko[2], V.G. Klochkova[3], V.E. Panchuk[3]

[1] Department of Astronomy, Odessa National University
T.G.Shevchenko Park, Odessa 65014 Ukraine, *igus@deneb1.odessa.ua*
[2] Ritter Observatory, University of Toledo
Toledo, OH 43606 USA, *asm0910@yahoo.com*
[3] Special Astrophysical Observatory, Russian Academy of Sciences
Nizhnij Arkhyz, Karachaevo-Cherkessia, 369167 Russia *valenta@sao.ru; panch@sao.ru*

ABSTRACT. We present the results of our analysis of high-resolution spectroscopic observations of Cepheid α UMi (Polaris A), and main-sequence type stars Polaris B, and HD 5914, an optical companion and a member of Polaris open cluster. The last ones are objects with high projected rotational velocities v $\sin i$ = 110 km s^{-1} and 100 km s^{-1}, respectively. The derived atmosphere parameters are: Polaris A: T_{eff}=6020 K; $\log g$=2.2; V_t=4.2 km s^{-1}; Polaris B: T_{eff}=6900 K; $\log g$=4.3; V_t=2.5 km s^{-1}; HD 5914: T_{eff}=8800 K; $\log g$=4.0; V_t=2.0 km s^{-1}. C, Na and Mg content in last two stars is close to solar, whereas for Polaris A these values are typical for Cepheid after the first dredge-up stage. The distances to Polaris B and HD 5914 are 109.5 and 108 pc, respectively. The *RV* pulsational amplitude of Polaris A increased to 7.5 km s^{-1} in 2003, decreased to 0.6 km s^{-1} in 2005 and increased anew to 2.5 s^{-1} in 2007.

Key words: Stars: abundances – Stars: distances - Stars: Cepheids – Stars: main-sequence stars – Stars: individual - α UMi (Polaris A), Polaris B, HD 5914

1. Introduction

S-Cepheid (DCEPS) α UMi named Polaris is an unique object for astrophysical research due to the following:

1. It is the nearest (d = 99 (Turner, 2005) – 132 pc (ESA, 1997)) yellow supergiant and Cepheid in the Galaxy.

2. Polaris is a well-known multiple system with three visual components (Polaris B (BD+88°9), C and D) that are main-sequence stars (Fernie, 1966), and the spectroscopic one (Polaris Ab) with an orbital period 29.71 yrs (Turner et al., 2006).

3. Polaris is a member of an anonymous open cluster, which contains late A-type and early F-type main sequence stars.

4. Polaris is one from four nearest Cepheid with the radius, 46±3 $R_\odot$, determined by means of optical interferometry (Nordgren et al., 1999).

5. CNO-abundances analysis data for Cepheid agree well with theoretically predicted ones for 3rd (or 5th) crossing of the Cepheids instability strip: [C/H]=-0.17 (predicted -0.18 dex), [N/H]=+0.42 (predicted +0.40 dex), [O/H]=-0.00 (predicted -0.02 dex) for evolutionary mass in ranges of 4.9 – 5.2 $M_\odot$ (Usenko et al, 2005).

Thus, the main task consist in:

1. To obtain the high-resolutioned spectra of Polaris ($F6 - F8I$), its the nearest visual companion Polaris B ($F3V$), and the brightest main-sequence member of Polaris cluster HR 5914 ($A3V$) to determine its atmospheric parameters, chemical composition (for the key evolutional elements), absolute magnitudes, masses and distances, respectively.

2. To measure the radial velocities of Polaris A during the lond observational period (1999-2007) to determine its pulsational amplitude changes.

2. Observations

Observations of these objects have been realized using:

1. 1m telescope – Ritter Observatory, University of Toledo (Toledo, OH, USA) – fiberfed echelle spectrograph ($\lambda\lambda$ 5800-6800 ÅÅ).

Table 1: Observational data of Polaris cluster's objects

Object	HJD	NS	T_{eff}	$\log g$	V_t
α UMi	2449513-9649 (1994)	6	5968±29	2.2	4.35
	2451240-2192 (1999)	4	5973±15	2.1	4.30
	2452416-2515 (2002)	9	6011±25	2.2	4.60
	2452782-2986 (2003)	11	6018±25	2.2	4.30
	2453005-3367 (2004)	10	6027±15	2.2	4.30
	2453686-3693 (2005)	6	6063±10	2.3	4.00
	2453751-4169 (2006)	7	6055±30	2.2	4.00
	2454169-4426 (2007)	4	6043±10	2.2	4.00
	Mean	57	6020±20	2.2	4.20
Polaris B		1	6900±50	4.3	2.50
HD 5914		1	8800±50	4.0	2.00

Table 2: Radial velocity data of α UMi during 2005-2007

HJD 2400000+	Number of orders	RV (km s^{-1})	σ	NL
53686.615	20	-17.68	1.05	198
53687.614	27	-17.82	1.00	616
53689.647	27	-18.24	1.20	589
53690.109	27	-17.80	1.13	566
53691.633	27	-17.82	1.06	550
53693.124	27	-17.93	1.06	549
53751.121	27	-16.83	1.21	581
53808.277	27	-18.78	1.55	933
53904.350	27	-17.87	1.09	506
53980.589	27	-17.40	1.29	569
54073.589	27	-18.43	1.15	579
54077.651	27	-17.58	1.21	406
54169.638	27	-19.18	1.09	415
54225.228	27	-18.92	1.25	592
54344.551	27	-19.41	1.04	464
54426.183	27	-16.65	1.19	603

2. 2.1m Otto Struve telescope – McDonald Observatory (Texas, USA) – SANDIFORD spectrograph ($\lambda\lambda$ 5500-7000 ÅÅ).
3. 6m telescope BTA – SAO RAS (Russia) – LYNX, PFES and NES spectrometers ($\lambda\lambda$ 5050-7100 ÅÅ).

The reduction was made using IRAF, MIDAS and DECH20 software (Galazutdinov, 1992). The observational log is given in Table 1. In Table 2 we present new radial velocity data of Polaris A, obtained during 2005-2007.

3. Atmosphere parameters and chemical composition

Atmosphere parametrs were determined:

1) Effective temperature T_{eff}: by line depth ratio (Kovtyukh & Gorlova, 2000) for Polaris (accuracy: 15–70 K); $(B-V)$-T_{eff}, $\log g$ and SYNTH for Polaris B and HD 5914 (accuracy: 50 K);

2) Surface gravity $\log g$: by adopting the same iron abundance for Fe I and Fe II lines. (accuracy: 0.15 dex) for Polaris; $(B-V)$-T_{eff}, $\log g$ and SYNTH for Polaris B (H_β); see Figure 1) and HD 5914 (H_α; see Figure 2)(accuracy: 0.15 dex);

3) Microturbulent velocity V_t: by assuming abundances of the Fe II lines independent of the W_λ for Polaris (accuracy: 0.25 km/s). For Polaris B and HD 5914 these V_t data were selected using SYNTH.

Table 3: Average abundances for Polaris cluster's objects

Elements	Polaris	Polaris B	HD 5914
[C/H]	-0.17±0.10	-0.00±0.05	-0.01
[N/H]	+0.42±0.00	+0.00	+0.00
[O/H]	-0.00±0.15	-0.00	-0.02±0.09
[Na/H]	+0.09±0.11	+0.03	-0.02
[Mg/H]	-0.21±0.12	+0.04±0.12	-
[Fe/H]	+0.07±0.10	+0.07±0.15	+0.05±0.15

The mean atmosphere parametrs are given in Table 1. It is necessary to note that Polaris B and HD 5914 are high-rotating objects with v $\sin i$ = 110 km s^{-1} and 100 km s^{-1}, respectively (see Figures 1 and 2).

As seen from Table 3, a comparison of chemical abundances (CNO-elements, sodium, magnesium and iron) for Cepheid, its visual companion and main-sequence star from open cluster reveals some interesting features. All three stars display essentially identical abundances of iron, whereas Polaris B and HD 5914 appears to have a solar carbon content. The same fact noticeable for sodium and manganise content for these stars. On the other hand Cepheid Polaris A exhibits an obvious deficit of carbon, overabundance of nitrogen, small overabundance of sodium and noticeable deficit of manganese. These features agrees well with theoretically predicted abundances for 5 $M_\odot$ star after 3rd or 5th crossing of the Cepheid instability strip (Usenko et al., 2005).

4. Colour-Excess and Reddening

Knowing the average T_{eff} and $(B-V)$ for the Cepheid and using the Gray's (1992) $(B-V)$ vs. T_{eff} relationship, we can calculate the intrinsic colour $(B-V)_0$, colour-excess E_{B-V}, and reddening A_V. For the mean T_{eff} = 6020 K we have E_{B-V} = 0.034 mag; A_V = 0.102 mag, R = 3.0 (Arellano Ferro, 1984) BC=0.01 mag (Bessell, Castelli & Plez, 1998).

5. Distances, Luminocities, Radii and Masses

The distance determination for Polaris system is problematical (Usenko et al. 2005), because the different methods give unequal estimates, from 99 pc (Turner, 2005) to 132 pc (ESA 1997; Norgren et al., 1999). Known that Polaris B is $F3V$ main-sequence star, then its radius is near 1.38 R_{odot} (Straižys, 1982). Using our mean T_{eff} value we can obtain its luminosity of 3.868 $L_\odot$, equivalent to an absolute magnitude M_V = +3.30 mag. Using our A_V = 0.102 mag we have obtained a distance d = 109.5 pc. This result coincide with Kamper's (1996) one of 110 pc, determined by astrometrical methods.

As known, for main-sequence stars $\log(L/L_\odot)$ =

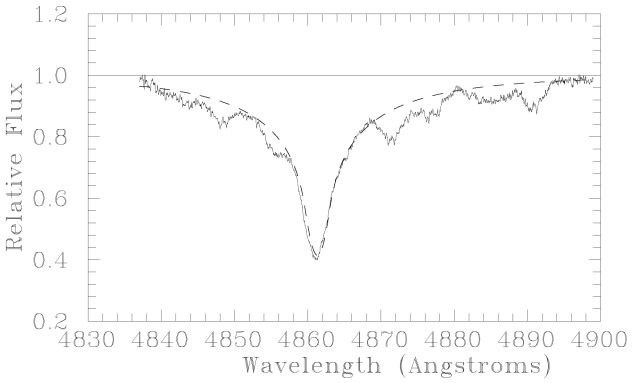

Figure 1: Fragment of Polaris B spectrum in the range 4930-4943 ÅÅwith synthetic spectrum (dashed line).

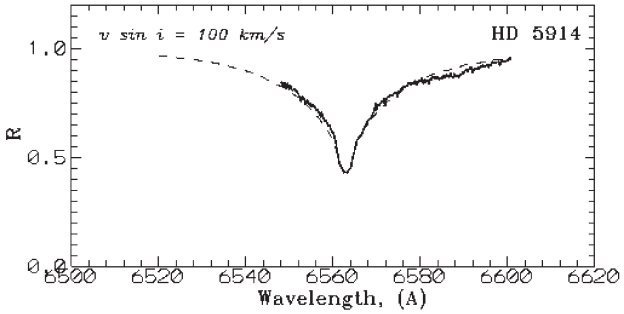

Figure 2: Fragment of HD 5914 spectrum in the range 6500-6620 ÅÅwith synthetic spectrum (dashed line).

4log($M/M_\odot$). Using our gravity and radius values for Polaris B, we can obtain its mass of 1.39 $M_\odot$, that agrees well with Polaris Ab $F4V$ type spectroscopic companion, – 1.38±0.61 $M_\odot$ (Evans et al., 2007).

In the case of HD 5914 we have obtained its radius of 2.14 $R_\odot$, M_V = +1.3 mag, d = 108 pc, and M = 1.66 $M_\odot$, respectively. Therefore, for Polaris A, in the case of distance d = 109.5 pc and T_{eff} = 6020 K, we have: M_V = -3.31 mag, log($L/L_\odot$) = 3.232, R = 38 $R_\odot$, and M = 5 $M_\odot$, respectively.

6. RV Pulsational Amplitude Changes

As seen from Figures 3-8 RV pulsational amplitude of Polaris during 2002-2007 undergoes the changes. It is interesting that it increased from 3 to 7.5 km s^{-1} during 2002-2003, after that we can see a decreasing from 2 to 0.6 km s^{-1} during 2004-2005, and new increasing to 2 km s^{-1} in 2006 and to 2.5 km s^{-1} in 2007.

7. Conclusions

We can summarize the results of our investigations as follows.

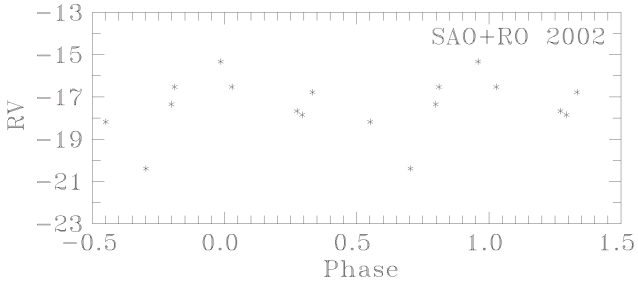

Figure 3: Radial velocity curve for Polaris A in 2002

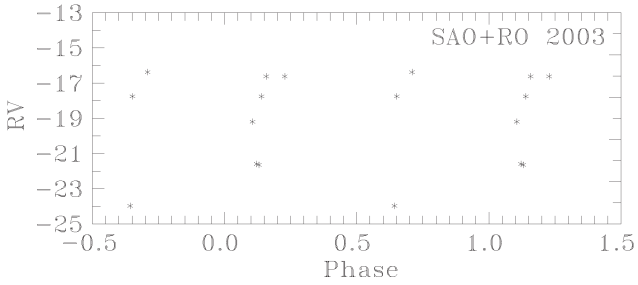

Figure 4: Radial velocity curve for Polaris A in 2003

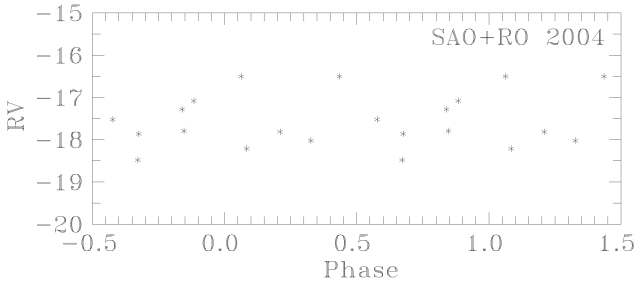

Figure 5: Radial velocity curve for Polaris A in 2004

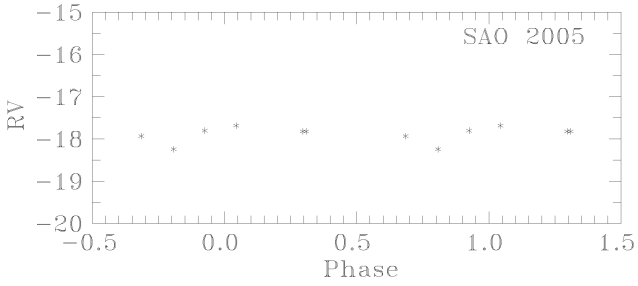

Figure 6: Radial velocity curve for Polaris A in 2005

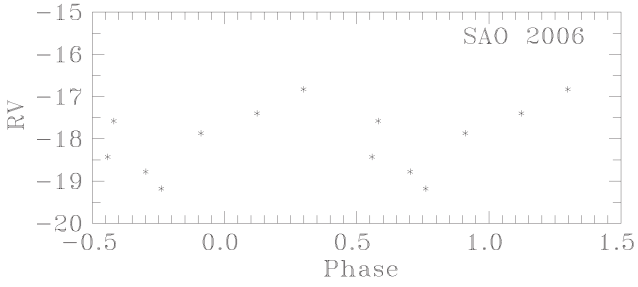

Figure 7: Radial velocity curve for Polaris A in 2006

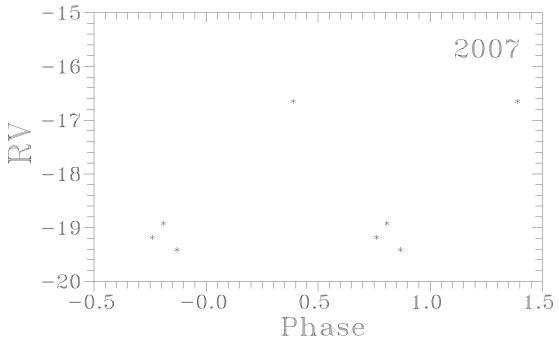

Figure 8: Radial velocity curve for Polaris A in 2007

1. A large projected rotational velocity v $\sin i$ = 110 km s^{-1} for Polaris B is an evidence that Polaris system is young and Polaris B is likely to be single, since most binaries of $A - F$ types have slow rotation, the angular momentum being tied up in orbital motion. Moreover, the rapid rotation's observation could be mean that we see the star nearly equator-on. Atmosphere parameters, obtaines for Polaris B are typical for $F3V$ star.

2. The same conclusions we can sum up for HD 5914 with its projected rotational velocity v $\sin i$ = 100 km s^{-1} and typical $A3V$ spectral type.

3. The majority of Polaris B and HD 5914 chemical elements shows abundances, equal to Polaris A and close to solar one. But carbon, sodium and magnesium in these stars close to solar content, therefore Polaris A demonstrates a typical for the first dredge-up yellow supergiants deficit of C and Mg and overabundance of N and Na (Usenko et al., 2005). Therefore we are eye-witnesses of evolutional history of three stars with different masses in the same stellar system.

4. Absolute magnitude +3.30 mag for Polaris B is equal to one from Fernie (1966). Spectroscopically determined T_{eff} = 6900 K combinating with radius of 1.38 $R_\odot$ give the distance near 109.5 pc, – a fine agreement with Kamper's (1996) one near 110 pc. This result is quite unexpected, because Turner (2005) denoted 101±3 pc to this object and Polaris system as a whole. Whereas HIPPARCOS parallax (ESA 1997) and optical interferometry (Nordgren et al., 1999) results give 132±9 pc to the Polaris A.

5. For HD 5914 we have the absolute magnitude +1.30 mag and for spectroscopically determined T_{eff} = 8800 K and radius of 2.14 $R_\odot$ the desired value of distance come to 108 pc. It is a real confirmation that this star is a member of Polaris open cluster.

6. The obtained mass of Polaris B near 1.39 $M_\odot$ has been founded as unexpected close to one of Polaris Ab spectroscopic companion, -1.38±0.61 $M_\odot$ (Evans et al., 2007), which is a main-sequence star of earlier than $F4V$ spectral type (Evans et al., 2002). The mass of HD 5914 near 1.66 $M_\odot$ is a typical for main-sequence early $A-$ type stars.

7. If the distance to Polaris A of 109.5 pc is true, then in case of mean T_{eff} = 6020 K its absolute magnitude is -3.31 mag, radius is near 38 $R_\odot$ and mass is equal to 5 $M_\odot$, respectively.

8. RV pulsational amplitude of Polaris A during last years undergoes sporadical changes minimized to 0.6 km s^{-1} in 2005 and culminated to 7.5 km s^{-1} (like before 1950) in 2003. In last year we can see its new increasing to 2.5 km s^{-1}.

References

Arellano Ferro A.: 1984, *MNRAS,* **209**, 481.
Bessel M.S., Castelli F., Pfelz B.: 1998, *A&A,* **333**, 231.
ESA 1997, *The Hipparcos and Tycho catalogues*, ESA-SP 1200.
Evans N.R., Sasselov D.D., Short C.I.: 2002, *ApJ,* **567**, 1121.
Evans N.R., Schaefer G., Bond H.E. et al.: 2007, *Proceed. IAU Symp.* **No.240** (in press).
Fernie J.D.: 1966, *AJ,* **71**, 731.
Galazutdinov G.A.: 1992, *Preprint SAO RAS*, **No.92**.
Gray D.: 1992, *Observation and Analysis of Stellar Atmospheres, (Cambrige Univ. Press, 2nd ed.)*
Kamper K.W.: 1996, *JRASC,* **90**, 140.
Kovtyukh V.V., Gorlova N.I.: 2000, *A&A* **358**, 587.
Nordgren T.E., Germain M.E., Benson J.A. et al.: 1999, *AJ*, **118**, 3032.
Straizys V.: 1982, *"Metal-Deficient Stars", Vilnius, "Mosklas"*, 300.
Turner D.G.: 2005, *OAP*, **18**, 115.
Turner D.G., Usenko I.A., Miroshnichenko A.S., Klochkova V.G., Panchuk V.E.: 2006, *AAS*, **208**, 4401.
Usenko I.A., Miroshnichemnko A.S., Klochkova V.G., Yushkin, M.V.: 2005, *MNRAS,* **362**, 1219.

NEW ASPECT OF SMALL-AMPLITUDE CEPHEID SU CAS

I.A. Usenko[1], V.G. Klochkova[2], N.S. Tavolzhanskaya[2]

[1] Department of Astronomy, Odessa National University
T.G.Shevchenko Park, Odessa 65014 Ukraine, *igus@deneb1.odessa.ua*
[2] Special Astrophysical Observatory, Russian Academy of Sciences
Nizhnij Arkhyz, Karachaevo-Cherkessia, 369167 Russia *valenta@sao.ru; tavolga@sao.ru*

ABSTRACT. New 17 high-resolutional spectra of small-amplitude Cepheid SU Cas have been obtained to determine its atmosphere parameters (T_{eff}=6353 K; $\log g$=2.38; V_t=3.25 km s^{-1}) and to measure its radial velocities. The last ones were added to the total RV list (378 values) and using the frequency analysis we can specify the pulsational and orbital periods of this Cepheid. With the well-known main pulsational period of 1.9493 days, classified as fundamental tone, we can detect the presence of two equidistant periods at a distance of ±0.003 c/d from it, and the secondary (possible first overtone) one of 2.0405 day. Their ratio P_1/P_0 = 0.96 supposed about an existence of non-radial pulsations in the Cepheid's atmosphere. Changes of the mean colour-index, effective temperature and γ-velocity confirmed the presence of one or more companions with possible periods of 463.7 – 483.8, 1738.8 and 7490.3 days.

Key words: Stars: Pulsational periods – Stars: Orbital periods – Stars: Cepheids – Stars: individual – SU Cas

1. Introduction

S-Cepheid (DCEPS) SU Cas is an interest object for astrophysical research due to the following aspects:

1. It is one of the nearest (d = 258 pc (Turner & Evans, 1984) Cepheid in the Galaxy.
2. SU Cas is a member of Cas OB2 association (Racine, 1968).
3. CNO-abundances analysis data for Cepheid agree well with theoretically predicted ones for 3rd crossing of the Cepheids instability strip in case if it mass is close to 3.7 $M_\odot$ (Usenko et al., 2001).
4. SU Cas has a close companion $B9.5 - -A5V$ (Turner & Evans, 1984; Usenko, 1990; Evans, 1991) with possible orbital periods of 462.5, 928, 1375 and 1682 days, respectively (Szabados, 1991).

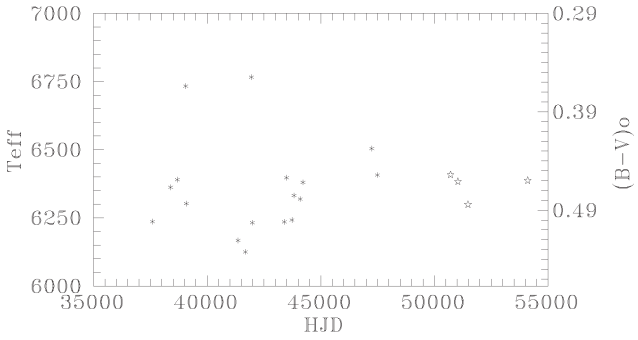

Figure 1: Variations of the mean effective temperature and colour-index during the last fourty years. Six-point stars, – the photometrical data from Mitchell et al. (1964), Wisniewski & Johnson (1968), Milone (1970), Sudzius (1969), Feltz & McNamara (1980), Szabados (1977), Niva & Schmidt (1979), Moffett & Barnes (1984); five-point stars, – the data obtained from spectroscopy (Usenko et al. 2001, Luck 2001, and this work).

Nevertheless there are some problems connected with unusual character of this Cepheid, namely:

1. Identification of its pulsational mode:
   a) Fundamental mode: R = 18.2 $R_\odot$; T_{eff} = 6328 K; d = 258 pc (Turner & Evans 1984); $\log g$ = 2.35 (Usenko et al., 2001);
   b) First overtone: R = 29 $R_\odot$; T_{eff} = 6600 K; d = 407 pc; M_{ev} = 4.3 $M_\odot$ (Gieren, 1976);
   c) Second overtone: R = 33.8 $R_\odot$; T_{eff} = 6300 K; d = 433 pc; (ESA 1997; Evans, 1991).
2. Noticeable variations of the mean $(B-V)_0$ during last decades (see Figure 1).
3. Relatively small number of radial velocity measurements (349 estimates from 1918 to 1999 in 20 observational sets).

Table 1: Observations and radial velocities of SU Cas

Spectrum	HJD 2400000+	RV ($\mathrm{km\,s^{-1}}$)	σ ($\mathrm{km\,s^{-1}}$)	NL
s482013	54074.392	1.52	1.3	512
s484026	54076.583	-7.41	1.3	463
s485017	54077.315	-8.72	1.2	559
s490017	54137.430	-13.79	1.4	599
s492002	54139.142	-14.76	1.6	471
s493012	54139.595	-15.91	1.2	472
s494020	54169.542	0.43	1.3	594
s495015	54170.449	-16.43	1.3	492
s497015	54225.247	-13.14	1.3	535
s498013	54226.241	2.53	1.3	518
s500036	54305.546	-5.89	1.3	571
s514035	54481.655	-10.32	1.4	538
s515022	54483.148	-2.15	1.1	599
s516012	54518.359	-0.38	1.2	580

Table 2: Atmosphere parameters of SU Cas

Spectrum	T_{eff} (K)	$\log g$	V_t ($\mathrm{km\,s^{-1}}$)
s482013	6298±11	2.30	3.00
s484026	6485±65	2.50	3.30
s485017	6256±38	2.25	2.70
s490017	6514±13	2.40	3.15
s492002	6548±38	2.55	4.30
s493012	6427±62	2.55	4.00
s494020	6162±17	2.30	2.85
s495015	6502±85	2.50	4.20
s497015	6502±9	2.40	3.00
s498013	6207±10	2.30	3.00
s500036	6250±11	2.30	2.80
s514035	6388±9	2.40	2.90
s515022	6272±15	2.40	3.20
s516012	6127±8	2.20	3.10
Mean	6353±28	2.38	3.25

Thus, the main task consist in:

1. To obtain the high-resolutioned spectra set of SU Cas ($F6IIb - -F8IIb$), to determine its atmospheric parameters and to compare its with the same from other authors.

2. To measure the radial velocities of SU Cas from this set.

3. To add these radial velocities to the tolal list, obtained during the long observational period (1918–2008).

4. To make more exact of SU Cas pulsational and possible orbital periods using Fourier analysis.

2. Observations

Observations of these objects have been realized using 6m telescope BTA – SAO RAS (Russia) equiped by LYNX (Panchuk et al., 1999), PFES (Panchuk et al., 1998), NES (Panchuk et al., 2002) spectrometers ($\lambda\lambda$ 4800–6600 ÅÅ.)

The reduction was made using IRAF software, the MIDAS context ECHELLE modified for extraction of echelle spectra obtained with an image slicer (Yushkin & Klochkova, 2005), DECH20 software (Galazutdinov, 1992). The observational log is given in Table 1.

3. Atmosphere parameters and chemical composition

Atmosphere parametrs were determined:

1) Effective temperature T_{eff}: by the line deph ratio (Kovtyukh & Gorlova, 2000).

2) Surface gravity $\log g$: by adopting the same iron abundance for Fe I and Fe II lines. (accuracy: 0.15 dex).

3) Microturbulent velocity V_t: by assuming abundances of the Fe II lines independent of the W_λ for Polaris (accuracy: 0.25 km $\mathrm{s^{-1}}$).

The mean atmosphere parametrs are given in Table 2.

4. Frequency analysis

Frequency analysis have been completed for SU Cas radial velocity data using **PERIOD 98** software (Sperl, 1998). **PERIOD 98** allows to search for and to fit sinusoidal patterns within the time series of data containing huge gaps. It used techniques of Fourier and Fast Fourier analysis with residuals minimization of sinusoidal fits to the data.

For calculations we have 378 radial velocities totally, obtained during the period of 1918-2008 (364 values from other authors and 14 our ones). The Fourier amplitude spectra were obtained over the frequency range 0–1 c/d at a resolution of 0.00002 c/d. These calculations were based on the original data (pulsational periods search), and the residuals at original (orbital periods search).

4a. Pulsational periods

As seen from Figure 2, we can observe the main pulsational period of 1.949329 days with two equidistant ones ±0.003 c/d (1.939059 days and 1.959787 days, respectively). And, the presence of secondary

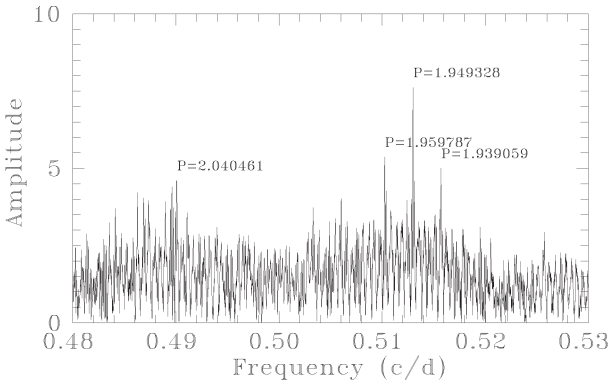

Figure 2: Fragment of Fourier amplitude spectrum of SU Cas over a narrow frequency range corresponding to pulsational periods with calculations based on the original data.

pulsational period is visible well too, – 2.040461 days. Their ratio consists 0.96 what is typical for non-radial pulsations. It is interesting that Stobie's model 9e for 5 $M_{\odot}$ star gives the period of 2.07 days in case of *first* harmonic (Stobie, 1969).

4b. Orbital periods

An existence of SU Cas hot companion is a notorious fact. Turner & Evans (1984), Usenko (1990) and Evans (1991) have predicted its spectral type within the limits of *B9.5 – A5 V*. Szabados (1991) has estimated its orbital period of 462.5, 928, 1375 and 1682 days, at that he has gave preference to the first value. In Table 3 we represented the γ – velocities, estimated for different observational sets. As seen from Figure 3, these changes show an evidence of SU Cas system orbital motion, at that the mean γ velocity is equal to -6.46 km s^{-1}.

To confirm Szabados' conclusions, we have began a search of peaks on the Fourier amplitude spectrum, which could be correspond to his orbital periods, mentioned above (see Figure 4). Evidently, these peaks are very slight and insignificant in case of calculations based on the original data. To improve this situation we calculated the Fourier amplitude spectrum based on the residuals at original ones (see Figure 5). As seen from this figure, the highest amplitude corresponds to 7490.3, 1738.8, 483.8 and 463.7 days, at that last two values are very close to Szabados' (1991) data.

5. Conclusions

1. According to our determination of T_{eff} and $(B-V)_0$ data, SU Cas demonstrates their sporadic changes with unestablished period.

Table 3: γ-velocities of SU Cas

HJD 2400000+	γ (km s^{-1})	σ (km s^{-1})	N	Reference
20229	-6.3	1.2	4	Adams & Shapley (1918)
21252	-8.0	1.2	4	Adams & Shapley (1918)
34307	-8.0	0.6	4	Abt (1959)
34621	-8.5	0.3	14	Abt (1959)
35051	-8.2	0.7	3	Abt (1959)
36451	-9.6	1.0	1	Abt (1959)
40943	-3.8	0.3	7	Niva & Schmidt (1979)
41962	-8.9	0.1	63	Gieren (1976)
43421	-7.2	0.4	39	Niva & Schmidt (1979)+ +Wilson et al. (1989)
43889	-5.6	0.3	72	Beawers & Eitter (1986)+ +Barnes et al. (1987)
44570	-6.4	0.2	15	Häupl (1988)+ +Barnes et al. (1987)
44895	-3.4	0.3	12	Häupl (1988)+ +Barnes et al. (1987)
46866	-4.9	0.4	2	Gorynya et al. (1992)
47126	-6.3	0.2	19	Bersier et al. (1994)
48630	-4.9	0.2	18	Gorynya et al. (1992, 1996)
49563	-7.0	0.3	14	Gorynya et al. (1996)
50035	-5.9	0.2	16	Sachkov et al. (1998)
50318	-5.4	0.3	9	Sachkov et al. (1998)
50741	-5.0	0.3	27	Sachkov et al. (1998) + Luck (2001)+SAO (2001)
54296	-6.5	0.3	14	This work

Reference: SAO (2001) – two spectra from Usenko et al. (2001) with radial velocities, measured by author.

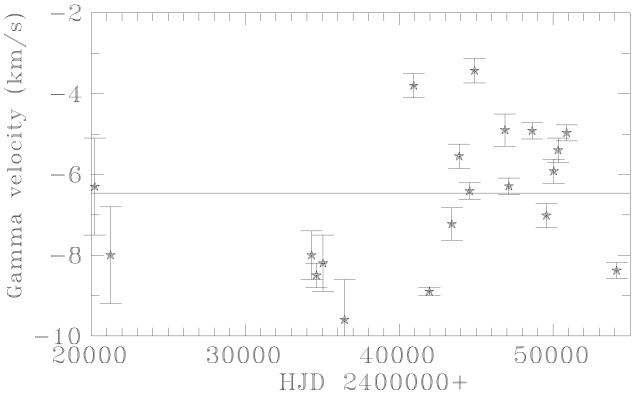

Figure 3: γ – velocity values of SU Cas during 1918 – 2008.

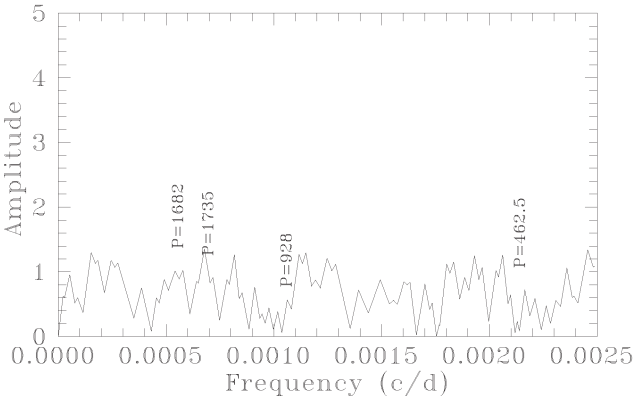

Figure 4: Fragment of Fourier amplitude spectrum of SU Cas over a narrow frequency range corresponding to orbital periods with calculations based on the original data. Periods values from Szabados (1991)

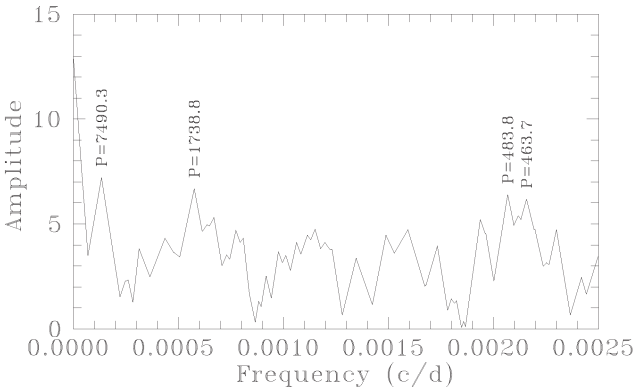

Figure 5: Fragment of Fourier amplitude spectrum of SU Cas over a narrow frequency range corresponding to orbital periods with calculations based on the residuals at original data.

2. In case of mean gravity value 2.35 – 2.40 we can consider SU Cas as *fundamental mode* pulsator with period of 1.949329 days.

3. The presence of two equidistant periods at a distance of ±0.003 c/d from the main pulsational period and possible *first overtone* period of 2.040461 days, and $P_1/P_0 = 0.96$ suggest an idea to an existence of non-radial pulsations in the Cepheid's atmosphere.

4. Szabados'(1991) 462.5 days orbital period need to be improved. Its value could be consist with in the limits of 463.7 – 483.8 days. We need as much as possible new radial velocity data to make it.

5. It is possible that SU Cas has one more companion(s) with long orbital periods near 7490.3 and 1738.8 days.

References

Abt H.A.: 1959, *ApJ*, **130**, 1021.
Adams W.S., Shapley H.: 1918, *ApJ*, **47**, 46.
Barnes T.G. III, Moffet T.J., Slovak M.H.: 1987, *ApJS*, **65**, 307.
Beavers W.I., Eitter J.J.: 1986, *ApJS*, *62*, 147.
Bersier D., Burki G. Mayor M., Duquennoy A.: 1994, *A&AS*. **108**. 25.
Evans N.R.: 1991, *ApJ*, **372**, 597.
Feltz K.A., McNamara D.H.: 1980, *PASP*, **92**, 609.
Galazutdinov, G.A.: 1992, *Preprint SAO RAS* **No.92**
Gieren W.: 1976, *A&A*, **47**, 211.
Gorynya N.A., Irsmambetova T.R., Rastorguev A.S., Samus N.N.: 1992, *SvA Lett.*, **18**, 777.
Gorynya N.A., Samus N.N., Rastorguev A.S., Sachkov M.E.: 1996, *SvA Lett.*, **22**, 198.
Gray D.: 1992, *Observation and Analysis of Stellar Atmospheres, (Cambrige Univ. Press, 2nd ed.)*
Häupl W.: 1988, *Astr. Nachr.*, **309**, 327.
Kovtyukh V.V., Gorlova N.I: 2000, *A&A*, **358**, 587.
Luck R.E.: 2001, *priv. comm.*
Milone E.F.: 1970, *IBVS*, **No. 482**.
Mitchell R.I., Iriarte B., Steinmetz D., Johnson H.L.: 1964, *Bol. Obs. Tonantzintla y Tacubaya*, **3**, No.24.
Niva G.D., Schmidt E.G.: 1979, *ApJ*, **234**, 245.
Panchuk V.E., Najdenov I.D., Klochkova V.G. et al.: 1998, *Bull. SAO RAS*, **44**, 127.
Panchuk V.E., Klochkova V.G., Najdenov I.D. et al.: 1999, *Preprint SAO RAS*, **No. 139**.
Panchuk V.E., Piskunov N.E., Klochkova V.G., Yushkin M.V., Ermakov S.V.: 2002, *Preprint SAO RAS*, **No. 169**.
Racine R.: 1968, *AJ*, **73**, 588.
Sachkov M.E., Rastorguev A.S., Samus N.N., Gorynya N.A.: 1998, *SvA Lett.*, **24**, 443.
Sperl M.: 1998, *PERIOD 98,* program.
Stobie R.S.: 1969, *MNRAS*, **144**, 511.
Sudzius J.: 1969, *Vilnius Observ. Bull.*, **No. 26**.
Szabados L.: 1977, *Bud. Mitt.*, **No. 70**.
Szabados L.: 1991, *Bud. Mitt.*, **11**, No.9, 125.
Turner D.G., Evans N.R.: 1984, *ApJ*, **83**, 254.
Usenko I.A.: 1990, *Kinemat. i Fizika Nebesn Tel*, **6**, No.3, 91.
Usenko I.A., Kovtyukh V.V., Klochkova V.G., Panchuk V.V., Yermakov S.V.: 2001, *A&A*, **367**, 831.
Wilson T.D., Carter M.W., Barnes T.G. III, van Citters G.W., Moffett T.J.: 1989, *ApJS*, **69**, 951.
Wisniewski W.Z., Johnson H.L.: 1968, *Commun. Lunar Planet. Lab.*, **7** , No. 112.
Yushkin M.V., Klochkova V.G.: 2005, *Prepint SAO RAS*, **No. 206**.

FIRST SUPERNOVAE IN DWARF PROTOGALAXIES

E.O. Vasiliev[1,2], E.I. Vorobyov[1,3], Yu.A. Shchekinov[4,5]

[1] Institute of Physics, Southern Federal University, Rostov-on-Don 344090 Russia, *eugstar@mail.ru*
[2] Institute of Astronomy, Russian Academy of Sciences, 119017 Moscow Russia
[3] Institute for Computational Astrophysics, Saint Mary's University, Halifax, B3H 3C3, Canada *vorobyov@ap.smu.ca*
[4] Department of Physics, Southern Federal University, Rostov-on-Don 344090 Russia, *yus@phys.rsu.ru*
[5] Special Astrophysical Observatory, Nizhny Arkhyz 369167 Russia

ABSTRACT. Using a two-dimensional hydrodynamics code with axial symmetry we explore the chemical, thermal, and dynamical evolution of a shell formed by a high-energy supernova explosion (10^{53} erg) in dwarf protogalaxies with a total (dark matter plus baryonic) mass 10^7 $M_\odot$ at a redshift $z = 12$. We consider two initial configurations for the baryonic matter, one without rotation and the other having the ratio of rotational to gravitational energy $\beta = 0.17$. The (non-rotating) dark matter halo is described by a quasi-isothermal sphere. We find that the dynamics of the shell is different in protogalaxies with and those without rotation. For instance, the Rayleigh-Taylor instability in the shell develops faster in protogalaxies without rotation. The fraction of a blown-away baryonic mass is approximately twice as high in models with rotation than in models without rotation. We argue that these differences are caused by different *initial* gas density profiles in non-rotating and rotating protogalaxies. On the other hand, the chemical evolution of gas in protogalaxies with and without rotation is found to be similar. The relative number densities of molecular hydrogen and HD molecules in the cold gas ($T \leq 10^3$ K) saturate at typical values of 10^{-3} and 10^{-7}, respectively. The clumps formed in the fragmented shell move with velocities that are at least twice as high as the escape velocity. The mass of the clumps is $\sim 0.1 - 10$ $M_\odot$, which is lower than the Jeans mass.

Key words: cosmology, galaxies, ISM, molecules, stars, shock waves.

1. Introduction

The detection of extremely metal-poor stars in our Galaxy with an iron abundance equal to or less than 10^{-3} of the solar value (Beers et al., 1992, Christlieb et al., 2002) has motivated scientists to put forward possible scenarios for the formation of such stars. According to Tsujimoto et al., (1999), extremely metal-poor (EMP) stars form in a dense shell produced by Type II supernova explosions of the first stars and accrete metals from the surrounding medium during the subsequent evolution. The formation of EMP stars is made possible by fragmentation of the primordial gas in a supernova shell due to efficient cooling by molecular hydrogen and HD molecules (see review by Nishi & Susa (1999), Salvaterra et al., (2004), Greif et al., (2007)). It now becomes evident that the formation of EMP stars due to fragmentation of supernova driven shells is a complicated phenomenon that depends on a variety of physical conditions in a host protogalaxy, which may vary from allowing star formation to shutting it off completely. In such circumstances, the construction of increasingly more sophisticated numerical models is justified. Here we perform axially symmetric numerical hydrodynamics simulations of high-energy supernova explosions (10^{53} erg) in a model dwarf protogalaxy with total mass 10^7 $M_\odot$. We seek to determine the effect of galactic rotation on the dynamical and chemical evolution of a supernova-driven shell.

2. Model protogalaxy

Our model protogalaxy consists of a baryonic component surrounded by a spherical dark matter halo. We assume that the dark matter halo profile is spherically symmetric and is determined by a modified isothermal sphere. The dark halo mass (M_h) in our numerical simulations is set to 10^7 $M_\odot$, which, at a redshift of $z = 12$, corresponds to 3σ perturbations in the ΛCDM model for the parameters determined from the third

year WMAP data.[1] The virial radius of our model protogalaxy is $r_{\rm v} = 520$ pc (Ciardi & Ferrara 2004).

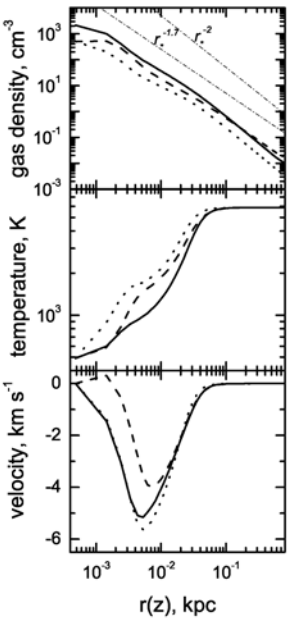

Figure 1: Profiles for the gas density (top panel), temperature (middle panel), and infall velocity (bottom panel) in the non-rotation model 1 (solid line) and rotating model 2 (dashed and dotted lines). In particular, the dashed and dotted lines show the radial and vertical profiles in model 2, respectively.

The initial distribution of the total gas density ($\rho_{\rm g}$) is found by solving numerically the steady-state momentum equations in cylindrical coordinates (z, r). We introduce a parameter $\beta < 1$, which is the ratio of rotational to gravitational energy. In the following text, we consider two models: model 1 without rotation, $\beta = 0$ and model 2 with rotation, for which we choose $\beta = 0.17$. The gas is assumed to be *initially* isothermal at a virial temperature $T_{\rm vir} = 5900$ K.

The dynamics of the gaseous component is followed by numerically solving a usual set of hydrodynamic equations in cylindrical coordinates (z, r, ϕ) using a finite-difference operator-split code (Stone & Norman 1992). The computational domain has a size of 750 pc in both the vertical (z) and horizontal (r) directions. The numerical resolution is 780×780 grid zones.

Once the equilibrium gas density distribution is constructed, we let our model galaxies evolve out of equilibrium. We stop this process when the temperature in the centre drops below 500 K. The resulted distributions are shown in Fig. 1. After we release 10^{53} erg of thermal energy in the central sphere with radius 5 pc. Such energetic supernovae are expected to result from explosion of massive metal-free stars (Heger & Woosley 2002).

[1]We assume a ΛCDM cosmology with the parameters $(\Omega_0, \Omega_\Lambda, \Omega_m, \Omega_b, h) = (1.0,\ 0.76,\ 0.24,\ 0.041,\ 0.73)$, and deuterium abundance 2.78×10^{-5} (Spergel et al., 2007).

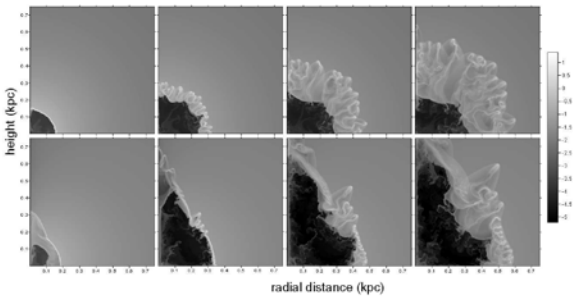

Figure 2: Distribution of density (in cm^{-3}) at t = 1, 4, 8, 12 Myr after SN explosion with $E_{SN} = 10^{53}$ erg in halo $M = 10^7\ M_\odot$ for the spin parameter $\beta = 0$ – *upper* and $\beta = 0.17$ – *low* row of panels.

The gas component of our model protogalaxy consists of a standard set of species: H, He, H^+, H^-, H_2, H_2^+, D, D^+, HD. The cooling rates are computed separately for temperatures below and above 2×10^4 K. In the low-temperature regime, the cooling rate includes cooling due to recombination and collisional excitation of atomic hydrogen (Cen 1992), H_2 (Galli & Palla 1998) and HD molecules (Lipovka et al., 2005). In the high-temperature regime, the cooling rates for zero metallicity are taken from (Sutherland & Dopita 1993). The list of chemical reactions and other details of solving chemical kinetics can be found in (Vasiliev et al 2008).

3. Results

Fig. 2 presents snapshots of the gas density distribution at four consecutive times after the supernova explosion. When the characteristic cooling time becomes shorter than the dynamical time (the age of a supernova remnant), an expanding shell becomes unstable to the Rayleigh-Taylor (RT) instability (Gull 1973). As a result, small ripples that distort a spherical shape of the shell appear in model 1 at $t = 1$ Myr. The subsequent evolution of the shell is governed by the RT instability, which acts mostly in the compressed gas of the shell outside the interface between hot supernova ejecta and the shell of compressed material. The characteristic time for the development of the RT instability is shorter for steeper initial gas density profiles and vice versa. Fig. 1 indicates that both the gas density distribution in model 1 and the *vertical* gas density distribution in model 2 have profiles similar to r_*^{-2}, where $r_* = (r^2 + z^2)^{1/2}$ is the distance from the galactic centre. On the other hand, the *radial* gas density distribution in model 2 is noticeably shallower and follows an $r_*^{-1.7}$ profile. Hence, we expect the RT instability to grow faster in the non-rotating model 1.

This is indeed seen in the top row of Fig. 2 – the shell has lost its spherical shape by $t = 4$ Myr and prominent spurs (or fingers) start to grow into the unperturbed medium. Model 2 shows little spurs at the same evolutionary time, though the shell has already started to show first signs of instability.

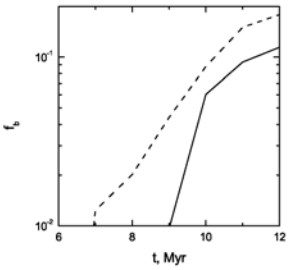

Figure 3: Fraction of the baryonic mass blown away by a supernova energy release of 10^{53} ergs in model 1 (solid) and in model 2 (dash).

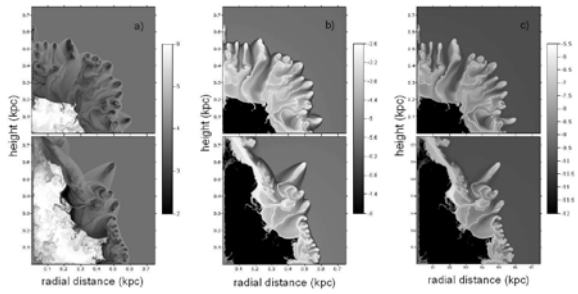

Figure 4: Logarithmic distribution of temperature (*left*), H_2 (*middle*) and HD (*right*) abundances at time $t = 12$ Myr after the explosion of SN with energy $E_{SN} = 10^{53}$ erg in halo with mass $M = 10^7\ M_\odot$ and the parameter $\beta = 0$ (upper) and $\beta = 0.17$ (lower).

Figure 2 shows that at $t = 12$ Myr some spurs are found outside the virial radius (520 pc) in the both models. This implies that a fraction of the baryonic mass is blown away by the supernova explosion (Fig. 3). We find that the spurs are characterized by mean mass-weighted velocities of the order of 26 km s^{-1} in model 1 and 22 km s^{-1} in model 2, whereas the escape velocity at the virial radius in both models is $v_e \approx 13$ km s^{-1}.

Fig. 4 shows the distribution of gas temperature, relative number densities of molecular hydrogen and HD molecules at $t = 12$ Myr. It is evident that low gas temperatures (below 10^3 K) are found in the shell and the spurs, where cooling takes place due to H_2 and HD molecules. In particular, the lowest temperatures found in the spur cores are of the order of 500 K and the relative number densities of H_2 and HD are approximately 10^{-3} and 10^{-7}, respectively.

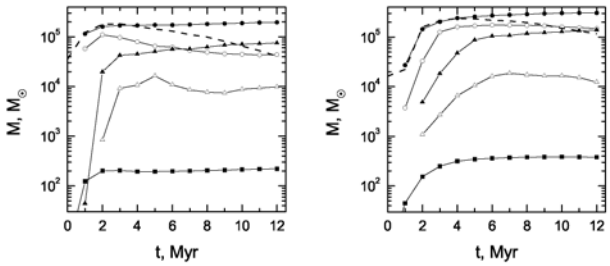

Figure 5: The total mass of gas in computational domain for model 1 with H_2 abundance higher than $x[H_2] = 5 \times 10^{-4}$ (filled circles), $x[H_2] = 10^{-3}$ (open circles), with temperature lower than $T \leq 10^3$ K (filled triangles), $T \leq 500$ K (open triagles). The line with filled squares represents the total H_2 mass. The dashed line shows the gas mass contained in fragments with density $\log n > -0.25$ and temperature $T < 5 \times 10^3$ K.

Figs. 5 present the temporal evolution of different molecular hydrogen tracers in model 1 and model 2. The comparison of those figures shows that the H_2 traces saturate during the evolution. The saturation is explained by the fact that we consider the gas evolution behind strong shock waves. The saturation times in model 2 are systematically longer than in model 1. This can be attributed to longer cooling times in model 2 due to a shallower initial gas density profile.

4. Evolution of fragments

One can see from Figs. 2 that the typical radial length of the most cold and dense regions is several parsecs. The clumps form due to desintegration of the shock wave under Rayleigh-Taylor instability which develops when gas behind the shock front starts cooling rapidly and the front decelerates. A typical size of fragments is expected to be close to the thickness of the compresses gas behind the front at the moment, when it becomes unstable.

Among possible mechanisms of cloud destruction stripping of the external layers of clouds seems the most efficient under the conditions of interest. This process operates mostly by Kelvin-Helmholtz instability. The stripping time for typical conditions in the case considered here equals ~ 3 Myr. This is short compared to the dynamical time, and from this point of view dense clumps should be destroyed quickly. However, the radiative cooling time is of the same order $t_c \sim 1 - 3$ Myr, which means that the density increase always connected with the radiative cooling can inhibite the destruction through stripping, so that the clumps can survive on longer dynamical time. The clumps however asymptotically are destroyed, which is seen from the fact that the mass contained in

relatively dense ($n > 0.56$ cm^{-3}) and cold ($T < 5 \times 10^3$ K) fragments decreases at $t > 3$ Myr as shown in Fig. 5 by dashed lines. Moreover, a typical mass of the most dense ($n > 1.8$ cm^{-3}) clumps $M \sim 0.1 - 10\ M_\odot$ (see Fig. 6) is much smaller than the Jeans mass for the corresponding conditions ($n \leq 1.8$ cm^{-3} and $T \sim 0.5 - 1 \times 10^3$ K). All this means that protostellar clouds do not form in the shell unless the clumps merge.

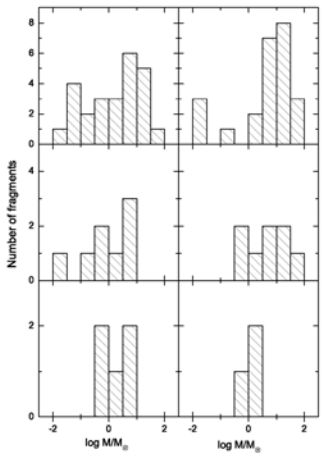

Figure 6: Number of fragments in the expanding shell at $t = 12$ Myr for a protogalaxy without (left) and with (right) rotation; panels from the uppermost to the lowermost correspond to the fragments with log $n > -0.25,\ 0,\ 0.25$, respectively; the mass of the fragments was calculated as $\bar{\rho} S^{3/2}$, where S is the area of a filamentary fragment on the "radius-height" plane, $\bar{\rho}$ is the mean density in it; note, the fragments of low density do look more filamentary and irregularly shaped than the dense ones, what therefore explains a higher spread of masses of fragments with lower density limit.

5. Conclusions

We have considered numerically the effect of energetic supernovae explosions (10^{53} erg) in non-rotating and rotating protogalaxies with the total mass $10^7\ M_\odot$ at a redshift of $z = 12$. We find the following:

- the process of the shell destruction is different for non-rotating and rotating protogalaxies;
- the supernova evacuates about 10% and 20% of the initial gas mass for models without and with rotation, respectively, to radial distances larger than the virial radius;
- the relative number densities of molecular hydrogen and HD molecules in the fingers and spurs are found to be quite large, approximately 10^{-3} and 10^{-7}, respectively. The typical temperature in the spur cores is of the order of 500 K at $t \geq 8$ Myr after the supernova explosion;
- the total gas mass with $x[\mathrm{H_2}] \geq 10^{-3}$ saturates at $2 \times 10^5\ M_\odot$, which corresponds to approximately 10% of the total baryonic mass in our model galaxy.

Finally, we would like to note that the typical masses of most fragments are $\sim 0.1 - 10\ M_\odot$. For the typical densities and temperatures in the fragments to be $\sim 0.5 - 1$ cm^{-3} and $(0.5 - 1) \times 10^3$ K, respectively, these masses are strongly sub-Jeans and the fragments are expected to be pressure-supported. Their further evolution depends on both the efficiency of cooling and destruction due to the Kelvin-Helmholtz instability. We do not expect that the low-mass stars can be formed in such conditions as suggested by Salvaterra et al. 2004. In our opinion, a more feasible mechanism for low-mass, metal-poor star formation is related with the re-collapse of a supernova bubble in protogalaxies, whose total gravitational binding energy is much larger than supernova energy.

Acknowledgements. We acknowledge Eugene Matvienko for his program of statistical processing. This work is supported by the RFBR grant 08-02-91321, the Federal Agency of Education grant RNP 2.1.1.3483. EOV is supported by the RFBR through the mobility programme grant 08-02-90706.

References

Beers T., Preston G., Shectman S.: 1992, *AJ*, **103**, 1987.
Burkert A.: 1995, *ApJ*, **447**, 25.
Cen R.: 1992, *ApJSS*, **78**, 341.
Ciardi B. & Ferrara A.: 2004, *SSR*, **116**, 625.
Christlieb N., Bessel M.S., Beers T.C., et al.: 2002, *Nature*, **419**, 904.
Galli D. & Palla F.: 1998, *A&A*, **335**, 403.
Greif T.H., Johnson J.L., Bromm V., Klessen R.S.: 2007, *ApJ*, **670**, 1.
Gull S.F.: 1973, *MNRAS*, **161**, 47.
Heger A. & Woosley S.E.: 2002, *ApJ*, **567**, 532.
Lipovka A., Núñez-López R., Avila-Reese V.: 2005, *MNRAS*, **361**, 850.
Nishi R. & Susa H.: 1999, *ApJ*, **523**, 103.
Salvaterra R., Ferrara A., Schneider R.: 2004, *NewA*, **10**, 113.
Spergel D.N., Bean R., Doré O. et al.: 2007, *ApJSS*, **170**, 377.
Stone J.M., Norman M.L.: 1992, *ApJSS*, **80**, 753.
Sutherland R. & Dopita M.: 1993, *ApJSS*, **88**, 253.
Tsujimoto T., Shigeyama T., Yoshii Y.: 1999, *ApJ*, **519**, 63.
Vasiliev E.O., Vorobyov E.I., Shchekinov Yu.A.: 2008, *A&A*, **489**, 505, arXiv/0807.3414.

CRITICAL METALLICITY FOR POPULATION II STARS

E.O. Vasiliev[1,2], Yu.A. Shchekinov[3,4]

[1] Institute of Physics, Southern Federal University, Rostov-on-Don 344090 Russia, *eugstar@mail.ru*
[2] Institute of Astronomy, Russian Academy of Sciences, Moscow 119017 Russia
[3] Department of Physics, Southern Federal University, Rostov-on-Don 344090 Russia, *yus@phys.rsu.ru*
[4] Special Astrophysical Observatory, Nizhnij Arkhyz, Karachai-Cherkess Republic 369167 Russia

ABSTRACT. We present simple arguments about metallicity of transition from first stellar generation (population III) to the second one. We consider the efficiency of fragmentation in gas induced by thermal instability in cold gas layers and filaments ($T < 10^4$ K), and in the shells formed by supernovae explosions from first stars. We estimate the metallicity at which the gas behind shock waves becomes unstable against thermal instability. We argue that this metallicity is inherited by population II stars and can be thus treated as the critical metallicity.

Key words: early universe, shock waves, mixing, heavy elements, supernovae, stars (Population III, Population II).

1. What determines the metallicity of stars

First stars formed at redshifts 20–30 and after a short (a few million years) lifetime exploded as a supernovae to enrich surrounding gas with heavy elements (metals). It is well known that cooling rate in metal lines is more efficient than in primordial molecular lines (H_2 and HD). Metals thus favour fragmentation in gas and formation low mass stars. The metallicity of gas, when metals become a dominant cooling agent, is called the critical metallicity. This value can be defined variously: *a)* this is the metallicity when cooling rates by metals and primordial molecules are equal to each other (Bromm & Loeb 2003), *b)* or the metallicity when cooling by metals is predominated over the gravitational heating during protostellar cloud collapse (Bromm et al 2001), *c)* or when cooling by metals and dust leads to fragmentation of gas in the process of protostellar collapse (Omukai et al 2005). Such defined critical metallicity is found to range between $10^{-5} - 3 \times 10^{-4}$.

In these estimates it is assumed implicitly that the metallicity increases gradually until it reaches the critical value. However, initially the metals locate in the supernovae ejecta and further mix with a swept-away supernovae shell. The shell fragments onto filaments due to Raileigh-Taylor and/or thermal instabilities, so that the filaments can contain different fractions of metals depending on how metals are mixed through the shell and where a fragment has formed. In other words the metallicity of filaments can vary in a wide range. In subsequent evolution the filaments may fragment onto smaller ones and merge with other filaments to form larger clumps. In the process of fragmentation and merging mixing efficiency depends on many factors (as density contrast between mergers, their sizes, relative velocities and so on), and in general is far from being complete (Vasiliev et al 2008). This means that filaments, clumps and clouds preceding formation of next generation of stars can have widely varying metallicity, above and below the critical value as defined earlier. In general, birth of stellar objects depends on thermal and dynamical evolution of protostellar clumps. The former is governed by cooling efficiency and self-gravitation, while the latter is determined by external influence, e.g. shock waves and collisions. Obviously, clouds with supercritical metallicity cool efficiently and form stellar objects, whereas evolution of clouds with subcritical metallicity is less clear: external shock waves can either compress or destroy clouds, however in first case under certain conditions clumps may form stars with subcritical metallicity. Since the metallicity of protostellar clouds can in principle be higher than the critical value in the sense defined above, we can meet among post-PopIII no stars belonging to the intermediate stellar population according to their metallicity level, rather misinterpreting them as PopII stars.

2. Thermal instability in cooling gas

We consider first the efficiency of fragmentation in gas induced by thermal instability (Fields, 1965) in shells formed by supernovae from first stars. The evo-

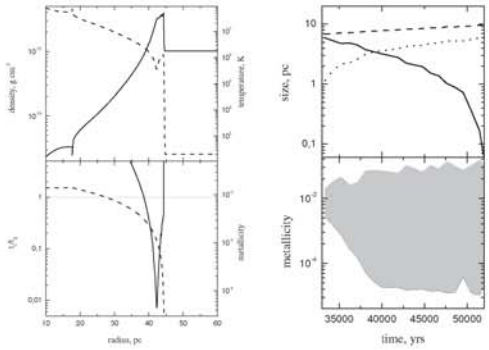

Figure 1: **Upper left panel:** Radial distributions of density (solid line), temperature (dashed line) at $t = 5 \times 10^4$ yrs after SN explosion with energy 10^{53} egs in the homogenious medium with $n = 10$ cm^{-3}; **Lower left panel:** the ratio of cooling to dynamical time (solid line) and distribution of metallicity (dashed line) at $t = 5 \times 10^4$ yrs after SN explosion. **Upper right panel:** Thickness of the unstable shell (dotted line), maximum (dashed) and minimum (solid line) thermally unstable length in the shell; **Lower right panel:** The allowed range of metallicity of fragments.

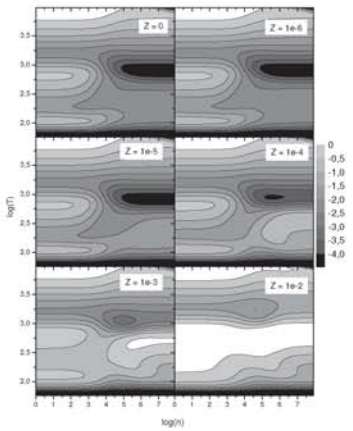

Figure 2: Thermal instability at various metallicities. Unstable regions are marked by white.

lution of supernovae remnant (SNR) can be divided onto two phases: adiabatic and radiative. The transition from the former to the latter occurs when dynamical time (the age of SNR) and cooling time equal. At this moment the SNR shell becomes unstable against thermal instability, and it is getting destroyed onto fragments when the size of perturbations turns to be shorter than the shell thickness.

In our one-dimensional gas dynamics we consider a simple model of metal mixing in SNR: initially metals are assumed to be confined in the supernovae ejecta; further on the fraction (relative density) of metals is prescribed constant inside the ejecta, whereas it linearly decreases in the shell. Figure 1 (left panels) presents radial distributions of density, temperature, metallicity and the ratio of cooling to dynamical time at $t = 5 \times 10^4$ yrs after SN explosion in a homogenious medium. Behind the shock wave a region where the ratio is less than one is readily seen, so this part of the shell becomes thermally instable. The average metallicity in this region is 10^{-3}. In the right upper panel of Figure 2 one can find the time dependence of the thickness of thermally unstable shell, maximum amd minimum length of the instability (size of fragments). On the right lower panel the metallicity range of thermally unstable fragments is shown. Note that the lower density is in the medium, the larger sizes and the lower metallicity have fragments.

Cooling of gas below 10^4 K is governed by H_2 and HD molecules, ionized carbon and neutral oxygen. Those coolants able to decrease temperature of gas down to the value of the cosmic microwave background temperature. Figure 2 shows the temperature-density range for various metallicities where the gas becomes thermally unstable. Similar diagrams were obtained by Smith et al (2007). It is clearly seen that the criterion of thermal instability is fulfilled only for high metallicity. Thus, fragments that can become protostellar clouds have high metallicity.

3. Conclusions

We briefly discussed what determines the transition from first stars to next stellar generations. The transition metallicity depends on mixing in SN shell and on efficiency of thermal instability in cooling gas. In our simple estimates the metallicity at which gas behind shock waves becomes unstable againt thermal instability and forms fragments vary in a wide range and at upper level can be higher than the critical metallicity.

Acknowledgements. This work is supported by the RFBR grant 08-02-91321, the Federal Agency of Education grant RNP 2.1.1.3483. EOV is supported by the RFBR through the mobility programme grant 08-02-90706.

References

Bromm V., Ferrara A., Coppi P.S., Larson R.B.: 2001, *MNRAS*, **328**, 969.
Glover S.C.O.: 2008, *AIP Conf. Proc.*, **990**, 25.
Field G.B.: 1965, *ApJ*, **142**, 531.
Omukai K., Tsuribe T., Schneider R., Ferrara A.: 2005, *ApJ*, **626**, 627.
Vasiliev E., Dedikov S., Shchekinov Yu.: in press.
Smith B., Sigurdsson S., Abel T.: 2008, *MNRAS*, **385**, 1443.

Non-LTE LINE FORMATION FOR Zr I/II IN COOL STARS

A.B. Vinogradova, L.I. Mashonkina

Institut of Astronomy of Russian Academy of Sciences
48 Pyatnitskaya st., Moscow 119017 Russia, *anna@inasan.ru*

ABSTRACT. Non-local thermodynamical equilibrium (non-LTE) line formation for neutral and singly-ionized zirconium is considered for the first time through a range of stellar parameters when the Zr abundance varies from the solar value down to [Zr/H] = – 3. The model atom includes 63 combined energy levels of Zr I, 247 levels of Zr II and the ground state of Zr III. It is shown that the Zr I levels are depopulated relative to their thermodynamic equilibrium populations in the line formation layers with $\log\tau_{5000} < 0.1$ resulting in weakening the Zr I lines relative to their LTE strengths. The ground state and low-excitation levels of Zr II keep their LTE populations throughout the atmosphere, while the excited levels of Zr II are overpopulated. This leads to weakening the Zr II lines arising from the ground state or low-excited levels. The role of inelastic collisions with hydrogen atoms in the statistical equilibrium of Zr I/II is estimated empirically from inspection of their different influences on Zr I and Zr II lines in the solar spectrum. The mean non-LTE abundance of zirconium in the solar atmosphere is determined as $\log\varepsilon_{\rm Zr,\odot} = 2.61\pm0.09$ from the lines of two ionization stages, Zr I and Zr II. The dependence of non-LTE effects on the atmospheric parameters is considered for a small grid of model atmospheres with T_{eff} = 5500K, logg = 2.0 and 4.0, [M/H] = –3.0, –2.0, –1.0, and 0.0. The departures from LTE increase with increasing the luminosity and decreasing metal abundance (metallicity).

Key words: Line: formation; Sun: atmosphere; stars: abundance; line: profiles

1. Introduction

One believes that elements beyond the iron group are produced by neutron-capture reactions which are distinguished into slow (s-) and rapid (r-) process depending on the neutron density flux available. In ones turn, the slow process is subdivided into the main and the weak components. The weak s-process can run in the cores of massive (M $\geq$ 20 $M_\odot$) stars during hydrostatic helium-core burning, and the main s-process occurs in intermediate-mass (2 - 4 $M_\odot$), asymptotic-giant-branch (AGB) stars during unstable burning in the double shell source. According to Käppeler et al. [10], the weak s-process produces nuclei with an atomic mass A $\leq$ 90. The r-process is associated with type II supernovae (SNeII). The different zirconium isotopes (A=90, 91, 92, 94, 96) can be produced by various types of n-capture reactions. The current nucleosynthesis models are unable to predict the yields of elements in the r-process and give only very approximate estimates for the weak s-process. Therefore, one needs to reconstruct the history of the heavy-element enrichment of the interstellar medium on an observational basis and to provide accurate observational constraints to nucleosynthesis models.

In our recent work [17], the zirconium abundance was determined at the assumption of local thermodynamical equilibrium (LTE) in the atmospheres of 52 stars belonging to the Galactic thin disk, thick disk and halo. In the halo stars, a large overabundance of zirconium relative to barium is found up to log(Zr/Ba) = 1.8 at [Ba/H] = −3.8 (Figure 1). The Zr/Ba ratio

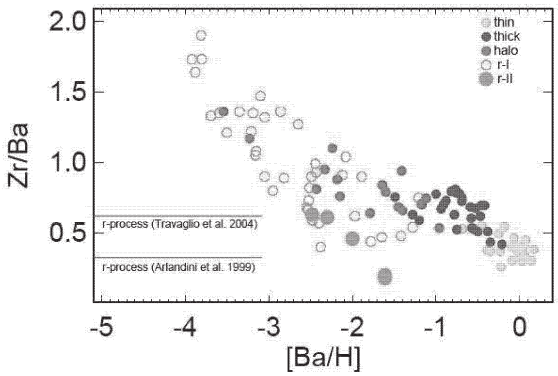

Figure 1: log(Zr/Ba) abundance ratios as a function of [Ba/H] plotted based on the data from [4] and [17].

decreases with increasing the barium abundance and approaches to solar value in the thin disk stars. According to the current conceptions, the heavy elements in the early Galaxy were synthesized by pure r-process. Travaglio et al. [21] and Arlandini et al. [2] predict that the [Zr/Ba] ratio must be constant at [Fe/H] < −1.5. The observed trend points to the existence in the early

Galaxy of some additional source of synthesis of zirconium with only little contribution to barium.

The aim of this work is to check whether the departures from LTE can affect the observational finding on an evolutionary behavior of the stellar zirconium abundances.

2. The model atom

Energy levels. In the atmospheres of cool stars with $T_{\rm eff}$ = 5500 - 6500 K, the major fraction of zirconium is represented by Zr II and a fraction of Zr I does not exceed several parts in a thousand. Zr II is a species of our main interest because only Zr II lines are observed in metal-poor stars. We use all measured energy levels of Zr II with an excitation energy up to $E_{\rm exc}$ = 8.75 eV available in the NIST (http://physics.nist.gov/PhysRefData) database and in Malcheva et al. [16]. However, an ionization energy of Zr II is 13.13 eV, and we use the predicted high-excitation levels from calculations of H. Nilsson [18] in order to provide close coupling to the next ionization stage. The model atom of Zr I includes the measured levels from the NIST and VALD (Kupka et al. [11]) databases with $E_{\rm exc}$ up to 4.25 eV. In total, the model atom is based on 148 levels of Zr I and 772 levels of Zr II. The levels with small energy differences were combined into single level. The resulting model atom consists of 63 levels of Zr I, 247 levels of Zr II, and the ground state of Zr III. Fine structure is allowed for low excited levels of Zr II with $E_{\rm exc} < 5$ eV.

Radiative bound-bound (b-b) rates. For Zr II, we take into account 1070 experimental oscillator strengths from [14] and 8266 theoretical ones from [18]. For Zr I, we use only experimental oscillator strengths taken from the NIST and VALD databases for 247 transitions.

Photoionization cross-sections. We apply hydrogenic approximation because no accurate data is available.

Collisional rates. The electron impact excitation is taken into account using the van Regemorter′s formula [22] for the allowed transitions and using a line collision strength, $\Omega_{\rm ij} = 1$ for the forbidden transitions. The electron impact ionization is calculated using the Drawin′s formula [8]. In the atmospheres of cool stars, a number of neutral hydrogen atoms is much larger than a number of electrons. Therefore, one also needs to take into account collisions with hydrogen atoms. We use the Steenbock & Holweger′s formula [19] for allowed transitions and Takeda′s approximation [20] for forbidden transitions. Since both formulas provide only an order of magnitude accuracy, we made test calculations varying a scaling factor to these formulas, $k_{\rm H}$, between 0 and 1 to determine it empirically.

3. Methods and codes

In our calculations, we use plane-parallel, homogeneous, blanketed model atmospheres computed using the MAFAGS code [9]. We set an α-element enhancement [α/Fe] = 0 for the models with [M/H] > -0.6 and [α/Fe] = 0.4 for the less metallicity models. We use a revised version of the DETAIL program [7] based on the accelerated Λ-iteration in order to solve the coupled radiative transfer and statistical equilibrium equations. The departure coefficients obtained from DETAIL are then applied to compute synthetic line profiles via the SIU program developed by T. Gehren and J. Reetz at the University of Munich. The list of spectral lines includes all atomic and molecular lines from tables of Kurucz [13].

4. Mechanisms of departure from LTE

Figure 2 shows the departure coefficients,

$$b_i = \frac{n_i}{n_i^*}$$

of the selected levels of Zr I and Zr II as a function of continuum optical depth τ_{5000} at $\lambda = 5000$Å in the solar atmosphere. Here, n_i and n_i^* are the statistical equilibrium and LTE (Saha-Boltzmann) number densities, respectively. We find that the ground state and low-excitation levels of Zr II keep their LTE populations, but other levels of Zr II are overpopulated due to radiative pumping from the ground state and low excited levels. When hydrogenic collisions are neglected for forbidden transitions, a small depopulation of some low exited levels is seen at $\log\tau_{5000} < -2$. Opposite, most Zr I levels are depopulated everywhere above $\log\tau_{5000} = 0$ due to ultraviolet overionization.

We find that for every Zr I and Zr II line used in the zirconium abundance analysis, the upper level is overpopulated relative to the lower level of the transition. In the visual spectral range, a line source function is

$$S_\nu \approx B_\nu \frac{b_j}{b_i},$$

where b_j and b_i are the departure coefficients of the upper and lower levels, respectively, and B_ν is the Planck function. Since the upper level is overpopulated relative to the lower level,

$$\frac{b_j}{b_i} > 1$$

is valid, and, consequently, $S_\nu > B_\nu$. As a result, the line is weakened. Thus, in order to fit the observed profile of the line, one needs to increase an abundance of the zirconium. The non-LTE effects lead to positive

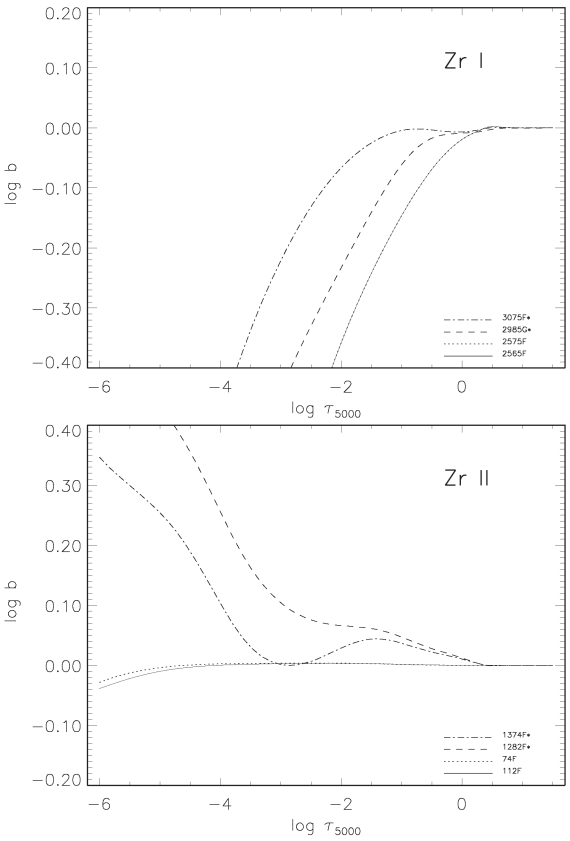

Figure 2: Departure coefficients of some Zr I/II levels as a function of $\log \tau_{5000}$ in the solar atmosphere.

non-LTE abundance corrections.

5. Analysis of the Zr I and Zr II lines in the solar spectrum

5.1. The spectral line sample

The abundance of zirconium in the solar atmosphere was determined in several papers under the LTE assumption. Biémont et al [5] used the equivalent width method for 34 lines of Zr I and 24 lines of Zr II. They have obtained the mean abundances derived from the lines of two ionization stages to be consistent, but with large abundance errors of up to 0.21 dex.

Ljung et al. [14] use the equivalent widths for 7 most reliable lines of Zr II and determine the solar Zr abundance with the abundance error of 0.02 dex. Bogdanovich et al. [6] apply theoretical oscillator strengths and determine the solar Zr abundance from 21 lines of Zr I and 15 lines of Zr II. Having inspected the zirconium lines in the solar flux spectrum [12] we find that many of them are blended and the equivalent width method cannot provide correct calculations of the blending lines effect. We conclude that most lines from the Biémont′s line list cannot be used in abundance analysis. We find only 6 relatively unblended lines of Zr I and 10 lines of Zr II which can be reliably used to determine the zirconium abundance in the solar atmosphere.

5.2 The zirconium abundance in the solar atmosphere

We make calculations for a model atmosphere with $T_{\rm eff}$ = 5780 K, logg = 4.44, microturbulence velocity $V_{\rm mic} = 0.9\ km\,s^{-1}$. Our synthetic flux profiles are convolved with a profile that combines a rotational broadening of 1.8 $km\,s^{-1}$ and broadening by macroturbulence with a radial-tangential profile of $V_{\rm mac}$ which was allowed to vary between 2.4 $km\,s^{-1}$ and 4 $km\,s^{-1}$ for different lines. Figure 3 shows the best fits of the selected Zr I and Zr II lines achieved with the Zr abundance $\log \varepsilon_{Zr} = 2.57$ dex for Zr I 4687 Å and 2.68 dex for Zr II 4208 Å .

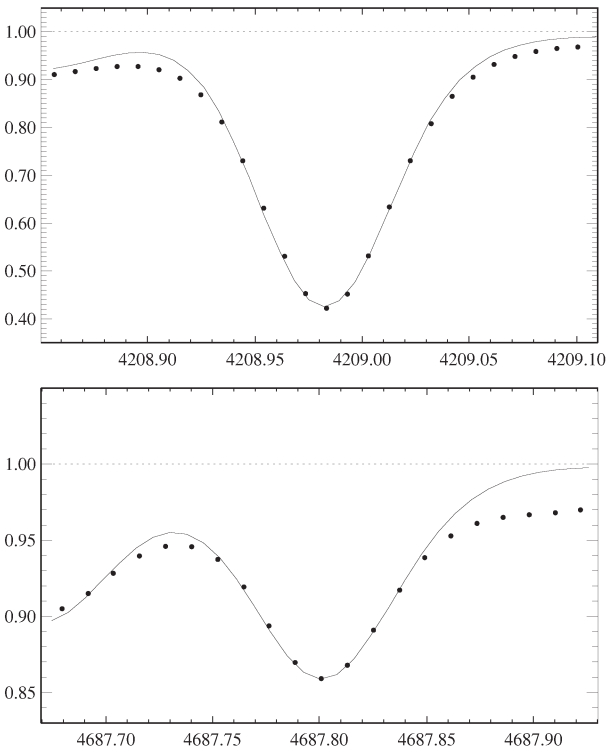

Figure 3: Best non-LTE fits of the solar Zr I 4687Å and Zr II 4208Å lines. See text for more details.

The largest uncertainty of our non-LTE calculations is connected with a treatment of hydrogenic collisions. According to various investigations, the Steenbock & Holweger′s formula [19] overestimates $C_{\rm ij}$(H). We determine a scaling factor, $k_{\rm H}$, to this formula from analysis of the Zr I and Zr II lines in the solar spectrum. The test calculations are performed for 8 cases, namely, LTE, non-LTE neglecting hydrogen collisions, non-LTE including hydrogen collisions only for allowed

transitions with $k_{\rm H}$ = 0.1, 0.33, 1.0, and non-LTE including hydrogen collisions for both allowed and forbidden transitions with $k_{\rm H}$ = 0.1, 0.33, 1.0. For each case, we determine the average element abundances from the Zr I lines and from the Zr II lines. The results are presented in Figure 4. It is evident, every non-LTE case provides the smaller discrepancy between the element abundances from two ionization stages than the LTE case where the abundance difference is $\log\varepsilon_{\rm ZrII} - \log\varepsilon_{\rm ZrI} = 0.27$.

If hydrogen collisions are neglected, the non-LTE effects are maximal. We prefer the case when hydrogen collisions are taken into account for both allowed and forbidden transitions with $k_{\rm H}$ = 0.1. In this case, a well agreement is simultaneously achieved between the element abundances from two ionization stages, $\log\varepsilon_{\rm ZrII} - \log\varepsilon_{\rm ZrI} = 0.04$, as well as between the solar average Zr abundance ($\log\varepsilon_{\rm Zr} = 2.61\pm0.09$) and the meteoritic value ($\log\varepsilon_{Zr}$ = 2.57 [3], 2.60 [15] and 2.61 [1]). We use an usual abundance scale where $\log\varepsilon_{\rm H}$ = 12 for hydrogen.

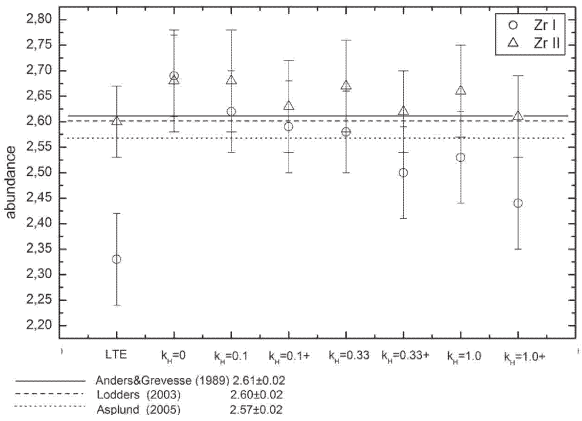

Figure 4: Mean abundances determined from the solar Zr I (circles) and Zr II (triangles) lines for various line formation treatments compared to the meteoritic Zr abundance from [1] (continuous line), [3] (dotted line), and [15] (dashed line). See text for more details.

6. Non-LTE effects as a function of stellar parameters

We calculate a non-LTE abundance correction, $\Delta_{\rm NLTE} = \varepsilon_{\rm NLTE} - \varepsilon_{\rm LTE}$, for the Zr II lines for a small grid of model atmospheres with an effective temperature $T_{\rm eff}$ = 5500 K, logg = 2.0 and 4.0, and [M/H] = –3.0, –2.0, –1.0, and 0.0. The results are shown in the Figure 5. It can be seen that the non-LTE effects are small for logg = 4.0: $\Delta_{\rm NLTE}$ does not exceed 0.06 dex. For logg = 2.0, $\Delta_{\rm NLTE}$ depends strongly on metallisity and increases from 0 up to 0.6 dex with decreasing [M/H] from 0 to –2.

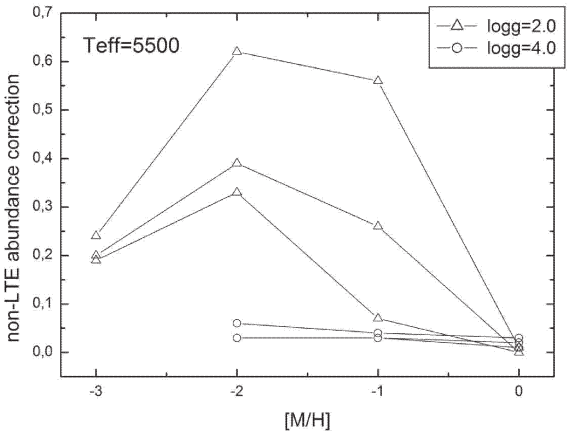

Figure 5: Non-LTE abundance corrections for lines of Zr II 3479, 3505, 4208 ÅÅ (the values at logg = 2, triangles), and Zr II 3505, 3714, 4208 ÅÅ (the values at logg = 4, circles) as a function of stellar parameters.

This is due to decreasing the electron number density and, hence, decreasing collisional rates. The non-LTE abundance corrections start to decrease with further decreasing [M/H] due to a shift of the line formation depth to deeper layers.

7. Conclusions

We have treated the model atom of Zr I/II including 63 combined levels of Zr I, 247 levels of Zr II and the ground state of Zr III. We show that the excited levels of Zr II are overpopulated relative to their LTE populations, while the Zr I levels are underpopulated. We deduce from analysis of the Zr I and Zr II lines in the solar spectrum that one needs to take into account hydrogenic collisions in SE calculations for both allowed and forbidden transitions with a scaling factor $k_{\rm H}$ = 0.1 to the Steenbock & Holweger's formula. In this case, the absolute abundance of zirconium in the solar atmosphere amounts 2.61±0.09 dex. Test calculations for the grid of model atmospheres with $T_{\rm eff}$ = 5500 K show that the non-LTE effects are small for dwarf stars with logg = 4.0. In giants (logg = 2.0), the non-LTE abundance corrections depend strongly on metallicity and increase from 0 up to 0.6 dex with decreasing [M/H] from 0 to –2. They start to decrease with further decreasing [M/H].

Acknowledgements. This research was supported by the the Russian Foundation for Basic Research with grant 08-02-00469-a and the Presidium RAS Programme "Origin and evolution of stars and the Galaxy".

References

1. Anders E. & Grevesse N.: 1989, *Geoch. & Cosmochim Acta*, **53**, 197.
2. Arlandini C., Kappeler F., Wisshak K. et al.: 1999, *Astrophys.J*, **525**, 886
3. Asplund M., Grevesse N. & Sauval A.J.: 2005 *ASP Conf. Ser.*, **336**, 25
4. Barklem P.S., Christlieb N., Beers T.C., et al.: 2005, *Astron. & Astrophys.*, **439**, 129
5. Biémont E. & Grevesse N.: 1981, *Astrophys. J.*, **248**, 867
6. Bogdanovich P., Tautvaisiene G., Rudzikas Z., Momkauskaite A.: 1996, *MNRAS*, **280**, 95
7. Butler K. & Giddings J.: 1985, *Newsletter on the analysis of astronomical spectra 9, University of London*
8. Drawin H. W.: 1961, *Z. Phys.*, **164**, 513
9. Fuhrmann K., Pfeiffer M., Frank C., et al.: 1997, *Astron. & Astrophys.*, **323**, 909
10. Käppeler F., Beer H., & Wisshak K.: 1989, *Rep. Prog. Phys*, **52**, 954
11. Kupka F., Piskunov N., Ryabchikova T.A., et al.: 1999, *Astron. & Astrophys.*, **138**, 119
12. Kurucz R. L., Furenlid I., Brault J., & Testerman, L.: 1984, *NSO Atlas No. 1: Solar Flux Atlas from 296 to 1300 nm, Sunspot, NSO*
13. Kurucz R.L.: 1994 *CD-Roms No. 18, 19*
14. Ljung G., Nilsson H., Asplund M., & Johansson S.: 2006, *Astron. & Astrophys.*, **456**, 1181
15. Lodders K.: 2003, *Astrophys.J*, **591**, 1220
16. Malcheva G., Blagoev K., Mayo R., et al.: 2006, *MNRAS*, **367**, 754
17. Mashonkina L.I., Vinogradova A.B., Ptitsyn D.A. et al.: 2007, *Astronomy Reports*, **51**, 11
18. Nilsson H.: 2007 (private communication)
19. Steenbock W. & Holweger H.: 1984, *Astron. Astrophys.*, **130**, 319
20. Takeda Y.: 1994, *PASJ*, **46**, 53
21. Travaglio C., Galli D., Gallino R., et al.: 1999, *Astrophys. J.*, **521**, 691
22. van Regemorter H.: 1962, *Astrophys. J.*, **136**, 906

ANALYSIS OF THE SPECTRAL ENERGY DISTRIBUTION OF THE COOLEST RCrB TYPE CARBON STAR DY Per

L.A.Yakovina[1], A.V.Shavrina[2], Ya.V.Pavlenko[3], A.F.Pugach[4]
Main astronomical observatory of the national academy of sciences of Ukraine, Kiev, Ukraine
[1]*yakovina@mao.kiev.ua,* [2]*shavrina@mao.kiev.ua,* [3]*yp@mao.kiev.ua,* [4]*pugach@mao.kiev.ua*

ABSTRACT. We analysed the spectral energy distribution of the evolved carbon star DY Per by spectral synthesis technique. The red giant shows the photometric features of R CrB type stars. We derived the atmosphere parameters of DY Per using three variants of molecular line lists. The range of T_{eff} estimations is $2900 < T_{eff} < 3300$ K. We adopted log g = 0. The star can be metal deficient and hydrogen deficient. The highest value of carbon abundance [C]=0.94 provides the combination of atmosphere parameters {T_{eff} =3100 K, [Fe/H] =0, log(C/O)=0.6, [N/Fe]=0, $(H/He)_\odot$} with Jorgensen's line lists for molecules C_2 and CN.

1. Introduction

The red giant DY Per shows photometric properties of R CrB type stars. Apparently, the star is the coolest among known stars of this type. DY Per is not typical R CrB type star and we cannot to classify one as a member of any known subclasses of C-stars.

Some authors estimate the effective temperature of DY Per $3500 < T_{eff} < 4740$ K by indirect methods (see Keenan & Barnbaum 1997). Yakovina et al. (2009) firstly determine $2900 < T_{eff} < 3000$ K for DY Per using fit of synthetic spectra to the observed spectral energy distribution (SED).

Molecular line lists in (Yakovina et al. 2009) were taken from database (Kurucz 1993-1994). This bank is the most full, but the accuracy of Kurucz's line lists is not always satisfactory. Because for some molecular systems are widely used data from other sources, it is possible to refine Kurucz's line lists. In this work we determine the atmosphere parameters of DY Per using the same observed material as in (Yakovina et al. 2009) and two other variants of line lists for molecules C_2 and CN.

The moderate resolution spectrum of DY Per was obtained 29.09.2003 with the spectrorgraph SPEM in Nesmith focus of 2.6-m telescope ZTSh of the Crimean astrophysical observatory. In the observed region $\lambda\lambda$ 400-730 nm the spectral resolution was $\sim$ 1.7 A/px, maximal S/N was about 280. Observed spectra reduction procedure is described in Yakovina et al. (2009).

Table 1: Systems of diatomic molecules accounted in computations of synthetic spectra. [1] - Urdahl et al. 1991, [2] - Huang et al. 1992, [3] - Tsuji 1973, [4] - Bernath et al. 1985.

Molecule	Transition	System	D_0 (eV)
$^{12}C^{12}C$	$d^3\Pi_g$ - $a^3\Pi_u$	Swan	6.297 [1]
$^{12}C^{12}C$	$A^1\Pi_u$ - $X^1\Sigma_g^+$	Phillips	6.297 [1]
$^{12}C^{14}N$	$B^2\Sigma^+$ - $X^2\Sigma^+$	Violet	7.738 [2]
$^{12}C^{14}N$	$A^2\Pi$ - $X^2\Sigma^+$	Red	7.738 [2]
^{12}CH	$A^2\Delta$ - $X^2\Pi$		3.47 [3]
^{12}CH	$B^2\Sigma^-$ - $X^2\Pi$		3.47 [3]
^{12}CH	$C^2\Sigma^+$ - $X^2\Pi$		3.47 [3]
^{24}MgH	$A^2\Pi$ - $X^2\Sigma^+$		1.27 [4]

2. Model atmospheres and synthetic spectra of DY Per

Model atmospheres of different T_{eff} and abundances (Pavlenko & Yakovina 2009) were calculated by SAM12 program (Pavlenko 2003). Microturbulent velocity V_t = 3 km/s was adopted. A reference set of the "solar" abundances we took from Gurtovenko & Kostik (1989).

Synthetic spectra were calculated by WITA6 program (Pavlenko 1997). Due to the high $^{12}C/^{13}C$ value in atmosphere of DY Per (Keenan & Barnbaum 1997), molecules contained ^{13}C were not accounted in our computations. We used the atomic line list from VALD (Kupka et al. 1999). The list of molecular systems accounted in synthetic spectra calculations we set in Table 1. Dissociation potentials are shown too.

In work (Yakovina et al. 2009) the line lists of all molecular systems had been taken from CD-ROM N18 of database (Kurucz 1993-1994). In this work we used two another versions:

First, we update line list of the Swan system of C_2 molecule from (Kurucz 1993-1994). For other molecular band systems we used the original Kurucz's line lists. The original Kurucz's list and modified one we name K18 and K18n, respectively.

Second, line lists of CN red system and C_2 (without dividing into the systems) were taken from Jorgensen's site http://stella.nbi.dk, other lists were taken from (Kurucz 1993-1994).

Line list of the CN red system on Jorgensen's site is well known list from tape SCAN-CN (see Jorgensen & Larsson 1990). Lists C_2 are the lists of Querci, described in (F.Querci et al. 1971, F.Querci et al. 1974). Jorgensen transformed Querci's lists to the SCAN-CN format. He updates oscillator strength (gf) when come new molecular data.

We updated Kurucz (1993-1994) line list of Swan band system using the Kuznetsova & Shavrina (1996) data and programs. The new values of gf for Swan system were calculated using information from databank RADEN (Kuznetsova et al. 1993) and the MOLEC program, developed in the Main astronomical observatory of NASU.

C_2 and CN spectra computed with three versions of molecular line lists are shown in Fig. 1. All theoretical spectra shown in this paper are convolved by gaussian of FWHM = 1.2 nm.

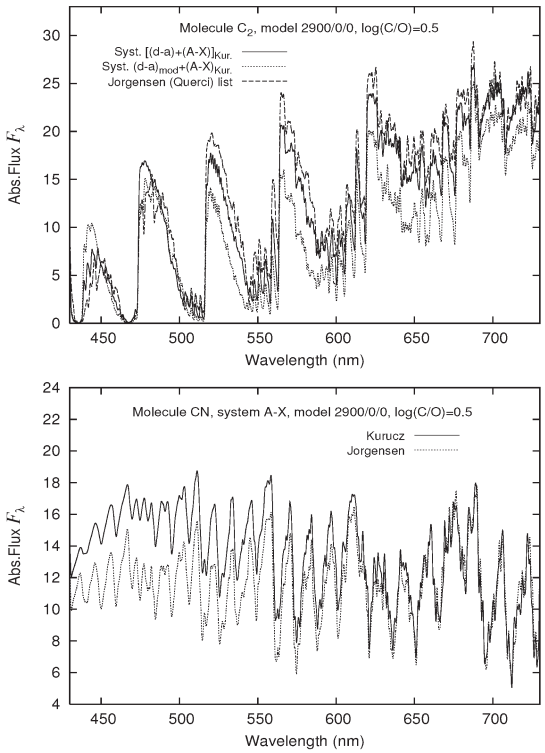

Figure 1: Theoretical spectra of C_2 and CN molecules computed with different molecular line lists. We computed gf-values for C_2 (d-a)$_{mod}$ lines following a procedure by Kuznetsova & Shavrina (1996)

3. Results

From the best fits of theoretical SEDs to observed fluxes of DY Per at $\lambda\lambda$ 430-730 nm we determined the atmosphere parameters $T_{\rm eff}$, [Fe/H], C/O, [N/Fe] and H/He.

To compare the observed and synthetic spectra we follow the next procedure.

First of all, we analyse the fit of synthetic spectrum to the selected narrow spectral regions of maximums or minimums in observed SED. Maximums of flux determine the gradient of SED in the investigated region. We found that gradient of SED is the important indicator of $T_{\rm eff}$. All selected regions we show on Fig. 2. We used them for determination of the next parameters:

– Swan bands were the main indicators of carbon abundance,

– bands of CH A-X system with Δv =-1 were the main indicators of the hydrogen abundance,

– resonance Na I doublet was the main indicator of atomic spectrum intensity,

– the band 3-0 of CN red system was the main indicator of nitrogen abundance.

In Fig.3 we show some fits of synthetic spectra, computed with different line lists, to the DY Per SED. These fits are rather similar.

We show in the Table 2 some new results combined with Yakovina et al. (2009) data.

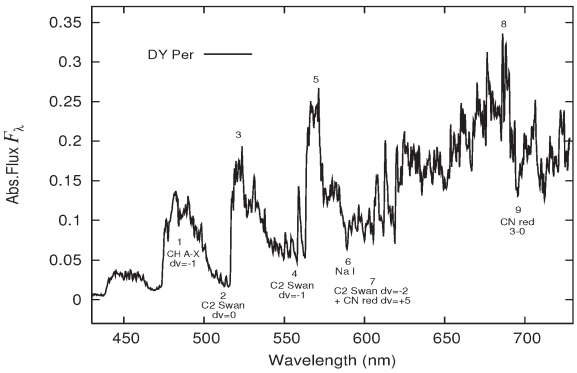

Figure 2: The main indicators for determination of atmosphere parameters in spectrum of DY Per. Here Δv =v'-v", v' and v"- vibrational quantum numbers of upper and low levels of transition, accordingly

Table 2: Sets of atmosphere parameters that provide the good fits of synthetic spectra to spectrum of DY Per. We adopt log g=0.0, $(H/He)_{\odot}$= 0.911/0.089 ≈ 9/1

T_{eff}	[Fe/H]	log C/O	[N/Fe]	H/He	[C]	Line list
2900	-0.5	0.3	0.0	Sun	+0.14	K18
2900	-1.0	0.5	0.2	7/3	-0.16	K18
2900	-1.5	0.6	0.4	3/7	-0.56	K18
2900	-2.0	0.6	0.5	1/9	-1.01	K18
3000	-0.5	0.4	0.0	Sun	+0.24	K18
3000	-1.0	0.5	0.3	Sun	-0.16	K18
3000	-1.0	0.5	0.2	8/2	-0.16	K18
3000	-1.5	0.8	0.5	5/5	-0.36	K18
3000	-2.0	1.0	0.8	3/7	-0.66	K18
3000	0.0	0.4	0.0	Sun	+0.74	Jorgensen
3100	0.0	0.6	0.0	Sun	+0.94	Jorgensen
3100	-0.5	0.4	0.0	4/6	+0.24	Jorgensen
3200	-2.0	1.2	1.5	Sun	-0.46	K18n
3200	-2.5	1.4	1.8	5/5	-0.76	K18n
3300	-2.0	1.6	1.4	Sun	-0.06	K18n
3300	-2.5	1.6	1.6	7/3	-0.56	K18n

Table 2 shows some ambiguousness of our DY Per parameters estimations. Values of effective temperature of DY Per are 2900 < T_{eff} < 3000 K if use line list K18 (Kurucz 1993-1994), 3000 < T_{eff} < 3100 K if use data of Jorgensen (http://stella.nbi.dk) and 3200 < T_{eff} < 3300 K if use K18n list.

In general, the uncertainty of other atmosphere parameters estimations - [Fe/H] , log(C/O), [N/Fe] and H/He - is considerably higher. We fixed the upper limits of metallicity for every T_{eff} and molecular line list:

$[Fe/H]_{max}$= -0.5 for K18 line list,

$[Fe/H]_{max}$= -2.0 for K18n list,

$[Fe/H]_{max}$= 0.0 for Jorgensen's data.

For all $[Fe/H]_{max}$ estimations of H/He are solar. If [Fe/H]decreases appears hydrogen deficiency, C/O and [C/Fe] increases but carbon abundance relatively solar value [C] decreases.

We cannot choose definitely the best variant of synthetic spectrum in frames of our spectral synthesis technique only. Qualitative analysis of observations of DY Per (Keenan & Barnbaum 1997, Zacs et al. 2007) shows that DY Per is of normal metallicity or slightly metal deficient star and, possibly, hydrogen deficient. From another hand, it is obviously that carbon abundance in atmosphere of DY Per is quite high. We see from Table 2 that only Jorgensen's molecular line lists support [C] values close to observed in atmospheres of R CrB type stars ([C]=1-2). The highest carbon abundance [C]=0.94 we get for model atmosphere {T_{eff} =3100 K, [Fe/H] =0, log(C/O)=0.6, [N/Fe]=0, $(H/He)_{\odot}$}. We note that these values of parameters are not in contradiction with rough estimations of other authors. The fit of theoretical fluxes to the observed SED of DY Per for this case is shown on Fig. 3c.

4. Discussion and conclusions

Results of this work and Yakovina et al. (2009) allows make the next conclusions:

- The effective temperature of DY Per is in range 2900 < T_{eff} < 3300 K. Our estimations of T_{eff} are below of estimations by indirect methods. So we confirm that DY Per is the coolest R CrB type star.
- For every value of T_{eff} spectral synthesis technique gives the large ambiguousness in the [Fe/H] , log(C/O), [N/Fe], H/He atmosphere parameters estimations. However, if account the qualitative analysis provided by some authors and physical constrains, the most real combination of atmosphere parameters of DY Per is {T_{eff} =3100 K, [Fe/H] =0, log(C/O)=0.6, [N/Fe]=0, $(H/He)_{\odot}$} with Jorgensen's line lists for molecules C_2 and CN.

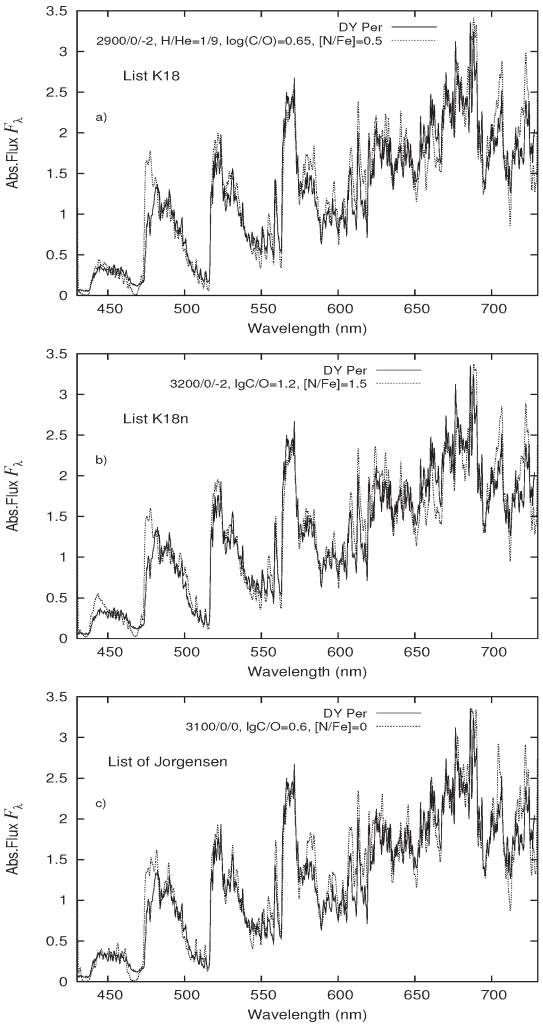

Figure 3: Fit of synthetic spectra computed with different line lists of C_2 and CN to the observed fluxes of DY Per.

- We believe that new observations of DY Per in wider spectral region, high resolution spectra of this star and independent methods of analysis allow us to increase a confidence of determination of atmosphere parameters of DY Per.

References

Bernath P.F., Black J.H., Brault J.W.: 1985, *ApJ*, **298**, 375.

Gurtovenko E.A., Kostik R.I.: 1998, *The system of solar oscillator strengths*, preprint MAO-98-3E, 63.

Huang Y., Barts S.A., Halpern J.B.: 1992, *J. Phys. Chem.*, **96**, 425.

Jorgensen U.G., Larsson M.: 1990, *A&A*, **238**, 424.

Keenan P.C., Barnbaum C.: 1997, *PASP*, **109**, 969.

Kupka F., Piskunov N., Ryabchikova T.A. et al.: 1999, *A&AS*, **138**, 119.

Kurucz R.L.: 1993-1994, Data Bank - CD-ROM NN 1-22.

Kuznetsova L.A., Shavrina A.V.: 1996, *Kinem. & Phys. of Celest. Bodies*, **12**, N 6, 75.

Kuznetsova L.A., Pazyuk E.A., Stolyarov A.V.: 1993, in: *Proc. IAU Coll.*, eds P.Thejll, U.G.Jorgensen, Copenhagen: Niels Bohr Inst., s.a., **146**, 63.

Pavlenko Ya.V.: 1997, *Ap&SS*, **253**, 43.

Pavlenko Ya.V.: 2003, *Astron. Rept.*, **47**, 59.

Pavlenko Ya.V., Yakovina L.A.: 2009, *Kinem. & Phys. of Celest. Bodies*, accepted.

Querci F., Querci M., Kunde V.G.: 1971, *A&A*, **15**, 256.

Querci F., Querci M., Tsuji T.: 1974, *A&A*, **31**, 265.

Tsuji T.: 1973, *A&A*, **23**, 411.

Urdahl R.S., Bao Y., Jackson W.M.: 1991, *Chem. Phys. Lett.*, **178**, 425.

Yakovina L.A., Pugach A.F., Pavlenko Ya.V.: 2009, *Astron. Rept.*, in press.

Zacs L., Chen W.P., Mondal S. et al.: 2007, *A&A*, **472**, 247.

ρ PUPPIS: THE POSSIBILITY OF NON-RADIAL PULSATIONS

A.V. Yushchenko[1,2], T.N. Dorokhova[2], V.F. Gopka[2], C. Kim[3]

[1] Astrophysical Research Center for the Structure and Evolution of the Cosmos (ARCSEC), Sejong University, Seoul, 143-747, Korea, *yua@sejong.ac.kr*

[2] Astronomical Observatory of Odessa National University, Marazlievskaya, 1v, 65014 Odessa, Ukraine, *astro@paco.odessa.ua*

[3] Department of Earth Science Education, Chonbuk National University, Korea, *chkim@chonbuk.ac.kr*

ABSTRACT. The profiles of spectral lines in the high resolution (R=80,000) and high signal to noise ratio (S/N more than 300) VLT spectrum of ρ Pup are not symmetric. Under the assumption that the asymmetry of the observed profiles is introduced by non-radial pulsations we estimated the pulsational degree l=3, the azimuthal order m=1, and amplitude of pulsation 15 km s^{-1}. The projected rotational velocity of the star is near $v \sin i$ =3.5 km s^{-1}. The obtained synthetic spectrum yield the better fit to the observed one in comparison with earlier known parameters.

Key words: stars: oscillation – stars: variables (ρ Pup, δ Scuti) – stars: individual (ρ Pup)

1. Introduction

ρ Pup (HR 3185, HD 67523) is a prototype of the group of metallic-line pulsating variables (Rodriguez & Breger 2001).

The enhanced metal abundance in the atmosphere of ρ Pup has been confirmed by Greenstein (1948), Bessell (1969), Breger (1970) and Kurtz (1976), however, the chemical composition was not yet determined in details with the use of a new high resolution and high signal to noise spectra.

As one of the bright star of the south sky ρ Pup (B=3.24, V=2.81, Sp F6 II) was an object of the first radial velocities surveys. The first radial velocities estimates (Reese 1903) revealed the variability with the peak-to-peak amplitude of 8.4 km s^{-1}.

The photometric variability of ρ Pup was detected considerably latter (Cousins 1951), and the star was considered as a radial monoperiodic pulsator (Campos & Smith 1980 and references therein). Only Mathias et al. (1997) found the evidence for additional two possible secondary non-radial pulsations (NRPs) at frequencies of 7.8 c/d and 6.3 c/d at a very low level.

ρ Pup with the sharp and well-defined lines was a "launch pad" for the line profile analysis (Aerts et al. 2008 and references therein) and a Van Hoof effect searching (Mathias et al. 1997).

2. Asymmetry of line profiles

For the present investigation we used the spectrum of ρ Pup from the VLT archive (Bagnulo et al. 2003) with the spectral resolving power R=80,000 and the signal to noise ratio S/N more than 300. Under this resolution the asymmetry of line's profiles in the observed spectrum becomes clearly detected. The reason of this asymmetry is, evidently, the line profile variations produced by NRP (see, for example, Aerts et al. 1992, Aerts et al. 1993). Yushchenko et al. (2005) detected this effect in the spectrum of δ Sct .

The use of the last version of URAN software (Yushchenko 1998) allow us to find the appropriate quantum numbers and amplitudes of the NRP for ρ Pup. The disk of the star was divided by several thousands regions. The number of these regions, the profile of pulsation over the stellar surface and the projected rotational velocity were selected to adjust the observed profile.

The synthetic spectra at the different distances from the center of the disk were calculated by Kurucz (1995) SYNTHE code. Only the velocity fluctuations have been taken into account. Integration over the stellar disk resulted in synthetic profile disturbed by NRP.

The Least Square Decomposition (LSD) profile (Reiners & Royer 2004) constructed from 34 clean iron lines was used as a mean observed profile to fit it by synthetic spectrum disturbed by NRP.

Figure 1 (upper panel) shows the observed profile of ρ Pup and the synthetic spectrum disturbed by NRP with the pulsational degree l=3, the azimuthal order m=1, the pulsational amplitude of 15 km s^{-1}, and additionally broadened by rotation with the projected rotational velocity $v \sin i$ =3.5 km s^{-1}. For the obtained synthetic profile the amplitude of pulsation occurs somewhat higher than the observed amplitudes 9.5 - 11.5 km s^{-1} found in different investigations by Yang et al. (1987) and Campos & Smith using Fe I and Fe II lines.

Mathias et al. (1997) using only the H$_\alpha$, Fe I λ 6393,

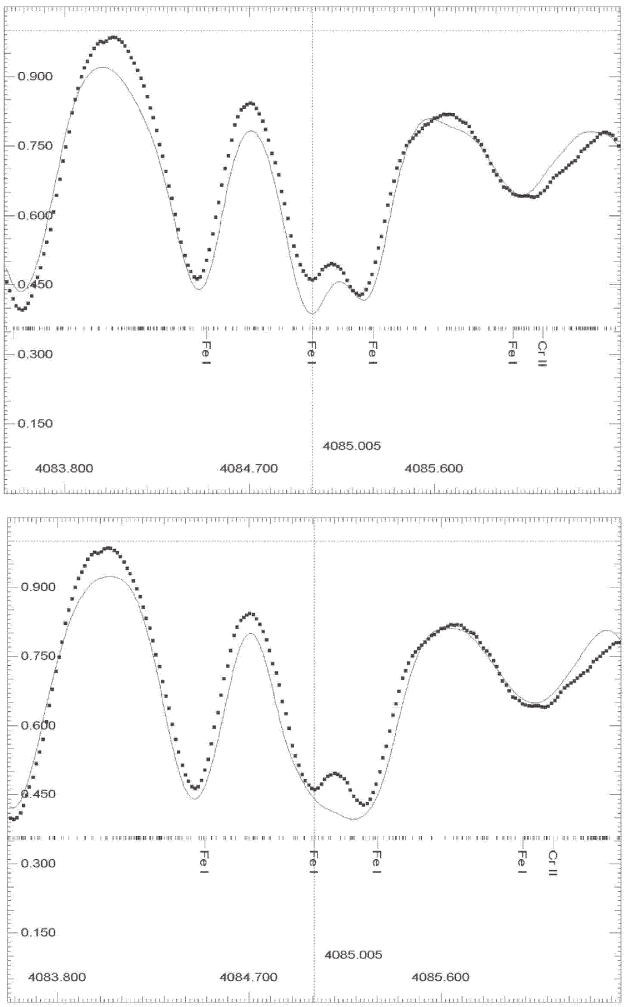

Figure 1: The observed (points) and synthetic (lines) spectra of ρ Pup in the vicinity of of Fe I λ 4085.005 Å line. The axes are the wavelength in angströms and the relative fluxes. The wavelengths of the spectral lines involved in the calculations are marked at the foot. For the strongest lines the identifications are given. The position of the Fe I λ 4085.005 Å line is marked by a vertical dotted line. Synthetic spectrum is convoluted with two sets of parameters. Upper panel: l=3, m=1, amplitude of pulsation 15 km s^{-1}, $v \sin i$ =3.5 km s^{-1}. Bottom panel: zero amplitude of pulsation, $v \sin i$ =15.3 km s^{-1}.

and Ca I λ 6122 lines found the observed amplitudes of 8.6 km s^{-1} and theoretical fit with amplitudes of 5.6 km s^{-1} of the radial pulsation (see also Aerts 1996).

However, the model with their value of $v \sin i$ =15.3 km s^{-1} fits the VLT spectrum too rough: the isolated lines may be fitted with comparable precision but the close pairs of lines cannot be reproduced with a rather high value of rotational velocity (Fig. 1, bottom panel).

The existence of NRP is in a contradiction with the commonly accepted persuasion that ρ Pup is a radial pulsator. However, from radial velocity variations Mathias et al. (1997) also identified the NRPs of a low-degree axisymmetric mode ($l = 3$; $m = 0$) and the one which is clearly non-axisymmetric ($m \neq 0$) besides of radial pulsations.

3. Conclusion

We are going to use the VLT spectrum of ρ Pup for the investigation of the chemical composition of the star, the dynamics of the atmosphere can not be found using the single spectrum. However, the spectrum synthesis method needs in the reliable profiles of spectral lines, that is why we were forced by high quality observed spectrum to find this profile and to clarify its physical meaning.

We assumed that the shape of the profile of ρ Pup may be explained by NRPs and found the appropriate combination of quantum numbers and amplitudes. The additional broadening could be explained by rotation with the projected rotational velocity $v \sin i$ =3.5 km s^{-1}. Our combination of parameters fits the observed VLT spectrum better than the previously found projected rotational velocity ($v \sin i$ =15.3 km s^{-1}: Mathias et al. 1997).

Acknowledgement. Work by AY was supported by the Astrophysical Research Center for the Structure and Evolution of the Cosmos (ARCSEC, Sejong University) of the Korea Science and Engineering Foundation through the Science Research Center program.

References

Aerts C., de Pauw M., Waelkens C.: 1992, *Astron. Astrophys.*, **266**, 294.
Aerts C., Waelkens C.: 1993, *Astron. Astrophys.*, **273**, 175.
Aerts C.: 1996, *Astron. Astrophys.*, **314**, 115.
Aerts C., Hekker S., Desmet M., et al.: 2008, in *Proc. of the ESO/Lisbon/Aveiro Conf.*, Ed. N.C.Santos, L. Pasquini, A.C.M.Correia, M.Romanielleo, 161-164.
Bessell M.S.: 1969, *Astrophys. J. Suppl.*, **16**, 167.
Bagnulo et al.: 2003, *Messenger*, **114**, 10.
Breger M.: 1970, *Astrophys. J.*, **162**, 597.

Campos A.J., Smith M.A.: 1980, *Astrophys. J.*, **238**, 667.
Greenstein J.L.: 1948, *Astrophys. J.*, **107**, 151.
Kurtz D.W.: 1976, *Astrophys. J. Suppl.*, **32**, 651.
Kurucz R.L.: 1995, CDROM No. 23 (Cambridge, MA, Smithsonian Astrophys. Obs.)
Mathias P., Gillet D., Aerts C., Breitfellner M.G.: 1997, *Astron. Astrophys.*, **327**, 1077.
Reese H. M.: 1903, *Astrophys. J.*, **17**, 308.
Reiners A., Royer F.: 2004, *Astron. Astrophys.*, **428**, 199.
Rodriguez E., Breger M.: 2001, *Astron. Astrophys.*, **366**, 178.
Yang S., Walker G. A. H., Bennett P.: 1987, *PASP*, **99**, 425.
Yushchenko A.V.: 1998, in *Proc. of the 20th Stellar Conf. of the Czech and Slovak Astronomical Institutes*, Ed. J. Dusek, 201.
Yushchenko A., Gopka V., Kim C., et al.: 2005, *MNRAS*, **359**, 865.

ATMOSPHERIC PARAMETERS AND CHEMICAL COMPOSITION OF PECULIAR STARS HR465, HD91375, and HD25354

V. Yushchenko[1], V. Gopka[2], A. Yushchenko[3,2], A. Shavrina [4], S. Hubrig [5], F. Musaev [6,7]

[1]Department of astronomy, Odessa National University, T.G. Shevchenko Park, Odessa, 65014, Ukraine, *12345678e@mail.ru*
[2]Astronomical observatory, Odessa National University, T.G. Shevchenko Park, Odessa, 65014, Ukraine, *gopkavera@mail.ru*
[3]Astrophysical Research Center for the Structure and Evolution of the Cosmos, Sejong University, Seoul, 143-747, Korea, *avyushchenko@gmail.com*
[4]Main Astronomical Observatory of National Academy of Sciences of Ukraine, 27 Zabolotnogo Str., 03680, Kyiv, Ukraine, *shavrina@mao.kiev.ua*
[5]European Southern observatory, Casilla 19001, Santiago 19, Chile, *shubrig@eso.org*
[6]Special Astrophysical Observatory, Russian Academy of Sciences, Nizhnii Arkhyz, Karachai-Cherkessian Republic, 357147, Russia *faig@sao.ru*
[7]International Center for Astronomical, Medical, and Ecological Research, Terskol, Kabarda-Balkarian Republic, 361605, Russia

ABSTRACT. We present the results of determinations of the atmospheric parameters and chemical composition of three chemically peculiar stars: HR465, HD91375, and HD25354. We used the observations made at 1.8 meter Bohuynsan observatory (Korea), 1.88 meter Haute-Provence observatory (France), 2.0 meter Terskol observatory (Russia), and 8.2 meter ESO telescopes. The effective temperatures of HR465 and HD25354 are higher than the values, found in earlier investigations. The detailed abundance pattern of HD91375 is found for the first time, the star is a typical member of Am or Ap group.

Key words: stars: abundances; stars: individual (HR465, HD91375, HD25354).

1. Introduction

The chemical composition of peculiar stars of the upper main sequence was one of the results which allowed Burbidge et al. (1957) to finalize the theory of synthesis of the chemical elements in stars. But up to now the nature of these stars is not fully explained. High resolution spectra allow to investigate the magnetic fields, the stratification of chemical elements, the spots, the unidentified lines, the radial and nonradial pulsations in the atmospheres of these objects. The interplay of above mentioned and other effects, like the radiative diffusion and the accretion of interstellar matter results in a variety of different anomalies.

In this paper we show the results of the determination of atmospheric parameters of three peculiar stars of upper main sequence, namely HR465, HD91375, and HD25354. The next sections of the paper are devoted to the description of observations, to the determinations of atmospheric parameters, and to the first iteration of abundance determinations in the atmospheres of these stars. For HR465 and HD25354 our values of temperatures are significantly higher, than it were found in earlier investigations.

2. Observations

HR465. The star was observed at 1.8 meter telescope of Bohuynsan observatory (Korea) in 2004. Spectral resolving power was R=60000, signal to noise ratio S/N>100 in red spectral region, the wavelength coverage was from λ=3800 Å to λ=9500 Å. We used also the spectrum of the star taken from the archive of Haute-Provence observatory 1.88 meter telescope. For this spectrum R=40000, S/N=50-100, the wavelength coverage is 4000-6800 Å. The spectrum was observed in 1996.

HD91375. We used the spectra of the star obtained at 8.2 meter ESO telescope. The wavelength coverage

is from λ=3060 Å to λ=9460 Å, R=80000, S/N is near 500 in the spectrum region from λ=5000 Å to λ=6000 Å. All spectra were obtained in ten minutes, the variability of profiles and the asymmetry of spectral lines were noticed. To find the equivalent widths of spectral lines the red and the blue wings of the profile were fitted by different Gauss profiles.

HD25354. Two observations of the spectrum of this star were made at 2.0 meter telescope of Terskol observatory. The wavelength coverage is from λ=3700 Å to λ=9400 Å, S/N=200, R=60000.

3. Atmosphere parameters

HR465. To find the effective temperature and the surface gravity of the star we measured the equivalent widths of 197 lines of neutral iron and 13 lines of ionized iron in 2004 year spectrum. Using the method, described by Yushchenko et al. (1999, 2005) we found the following set of parameters: the effective temperature $T_{\rm eff}$=11840 K, the surface gravity $\log g$=4.3, the microturbulent velocity $v_{\rm micro}$=1.66 km s^{-1}, the iron abundance logN(Fe)=8.68 in the scale logN(H)=12.00.

The variability of the spectrum of HR465 with period near 23 years is known (Preston 1970), that is why to check the stability of effective temperature we analyzed the spectral energy distribution in the ultraviolet region using IUE spectra and the magnitudes and the colors using the observations of HIPPARCOS and TYCHO satellites. The results are shown in Figures 1-3. It is clear that no significant variability of the temperature can be expected, but the total flux of the star is variable. That is why we used the same set of parameters for processing of the observations obtained in 2004 and in 1996 years.

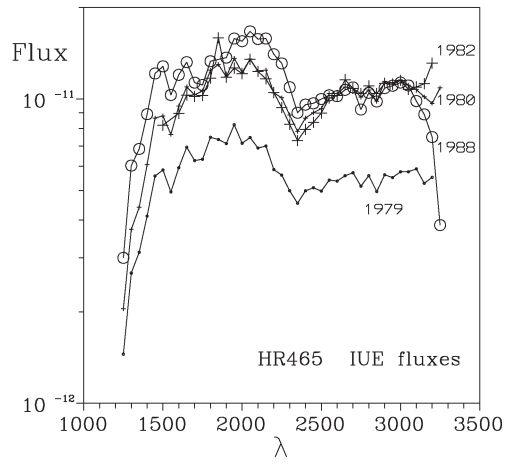

Figure 1: IUE fluxes of HR465. The axes are the wavelength in angstroms and the flux in erg/cm^2/s. The mean spectrum was calculated using all observations obtained during the specified year. Observations of different years are denoted by different symbols.

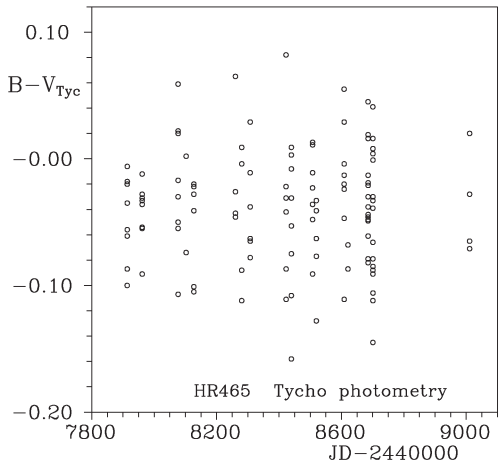

Figure 2: Colors of HR465 observed by TYCHO satellite. The axes are the Julian dates and colors in magnitudes. No significant trend can be found during three years.

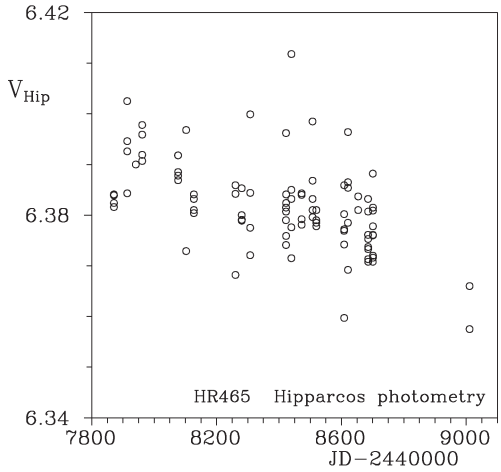

Figure 3: Magnitudes of HR465 observed by HIPPARCOS satellite. The axes are the Julian dates and the magnitudes. The mean flux of the star decreased by at least 0.02^m in three years.

Table 1 shows the effective temperatures and the surface gravities of HR465 obtained by different investigators. The majority of previous determinations of the temperature are lower than our value. It should be noted that the use of calibrations developed for normal stars can lead to strange results for peculiar stars. The metallicity of HR465 is significantly higher than the solar one, that is why only high dispersion spectroscopy and individual atmosphere models can help to find the reliable set of atmospheric parameters.

HD91375. The effective temperature and the surface gravity of the star were found using the equivalent widths of 25 lines of neutral iron and 34 lines of ionized one. The effective temperature appeared to be equal $T_{\rm eff}$=9100 K, the surface gravity – $\log g$=3.8, the mi-

Table 1: The determinations of atmospheric parameters of HR465.

$T_{\rm eff}$	$\log g$	Reference
10723	3.7	Aller (1972)
10500		Cowley & Aikman (1980)
11500		Floquet (1981)
9450	3.8	Guhtrie (1982)
10600	3.4	Guhtrie (1982)
9700		Carrier et al. (2002)
11840	4.3	This paper

croturbulent velocity – $v_{\rm micro}$=2.12 km s^{-1}, the iron abundance – logN(Fe)=7.66.

Lemke (1989) found for HD91375 the values $T_{\rm eff}$=9300 K, $\log g$=3.65, $v_{\rm micro}$=3.0 km s^{-1}, and the iron abundance logN(Fe)=7.56 in the case of LTE, These results are in the error boxes of our determinations.

HD25354. Wolff (1967) pointed that the temperature of HD25354 is in the range of 11000-12500 K. Pyper & Hartoog (1975) pointed that the temperature of the star is close to $T_{\rm eff}$=11000 K. Floguet (1982) derived the effective temperature and the surface gravity of the star to be equal $T_{\rm eff}$=9050 K, $\log g$=3.5. Kochukhov & Bagnulo (2006) found $T_{\rm eff}$=9840 K using the observations of the star in Geneva photometrical system.

Our attempts to describe the observed spectrum with by synthetic spectrum caclulated with low (near 9000 K) temperature failed. It was necessary to increase the temperature to 12500–13000 K. These value was supported also by the investigation of the profiles of hydrogen lines. Using the equivalent widths of 83 lines of ionized iron and 8 lines of doubly ionized iron we found the effective temperature $T_{\rm eff}$=12900 K, the surface gravity $\log g$=4.5, the microturbulent velocity $v_{\rm micro}$=0.23 km s^{-1}, the iron abundance logN(Fe)=8.44.

It should be noted the the lines of the third spectra of different chemical elements are present in the spectrum of HD25354. Aikman et al. (1979) found the lines of Dy III, Pyper & Hartoog (1975) – the lines of Ce III, Pr III, Yb III. Detectability of the lines of third spectra confirms the high temperature of the star. The second spectra of the elements with high ionization potentials, like Hg, Pt, Ta, Au, were also detected by Pyper & Hartoog (1975).

3. Chemical composition

Using the parameters, derived here before, we calculated the synthetic spectra of investigated stars in the whole observed wavelength region. These synthetic spectra allowed to make the reliable identification of spectral lines. To find the chemical composition of the atmospheres we used Kurucz (2000) programs WIDTH9 and SYNTHE, and Yushchenko (1998) URAN software. Atmosphere models were interpolated from Kurucz (2000) grid of stellar models. The full description of used methodic can be found in Yushchenko et al. (2005).

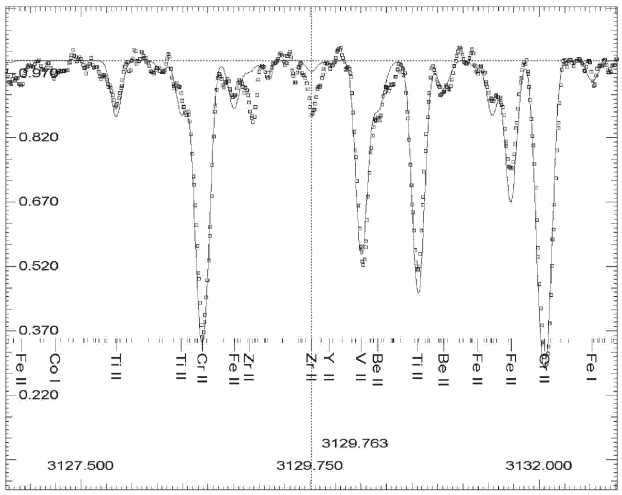

Figure 4: Observed spectrum of HD91375 (open squares) and synthetic spectrum (line) in the vicinity of Zr II line λ 3129.763 Å. The berillium dublet is in the right part of the figure. The axes are the wavelengths in angstroms and the relative fluxes. The positions of the lines used for calculation of synthetic spectrum are marked in the bottom part of the figure. The identification of part of the strong lines are shown. Synthetic spectrum was calculated with solar abundances of heavy elements, that is why the depths of zirconium lines in the synthetic spectrum do not fit the observed one.

Figures 4-6 show the examples of observed and calculated spectra in the vicinities of lines of heavy elements for HD91375 and HD25354.

Figures 7-9 show the results of our determinations of the abundances of chemical elements in the atmospheres of HR465, HD91375, and HD25354 with the parameters, found in the previous section.

HR465. The variability of the strengths of absorption lines in the spectrum is clearly observed. It results in the variation of abundances of chemical elements. The lines of chromium and the lines of lanthanides and actinides vary in the opposite phases. The differences in the lanthanides abundances are as high as 1-2 dex. The abundance of chromium in 2004 is 0.7 dex lower than in 1996. (Gopka, Shavrina,Yushchenko, 2007)

The overabundances of lanthanides can reach 6-7 dex with respect to the solar values. It should be noted that HR465 is a spectroscopic binary with orbital period near 273 days (Carrier et al. 2002). The lines of the

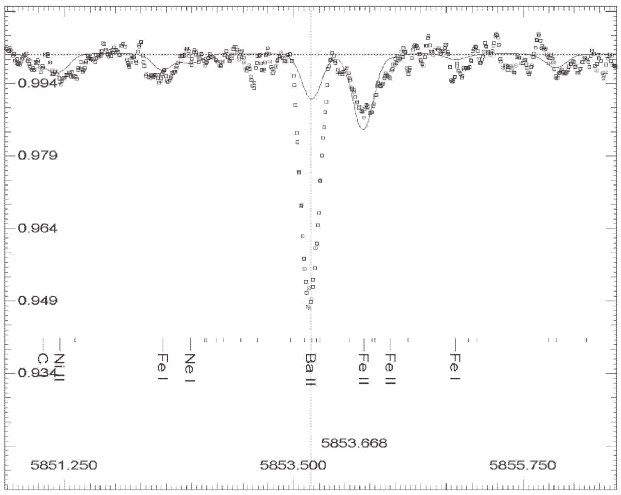

Figure 5: The same as Fig. 4 but in the vicinity of barium line λ 5853.668 Å.

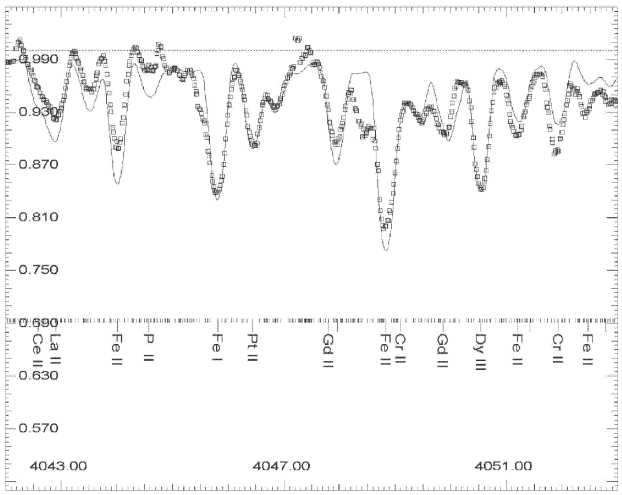

Figure 6: The same as Fig. 5 but for HD25534. The abundances of heavy elements are enhanced in accordance with our result. Note the line of ionized platinum in the central part of the figure.

secondary component are not detected in the spectrum. If the unvisible companion is a neutron star (NS), the chemical composition of HR465 should be influenced by NS (Gopka et al., 2007, 2008).

HD91375. No detailed investigation of the chemical composition of this star was made earlier. Holweger et al. (1986) compared the relative intensities absorption lines of iron group elements, helium, carbon, magnesium, and barium in the spectra of several stars including HD91375. Lemke (1989, 1990) derived the abundances of iron, titanium, carbon, silicon, calcium, strontium, and barium. The abundances of carbon, silicium, and iron were found by Holweger & Sturenburg (1993), the abundances of sodium and sulfur – by Rentzsch-Holm (1997). Mathys & Hubrig (2006) investigated the magnetic field of the star and found the value 1662 gauss for quadratic magnetic field using the lines of neutral iron, but only the upper limit of the strength of magnetig field was found using the lines of ionized iron (<2681 gauss).

We found the abundances of 34 chemical elements in the atmosphere of HD91375. The abundance pattern is typical for Ap stars. HD91375 is a member of Sirius group (Palous & Hauck 1986), so it will be very interesting to compare the chemical composition of HD91375 and the chemical composition of Sirius A. The temperature of Sirius A is only 800 K higher than the temperature of HD91375, but no detectable magnetic field was found for Sirius A.

The chemical composition of HD91375 is typical for Am stars but the existence of magnetic field (liked *o* Peg).

HD25354. The abundances of 18 chemical elements from oxygen to erbium are found in the atmosphere of this star. The lines of helium, strontium, gadolinium, platinum, and several other elements were identified, but it will be analyzed later, when the new atmosphere model will be constructed. The abundance pattern is similar to that of HR465. It is necessary to note that the intensities of helium lines in the observed spectrum are significantly weaker than in the synthetic one. Maybe the star is a helium weak object.

4. Summary

The use of high resolution spectral observations allow to find the atmosphere parameters of the investigated stars. For two of them the derived temperatures appeared to be higher than the earlier determinations. For HR465 the difference with the highest previously published value is 340 K, for HD25354 – 400 K.

The detailed abundance pattern of HD91375 is found for the first time. The star appeared to be a typical Am or Ap type star. The selection between these two possibilities needs additional investigation. The chemical composition of HR465 and HD25354 shows the high overabundances of heavy elements – up to 6-7 dex.

The obtained results will be used to construct the individual atmosphere models of these objects. The models will be used to find more precise chemical composition.

Work by AY was supported by the Astrophysical Research Center for the Structure and Evolution of the Cosmos (ARCSEC, Sejong University) of the Korea Science and Engineering Foundation (KOSEF) through the Science Research Center (SRC) program.

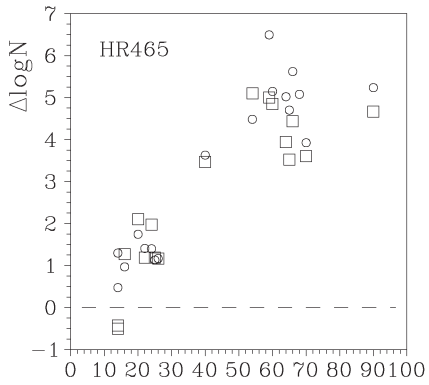

Figure 7: Chemical composition of HR465. The axes are the atomic numbers of the elements and the chemical composition with respect to the solar one. Circles and squares denote the observations made in 2004 and 1996 respectively.

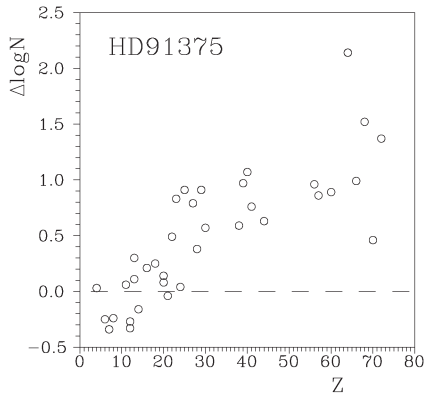

Figure 8: Chemical composition of HD91375.

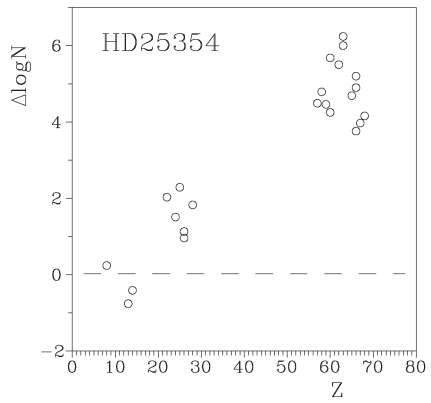

Figure 9: Chemical composition of HD25354.

References

Aikman G.C.L., Cowley C.R., Crosswhite H.M.: 1979, *ApJ*, **232**, 812.

Aller M.F.: 1970, *A&A*, **19**, 248.

Burbidge E.M., Burbidge G.R., Fowler W.A., Hoyle F.: 1957, *Reviews of Modern Physics*, **29**, 547.

Carrier F., North P., Udry S., Babel J.: 2002, *A&A*, **394**, 151.

Cowley C.R., Aikman G.C.L.: 1980, *ApJ*, 1980, **242**, 684.

Floquet M.: 1981, *A&A*, **101**, 176.

Floquet M.: 1982, *A&A*, **112**, 299.

Gopka V.F., Ulyanov O.M., Andrievsky S.M.: 2007, *Odessa Astron. Publ*, **20**, 57.

Gopka V.F., Ulyanov O.M., Andrievsky S.M.: 2008, *AIP Conf. Proc.*, **1016**, 460.

Gopka V.F., Shavrina A.V., Yushchenko V.A.: 2007, *Izv. KrAO*, **104**, 223.

Guthrie B.N.G.: 1982, *Astrophysics and Space Science*, **85**, 315.

Holweger H., Steffen M., Gigas D.: 1986, *A&A*, **163**, 333.

Holweger H., Sturenburg S.: 1993, *Peculiar versus Normal Phenomena in A-type and Related Stars*, IAU Col. 138, Eds. M.M. Dworetsky, F. Castelli, R. Faraggiana; ASP, San Francisco, CA, P. 356.

Kochukhov O., Bagnulo S.: 2006, *A&A*, **450**, 763.

Kurucz R.: 2000, http:*kurucz.harvard.edu*

Lemke M.: 1989, *A&A*, **225**, 125.

Lemke M.: 1990, *A&A*, **240**, 331.

Mathys G., Hubrig S.: 2006, *A&A*, **453**, 699.

Palous J., Hauck B.: 1986, *A&A*, **162**, 54.

Preston G.W.: 1970, *PASP*, **82**, 878.

Pyper D.M., Hartoog M.R.: 1975, *ApJ*, **198**, 555.

Rentzsch-Holm I.: 1997, *A&A*, **317**, 178.

Wolff S.C.: 1967, *ApJS*, **15**, 21.

Yushchenko A.V., Gopka V.F., Khokhlova V.L., Musaev F.A., Bikmaev I.F.: 1999, *Astronomy Letters*, **25**, 453.

Yushchenko A.V.: 1998, *Proceedings of the 20th Stellar Conference of the Czech and Slovak Astronomical Institutes*, Brno, Czech Republic. ed. Dusek J., pp. 201-203, ISBN 80-85882-08-6.

Yushchenko A., Gopka V., Goriely S., Musaev F., Shavrina A., Kim C., Kang Y.-W., Kuznietsova J., Yushchenko V.: 2005, *A&A*, 2005 **430**, 255.

Yushchenko A., Gopka V., Shavrina A., Nazarenko V., Kang Y.-W., Kim C., Yushchenko V.: 2008, *The First Thailand-Korea Joint Workshop on Stellar Astrophysics*, Eds. Kang Y.-W. & Soonthornthum B., pp. 75-86. Chiang Mai University Press, Chiang Mai, Thailand. ISBN 978-974-229-620-9.

THE INFLUENCE OF ATMOSPHERIC ABSORPTION ON VISIBILITY OF GALAXIES

M. Biernacka[1], M. Chudy[2], P. Flin[1], M. Michniak[3], E. Panko[4,5]

[1] Jan Kochanowski University, Institute of Physics
ul. Swietokrzyska 15, Kielce 25-406 Poland, *bmonika@pu.kielce.pl*, *sfflin@cyf-kr.edu.pl*
[2] Youth Astronomical Observatory
ul Kopernika 2, Niepolomice 32-005 Poland, *monika@moa.home.pl*
[3] Pedagogical Academy, Institute of Physics
ul. Podchorazych 2, Krakow, 30-084 Poland
[4] Odessa National University, Department of Astronomy
T.G.Shevchenko Park, Odessa 65014 Ukraine
[5] Nikolaev State University, Astronomical Observatory
Nikolskaya, 24, Nikolaev 54030 Ukraine, *tajgeta@sp.mk.ua*

ABCTRACT. We discuss the influence of atmospheric extinction to visibility of galaxies in the visual region of the spectrum. For this purpose the plates covering the same, small region of the sky taken with 2-m telescope, at different zenith distances were obtained. We investigated the relation between galaxy counts and the zenith distance. We show that the influence of the atmospheric mass to the visibility of galaxies is the same as for stars.

Key words: atmospheric absorption; teaching of astronomy.

1. Introduction

The quality of astronomical observations strongly depends on conditions of the Earth atmosphere. There are several factors influencing the accuracy of observations. The atmospheric refraction lowers the accuracy of astrometry; atmospheric absorption causes significant errors in photometric and spectrophotometric measurements, different for point-like images, i.e. stars, and extended objects such as nebulae and galaxies.

For stars at zenith distances $z < 30^\circ$ secans law describing the atmospheric mass works well. The zenith distance is the distance of an object from the zenith of a observer, equal to 90° minus altitude of an object. For greater zenith distances the formula with higher powers of the series expansion of the $\sec z$ is applied (Goley, 1974; Walker, 1987).

For galaxies the atmospheric influence is not the same for inner and outer parts of a galaxy. The counts of galaxies can be seriously biased by selection effects, mainly due to the brightness of the night sky (Disney, 1976). It is even possible that dim external regions of galaxies can be invisible, causing that galaxy can appear as star. Such phenomenon obviously changes galaxy counts. The photometry of galaxies has a number of features and interpretations directly or indirectly concern numerous questions of physics of galaxies. Effect of seeing and its influence on galaxy photometry has been carefully studied by Saglia et al. (1993). It is interesting to point out that the first results of the correlation function based on Lick counts (Shane & Virtanen, 1967) as presented by Groth & Peebles (1977) led to the discussion on the factors influencing galaxy counts (Geller et al., 1984, Groth & Peebles, 1986a, 1986b; de Lapperent et al., 1986; Brown & Groth, 1989).

In order to check the influence of atmospheric mass to galaxy counts we obtained the adequate data and we investigate the relationship between the number of galaxies seen on the plate and the zenith distance.

2. Observational data

The direct photographs of the one square degree of the sky were taken using the two-meter telescope of the Rozhen National Observatory (Bulgaria).

The involved photographic material consists of 30×30 cm plates ORWO ZU-21, in the photometric system close to IP_v obtained at 6 different zenith distances. Plates were developed in standard manner. All plates were taken during one non-photometric night, but with stable seeing. The centre of each negative has

Table 1: The number of galaxies for individual plates.

z°	Galaxy counts							
	1	2	3	4	5	6	7	8
64	457	567	432	444	416	449	429	456
55	801	904	667	659	672	663	675	720
45	1067	1214	1005	1011	1066	1097	1076	1077
36	1385	1582	1381	1478	1421	1392	1371	1430
28	1697	1777	1741	1728	1732	1738	1746	1737
21	1999	2199	2118	2126	2123	2135	2114	2116

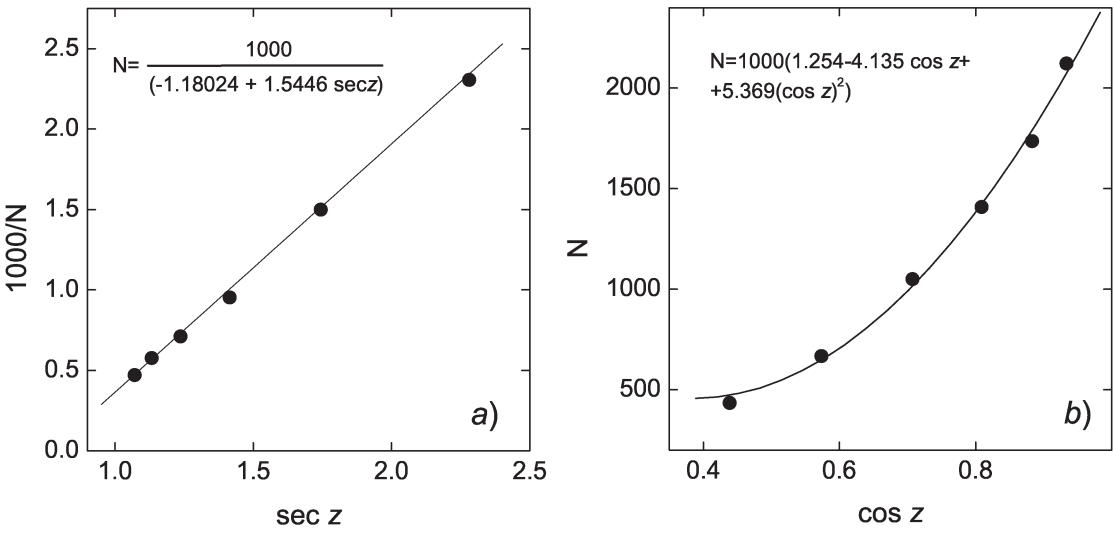

Figure 1: Dependence of galaxy numbers on $\cos z$ (a) and $\sec z$ (b).

coordinates $\alpha = 11^h21^m07^s$ $\delta = 35°07'30''$. We have accepted the middle time of exposure as observation time and the zenith distance was calculated for this moment. The counts of galaxies were performed using light table and a small magnifier. The used magnifications were $6^\times$ and $10^\times$.

3. The results and discussion

We performed galaxy counts independently on each plate. Results are presented in Table 1. Co1umns 1 and 2 give results of galaxy counts made by the same observer, without and with magnifier accordingly. In columns 3–7 counts of other observers are presented and in column 8 the mean of counts is given.

We found the dependence of galaxy number on the zenith distance. Two different variants of the representation of the relation are shown in Fig.1*a* and *b*.

Correlation coefficient in both cases is equal 0.99. So, we found a very good correlation among galaxy counts and the zenith distance. The relation among investigated parameters can be expressed as:

$$N = a + b\cos z + c\cos^2 z \text{ or } N = a/(b + c\sec z)$$

It is clear that the atmosphere mass drastically diminishes the number of seen galaxies. The optical thickness of the atmosphere decreases with the zenith distance, so the faint external parts of galaxies are disappearing, causing the indistinguishability galaxies and stars. We show that the atmosphere mass diminishes the number of galaxies in the same manner as stars.

4. Conclusions or methodical remarks

The presented considerations allow us to prepare a special exercise for student and pupils. Because we have in our disposal photographic plates it was very easy to built a light table. The magnification glass is also not a problem. It is not very difficult to obtain photographic material even using own equipment, because this exercise does not need data from 2-m telescope. Smaller aperture can be also useful. From the methodical point of view this laboratory exercise allows pupils and students to have contact with a part of real astronomical work. Moreover, the look to objects registered on the plate permit one to have filling of the enormous number of shapes of astronomical objects.

Even such simple procedure as counts of objects leads to discovery of the law describing the influence of the atmosphere to the visibility of objects. In practical manner such exercise shows the influence of dark sky to the visibility of galaxies and well known conclusion why astronomers prefer clear, moonless nights, without bright background and observed object at small zenith distances. Therefore, it can be very instructive for students why we should preserve the darkness of the night sky and to exhibit great efforts to keep the night sky clear for the next generations.

Of course the present day astronomy is using plates rather rarely, preferring modern electronic devices, like e.g. CCD. Nevertheless, the problems occurring in this exercise are not easy solvable when the modern devices are in use too. Moreover, the acquaintance with so great variety of extended structures in astronomy gives students the filling how complicated are the problems with pattern recognition, and how difficult is to construct programmes teaching computer how to separate and classified images of different structures. Students will be well informed on the high complexity of such problems also when possible solution is based on neural networking.

References

Brown, M.E., Groth, E.J.: 1989, *ApJ*, **338**, 605.
Disney, M.J.: 1976, *Nature*, **263**, 573.
Geller, M.J., De Lapperent, V., Kurtz, M.J.: 1984, *ApJ*, **287**, L55.
Goley, M.: 1974, "Introduction to Astronomical Photometry", D. Reidel Publ. Co., Dordrecht.
Groth, E.J., Peebles, P.J.E.: 1986a, *ApJ*, **310**, 499.
Groth, E.J., Peebles, P.J.E.: 1986b, *ApJ*, **310**, 507.
Groth, E.J., Peebles, P.J.E.: 1977, *ApJ* **217**, 385.
de Lapperent, V., Kurtz, M.J., Geller, M.J.: 1986, *ApJ*, **304**, 505.
Saglia, R.P., Bertschinger, E., Baggley, G. et al.: 1993, *MNRAS*, **264**, 961.
Shane, C.D., Wirtanen , C.A.: 1967, *Publ. Lick Obs., Vol. XXII*, part 1.
Walker, G.: 1987, "Astronomical Observations, an optical perspective", Cambridge Univ. Press, Cambridge.